AD-A119 264 CALIFORNIA INST OF TECH PASADENA F/G 20/5
OPTICAL PROPERTIES OF SMALL BAND GAP SEMICONDUCTORS SUBJECT TO --ETC(U)
1982 T C MCGILL, D L SMITH AFOSR-77-3216
UNCLASSIFIED AFOSR-TR-82-0678 NL

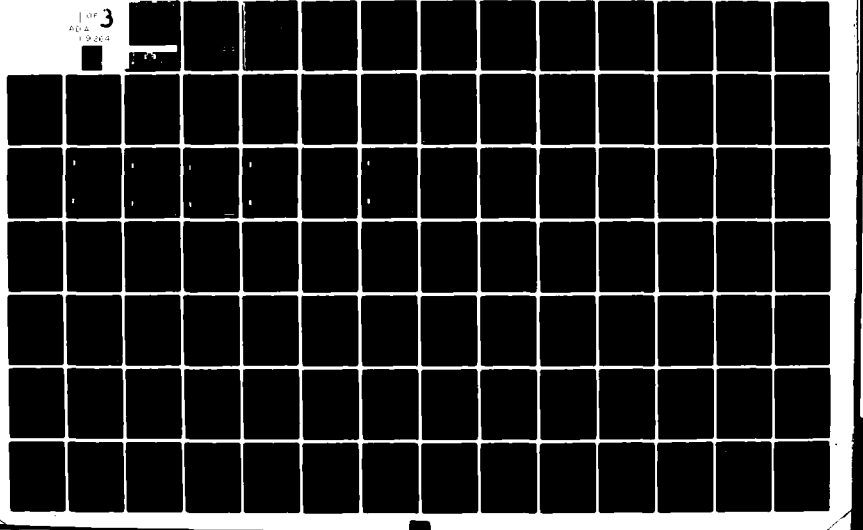

AD A119264

AFOSR-TR- 82-0878

(10)

DTIC
ELECTE
SEP 16 1982
S D

Approved for public release;
distribution unlimited.

82 09 15 048

FINAL TECHNICAL REPORT

TO

AIR FORCE OFFICE OF SCIENTIFIC RESEARCH

GRANT NO. 77-3216

Title: (1/1/77 - 7/31/79)

OPTICAL PROPERTIES OF SMALL BAND GAP SEMICONDUCTORS

SUBJECT TO LASER EXCITATION

Title: (8/1/79 - 2/28/82)

NONLINEAR INFRARED PROPERTIES OF SEMICONDUCTORS

SUBMITTED

BY

T. C. McGill and D. L. Smith*
California Institute of Technology
Pasadena, California 91125

* Present address: Honeywell Systems & Research Center
Mail Code: MN17-2328
2600 Ridgeway Parkway
Minneapolis, Minnesota 55413

UNCLASSIFIED

SECURITY CLASSIFICATION OF THIS PAGE (When Data Entered)

REPORT DOCUMENTATION PAGE		READ INSTRUCTIONS BEFORE COMPLETING FORM
1. REPORT NUMBER AFOSR-TR- 82-0678	2. GOVT ACCESSION NO. AD-A119264	3. RECIPIENT'S CATALOG NUMBER
4. TITLE (and Subtitle) OPTICAL PROPERTIES OF SMALL BAND GAP SEMICONDUCTORS SUBJECT TO LASER EXCITATION & NONLINEAR INFRARED PROPERTIES OF SEMICONDUCTORS		5. TYPE OF REPORT & PERIOD COVERED FINAL REPORT 01 January 77 to 28 February 82 6. PERFORMING ORG. REPORT NUMBER
7. AUTHOR(s) T.C. McGILL & D.L. SMITH		8. CONTRACT OR GRANT NUMBER(s) AFOSR-77-3216
9. PERFORMING ORGANIZATION NAME AND ADDRESS California Institute of Technology Pasadena, CA 91125		10. PROGRAM ELEMENT, PROJECT, TASK AREA & WORK UNIT NUMBERS 2306/C1 61102F
11. CONTROLLING OFFICE NAME AND ADDRESS Air Force Office of Sciences Research Building #410 Bolling AFB, Washington, DC 20332		12. REPORT DATE 1982 13. NUMBER OF PAGES 196
14. MONITORING AGENCY NAME & ADDRESS(if different from Controlling Office)		15. SECURITY CLASS. (of this report) UNCLASSIFIED 15a. DECLASSIFICATION DOWNGRADING SCHEDULE

16. DISTRIBUTION STATEMENT (of this Report)

Approved for public release;
distribution unlimited.

17. DISTRIBUTION STATEMENT (of the abstract entered in Block 20, if different from Report)

18. SUPPLEMENTARY NOTES

19. KEY WORDS (Continue on reverse side if necessary and identify by block number)

20. ABSTRACT (Continue on reverse side if necessary and identify by block number)

A theoretical and experimental study of the optical properties of small band gap semiconductors subject to laser excitation and the nonlinear infrared properties of small band gap semiconductors subject to laser excitation and the nonlinear infrared properties of semiconductors has been carried out. These studies have led to an understanding of the nonradiative recombination mechanisms due to impurties via an Auger process. Predictions about the role of radiative and nonradiative processes in narrow band gap semiconductors have been made. Experiments performed

- OVER -

DD FORM 1 JAN 73 1473 EDITION OF 1 NOV 65 IS OBSOLETE

UNCLASSIFIED

SECURITY CLASSIFICATION OF THIS PAGE (When Data Entered)

on HgCdTe alloys with different composition provided the first systematic study of photoluminescence in these alloys and gave data that supported the conclusions on the relative importance of radiative and nonradiative processes in alloys. The study of the nonlinear infrared properties in the semiconductors resulted in the first complete theory of the phenomenon. Experiments to measure the role of impurities on the saturation intensity have given results in good agreement with theory.

ABSTRACT

We have carried out a theoretical and experimental study of the optical properties of small band gap semiconductors subject to laser excitation and the nonlinear infrared properties of semiconductors. These studies have led to an understanding of the nonradiative recombination mechanisms due to impurities via an Auger process. We have made predictions about the role of radiative and nonradiative processes in narrow band gap semiconductors. Experiments performed on HgCdTe alloys with different composition provided the first systematic study of photoluminescence in these alloys and gave data that supported the conclusions on the relative importance of radiative and nonradiative processes in alloys. The study of the nonlinear infrared properties in the semiconductors resulted in the first complete theory of the phenomenon. Our experiments to measure the role of impurities on the saturation intensity have given results in good agreement with our theory.

I. SCIENTIFIC OBJECTIVES

The major scientific objectives of this program were:

(1) To determine the nature of quantum states formed by excited electrons and holes in small gap semiconductors under different conditions of carrier density and temperature;

(2) To determine the energy and lifetime of these states;

(3) To determine the effect carriers in these states have on the optical properties of the material;

(4) To determine the effect of impurities on the recombination of photoexcited carriers in small band gap semiconductors;

(5) To determine the influence of high intensity below band gap radiation on the free carrier distribution function in semiconductors;

(6) To determine the consequences of this change in the distribution function on the optical and electrical properties of the semiconductors.

II. SIGNIFICANT RESULTS

Over a period of five years a program, such as this one, produces a large number of important results. To indicate the development of our ideas and results, I will order the results approximately chronologically.

A. Auger Rates and Oscillator Strengths for Acceptor Bound Excitons in Si and Ge

The major recombination mechanisms for excitons in moderately and heavily doped indirect semiconductors are due to Auger processes. In this process an exciton bound to a neutral impurity recombines with the energy being absorbed by carrier originally bound to the neutral impurity. Under this program, the first theoretical calculations of this effect were carried out for acceptors in Si (see publication list item 1 and 2) and experiments measuring the decay rates of bound excitons were carried which confirmed the predictions of the theory (see publication list item 3). The theory was extended to cover the case of excitons bound to acceptors in direct band gap materials (see publication list item 4). The theoretical results also included a calculation of the oscillator strength for radiative recombination in the no-phonon channel (see publication list item 4).

B. Auger Decay Versus Radiative Decay in HgCdTe Alloys

Theoretical predictions of radiative decay and the Auger decay were made for $Hg_{(1-x)}Cd_xTe$ alloys as a function of alloy composition x. It was found that alloys with a band gap of less than 0.5 eV the radiative recombination mechanism dominates while alloys with a band gap of greater than 0.5 eV the

Auger recombination mechanism dominates (see publication list items 2 and 4). These results are supported by the experimental results obtained on HgCdTe alloys with differing x (see publication list items 5 and 6).

C. Near Band Photoluminescence of HgCdTe Alloys

We made the first published study of the photoluminescence spectra of $Hg_{(1-x)}Cd_xTe$ alloys for $x \simeq 0.3$ and $x \simeq 0.4$. The small x material shows spectral features which we interpret as band-to-band, and donor-acceptor recombination. The large x material shows spectral features which are band-to-band, donor-acceptor, and bound exciton recombination. These results are presented in publications 5 and 6. The results support the theoretical results discussed in Section B. The variation of the energy of the luminescence with position on the sample offers a method for measuring the variation in composition and band gap across the layer (see publication 6).

D. Theory of Nonlinear Absorption in p-type Semiconductors

The first realistic solid state theory of the nonlinear optical absorption in p-type semiconductors was presented in publications 8 and 9. This theory was very successful in accounting for the first time for the saturation in the absorption observed at high laser intensities at 10.6 μm in Ge. This theory was generalized to include the effects of ionized impurity scattering, residual (non-carrier induced) absorption and the effects of hole-hole scattering in publication 10. In publication 11 this theory was extended from Ge to the III-V semiconductors with large spin-orbit splitting. These included GaAs, GaSb, InAs, AlSb as well as Ge. The theory was further extended

to include the effects of the spin orbit split-off valence band in publication 12.

E. Theory of Pump and Probe Experiments

To develop an understanding of the hole distribution in p-type semiconductors under intense 10.6 μm irradiation experiments pump and probe experiments have been performed. In these experiments the sample is irradiated with an intense 10.6 μm laser pulse and the transmission through the sample is measured at 3 μm. In publication 13, a theory of what should be observed in these experiments was developed and compared with experiment. The agreement between the theory and experiment are very good.

F. Photoconductivity of Ge under 10.6 μm Radiation

It is known that the response of carriers to 10.6 μm radiation in Ge produces a change in the conductivity due to the holes. This occurs because the high intensity radiation changes the carrier distribution and hence the effective mobility. In publication 14, the theory of this phenomenon is presented. Again the agreement between theory and experiment is quite good.

G. Nonlinear Refractive Index of p-type Semiconductors

A theory of the change in the refractive index of p-type semiconductors due to the changes in the carrier distribution was presented in publication 15. At present, there is no experimental data on this phenomena although the theory predicts that such changes in the refractive index should be observable for samples doped higher than $3 \cdot 10^{15} cm^{-3}$.

H. Experimental Measurements of the Saturation in Absorption in p-type Ge

An experimental apparatus was constructed to measure the absorption as a function of intensity using a CO_2 laser. Experiments were performed on Ge and Si samples in which for the first time the saturation as a function of doping was measured. The results were found to be in good agreement with the theory. The experimental results were presented in publication 7.

I. Review on Theory of Nonlinear Optical Absorption Associated with Free Carriers in Semiconductors

From above one can see that a major program was carried out to study the nonlinear optical effects associated with free carriers in semiconductors. The results of this study are presented in an invited review article to be published in the IEEE Journal of Quantum Electronics. A preprint of this article is included in Appendix B which will be published in the November 1982 issue of this journal.

III. INFORMATION TRANSMITTAL

A. Oral Presentations:

D. L. Smith, Physics Seminar at University of California, San Diego, February 7, 1978

D. L. Smith, Applied Physics Seminar at Stanford University, March 16, 1978

D. L. Smith, APS Meeting, Chicago, March, 1979.

G. C. Osbourn, APS Meeting, Chicago, March, 1979.

D. L. Smith, Seminar at Iowa State University, March, 1980.

D. L. Smith, Seminar at Texas A & M University, April, 1980.

R. B. James (Invited Talk)
Grenoble, France, December, 1980.

D. L. Smith, APS Meeting, Phoenix, March, 1981.

R. B. James, APS Meeting, Dallas, March, 1982

D. L. Smith, Seminar at University of Minnesota, Minneapolis, January, 1981.

D. L. Smith, APS Meeting, New York, March, 1980.

B. LIST OF PUBLICATIONS SUPPORTED BY THIS GRANT

1. G. C. Osbourn and D. L. Smith , "Auger Transition Rates for Excitons Bound to Acceptors in Si and Ge", Phys. Rev. B16, 5426 (1977).
2. G. C. Osbourn, S. A. Lyon, K. R. Elliott, D. L. Smith, and T. C. McGill, "Auger and Radiative Recombination of Acceptor Bound Excitons in Semiconductors", Solid State Electron. 21, 1339 (1978).
3. S. A. Lyon, G. C. Osbourn, D. L. Smith, and T. C. McGill, "Bound Exciton Lifetimes for Acceptors in Si", Solid State Commun. 23, 425 (1977).
4. G. C. Osbourn and D. L. Smith, "Auger and Radiative Transition Rates for Acceptor Bound Excitons in Direct Gap Semiconductors", Phys. Rev. B20, 1556 (1979).
5. A. T. Hunter, D. L. Smith, and T. C. McGill, "Near Band Gap Photoluminescence of $Hg_{1-x}Cd_xTe$", Appl. Phys. Lett. 37, 200 (1980).
6. A. T. Hunter and T. C. McGill, "Luminescence from HgCdTe Alloys", J. Appl. Phys. 52, 5779 (1981).
7. R. B. James, Edgard Schweig, D. L. Smith, and T. C. McGill, "Experimental Investigation of the Infrared Absorption Saturation in p-Type Germanium and Silicon", Appl. Phys. Lett. 40, 3 (1982).
8. R. B. James and D. L. Smith, "Theory of Nonlinear Infrared Absorption in p-Type Germanium", Phys. Rev. Lett. 42, 1495 (1979).
9. R. B. James and D. L. Smith, "Saturation of Intervalence Band Transitions in p-Type Semiconductors", Phys. Rev. B21, 3502 (1980).
10. R. B. James and D. L. Smith, "Dependence of the Saturation Intensity of p-Type Germanium on Impurity Concentration and Residual Absorption at 10.59 μm", Solid State Commun. 33, 395 (1980).

11. R. B. James and D. L. Smith, "Saturation Characteristics of p-Type Semiconductors over the CO_2 Laser", J. Appl. Phys. 51, 2836 (1980).

12. R. B. James and D. L. Smith, "Absorption of High-Intensity CO_2 Laser Light in p-Type Semiconductors with Small Spin-Orbit Splittings", J. Appl. Phys. 52, 4238 (1981).

13. R. B. James and D. L. Smith, "Calculation of 3 μm Probe Transmission in p-Ge Excited by a CO_2 Laser", Solid State Commun. 37, 379 (1981).

14. R. B. James and D. L. Smith, "Theoretical Description of Intervalence-Band Photoconductivity of p-Ge at 10.6 μm", Phys. Rev. B23, 4049 (1981).

15. R. B. James and D. L. Smith, "Laser-Induced Changes in the Dispersive Properties of p-Ge Due to Intervalence Band Transitions, Phys. Rev. B23, 4044 (1981).

16. A. T. Hunter and T. C. McGill, "Luminescence Studies of HgCdTe Alloys", Proceedings on HgCdTe Workshop, Minneapolis, Minn., Journal of Vacuum Science and Technology (to be published).

17. M. B. Weimer and D. L. Smith, "Photoionization of Shallow Acceptors in Ge", Solid State Commun. 36, 761 (1980).

STUDENTS SUPPORTED UNDER THIS PROGRAM

In Table I we present a list of the students whose Ph.D. research was supported in part by this grant, the date of their Ph.D. and their current position. From the table you can see that four students have had substantial parts of their Ph.D. research supported by this grant. The four students are all employed by major government laboratories, industrial laboratories or universities in the United States. Other students which have been supported in part by this program have not completed their Ph.D. (e.g., M. Weimer).

TABLE I. Students whose research was supported in part by this Air Force Office of Scientific Research Grant

Name	Date of Ph.D.	Current Position
S. A. Lyon	7/78	Assistant Professor of EE Princeton University
G. C. Osbourn	5/79	Member of Technical Staff Sandia Laboratories
R. B. James	11/80	Wigner Fellow Oak Ridge National Laboratory
A. T. Hunter	8/81	Member of Technical Staff Hughes Research Laboratories

IV. PATENTS AND DISCLOSURES

No patents or disclosures resulted from this work.

APPENDIX A

PUBLICATIONS

PHYSICAL REVIEW B VOLUME 16, NUMBER 12 15 DECEMBER 1977

Auger transition rates for excitons bound to acceptors in Si and Ge†

G. C. Osbourn and D. L. Smith
California Institute of Technology, Pasadena, California 91125
(Received 28 June 1977)

We present calculations of the phononless Auger transition rates for excitons bound to the four common shallow acceptors (B, Al, Ga, and In) in Si and Ge. The calculated rates for the bound excitons in Si vary significantly for the different acceptors, increasing rapidly as the acceptor binding energy increases. This is in agreement with the rapid decrease with increasing acceptor binding energy of measured acceptor bound-exciton lifetimes in Si. Numerically, the calculated Auger rates are within about a factor of 3 of the measured recombination rates for the different acceptors. The dependence of the Auger rates on acceptor binding energy is due to an increased spreading in momentum space of the bound-exciton wave function. In Ge, the calculated Auger rates are orders of magnitude less than the measured free-exciton recombination rate in undoped Ge, suggesting that the phononless Auger transition is not important for acceptor bound excitons in Ge. This is consistent with the experimental observation that light doping with shallow acceptors has little effect on the lifetimes of photoexcited carriers at low temperatures in Ge; whereas, in Si the carrier lifetimes can be decreased by orders of magnitude. The principal difference between Si and Ge is that the acceptor binding energies are much greater in Si than they are in Ge.

I. INTRODUCTION

A bound exciton (BE) consists of three carriers (two holes and one electron for acceptor BE; two electrons and one hole for donor BE) bound to a charged impurity. Because in a BE three carriers are localized in the same region of space, an Auger transition, in which an electron recombines with a hole and the energy is carried off by the third carrier, can occur. Auger transitions are believed to limit the lifetimes of bound excitons in many cases.[1-5] Auger transitions have also been shown to be important in band-to-band recombination and carrier capture at a trap site.[4,5] These processes have been studied theoretically,[4,5] but to our knowledge, no quantitative calculations of BE Auger rates in semiconductors have been presented.

The bound-exciton lifetimes for the four common shallow acceptors in Si(B, Al, Ga, In) have recently been measured.[3] The BE lifetime was found to be significantly shorter than the free-exciton (FE) lifetime in undoped Si for each type of acceptor. The BE lifetime was strongly dependent on the type of acceptor, decreasing rapidly (at least a factor of 200 from Si:B to Si:In) as the acceptor binding energy increased. The lifetimes were interpreted as due to Auger transitions without phonon assistance. Qualitatively similar behavior has been observed for excitons bound to acceptors in GaP.[2] The lifetimes for the BE in GaP were also interpreted as limited by phononless Auger transitions.

Because the BE lifetimes are shorter than the FE lifetimes in undoped Si, the addition of small concentrations of shallow acceptors can greatly change the decay rate of photoexcited carriers in Si at low temperatures. For example, the free-exciton lifetime in undoped Si is 2.6 μsec.[6] If Si is doped with In at the 10^{15} cm^{-3} level (or greater), the lifetime of photoexcited carriers (low excitation) is reduced to less than 5 nsec.[3] This dramatic reduction in carrier lifetime is most likely due to capture of a FE at the impurity to form a BE (the cross section for this process has recently been shown to be very large for Si:In at temperatures less than 10 °K[7]) followed by Auger recombination of the BE. The rate limiting step in the process is the Auger recombination rate (for doping in the 10^{16} cm^{-3} or greater level and temperatures less than 10 °K).[7]

In contrast to Si, doping Ge with shallow acceptors at the 10^{15} cm^{-3} level has little effect on the lifetime of photoexcited carriers for temperature and excitation conditions at which electron-hole drops are not formed.[8,9] Both FE and BE are observed in the luminescence spectrum of Ge under these conditions and both decay with the lifetime of the FE in undoped Ge. Thus, it appears that Auger transitions for the BE in Ge are slow processes.

In this paper, we present calculations of the BE Auger rates for the common shallow acceptors in Si and Ge. The purpose of the calculation is to understand the strong dependence of the Auger rate on acceptor type in Si and the qualitatively different effect doping with shallow acceptors has on the lifetime of photoexcited carriers in Si and Ge. The result of the calculation shows the observed dependence of the BE lifetime on acceptor type in Si and is within about a factor of 3 of the measured lifetime in absolute value. The computed BE Auger rates in Ge are found to be much slower than the measured free-exciton lifetime in Ge. The impor-

tant difference in the two materials is that the holes are much more strongly bound to the acceptors in Si than they are in Ge.

The paper is organized in the following way: the qualitative physics of the Auger transition is discussed in Sec. II. In Sec. III, the calculation is presented, and the result of the calculation is compared with experiment. Our conclusions are given in Sec. IV. Calculational details are included in Appendix A. Appendix B contains a calculation of BE no-phonon oscillator strengths used to test the BE wave function used in the Auger calculation.

II. QUALITATIVE PHYSICS OF THE AUGER TRANSITIONS

In their work on GaP, Dean and co-workers argued that the dependence of acceptor BE lifetimes on acceptor type could be understood as due to an increased localization (hence, an increased spreading in K space) of the hole wave function in the BE for the more tightly bound acceptors.[2] (They did not, however, present quantitative calculations of the BE Auger rates to support their arguments.) We believe that the physical picture they suggest also applies to Si and can be used to understand the qualitatively different effect of doping with shallow acceptors on carrier lifetimes in photoexcited Si and Ge.

In the acceptor BE (initial state of the Auger transition) there are two holes near the valence-band maximum and an electron near the conduction-band minimum. The final state of the acceptor BE Auger transition has one hole in the valence band. The holes in the BE are spread in K space because they are localized about the acceptor. The electron state will also be spread in K space, but the spreading will be small compared to that of the holes because the electron is not localized as much as the holes. The wave vector of the final-state hole lies on a constant energy surface as required by energy conservation in the transition. Carrier-carrier scattering, which conserves total wave vector, is the dominant interaction responsible for an Auger transition. Thus, for the Auger transition to take place, the initial BE state must have an amplitude to contain wave vectors which are accessible to the final-state hole. The conduction-band minimum is rather far in K space from the constant energy surface of the final-state hole. Since the BE wave function is peaked at the conduction-band minimum, spreading of the BE wave function in K space is essential for the Auger transition to occur. In Si, the holes in the acceptor BE are well localized, resulting in large hole wave function spreading and fast Auger rates. The dependence on acceptor type occurs because the acceptors with larger binding energy bind the holes in the BE more tightly leading to faster Auger rates. In Ge, the holes in the acceptor BE are not tightly bound, so that the hole wave-function spreading is small and the Auger rates are slow.

In principle, the Auger transition could be phonon assisted. In contrast to the phononless Auger transition, an Auger transition involving a phonon should not be sensitive to the wave-function spreading in the BE because the phonon would make up the difference in wave vector between the peak in K space of the BE wave function and the final-state hole. As a result the phonon-assisted Auger transition rate should be insensitive to the acceptor type. Since the observed BE lifetimes in Si are, in fact, very sensitive to the acceptor type, the acceptor BE Auger transitions in Si most likely occur without phonon assistance. In Ge, it is very difficult to know whether the phonon-assisted or no-phonon Auger transition is more likely. Experimentally, neither process appears to be important. We will show that the no-phonon Auger process (which dominates in Si) is slow in Ge.

In order to compute the BE Auger rate, it is necessary to know the BE wave function. It is very difficult to compute this wave function accurately, and we use an idealized model. In particular, we describe the interaction of the holes with the charged acceptor by a Coulomb potential and a short-range square well. For Si:Al and Ge:Ga (the impurity has the same core structure as the host) the strength of the short-range well was taken to be due only to the wave-vector dependence of the dielectric function. For the other impurities, it was adjusted to produce the observed acceptor binding energies for a simple hydrogenic model of the acceptor. In order to check the approximate validity of the model BE wave function, we used it to compute no-phonon oscillator strengths for BE absorption. For Si:Al, Si:Ga, and Si:In the results are within a factor of 2 of the measured values.[10] For Si:B, the computed oscillator strength is about a factor of 4 too large. We readjusted the strength of the square wells so as to give wave functions which produce the measured oscillator strengths. This procedure is appropriate because both the no-phonon oscillator strength and the Auger transition rate depend sensitively on the extent of K-space spreading of the hole wave function and hence on the strength of the short-range potential. In contrast, the acceptor binding energy is not as strongly dependent on the strength of the short-range potential. For Ge, the computed oscillator strengths were so small that they are probably not observable. This is consistent with the lack of no-phonon BE optical transitions for Ge doped with acceptors, but is not of much help in the Auger rate calculations.

III. CALCULATION OF AUGER TRANSITION RATES

From time-dependent perturbation theory, the BE Auger transition rate is given by

$$\frac{1}{\tau} = \frac{2\pi}{\hbar} \sum_{F;\text{all}\,I} |\langle F|H|I\rangle|^2 \delta(E_I - E_F) \,. \tag{1}$$

Here $|F\rangle$ is the final state which consists of a free hole, $|I\rangle$ is the BE initial state, and H is the Hamiltonian for the solid. (The states $|I\rangle$ and $|F\rangle$ are only approximate eigenstates of H.) The BE wave function has the form

$$|I\rangle = \sum_{k_h, k_h', k_e, m_1 m_2} A^{JM}_{m_1 m_2}(k_h, k_h', k_e)\, \Psi(k_h m_1; k_h' m_2; k_e \sigma_e), \tag{2}$$

where $\Psi(k_h m_1; k_h' m_2; k_e \sigma_e)$ is a Slater determinant with the valence-band states $(k_h m_1)$ and $(k_h' m_2)$ empty and the conduction-band state $(k_e \sigma_e)$ occupied. Here m_1 and m_2 label the four hole bands degenerate at the valence-band maximum and σ_e labels the electron spin. For simplicity, we neglect valley orbit-splitting effects in the BE and restrict the electron to a particular conduction-band minimum. $A^{JM}_{m_1 m_2}$ is the amplitude that a particular determinant is contained in the BE wave function; J is the total hole spin (2 or 0) with projection M along the Z axis. The final state is

$$|F\rangle = \Psi(k_f \sigma_f) \,, \tag{3}$$

where $\Psi(k_f \sigma_f)$ is a Slater determinant with the valence-band state $(k_f \sigma_f)$ empty and σ_f is the final-state hole spin. (We neglect spin-orbit splitting in the final state and the hole band index is included with σ_f.)

Using the wave functions given by Eqs. (2) and (3), the transition-matrix element becomes[11]

$$\begin{aligned}\langle F|H|I\rangle = \sum_{k_e k_h k_h' m_1 m_2} & A^{JM}_{m_1 m_2}(k_h, k_h', k_e) \\ & \times (\langle \phi_{k_h m_1}; \phi_{k_h' m_2}|V_{ee}|\phi_{k_f \sigma_f} \phi_{k_e \sigma_e}\rangle \\ & - \langle \phi_{k_h' m_2}; \phi_{k_h m_1}|V_{ee}|\phi_{k_f \sigma_f} \phi_{k_e \sigma_e}\rangle),\end{aligned} \tag{4}$$

where ϕ is a one-electron Bloch function and V_{ee} is the Coulomb interaction. The two-electron matrix elements in Eq. (4) can be written

$$\begin{aligned}\langle \phi_{k_h m_1}; \phi_{k_h' m_2}|V_{ee}|\phi_{k_f \sigma_f} \phi_{k_e \sigma_e}\rangle \\ = \sum_{GG'} U_{k_h m_1; k_f \sigma_f}(G)\, U_{k_h' m_2; k_e \sigma_e}(G') \\ \times \frac{e^2 (2\pi)^3 \delta(\vec{k}_f + \vec{k}_e - \vec{k}_h - \vec{k}_h' + \vec{G} - \vec{G}')}{\epsilon(\vec{k}_f - \vec{k}_h + \vec{G})|\vec{k}_f - \vec{k}_h + \vec{G}|^2} \,.\end{aligned} \tag{5}$$

Here ϵ is the dielectric function, G and G' are reciprocal-lattice vectors, and

$$U_{k_h m; k_0 \sigma_0}(G) = \frac{1}{\Omega} \int d^3r\, e^{-i\vec{G}\cdot\vec{r}}\, u_{k_h m}(r) u^*_{k_0 \sigma_0}(r) \,, \tag{6}$$

where u is the periodic part of the Bloch function and Ω is the sample volume.

The maximum contribution to the matrix element comes from terms with $G = 0$ so that the denominator can be small. The δ function in Eq. (5) requires that

$$\vec{k}_f + \vec{k}_e - \vec{k}_h - \vec{k}_h' + \vec{G}' = 0 \tag{7}$$

for $G = 0$. The amplitude function, A, will be peaked at $\vec{k}_h - \vec{k}_h' = 0$ and $\vec{k}_e - \vec{k}_{e0}$ where k_{e0} is the conduction-band minimum. The wave vector $\vec{k}_f$ lies on a constant energy surface. For Si, $\vec{k}_{e0}$ is about 82% of the way out in the Brillouin zone in the [100] direction[12] and k_f is approximately 25% of the way out in the zone with the value varying somewhat with the direction of $\vec{k}_f$. Under these conditions, the most important term in the sum over $\vec{G}'$ will be with $\vec{G}' = 0$. For Ge, $\vec{k}_{e0}$ is at the zone edge in the [111] direction so that there is a nonzero $\vec{G}'$ that puts $\vec{k}_{e0} + \vec{G}'$ at the zone edge in the $[\bar{1}\bar{1}\bar{1}]$ direction. Both this term and the one with $\vec{G}' = 0$ will be significant in the sum on $\vec{G}'$. These two terms are important for different values of k_f so there is no interference between them, and they give the same contribution to the Auger rate. Thus, we evaluate the contribution to one of the terms and multiply this by a factor of 2. (Since our conclusion will be that the BE Auger rate in Ge is several orders of magnitude smaller than the measured free-exciton lifetime, this factor of 2 is not important.) Thus, for Si and Ge we need only consider the term $\vec{G} = \vec{G}' = 0$ in Eq. (5).

The wave-function amplitude function is taken to have the form

$$A^{JM}_{m_1 m_2}(k_h, k_h', k_e) = C^{JM}_{m_1 m_2} f_h(k_h) f_h(k_h') f_e(k_e) \,, \tag{8}$$

where the coefficients C are chosen to give wave functions that are eigenstates of the total spin of the two holes. In particular, we have

$$C^{22}_{\frac{3}{2}\frac{1}{2}} = C^{21}_{\frac{3}{2}-\frac{1}{2}} = C^{2-1}_{\frac{1}{2}-\frac{1}{2}} = C^{2-2}_{\frac{1}{2}-\frac{1}{2}} = 1 \tag{9a}$$

and

$$C^{20}_{\frac{3}{2}-\frac{1}{2}} = C^{20}_{\frac{1}{2}-\frac{1}{2}} = C^{00}_{\frac{3}{2}-\frac{1}{2}} = -C^{00}_{\frac{1}{2}-\frac{1}{2}} = \frac{1}{\sqrt{2}} \tag{9b}$$

and all others are zero. The BE wave function is properly normalized so long as the one-electron functions f_h and f_e are. Using this notation, Eq. (4) becomes

$$\langle F|H|I\rangle = \sum_{k_h k_f k_e m_1 m_2} f_h(\vec{k}_h) f_h(\vec{k}_h') f_e(\vec{k}_e) U_{k_h m_1 : k_f \sigma_f} U_{k_h m_2 : k_e \sigma_e} \frac{e^2(2\pi)^3 \delta(\vec{k}_f + \vec{k}_e - \vec{k}_h - \vec{k}_h')}{\epsilon(\vec{k}_f - \vec{k}_h)|\vec{k}_f - \vec{k}_h|^2} (C^{JM}_{m_1 m_2} - C^{JM}_{m_2 m_1}) . \quad (10)$$

We next consider the overlap integrals U. Both k_f and k_h are toward the zone center and in the upper valence band. From the $\vec{k}\cdot\vec{p}$ calculations of Cardona and Pollak,[13] we see that overlap integrals of the form $U_{k_h m_1 : k_f \sigma_f}$ are not strongly dependent on the magnitude of $\vec{k}_f$ or $\vec{k}_h$ in Si and Ge, and we make the approximation

$$U_{k_h m_1 : k_f \sigma_f} \approx \lim_{k_f \to 0} U_{0 m_1 : k_f \sigma_f} . \quad (11)$$

The value depends on m_1, σ_f, and the final-state hole band index b_f. An analogous approximation cannot be used for $U_{k_h' m_2 : k_e \sigma_e}$ in Si because it is zero at $\vec{k}_h' = 0$ and $\vec{k}_e = \vec{k}_{e0}$. Since the spreading in K-space of the holes in the BE is much greater than that for the electron, we set $\vec{k}_e = \vec{k}_{e0}$ and expand in $\vec{k}\cdot\vec{p}$ perturbation theory for k_h' away from the zone center. Using the $\vec{k}\cdot\vec{p}$ perturbation theory, the periodic part of the hole Bloch function is

$$u_{k_h' m_2}(r) = u_{0 m_2}(r) + \frac{\hbar}{m} \sum_{b\sigma''} u_{0 b\sigma''}(r) \times \frac{\langle u_{0 b\sigma''} | \vec{k}_h' \cdot \vec{p} | u_{0 m_2} \rangle}{E_0 - E_b} , \quad (12)$$

where b labels bands and σ' spins. Then we have

$$U_{k_h' m_2 : k_e \sigma_e} \approx \vec{k}_h' \cdot \vec{M}_{0 m_2 : k_{e0} \sigma_e} , \quad (13a)$$

where

$$\vec{M}_{0 m_2 : k_{e0} \sigma_e} = \frac{\hbar}{m} \sum_{b\sigma''} U_{0 b\sigma'' : k_{e0} \sigma_e} \frac{\langle u_{0 b\sigma''} | \vec{p} | u_{0 m_2} \rangle}{E_0 - E_b} . \quad (13b)$$

The only band which makes a significant contribution to the sum in Eq. (13b) for Si is the Γ_{15} conduction band. If $\vec{k}_{e0}$ is taken to define the Z direction, the Z component of $\vec{M}$ is zero.

In Ge, $U_{0 m_2 : k_{e0} \sigma_e}$ is not zero as it is in Si. However, the $\vec{k}\cdot\vec{p}$ calculations of Cardona and Pollak[13] show that this overlap integral is small. We have computed the Auger rates in Ge both approximating $U_{k_h m_2 : k_e \sigma_e}$ by $U_{0 m_2 : k_{e0} \sigma_e}$ and using the $\vec{k}\cdot\vec{p}$ expansion similar to Si (that is, setting $U_{0 m_2 : k_{e0} \sigma_e}$ equal to zero). The second result gave almost an order of magnitude larger Auger rates. It is the one we report.[14] For Ge, the Γ_2' conduction band makes the dominant contribution to the sum in Eq. (13b).

With these approximations, the transition-matrix element becomes

$$\langle F|H|I\rangle = \sum_{m_1 m_2} (C^{JM}_{m_1 m_2} - C^{JM}_{m_2 m_1}) \times U_{0 m_1 : k_f \sigma_f} \vec{M}_{0 m_2 : k_{e0} \sigma_e} \cdot \vec{\beta}(\vec{k}_f) , \quad (14a)$$

where

$$\vec{\beta}(\vec{k}_f) = \left(\frac{1}{2\pi}\right)^3 \frac{1}{2\pi^2} \int d^3k_h d^3k_h' f_h(\vec{k}_h) f_h(\vec{k}_h') \times f_e(\vec{k}_h + \vec{k}_h' - \vec{k}_f) \times \frac{e^2 \vec{k}_h'}{\epsilon(\vec{k}_h - \vec{k}_f)|\vec{k}_h - \vec{k}_f|^2} . \quad (14b)$$

To obtain the transition rate, the matrix element is squared, averaged over the initial BE states and summed over final states. The most important final hole states are in the two upper valence bands; these two bands are degenerate in the [100] and [111] directions. We include only these two bands in the summation and neglect the fact that they are not degenerate in all directions.[15] The remaining summations on discrete indices can be performed in a straightforward but tedious way. The result becomes

$$1/\tau = |D|^2 B , \quad (15a)$$

where

$$|D|^2 = [2](\tfrac{2}{3})^2 |\langle u_\Gamma | u_c \rangle|^2 \left(\frac{\hbar}{m}\right)^2 \frac{|\langle u_\Gamma | p_x | u_{\Gamma 25'} \rangle|^2}{(E_\Gamma)^2} \quad (15b)$$

and

$$B = \frac{2\pi}{\hbar} \frac{1}{(2\pi)^3} \int d^3k_f \beta_x^2(\vec{k}_f) \delta(E_I - E_F) . \quad (15c)$$

The factor of 2 in square brackets is to be included for Ge but not for Si. In Eq. (15), Γ refers to the Γ_{15} conduction-band state for Si and the Γ_2' conduction-band state for Ge; c refers to the conduction-band minimum (Δ_1 in Si and L_1 in Ge) and p_x is the x component of the momentum operator. (The minimum of the conduction band is taken to define the Z axis; the x and y components which appear in the product $\vec{M}\cdot\vec{\beta}$ give equal contributions to the transition rate.)

To evaluate $\vec{\beta}(\vec{k}_f)$, it is necessary to obtain the envelope functions $f_h(\vec{k}_f)$ and $f_e(\vec{k}_e)$. As a first approximation, we use effective-mass theory with a simplified model for the band structure. The electron effective mass is taken to be spherical with a value[16]

$$1/m_e = \tfrac{1}{3}(2/m_t + 1/m_e) , \quad (16)$$

where m_t is the transverse electron effective mass and m_e is the longitudinal electron effective mass. The interaction between the holes and the charged acceptor is taken to be a Coulomb part, screened by the static dielectric function, plus a short-range square well. The radius of the square well

is taken to be the covalent radius of the host. For Si : Al and Ge :Ga (the impurity with the same core structure as the host), the square well is taken to be due only to the dielectric function. In Appendix A, we obtain an expression for the depth of square well for Si : Al and Ge : Ga based on this assumption. The hole effective mass is taken to be spherical. We chose a value for the hole effective mass by making a variational calculation for the Si : Al and Ge : Ga acceptors, using a 1s hydrogenic wave function and fitting the measured binding energy. For impurities other than Al in Si and Ga in Ge, we determine the depth of the square well by making a variational calculation for the acceptor using a 1s hydrogenic wave function and fitting the measured binding energy. The interaction between the electron and the charged acceptor was taken to be the same as for holes but with the sign changed.

As a first approximation, f_h and f_e are assumed to have a 1s hydrogenic form

$$f_h(k) = \left(\frac{\pi}{a^5}\right)^{1/2} \frac{8}{[k^2 + (1/a)^2]^2}, \tag{17a}$$

$$f_e(k) = \left(\frac{\pi}{b^5}\right)^{1/2} \frac{8}{[k^2 + (1/b)^2]^2}. \tag{17b}$$

The Bohr radii for the holes and electrons are determined from a variational calculation.

There are corrections to the effective-mass approximation for wave vectors far from the band extrema because the hole dispersion curves are not parabolic at large $\vec{k}$. We take these corrections into account by substituting the hydrogenic form into the Hartree equation for the holes in the BE

$$f_h(k) = \frac{1}{E(k) + E_B} \sum_{k'} V_{kk'} f_h^H(k'). \tag{18}$$

Here $E(k)$ is the hole dispersion curve, E_B is the one hole Hartree energy, f_h^H is the hydrogenic form for the hole wave function [Eq. (17a)] and V is the Hartree potential seen by the hole computed taking the hydrogenic forms for the envelope function

$$V(r) = \frac{-e^2}{\epsilon(0) r} + \frac{e^2}{\epsilon(0)} \times \int \frac{|f_h^H(r')|^2}{|r - r'|} d^3r' \frac{-e^2}{\epsilon(0)} \times \int \frac{|f_e^H(r')|^2}{|r - \cdot|} d^3r' \frac{-4\pi}{3} V_0 R^3 \delta(r). \tag{19}$$

Here the short-range square well of radius R and depth V_0 has been replaced by a δ function for convenience. (The Fourier transform of the square well is effectively constant for the range of wave vectors of interest.) Evaluating the integrals using the hydrogenic functions and using the fact that the hole Bohr radius is much smaller than the electron Bohr radius gives

$$V(r) \simeq \frac{-e^2}{\epsilon(0)} e^{-2r/a} \left(\frac{1}{r} + \frac{1}{a}\right) \frac{-4\pi}{3} V_0 R^3 \delta(r). \tag{20}$$

Using this form for the potential, the iterated wave function is

$$f_h(k) = \frac{e^2}{\epsilon(0)} \frac{4\pi}{(\pi a^5)^{1/2}} \frac{1}{E(k) + E_B} \times \left(\frac{1}{k^2 + 9/a^2} + \frac{6}{a^2(k^2 + 9/a^2)^2} + \frac{V_0 R^3}{6e^2/\epsilon(0)}\right). \tag{21}$$

Although this function appears to be quite different than the hydrogenic form, they are numerically rather close at small $\vec{k}$. At large $\vec{k}$, where both functions are small, the iterated functions dies off more slowly with increasing $\vec{k}$ than the hydrogenic form. We compare the two functions for $\vec{k}$ in the [111] direction for Si : Ga in Fig. 1.[17] (Si : Ga represents a case with an intermediate value for the strength of the short range potential. The [111] direction is the one of greatest interest because the hole dispersion curves for Si and Ge drop off most slowly in this direction so that the hole wave function is spread most effectively in this direction.) In the calculations of Auger rates and no-phonon oscillator strengths, we will only need the

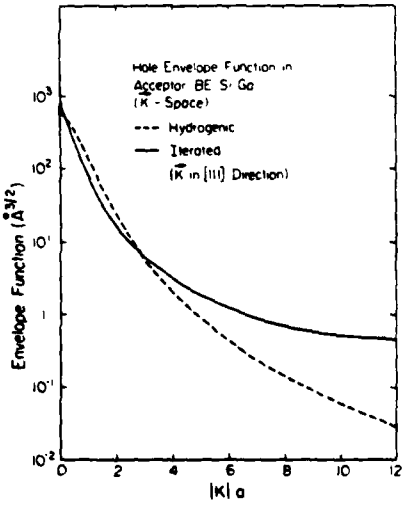

FIG. 1. Hole envelope function for the BE in Si:Ga vs wave vector in units of the hole Bohr radius. The dashed line is the hydrogenic form for the envelope function [see Eq. (17a)] and the solid line is the iterated form [see Eq. (21)]. The wave vector is in the [111] direction; $|K|a = 12$ corresponds to the zone edge.

TABLE I. No-phonon oscillator strengths for acceptor BE in Si.

	Measured	Calculated
Si : B	$\sim 2 \times 10^{-6}$ [a,b]	8.7×10^{-6}
Si : Al	7×10^{-6} [a]	3.5×10^{-6}
Si : Ga	1×10^{-6} [a]	9.0×10^{-6}
Si : In	9×10^{-6} [a]	9.3×10^{-5}

[a] Reference 10.

[b] Estimated from the measured TO-phonon oscillator strength of Ref. 10 and the ratio of TO to no-phonon emission intensity given by R. Sauer and J. Weber [Phys. Rev. Lett. 36, 48 (1976)].

iterated form of the hole wave function in the tail region.

In order to test the validity of the BE wave function, we have used this function to compute no-phonon oscillator strengths for acceptor BE in Si and Ge. The details of this calculation are given in Appendix B. In Ge, the acceptor BE no-phonon optical transitions are too weak to observe.[18] Our calculation produces very small oscillator strengths[19]; this is consistent with experiment, but not very helpful. In Si, the acceptor BE no-phonon oscillator strengths have been measured.[10] In Table I, we list the measured oscillator strengths and the computed values for Si. For Si : Al, Si : Ga and Si : In, the results are within about a factor of 2 of the measured values; for Si : B, the calculated oscillator strength is about a factor of 4 too large. Si : B is different than the other cases because the square-well potential is repulsive for holes in this case. The binding energy for the acceptor is not very sensitive to the strength of this potential; the no-phonon oscillator strength is rather sensitive to it. In addition, the no-phonon oscillator strength is sensitive to the tail (in k space) of the hole wave function in much the same way as the Auger transition rate. We adjust the depth of the square-well potential to produce the measured oscillator strength. This adjustment is most significant for Si : B, if we had not made the adjustment, the calculated Auger rate for Si : B would be about a factor of 3 larger than that which we report.

In Table II, we list the square-well parameters and resulting Bohr radii determined by the acceptor binding energy and by the no-phonon oscillator strengths. We also list the acceptor binding energies produced by the square wells determined by the no-phonon oscillator strengths. In Si : B, the strength of the repulsive square well is reduced to produce the measured oscillator strengths, and as a result the corresponding acceptor binding energy is greater than the measured value.

With the approximate expressions for the envelope functions, f_h and f_{e0}, we can perform the integral in Eq. (14b). First, we note that the function f_e is much more sharply peaked than the other function (the electron Bohr radius is large) and replace it by a normalized δ function,

$$f_e(\vec{k}_e) = [(2\pi)^3/(\pi b^3)^{1/2}]\delta(\vec{k}_e - \vec{k}_{e0}) . \tag{22}$$

Then we have

$$\tilde{\beta}(\vec{k}_f) = \frac{1}{2\pi^2} e^2 \frac{1}{(\pi b^3)^{1/2}} \int d^3k_h \frac{f_h(\vec{k}_h) f_h(\vec{k}_{e0} + \vec{k}_f - \vec{k}_h)(\vec{k}_f + \vec{k}_{e0} - \vec{k}_h)}{\epsilon(\vec{k}_h - \vec{k}_f)\,|\vec{k}_h - \vec{k}_f|^2} . \tag{23}$$

The calculation would still be very lengthy if it was done without further simplicifation because both the integration in $\tilde{\beta}(\vec{k}_f)$ and the final-state integration $\vec{k}_f$ involve evaluation of valence-band energies at every point. We have examined the integration in Eq. (23) numerically and found that nearly all the contribution to the integral comes from the region near $\vec{k}_h = 0$. This occurs because the function $f_h(\vec{k}_h)$ is peaked at $\vec{k}_h = 0$. There is no corresponding contribution at $(\vec{k}_{e0} + \vec{k}_f = \vec{k}_h)$ because

TABLE II. Square-well parameters and Bohr radii for acceptor BE in Si. The diameter of the square well is taken as the covalent radius of Si (1.11 Å). The unprimed numbers are determined by fitting acceptor binding energies and the primed numbers are determined by fitting no-phonon oscillator strengths.

	V_0R^3 (eV Å^3)	E_A (meV)	a (Å)	b (Å)	$V_0'R^3$ (eV Å^3)	E_A' (meV)	a' (Å)	b' (Å)
Si : B	−27.1	46	18.7	51.5	−12.0	53	16.4	48.2
Si : Al	2.8	67	13.0	43.3	4.9	70	12.4	42.5
Si : Ga	5.7	71	12.2	42.1	6.2	72	12.0	41.9
Si : In	14.8	154	7.7	34.9	14.8	154	7.7	34.9

of the factor $(\vec{k}_f + \vec{k}_{e0} - \vec{k}_h)$ and because the denominator $|\vec{k}_h - \vec{k}_f|^2$ is large in this region. As long as $a|\vec{k}_{e0} + \vec{k}_f|$ is much larger than unity, the integral in Eq. (23) is that of a sharply peaked function times a smoothly varying one in the region which contributes. In this case, the sharply peaked function can be reasonably approximated by a normalized δ function. Since we are only concerned with the part of $f_h(\vec{k}_h)$ where the function is large (i.e., near $\vec{k}_h \approx 0$) we use the hydrogenic form to determine the normalization.

$$f_h(k_h) \approx [(2\pi)^3/(\pi a^3)^{1/2}]\delta(\vec{k}_h) . \tag{24}$$

To check the validity of this approximation, we have used it for the integral with $f_h(\vec{k}_{e0} + \vec{k}_f - \vec{k}_h)$ being hydrogenic. For the hole Bohr radius parameters used here the approximate result was within 50% of the exact value determined by numerical integration for all cases except Si : In. For Si : In the approximate result was within a factor of 2 of the exact result. When Eq. (21) is used for $f_h(\vec{k}_{e0} + \vec{k}_f - \vec{k}_h)$, the approximation should be better than for the hydrogenic form because $f_h(\vec{k}_{e0} + \vec{k}_f - \vec{k}_h)$ is more slowly varying near $\vec{k}_h = 0$ in this case. With this approximation, we have

$$\vec{\beta}(\vec{k}_f) = \left(\frac{e^2}{2\epsilon(0)a}\right)^2 \frac{64\sqrt{\pi a}}{ak_f} \left(\frac{a}{b}\right)^{3/2} (\vec{k}_{e0} + \vec{k}_f) \frac{1}{E(\vec{k}_{e0} + \vec{k}_f) + E_B} \frac{\epsilon(0)}{\epsilon(\vec{k}_h - \vec{k}_f)}$$
$$\times \left(\frac{1}{|\vec{k}_{e0} + \vec{k}_f|^2 a^2 + 9} + \frac{6}{(|\vec{k}_{e0} + \vec{k}_f|^2 a^2 + 9)^2} + \frac{V_0 R^3}{6[e^2/2\epsilon(0)a]a^3}\right) \tag{25}$$

Here E_B is negligible compared to $E(\vec{k}_{e0} + \vec{k}_f)$; thus, it plays no role in the calculation of Auger rates.

The final-state integral in Eq. (15c) is performed numerically. The valence-band structure was obtained from a tight-binding band-structure calculation using essentially the parameters of Chadi and Cohen.[20] We have changed the second-nearest-neighbor interaction parameter (u_{zz} in the notation of Ref. 20) by 0.21 eV in Si and 0.16 eV in Ge in order to produce the known energies at the L_3 valence-band points.[21] It is desirable to get this point as accurately as possible because the largest contribution to the density of final hole states for the Auger transition in Si and Ge come with $\vec{k}$ in the [111] directions. In Table III, we list parameters used in the calculation.

In Fig. 2 we show the result of the calculation for Si along with experimental bound-exciton lifetimes for the four common shallow acceptors.[3,22] The calculated lifetimes show the same dependence on acceptor type as the observed lifetimes and have numerical values that differ by about a factor of 3 from the experimental lifetimes. Considering the simplified BE wave functions used in the calculation, we consider this agreement between the calculated Auger rates and measured lifetimes to be quite reasonable. The results indicate that the BE lifetimes are limited by phononless Auger transitions for acceptors in Si.

In Ge, it is difficult to determine the appropriate square-well parameters because the no-phonon acceptor BE oscillator strengths are so weak that these optical transitions have not been observed. In addition, the acceptor binding energies for the different acceptors are nearly the same in Ge, and they are not very sensitive to a short-range potential (due to the large Bohr radii of the acceptors in Ge). In Fig. 3, we plot calculated Auger rates for acceptor BE in Ge versus the square-well parameter V_0R^3. In the lower panel of the figure, we show the electron and hole Bohr radii. The range of the square-well parameter shown in the figure is over four times that used for Si : In. (The binding energy of the Ge : In acceptor is produced by a well parameter of 37 eV Å^3.) Over the entire range of the square-well parameters, the calculated Auger rate is almost two order of magnitude (or more) slower than the measured FE recombination rate in Ge. (The measured FE lifetime in undoped Ge is about 8 μsec.[23]) Since it seems unreasonable that the appropriate square-well depth for the shallow acceptors in Ge should be many times larger than that for Si : In, the calculation indicates that the phononless Auger rate for acceptor BE in Ge is too slow to significantly

TABLE III. Parameters used in the calculation. All symbols are defined in the text.

	Si	Ge
R	1.11 Å	1.22 Å
m_e	$0.26m$	$0.12m$
m_h	$0.60m$	$0.19m$
$\langle u_\Gamma \vert u_C \rangle$	0.8 [a]	0.6 [a]
$\vert\langle u_\Gamma \vert P_x \vert u_{\Gamma_{25'}}\rangle\vert$	0.53 a.u. [a]	0.68 a.u. [a]
E_Γ	3.4 eV [a]	1.0 eV [a]
$\vert\langle u_{\Delta_5} \vert P_y \vert u_{\Delta_1}\rangle\vert$	0.57 a.u. [a]	...
$\vert\langle u_{\Delta_2} \vert P_y \vert u_{\Delta_1}\rangle\vert$	...	0.65 a.u. [a]

[a] Reference 13.

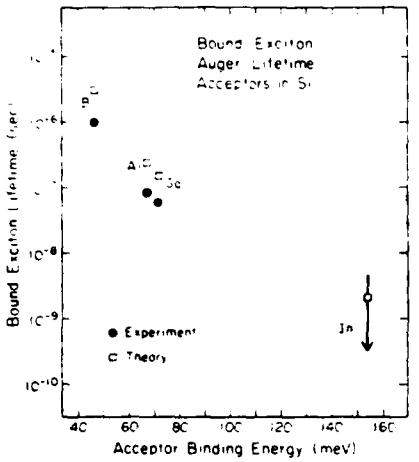

FIG. 2. Bound-exciton lifetimes vs impurity binding energy for the four common acceptors in Si. The hollow squares are our calculations of the Auger lifetime and the solid circles are the measure values from Ref. 3. Only an upper bound of 5 *nsec* (indicated by the top of the arrow) was set on the BE lifetime for Si:In in Ref. 3.

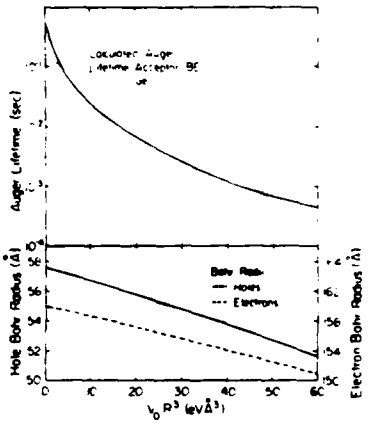

FIG. 3. Calculated Auger lifetimes for acceptor BE in Ge vs the square-well parameter V_0R^3. The range of square-well parameter is over four times that appropriate for Si:In. Even for this unrealistically large value, the calculated no-phonon Auger lifetime is almost two orders of magnitude greater than the measured FE lifetime in Ge indicating that the phononless Auger transition is not an important process for acceptor BE in Ge. In the lower panel, the hole and electron Bohr radii are shown.

influence the BE lifetime.[24] The slow Auger rates in Ge follow from the large Bohr radii.

IV. SUMMARY AND CONCLUSION

We have presented a calculation of phononless Auger transition rates for excitons bound to shallow acceptors in Si and Ge. We used a simplified model for the BE wave function and did not expect to produce numerically precise results (It would be a very formidable task to calculate a high-precision BE wave function. It would be necessary to include the degenerate valence-band structure, conduction-band anisotropies, and a realistic impurity-carrier potential in a three-body problem.) The purpose of the calculation was to understand the very large (almost three orders of magnitude) dependence of acceptor BE lifetimes observed in Si,[3] and the fact that shallow acceptors do not significantly effect the lifetime of photoexcited carriers in Ge at low temperature[9] (qualitatively different behavior than in Si). These are large effects and qualitative differences which can be accounted for in an approximate calculation.

The results of the calculation produced the strong dependence of the Auger rate on acceptor type for BE in Si. The calculated results deviated from the measured BE lifetimes by about a factor of 3. For Ge, the calculation gave Auger rates at least two orders of magnitude slower than the observed FE recombination rate in undoped Ge. We conclude that phononless Auger transitions limit the acceptor BE lifetime in Si, but are ineffective in Ge. The principal difference between the two materials is that the holes are much more tightly bound to the charged acceptor in Si than in Ge. Because the holes are more tightly bound in the Si BE, the hole wave function is more strongly spread in K space and the Auger rates are faster. This effect enters the calculation primarily through the hole Bohr radii which are much smaller in Si than in Ge. The increased spreading in K space for more tightly bound acceptors also accounts for the dependence of the Auger rate on acceptor type observed in Si.

ACKNOWLEDGMENTS

We thank S. A. Lyon, M. Chen, K. R. Elliott, D. S. Pan, J. N. Schulman, and T. C. McGill for valuable discussion on subjects related to this work. We thank P. J. Dean for drawing our attention to Ref. 2.

APPENDIX A: DIELECTRIC-FUNCTION CONTRIBUTION TO SHORT-RANGE POTENTIAL

In this appendix, we estimate the contribution to the short-range potential due to the frequency dependence of the dielectric function. We set the integrated value of the short-range potential equal to that for a square well,

$$\frac{4\pi}{3}V_0R^3 = \int V_s(r)\,d^3r = V_s(q=0)\,. \tag{26}$$

For the short-range potential, we take

$$V_s(q) = (4\pi e^2/q^2)[1/\epsilon(q) - 1/\epsilon(0)]. \quad (27)$$

We use the form of $\epsilon(q)$ suggested by Nara and Morita[25] for Si; this gives 2.83 eV Å for V_0R^3.

For Ge, we use the same form for the dielectric function as in Si, but replace $\epsilon(0)$ with the measured value for Ge, 15.36. This form is a reasonable parametrization of the dielectric function calculation in Ge by Brust.[26] For Ge, we have $V_0R^3 = 2.89$ eV Å^3.

APPENDIX B NO-PHONON OSCILLATOR STRENGTHS

In this appendix, we use the BE wave function to compute the no-phonon oscillator strengths for acceptor BE. The oscillator strength is defined as

$$f = (2/\hbar\omega m)|\langle I|P_y|F\rangle|^2. \quad (28)$$

Here $|F\rangle$ is the final-state acceptor BE, $|I\rangle$ is the initial-state acceptor, P is the momentum operator, and $\hbar\omega$ is the photon energy required in the optical transition; Eq. (28) is to be averaged over the initial acceptor states and summed over the final BE states. Using the BE wave function in Eq. (8) and an acceptor wave function of the form

$$|I\rangle = \sum_{\vec{k}} F_m(k)\Psi(km). \quad (29)$$

The matrix element can be written

$$\langle I|P_y|F\rangle = \sum_{\vec{k}_h\vec{k}_h'} \sum_{m_1m_2\sigma_e} f_h(\vec{k}_h) f_h(\vec{k}_h') f_e(\vec{k}_h) F_{m_2}(\vec{k}_h') \langle u_{\vec{k}_h m_1}|P_y|u_{\vec{k}_h\sigma_e}\rangle (C^{JM}_{m_1m_2} - C^{JM}_{m_2m_1}). \quad (30)$$

Here $u_{\vec{k}_h\sigma_e}$ is the periodic part of the electron Bloch function and $u_{\vec{k}_h m_1}$ is the periodic part of the hole Bloch function. We assume that the acceptor envelope function $F(\vec{k}_h')$ does not depend on the hole spin state m_2 and that near $\vec{k}_h = 0$ where $F(\vec{k}_h)$ and $f_h(\vec{k}_h)$ are large, they may be reasonably approximated by hydrogenic functions with Bohr radii a_A and a, respectively. In this case we have

$$\sum_{\vec{k}_h} f_h(\vec{k}_h')F_{m_2}(\vec{k}_h') = \frac{8}{(1+a_A/a)^3}\left(\frac{a_A}{a}\right)^{3/2}. \quad (31)$$

Next we use the fact that the spread of the electron envelope function in K space is very small compared to that for holes and replace $f_e(\vec{k}_h)$ with the normalized δ function given in Eq. (22). The matrix element becomes

$$\langle I|P_y|F\rangle = f_h(\vec{k}_{e0})\frac{1}{(\pi b^3)^{1/2}}\frac{8}{(1+a_A/a)^3}\left(\frac{a_A}{a}\right)^{3/2} \times \sum_{m_1m_2\sigma} \langle u_{\vec{k}_{e0}m_1}|P_y|u_{\vec{k}_{e0}\sigma_e}\rangle \times (C^{JM}_{m_1m_2} - C^{JM}_{m_2m_1}). \quad (32)$$

The spin sums in Eq. (32), initial-state averages, and final-state sum can be performed in a straightforward but tedious way. In Si, the result is

$$f = \frac{2}{\hbar\omega m}|\langle u_{\Delta_5}|P_y|u_{\Delta_1}\rangle|^2 \times 4\left[\frac{8}{(1+a_A/a)^3}\left(\frac{a_A}{a}\right)^{3/2}\right]^2\left(\frac{f_h(\vec{k}_{e0})}{(\pi b^3)^{1/2}}\right)^2. \quad (33)$$

Here u_{Δ_5} is the periodic part of the hole Bloch function in the Δ_5 valence band at $\vec{k}_{e0}$ and u_{Δ_1} is the periodic part of the electron Bloch function at this point. The conduction-band minimum is in the z direction (a [100] direction).

For Ge, the result is

$$f = \frac{2}{\hbar\omega m}|\langle u_{\Lambda_3}|P_y|u_{\Lambda_1}\rangle|^2 \times \frac{8}{3}\left[\frac{8}{(1+a_A/a)^3}\left(\frac{a_A}{a}\right)^{3/2}\right]^2\left|\frac{f_h(\vec{k}_{e0})}{(\pi b^3)^{1/2}}\right|^2. \quad (34)$$

Here u_{Λ_3} and u_{Λ_1} are periodic parts of the hole and electron Bloch functions at the conduction-band minimum. The conduction-band minimum is in the z direction (a [111] direction).

*Work supported in part by AFOSR under Grant No. 77-3216.

[1] D. F. Nelson, J. D. Cuthbert, P. J. Dean, and G. D. Thomas, Phys. Rev. Lett. 17, 1262 (1962).
[2] P. J. Dean, R. A. Faulkner, S. Kimura, and M. Ilegems, Phys. Rev. B 4, 1926 (1971).
[3] S. A. Lyon, G. C. Osbourn, D. L. Smith, and T. C. McGill, Solid State Commun. 23, 425 (1977).
[4] P. T. Landsberg, Phys. Status Solidi 41, 457 (1970).
[5] P. T. Landsberg and M. J. Adams, J. Lumin. 7, 3 (1973).
[6] J. D. Cuthbert, Phys. Rev. B 1, 1552 (1970).
[7] K. R. Elliott, D. L. Smith, and T. C. McGill (unpublished).
[8] M. Chen, D. L. Smith, and T. C. McGill, Phys. Rev. B 10, 4983 (1977).
[9] At temperatures and excitation conditions for which electron-hole drops are formed, the decay of the drops is slower in lightly doped Ge than in undoped Ge. This effect can be understood as due to a reduction

in the exciton diffusion away from the drops resulting in slower net evaporation of carriers [M. Chen, S. A. Lyon, K. R. Elliott, D. L. Smith, and T. C. McGill, Nuovo Cimento B 39, 622 (1977)]. At doping levels of 10^{17} cm^{-3} or greater, the luminescence spectrum of Ge at low temperatures is complicated and shows complicated decay transients (see Ref. 8); however, the decay is slower than in pure Ge. This behavior is qualitatively different than in Si.

[16]P. J. Dean, W. F. Flood, and G. Kaminsky, Phys. Rev. 163, 721 (1967).

[11]We have dropped a term in Eq. (4) which corresponds to interband scattering by the impurity potential. This term makes a negligible contribution to the Auger transition rate for two reasons: first, it depends on the small expansion of a hole orbital going from the acceptor to the BE; second, the lowest-order term in the $\vec{k}\cdot\vec{p}$ expansion [see Eq. (12)] does not contribute to this term.

[12]W. P. Dumke, Phys. Rev. 118, 938 (1960).

[13]M. Cardona and F. H. Pollak, Phys. Rev. 142, 530 (1966).

[14]In Ref. 13, $\langle u_{\Gamma_{25}} | u_{L_1} \rangle$ is found to be about 0.1; whereas, $\langle u_{\Gamma_{15}} | u_{L_1} \rangle$ is about 0.6. These overlap integrals are squared in the Auger rates. Because the overlap which appears in the first-order $\vec{k}\cdot\vec{p}$ expansion is considerably larger than that which appears in the zeroth-order term, the first-order term dominates. If these two overlap integrals were comparable, the zeroth-order term would be the more important.

[15]When performing the final state integration over k_f, we integrated over both bands and averaged the result. The integrations for the two bands differed by about 50%.

[16]W. F. Brinkman and T. M. Rice, Phys. Rev. B 7, 1508 (1973).

[17]In Fig. 1, we estimate the hole Hartree energy by the BE dissociation energy. This energy only effects the iterated wave function illustrated in Fig. 1 for $|K|a \leq 0.5$ and does not come into the actual Auger calculation at all since we use the hydrogenic form in the small-$|K|$ region.

[18]E. F. Gross, B. V. Nokikov, and N. S. Sokolov, Fiz. Tverd. Tela. 14, 443 (1972) [Sov. Phys.-Solid State 14, 368 (1972)]

[19]We compute a no-phonon oscillator strength of 2×10^{-5} for a square well parameter (V_0R^2) of 37 eV Å which produces the Ge:In acceptor binding energy. This is about an order of magnitude smaller than the weak no-phonon oscillator strength in Si:B. The calculated oscillator strengths for square-well parameters which produce the binding energies for the other acceptors in Ge are much less than that for Ge:In. The calculated no-phonon oscillator strengths in Ge are small because the hole Bohr radii are large.

[20]D. J. Chadi and M. L. Cohen, Phys. Status Solidi B 68, 405 (1975).

[21]See, for example, J. C. Phillips, Solid State Phys. 18, 55 (1966).

[22]In Ref. 3, the measured lifetime for the BE in Si:Al was reported to be 104 nsec. Following discussions with M. H. Pilkuhn and W. Schmid, the BE lifetime in Si:Al was remeasured using lower excitation intensity. The lifetime decreased slightly to 80 nsec suggesting that there was saturation of the Al impurities in the earlier measurement. Lifetimes for the other impurities showed no change (higher doping levels were used for the other impurities). [S. A. Lyon (private communication)].

[23]Ya. Pokrovskii, Phys. Status Solidi A 11, 385 (1972).

[24]Except at very low temperatures, excitons probably ionize rapidly from shallow acceptors in Ge because the dissociation energy is only about 1 meV (see Ref. 16). Thus, unless the acceptor BE has decay channels available to it (such as an Auger transition) which are rapid compared to the processes responsible for FE decay both the BE and FE densities will decay at a rate governed by the processes responsible for FE decay. At temperatures low enough that dissociation of the BE in Ge is slow compared to the FE lifetime (probably less than 2°K) photoexcited carriers in Ge form electron-hole drops.

[25]H. Nara and A. Morita, J. Phys. Soc. Jpn. 21, 1852 (1966).

[26]D. Brust, Phys. Rev. B 5, 435 (1972).

Solid-State Electronics Vol. 21, pp. 1339–1342
© Pergamon Press Ltd., 1978 Printed in Great Britain

AUGER AND RADIATIVE RECOMBINATION OF ACCEPTOR BOUND EXCITONS IN SEMICONDUCTORS

G. C. OSBOURN, S. A. LYON, K. R. ELLIOTT,
D. L. SMITH and T. C. MCGILL
California Institute of Technology, Pasadena, CA 91125, U.S.A.

Abstract—We report on a theoretical and experimental study of acceptor bound exciton recombination. We present calculations of phononless Auger and radiative recombination in direct and indirect band gap materials. We consider hydrogenic acceptors in the direct band gap material $Hg_{1-x}Cd_xTe$ in which the band gap can be varied by changing alloy composition. We present calculations of the Auger transition rate and no-phonon oscillator strengths for the common acceptors in Si and Ge. We have measured the bound exciton lifetimes and no-phonon oscillator strengths for the acceptors in Si and find reasonable agreement with the calculated values.

1. INTRODUCTION

A bound exciton (*BE*) is formed when an electron-hole pair becomes attached to a neutral acceptor or donor. Once formed the bound exciton has a number of possible decay modes available to it. Recombination can occur radiatively (with or without phonon assistance) as well as non-radiatively by an Auger transition (with or without phonon assistance)[1–8]. The relative importance of these decay mechanisms is dependent on the particular semiconductor considered. At low temperature, decay from a bound exciton state is often the principal decay route of a nonequilibrium concentration of electrons and holes. In indirect band gap materials, *BE* recombination can be dominated by the Auger transition[1–8]. Lightly doped Si is an example of an indirect material in which Auger transitions from bound exciton states provide the dominant decay mechanism for a non-equilibrium concentration of electrons and holes[3, 7, 8]. In Ge, however, small concentrations of acceptors or donors do not significantly affect the decay rate of a nonequilibrium concentration of electrons and holes[9]. In direct gap materials, radiative decay of *BE* is generally larger than Auger recombination[10]. For small band gap direct materials, however, Auger recombination can be faster than radiative decay.

To understand and compare the Auger and radiative decay mechanisms in both direct and indirect semiconductors, we calculate their transition rates for the common acceptors in Si and Ge (indirect) and for hydrogenic acceptors in $Hg_{1-x}Cd_xTe$ (direct). $Hg_{1-x}Cd_xTe$ provides a particularly interesting case because the band gap can be varied by changing the alloy composition[11]. Some of our results for Si and Ge have been previously published[3, 7, 12], and we review these results here briefly for comparison with the direct band gap case. The calculations for the direct gap material $Hg_{1-x}Cd_xTe$ have not been previously discussed.

2. QUALITATIVE PHYSICS

In the acceptor *BE*, there are 2 holes near the valence band maximum and 1 electron near the conduction band minimum. This leads to a *BE* wavefunction which is spread in k-space about a point of maximum amplitude at the conduction band minimum, with most of the spreading due to the more tightly bound holes. Because of the different points in k-space at which the *BE* wavefunction is peaked, the Auger and radiative transitions exhibit qualitatively different behavior in indirect and direct gap materials.

In indirect materials, the initial state *BE* has a total wavevector of maximum amplitude far out in the Brillouin zone. In the Auger transition, the final state is an ionized acceptor with a hole at a k-vector that lies on a surface of constant energy determined by energy conservation. The Auger transition depends on the amplitude for the *BE* to have k values that are accessible to the final state hole. Since the *BE* wavefunction peaks near the zone edge and the final state wavevector is not as far out in the zone, the Auger rate will depend sensitively on *BE* wavefunction spreading in k-space, with faster rates corresponding to larger spreading. In Si, there is a large spreading of the *BE* wavefunction because the holes are well localized about the impurity; this leads to fast Auger rates. The different acceptors in Si have significantly different binding energies, and they localize the *BE* holes by varying amounts. Increased localization leads to more k-space spreading, so that there is a rapid increase in Auger rates with increasing acceptor binding energy. In Ge, the holes in the *BE* are bound weakly to the impurity, so there is small k-space spreading and slow Auger rates. The calculated lifetimes for this transition are too slow to be important in Ge.

For radiative transitions in indirect materials, k is conserved, so that these transitions require large k-space spreading of the *BE* wavefunction or phonon assistance. Since the phononless radiative transition requires k-space spreading, it depends on acceptor type in a manner similar to the Auger transition (although less sensitively). The photon assisted radiative transitions do not depend on k-space spreading and phonon assisted oscillator strengths are nearly independent of acceptor type[13]. In Si, the relatively strong localization of the holes in the acceptor *BE* causes the no-phonon oscillator strengths to be comparable in magnitude to the phonon assisted

oscillator strengths[13]. In Ge, the holes are weakly bound to the acceptor and no-phonon optical transitions are not observed for the acceptor *BE*[9].

For direct gap materials, the *BE* wavefunction is peaked at the zone center. In the Auger transition, the final state again has a wave vector that lies on the surface of constant energy determined by conservation of energy. The Auger rate again requires k-space spreading to be significant, but the spreading required is only over a small portion of the zone for small band gap materials. The dependence on spreading leads to a dependence of the Auger rate on acceptor type with increasing rates corresponding to increasing acceptor binding energies. For a fixed acceptor, the Auger rate also depends on the size of the band gap. As the band gap decreases, the final state wavevector gets closer to the zone center, so that smaller k values in the *BE* wavefunction contribute. This provides larger amplitudes for the initial and final state k values to match up so that the Auger rate increases with decreasing gap.

For direct gap materials, radiative decay can be very fast because phonon assistance and large wavefunction spreading are not necessary. The radiative decay depends on the overlap of the electron and hole wavefunctions. This leads to a dependence of the radiative transition rate on band gap because as the gap decreases, the electron effective mass becomes smaller (from $k \cdot p$ theory) and the electron Bohr radius increases[14]. As a result, the overlap of electron and hole wavefunctions decrease as the gap decreases. In addition, the density of photon states decreases with the band gap further reducing the radiative transition rate for small gap materials.

The dependences of the Auger and radiative decay rates on band gap size cause the radiative decay to be dominant for larger gaps and the Auger decay to be dominant for smaller gaps. At some gap size a crossover will occur. We estimate this crossover gap for $Hg_{1-x}Cd_xTe$ (in which the gap can be made arbitrarily small as x gets small) with a hydrogenic acceptor and find a crossover at a gap of about 0.5 eV (or $x \approx 0.4$).

3. RESULTS AND DISCUSSION

The details of the calculation of the *BE* Auger rate for indirect materials have been previously discussed[7], and we will just state the result here. The values of the *BE* lifetime τ calculated for each acceptor in Si are presented in Fig. 1 along with the experimentally observed *BE* lifetimes. The experimental procedure used to measure the *BE* lifetime has been described elsewhere[3]. The agreement of the calculated lifetimes with experiment is reasonable (within a factor of 3 in all cases), and we conclude that the *BE* lifetimes in Si are determined by the phononless Auger transition. We have also estimated the Auger rate for Si:Tl using the measured oscillator strengths and the radiative efficiency determined by comparing the intensity of the *BE* luminescence in Si:Tl with that of Si:Al in which the radiative efficiency is known[3, 12]. We find that the Auger lifetime in Si:Tl is between 75 and 300 psec.

The calculated Auger lifetimes for acceptor *BE* in Ge are all greater than 10^{-3} sec, which is 2 orders of magnitude slower than the free exciton lifetimes[15]. We conclude that the phononless Auger transition does not determine the lifetimes in Ge. This result is consistent with the observation that light doping of Ge with shallow acceptors has little effect on the lifetimes of photoexcited carriers[9].

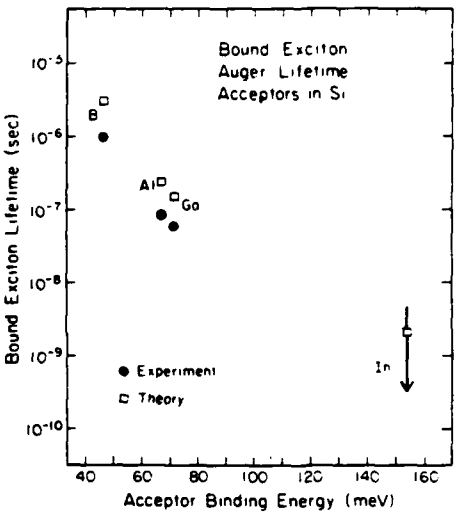

Fig. 1. Bound exciton lifetimes vs impurity binding energy for the four common acceptors in Si. The hollow squares are our calculations of the Auger lifetime and the solid circles are our measured values. In Si:In, we have only been able to set an upper bound on the measured lifetime of 5 nsec (indicated by the top of the arrow). Schmid[8] has recently found a measured lifetime of 2.7 nsec for Si:In.

The details of the calculation of the no-phonon oscillator strengths have been discussed elsewhere[7], we state the result here. In Table 1 we present the calculation results for Si and the observed results for Si. The experimental details have been presented elsewhere[12]. We also show the no-phonon radiative lifetime determined from the measured oscillator strengths[2] and the radiative efficiency of the no-phonon transition. We see that the no-phonon radiative efficiency

Table 1. No-phonon oscillator strengths and no-phonon radiative lifetimes for acceptor bound excitons in Si. The oscillator strengths are denoted by f, the lifetimes by τ and the no-phonon radiative efficiency by η; τ and η are determined by the measured f

	f measured	f calculated	τ (sec)	η
Si:B	$1\text{–}2\cdot10^{-6}$ [a]	$8.7\cdot10^{-6}$	$\sim7\cdot10^{-3}$	$\sim1\cdot10^{-4}$
Si:Al	$5\cdot10^{-6}$	$3.5\cdot10^{-6}$	$2\cdot10^{-3}$	$4\cdot10^{-5}$
Si:Ga	$7\cdot10^{-6}$	$9.0\cdot10^{-6}$	$1\cdot10^{-3}$	$4\cdot10^{-5}$
Si:In	$8\cdot10^{-5}$	$9.3\cdot10^{-5}$	$1\cdot10^{-4}$	$2\cdot10^{-5}$
Si:Tl	$4\cdot10^{-4}$	----	$2\cdot10^{-5}$	$\sim4\cdot10^{-6}$

[a] Ref. 13.

drops as the acceptor binding energy increases. The calculated results for Si agree within a factor of 2 with all the experimental results except Si:B, which is within about a factor of 4 of the observed value.

For Ge, the calculated no-phonon oscillator strengths are very small (less than 2×10^{-7} in all cases). These small oscillator strengths are due to the weak binding of the holes to the acceptor in the *BE* in Ge and are consistent with the fact that no-phonon optical transitions have not been observed for acceptor *BE* in Ge[9].

For the direct band gap case we have calculated the *BE* Auger and radiative decay rates for a hydrogenic acceptor as a function of band gap for the alloy $Hg_{1-x}Cd_xTe$, in which the band gap can be varied with composition[11]. The details of the calculations are somewhat different than the indirect gap case because the conduction band minimum is at the zone center. Here, we will concentrate on the smaller gap alloys. For these materials, the band gap is less than the energy separation between the top of the valence band and the split off valence band (~1.0 eV)[11]. As a result the split off band is not an accessible final state. In this calculation we approximate the light and heavy hole bands by a single parabolic valence band. We take the acceptor binding energy to be independent of alloy concentration for the range of x considered since this behavior has been deserved experimentally[16].

Proceeding as in the indirect band gap case, we find the Auger rate to be

$$\frac{1}{\tau} = |D|^2 \frac{e^4}{\epsilon_0^2} \frac{(32)^2}{6\pi^2 b^3 \hbar} \frac{1}{\sqrt{E_h}} \sqrt{\left(\frac{2m_h}{\hbar^2}\right)} (I(x_f))^2 \quad (1a)$$

$$|D|^2 = \left(\frac{\hbar}{m}\right)^2 \frac{|\langle u_{\Gamma_1}|P_x|u_{\Gamma_{15}}\rangle|^2}{Eg^2}. \quad (1b)$$

Here E_h is the energy of the final hole state and

$$I(x_f) = \int dx \left(\frac{1}{1+x^2}\right)^2 \left\{\frac{-1}{(x-x_f)^2+1} \frac{-1}{(x+x_f)^2+1} \frac{-1}{2xx_f} \ln\left[\frac{(x-x_f)^2+1}{(x+x_f)^2+1}\right]\right\} \quad (1c)$$

where

$$x_f = k_f a$$

and k_f is the final state hole wavevector. We determine the electron and hole Bohr radii (b and a, respectively) from a variational calculation. For the hydrogenic acceptor, the hole *BE* Bohr radius is 22 Å (independent of alloy concentrations for the small gap alloy case) and the electron *BE* Bohr radius varies with the alloy band gap from 150 to 730 Å for the range of alloy gaps 0.8–0.14 eV. Because the electron effective mass is much smaller than the hole effective mass, the hole Bohr radius is nearly that for the H^- ion, that is $a \approx (16/11)a_A$ where a_A is the acceptor Bohr radius and the electron Bohr radius is nearly that for the neutral donor. The electron effective mass is determined from the result of $k\cdot p$ perturbation theory[14].

$$\frac{m}{m_e} = 1 + \frac{P^2}{3}\left(\frac{2}{Eg} + \frac{1}{Eg+\Delta}\right) \quad (2a)$$

where

$$P^2 = \frac{2}{m}|\langle u_{\Gamma_1}|\mathbf{P}|u_{\Gamma_{15}}\rangle|^2 \quad (2b)$$

and Δ is the energy difference between the top of the valence band and the split off band.

The results of the *BE* Auger lifetimes as a function of band gap are presented in Fig. 2. The Auger lifetimes get very short for small gaps and rapidly increase with increasing gap. The various parameters used in the computation are given in Table 2.

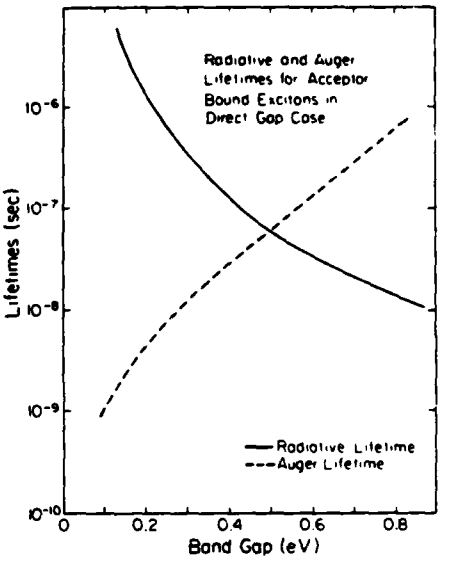

Fig. 2. Radiative and Auger transition rates for an acceptor bound exciton in the direct gap material $Hg_{1-x}Cd_xTe$ vs the band gap of the material.

Table 2. Parameters used in the Auger and radiative transition rate calculations for $Hg_{1-x}Cd_xTe$

$m_h = 0.5\ m_0$	[a]
$\epsilon_0 = 14.6$	[a]
$P^2 = \frac{2}{m}\lvert\langle u_{\Gamma_1}\rvert P_x \rvert u_{\Gamma_{15}}\rangle\rvert^2 = 18$ eV	[a]
$\Delta = 1$ eV	[a]

[a] Ref. 11.

Proceeding as in the indirect gap case, we find the no-phonon oscillator strength to be

$$f = \frac{2}{\hbar\omega m}|\langle u_{\Gamma_1}|P_x|u_{\Gamma_{15}}\rangle|^2 \left[\frac{8}{(1+a_A/a)^3}\left(\frac{a_A}{a}\right)^{3/2}\right]^2 \left[\frac{8}{(1+b/a)^3}\left(\frac{b}{a}\right)^{3/2}\right]^2. \quad (3)$$

The radiative transition rate is determined from the oscillator strength[2].

The numerical results for the radiative lifetimes are presented in Fig. 2 along with the Auger lifetimes. The radiative lifetimes show a strong dependence on the gap and cross the Auger lifetimes at a gap of about 0.5 eV. For gaps smaller than 0.5 eV, the *BE* decay will be primarily non-radiative, and for gaps larger than 0.5 eV radiative decay dominates. The radiative transition rate decreases with band gap for two reasons: the photon density of states becomes smaller and the overlap of the electron and hole wavefunctions becomes small as the electron effective mass becomes small and the electron Bohr radius becomes larger (the factor $[8/[(1+b/a)^3](b/a)^{3/2}]^2$ in eqn 3).

Acknowledgements—This work was supported in part by the Air Force Office of Scientific Research under Grant No. AFOSR-77-3216 and in part by the Alfred P. Sloan Foundation.

REFERENCES

1. D. F. Nelson, J. D. Cuthbert, P. J. Dean and G. D. Thomas, *Phys. Rev. Lett.* 17, 1262 (1962).
2. P. J. Dean, R. A. Faulkner, S. Kimura and M. Ilegems, *Phys. Rev.* B4, 1926 (1971).
3. S. A. Lyon, G. C. Osbourn, D. L. Smith and T. C. McGill, *Solid-State Commun.* 23, 425 (1977).
4. P. T. Landsberg, *Phys. Status Solidi* 41, 457 (1970).
5. P. T. Landsberg and M. J. Adams, *J. Lum.* 7, 3 (1973).
6. P. T. Landsberg and M. J. Adams, *Proc. R. Soc. Lond.* A334, 523 (1973).
7. G. C. Osbourn and D. L. Smith, *Phys. Rev.* B16, 5426 (1977).
8. W. Schmid, *Phys. Status Solidi* B84, 529 (1977).
9. M. Chen, D. L. Smith and T. C. McGill, *Phys. Rev.* B15, 4983 (1977).
10. C. H. Henry and K. Nassau, *Phys. Rev.* B1, 1628 (1970).
11. See for example, R. Dornhaus and G. Nimtz in *Springer Tracts in Modern Physics* (Edited by G. Höhler), Vol. 78, p. 1ff. Springer, Berlin (1976).
12. K. R. Elliott, G. C. Osbourn, D. L. Smith and T. C. McGill, *Phys. Rev.* B17, 1808 (1978).
13. P. J. Dean, W. F. Flood and G. Kaminsky, *Phys. Rev.* 163, 721 (1967).
14. E. O. Kane, *J. Phys. Chem. Solids* 1, 249 (1957).
15. Ya. Pokrovskii, *Phys. Status Solidi* A11, 385 (1972).
16. C. T. Elliott, I. Melngailis, T. C. Harman and A. G. Foyt, *J. Phys. Chem. Sol.* 33, 1527 (1972).

PUBLICATION #3

Solid State Communications, Vol. 23, pp. 425 - 428, 1977. Pergamon Press. Printed in Great Britain.

BOUND EXCITON LIFETIMES FOR ACCEPTORS IN Si*

S. A. Lyon, G. C. Osbourn, D. L. Smith and T. C. McGill†

California Institute of Technology
Pasadena, California 91125

We present measurements of the bound exciton lifetimes for the four common acceptors in Si and for the first two bound multiple exciton complexes in Si:Ga and Si:Al. We present a calculation of the Auger transition rate for the acceptor bound excitons in Si which accounts for the observed lifetimes and their dependence on the acceptor type.

A great deal of interest has recently been shown in the properties of bound excitons (BE) in Si. This interest has been stimulated, in part, by the observation of a large number of related emission lines (whose physical origin is not certain at present) in Si doped with the common shallow donors and acceptors[1]. The current explanation for these emission lines (this explanation is not universally accepted[2]) is that they are due to recombination of an electron hole pair in a complex of several excitons bound to a single impurity, a bound multiple exciton complex (BMEC).[1] If this explanation is correct, the energy position of the emission lines are such that the binding energy of the last exciton in a complex increases with the number of excitons already bound to the complex. Thus, the smaller complexes are thermodynamically unstable to formation of larger complexes. Since the small complexes are observed and the maximum binding energy is not reached, the relative concentration of complexes of different sizes must be determined by kinetics rather than energy considerations[3]. Thus, it is important to understand the decay and formation kinetics of bound excitons.

In any discussion of BE and BMEC kinetics, the bound exciton lifetime will play an important role. In Si, BE lifetimes have been measured for the donors Li[4], P[1] and As[5]; among acceptors, only the lifetimes for B[1] has been reported. In this communication, we present measurements of the BE lifetimes for the four common acceptors in Si (B, Al, Ga and In) and lifetimes of the first two BMEC in Si:Al and Si:Ga. (For Si:In, we are only able to set an upper limit on the BE lifetime). We find very different lifetimes for the BE associated with the different acceptors; the lifetimes decrease rapidly (by about three orders of magnitude) as the binding energy of the acceptor increases.

The lifetime of the acceptor BE in Si is most likely limited by Auger transitions in which an electron recombines with one of the holes in the BE and the energy is carried off by the second hole. We present a calculation of transition rates for this process. The calculation accounts for the strong dependence of the BE lifetime on acceptor binding energy and is in approximate quantitative agreement with the measured lifetimes.

Experiments were performed using samples of Si prepared by lapping and then etching with HNO_3:HF (6:1) and cleaning with methanol. The sample was placed in a variable temperature helium cryostat and bath temperature was measured using a Ge temperature sensor in the sample block. The sample was optically excited with a GaAs laser diode. The laser spot diameter on the sample was approximately 1 mm. The BE luminescence (TO phonon line for Si:B, zero phonon line for Si:Al, Si:Ga and Si:In) was selected with a Spex 1400-II spectrometer and was detected with a cooled S-1 photomultiplier in conjunction with a gated photon counting system. The minimum system response time was tested by measuring the fall time of the laser pulse; it was approximately 5 nsec. In measurements on Si:B, a 200 nsec gate was used; for Si:Al,Si:Ga and Si:In,the 5 nsec gate was used. The laser excitation power was selected so that the BE luminescence dominated the spectrum. Thus, the results should not be complicated by exciton capture and BMEC decay. The decay of the BE luminescence was exponential for over an order of magnitude drop in the intensity.

The measurements were made at 4.2°K and 10° K. There was a small increase in the observed lifetime as the temperature was raised to 10°K. This increase is most likely due to dissociation of the BE in Si:B at the higher temperature. (There was a reasonably large free exciton emission signal at 10°K, but this emission signal was very weak compared to the BE emission at 4.2°K.) In the case of Si:Ga, the BE has an excited state 1.67 meV above the ground state[6]. At 10°K this excited state is populated with a probability comparable to that for the ground state. If the Auger rate for the excited state is slower than for the ground state, population of the excited BE state in Si:Ga (as well as exciton dissociation) can increase the observed lifetime as the temperature is raised.

* Work supported in part by AFOSR under Grant No. 77-3216.
† Alfred P. Sloan Foundation Fellow.

Table I: Measured lifetimes for bound excitons (BE) and bound multiple exciton complexes for acceptors in Si; b_1 and b_2 label the first and second BMEC, respectively; E_A is the acceptor binding energy and N_A is the acceptor concentration.

	τ(4.2°K)	τ(10°K)	E_A	N_A	Excitation Conditions
Si:B(BE)	1.0 μsec	1.15 μsec	46 meV	$2\cdot10^{15}cm^{-3}$	6 μsec at 0.1 watt
Si:Al(BE)	104 nsec		67 meV	$5\cdot10^{14}cm^{-3}$	350 nsec at 0.5 watt
b_1(J=2)	59 nsec			$5\cdot10^{14}cm^{-3}$	350 nsec at 0.5 watt
b_2	46 nsec			$5\cdot10^{14}cm^{-3}$	350 nsec at 0.5 watt
Si:Ga(BE)	58 nsec	67 nsec	71 meV	$3\cdot10^{16}cm^{-3}$	350 nsec at 0.5 watt
b_1(J=2)	39 nsec			$2\cdot10^{15}cm^{-3}$	300 nsec at 0.5 watt
b_2	35 nsec [a]			$2\cdot10^{15}cm^{-3}$	300 nsec at 0.5 watt
Si:In(BE)	<5 nsec		154 meV	$2\cdot10^{16}$	200 nsec at 0.5 watt

a) The b_2 line for Si:Ga was very weak and there was a background which decayed with a 47 nsec lifetime beneath it. The presence of the background may cause the measured decay time to be somewhat larger than the actual lifetime.

The measured BE lifetimes for the four acceptors are listed in Table I. We have also listed the decay time for the first two BMEC in Si:Al and Si:Ga. The result for Si:B at 4.2°K is identical to that previously reported[1]. (We did not measure the BMEC decay for Si:B because they are already available in the literature[1].) The BE exciton lifetime in Si:In was shorter than our system response time, and we can only set an upper bound on it.

From Table I, we see that the BE lifetime decreases rapidly as the acceptor binding energy increases. This behavior is similar to that observed for acceptor BE lifetimes in GaP.[7] This effect can be understood as due to an increased spreading in K-space of the BE wavefunction as the acceptor binding energy increases[7]. To quantify this idea, we have carried out calculations of the BE Auger rates for acceptor BE in Si. The details of these calculations will be presented elsewhere[8], here we give the physical picture and the results of the calculation.

From time dependent perturbation theory, the BE Auger transition rate is given by

$$\frac{1}{\tau} = \frac{2\pi}{\hbar} \sum_F |\langle F|V|I\rangle|^2 \, \delta(E_F - E_I) \ , \qquad (1)$$

here $|F\rangle$ is the final state which consists of a free hole, $|I\rangle$ is the initial state which consists of two holes and an electron bound to the charged acceptor and the interaction which leads to the transition, V, is the Coulomb interaction between the carriers.

The final hole state is an eigenstate of wavevector. The possible final states are restricted by energy conservation. The initial BE state is not an eigenstate of wavevector because the carriers are localized in space by the impurity potential. In order for the Auger transition to occur, the initial BE state must have an amplitude to contain wavevectors which are accessible to the final state hole. Because the wavefunction for the holes in the BE in K-space are peaked at the zone center and that for electrons is peaked at the conduction band minimum, the total wavevector for the BE is peaked at the conduction band minimum. This point is rather far, in K-space, from the constant energy surface accessible to the final state hole. Thus, spreading of the BE wavefunction, in K-space, is essential for the Auger transition to occur. For the acceptor BE, the holes are more highly localized in space than the electron and the spreading of the BE wavefunction in K-space is due primarily to the holes. The extent of this spreading depends on the impurity, it increases as the binding energy of the acceptor increases because the holes are more strongly localized in space for the more tightly bound acceptors.

In principle, it is possible that the Auger transitions are phonon assisted. If this were the case, the phonon would supply the wavevector necessary for the transition to occur and the transition rate would not depend on the K-space spreading of the BE wavefunction. Thus, one would expect the phonon assisted Auger rates to be insensitive to the acceptor type. Since the observed lifetimes are, in fact, very sensitive to the acceptor type, we believe the Auger transitions occur without phonon assistance.

The bound exciton wavefunction can be written as a linear combination of determinants which contain two holes and one electron

$$|I\rangle = \sum_{k_e,k_h,k_h'} A(k_e,k_h,k_h') \, \varphi(k_e,k_h,k_h') \qquad (2)$$

As a first approximation, the Fourier transform of the amplitude function, A, can be obtained from effective mass theory. To describe the interaction of the carriers with the charged acceptor, we used a Coulomb potential with a short range spherical well. The strength of the short range well for Al (same core structure as Si) was taken to be due only to the wavevector dependence of the dielectric function. For the other impurities, it was adjus-

ted to produce the known acceptor binding energies for a hydrogenic acceptor wavefunction. For the BE wavefunction, a variational form

$$A(k_e, k_h, k_h') = f_e(k_h)\, f_h(k_h)\, f_h(k_h') \qquad (3)$$

was chosen. Here f is the Fourier transform of a 1s hydrogen function

$$f_i(k) = \sqrt{\frac{\pi}{a_i^5}}\ \frac{8}{(k^2 + (1/a_i)^2)^2} \qquad (4)$$

Here a is the Bohr radius and the subscript refers to electrons (i=e) or holes (i=h). The Bohr radii were chosen by a variational calculation. For more strongly bound acceptors, the hole Bohr radius is smaller corresponding to a greater spreading in K-space.

There are corrections to the effective mass approximation for wavevectors far from the band extrema because the carrier dispersion curves are no longer parabolic. We take these corrections into account by substituting the hydrogenic form into the Hartree equation for the hole in the BE

$$f_h(k) = \frac{1}{\varepsilon(k)+E} \sum_{k'} V_{kk'}\, f_h^H(k') \qquad (5)$$

Here $\varepsilon(k)$ is the hole dispersion curve, E is the one hole Hartree energy, V is the Hartree potential seen by the hole (computed taking the hydrogenic forms for the carrier wavefunctions) and f_h^H is the hydrogenic form for the hole wavefunction (Eq. (3)). The hole wavefunction produced by this procedure differs from the hydrogen form in that it has a longer tail region at large k. (This tail is due to the fact that $\varepsilon(k)$ increases slower than k^2 at large k.) In the region of K-space where the two functions are large, they are nearly equal.

The BE wavefunction was tested by computing no-phonon oscillator strengths. For Si:Al,Si:Ga and Si:In, the results were within a factor of two of the measured result[9]. For Si:B, the computed oscillator strength was about a factor of four too large. We adjusted the square well potential to produce the measured oscillator strengths.

The Auger transition rates for the acceptor BE was computed using the wavefunction described above. The details are complicated and will be given elsewhere[8]. The results of the calculation are shown in Fig. (1). The calculation is seen to describe the observed dependence of the lifetime on acceptor binding energy reasonably well. The computed lifetimes are larger than the experimental values by about a factor of three for all the impurities. Considering the sensitivity of the calculated lifetimes on the BE wavefunction, we consider this agreement to be reasonable.

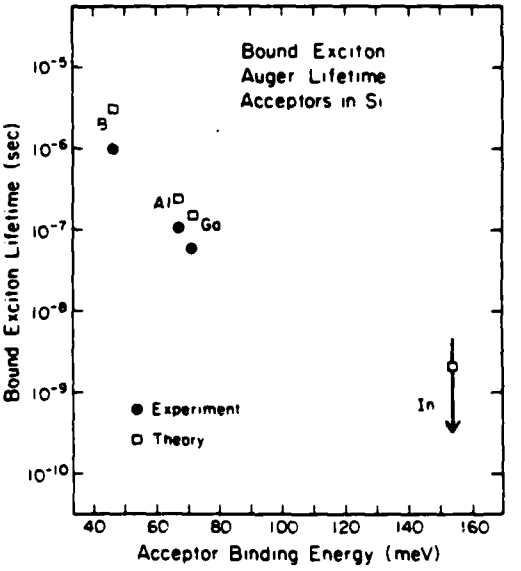

Fig. 1. Bound exciton lifetimes vs impurity binding energy for the four common acceptors in Si. The solid circles are measured values and the hollow squares are calculations of the Auger lifetime. For Si:In, the lifetime was shorter than our system response time, and we can only set an upper limit on it.

Summarizing, we have presented measurements of the BE lifetime for the common shallow acceptors in Si and for the first two BMEC in Si:Al and Si:Ga. The lifetime of the BE was found to decrease rapidly as the acceptor binding energy gets larger. We interpreted the lifetime as being limited by phononless Auger transitions. We presented a calculation of the phononless Auger rate for the acceptor BE in Si which produced the observed dependence of the lifetime on acceptor binding energy and is within about a factor of three of the measured lifetimes in absolute magnitude.

Acknowledgement- It is a pleasure to acknowledge W. H. Winston and M. H. Young from the Hughes Research Laboratories for providing samples. M. Chen, K. R. Elliott, and D. S. Pan provided us with numerous useful discussions.

References

1. See, for example, Sauer R., Proc. Twelfth Int. Conf. Physics of Semiconductors (Stuttgart, 1974), p. 42 and references therein.
2. Sauer R., and Weber J., Phys. Rev. Lett. 36, 48 (1976).
3. Sauer R., Phys. Rev. Lett. 31, 376 (1973).
4. Kosai K., Gershenzon M., Phys. Rev. B9, 723 (1974).
5. Nelson D. F., Cuthbert J. D., Dean P.J., and Thomas G. D., Phys. Rev. Lett. 17, 1262 (1966).

6. Vouk M. A. and Lightowlers E. C., Proc. Thirteenth Int. Conf. Physics of Semiconductors, (Rome, 1976).
7. Dean P. J., Faulkner R. A., Kimura S., and Ilegems M., Phys. Rev. B4, 1926 (1971).
8. Osbourn G. C., and Smith D. L., to be published.
9. Dean P. J., Flood W. F., and Kaminsky G., Phys. Rev. 163, 721 (1967).

PHYSICAL REVIEW B VOLUME 20, NUMBER 4 15 AUGUST 1979

Auger and radiative transition rates for acceptor bound excitons in direct-gap semiconductors

G. C. Osbourn and D. L. Smith
California Institute of Technology, Pasadena, California 91125
(Received 5 March 1979)

We present calculations of the Auger and radiative recombination rates for acceptor bound excitons in the HgCdTe alloy system and in GaAs. The transition rates are computed as a function of band gap in the HgCdTe alloy and as a function of the acceptor binding energy. The Auger rate is found to increase and the radiative rate to decrease with increasing acceptor binding energy. The radiative recombination rate is found to increase with increasing band gap. The Auger rate decreases with increasing band gap except when the band gap first exceeds the spin-orbit splitting in the valence band and for band gaps less than about 0.2 eV where the density of final hole states and the electron-hole overlap becomes small. We find that Auger recombination is dominant for hydrogenic acceptors in HgCdTe for materials with a band gap less than about 0.35 eV and radiative recombination is dominant for larger gap materials. For deeper acceptors, this crossover occurs at larger band gaps. For GaAs, we find that radiative recombination dominates for all reasonably shallow acceptors.

I. INTRODUCTION

A bound exciton (BE) is formed when an electron-hole pair becomes attached to a neutral impurity. At low temperatures, recombination from bound-exciton states is often the principal decay route of a nonequilibrium concentration of electrons and holes. There are two main decay mechanisms available to an exciton bound to a shallow neutral impurity: Auger[1-7] recombination and radiative recombination.[8-12] The relative importance of these two decay processes depends on the semiconductor and on the impurity. In indirect-band-gap materials, radiative recombination is rather slow and the Auger mechanism usually dominates the recombination.[3-7] In direct-band-gap materials, radiative recombination is quite fast and may dominate the recombination.[10-12] Auger recombination of bound excitons in indirect materials has recently been studied theoretically by the present authors[6] and by Schmid.[7]

In this paper, we present a theoretical study of Auger and radiative recombination of excitons bound to shallow neutral acceptors in direct-band-gap semiconductors. We consider the dependence of these two transition rates on the band gap of the semiconductor and on the binding energy of the impurity. We concentrate on the alloy system $Hg_{1-x}Cd_xTe$. This is a particularly interesting system because the band gap can be varied by changing alloy composition. We also present calculations for GaAs. We find that radiative recombination dominates Auger recombination for shallow acceptors except in rather small-band-gap materials ($E_g \lesssim 0.35$ eV). In these small-band-gap materials, the Auger rate is dominant. Radiative recombination for bound excitons in direct-band-gap materials has been previously studied theoretically by Rasba and Gurgenishvili.[8,9] We use a different model for the BE wave function than used by these authors, but our results are qualitatively similar to theirs. Except for a simple model calculation by us,[13] we are unaware of previous calculations of Auger recombination of BE in direct-gap materials.

The paper is organized in the following way: in Sec. II we discuss the qualitative behavior of Auger and radiative transition rates for acceptor BE in direct-gap materials; in Sec. III, detailed calculations are presented; Sec. IV contains a summary of our conclusions.

II. QUALITATIVE BEHAVIOR OF AUGER AND RADIATIVE TRANSITIONS

In the acceptor BE there are two holes and one electron bound to a charged acceptor. In direct-band-gap materials, the electron effective mass is generally considerably smaller than the hole effective mass. As a result, the two holes are bound relatively close to the acceptor and the electron is not as localized as the holes. In a k-space picture the holes are relatively spread out about the $k=0$ valence-band maximum and the electron is relatively well localized near the $k=0$ conduction-band minimum. In the HgCdTe alloy system, the electron effective mass is a sensitive function of the material band gap (alloy composition). From $\vec{k}\cdot\vec{P}$ perturbation theory, the electron effective mass decreases with decreasing band gap[14]

$$\frac{m}{m_e^*} = 1 + \frac{P^2}{3}\left[\frac{2}{E_g} + \frac{1}{E_g+\Delta}\right] . \tag{1a}$$

where

$$P^2 \approx \frac{2}{m}|\langle S|P_x|X\rangle|^2 \quad (1b)$$

Here m_e^* is the electron effective mass, E_g is the band gap, Δ is the spin-orbit splitting, m is the free-electron mass, S and X refer to periodic parts of the Bloch functions at the conduction-band minimum and valence-band maximum (without spin-orbit splitting) and P is the momentum operator. The hole effective mass and the static dielectric function of the material are only weakly dependent on band gap. Thus the acceptor binding energy and hole wave function in both the acceptor and the BE are not strongly dependent on the alloy composition.[15]

In the Auger transition, the initial state is the BE and the final state is a free hole in an accessible valence band. The heavy and light hole bands are always accessible. If the band gap is greater than the spin-orbit splitting of the valence band, the split-off valence band is also accessible. Energy conservation requires that the energy of the final state hole measured from the valence-band maximum is approximately the band gap. The dominant interaction responsible for the Auger transition is carrier-carrier scattering which conserves total wave vector.[16] Thus the transition rate depends on the amplitude for the BE to have wave vectors which are accessible to the final state hole. This amplitude depends on the strength of the impurity potential and on the band structure of the semiconductor.

In direct gap materials, the k-space BE wave function is peaked at the zone center and falls off with increasing $|k|$. The possible values of the final state hole wave vector (k_f) depends on the band gap of the material and on the valence-band structure. For materials with a very small band gap, the final state hole will be in the heavy or light hole band near the zone center. For these very small gap materials, the amplitude of the BE wave function to contain wave vectors accessible to the final state hole will be large. However, for very small gap materials the density of final hole states is small and the electron effective mass is small. Because of the small electron effective mass, the electron is weakly bound to the BE and is not well localized near the holes. As a result of the small density of final states and the small electron-hole overlap, the Auger transition is slow for very small gap materials. As E_g increases from zero, the density of final states and the electron-hole overlap increase so the Auger transition rate increases. As E_g continues to increase, the possible values of k_f become large enough that the amplitude for the BE wave function to contain k_f becomes small. As a result the transition matrix element begins to decrease rapidly, overcoming the effects of the increasing density of final states and increasing electron-hole overlap, and the transition rate decreases. We find that this change in slope of the transition rate occurs at about 0.2 eV for hydrogenic acceptors in the HgCdTe system. When E_g first exceeds the spin-orbit splitting of the valence band ($\Delta \approx 0.9$ eV in HgCdTe), final states in the split-off band with k_f near the zone center become available. There is a rapid increase in the Auger transition rate when this new set of final states becomes accessible. As E_g continues to increase, the possible values of k_f become large and the transition matrix element and hence the transition rate decreases.

The extent of the spread in k space of the BE wave function depends on the strength of the impurity potential. Stronger impurity potentials (resulting in larger acceptor binding energies) lead to an increased localization of the holes in the BE in position space and hence an increased spread of the BE wave function in k space. For those values of the band gap that have final states with large k_f, an impurity with a stronger attractive potential (hence larger acceptor binding energy) will have a faster Auger rate than an impurity with a weaker potential. For those values of the band gap that have final states with small k_f, the Auger transition rate does not depend strongly on the impurity potential.

For radiative transitions, the BE is the initial state and the neutral acceptor is the final state. Radiative transition rates decrease monotonically as the band gap is decreased. There are two reasons for this decrease in the radiative transition rate with band gap: first, the density of final photon states is smaller for the lower-energy photons emitted from the small-band-gap material; second, because the electron effective mass is small in small gap materials the electron-hole overlap is small. The radiative rate also depends on the strength of the impurity potential. The holes in the acceptor BE are bound close to the impurity and their wave functions are sensitive to the short-range part of the impurity potential. The electron is bound relatively loosely about the impurity (held in the complex by its interaction with the holes) and its wave function is relatively insensitive to short-range parts of the impurity potential. As the impurity potential becomes increasingly attractive to holes, the hole wave function will be more closely bound to the impurity. As a result, the electron-hole overlap will decrease and the radiative transition rate will decrease.

The radiative lifetime is a monotonically decreasing function of band gap. The Auger lifetime is a more complicated function of band gap, but for most values of the band gap it is an increasing function. As a result, radiative recombination tends to dominate in large gap materials and Auger recombination tends to dominate in small gap materials. The radiative lifetime is an increasing function of acceptor binding energy; whereas, the Auger lifetime is a decreasing function of acceptor binding energy. Thus,

in large-band-gap materials (where radiative recombination is dominant), the lifetime increases with acceptor binding energy and in small gap materials (where Auger recombination is dominant), the lifetime decreases with acceptor binding energy.

III. CALCULATION OF AUGER AND RADIATIVE TRANSITION RATES

From time-dependent perturbation theory, the recombination rate of a BE due to a perturbation v is given by

$$\frac{1}{\tau} = \frac{2\pi}{\hbar} \sum_{\text{all } I,F} |\langle F|v|I\rangle|^2 \delta(E_I - E_F) \quad , \tag{2}$$

where $|I\rangle$ is the initial BE state and $|F\rangle$ is the final state (free hole for Auger transition, neutral acceptor and photon in the radiative transition). We take the BE wave function to have the form

$$|I\rangle = \sum_{k_h k_h' k_e m_1 m_2} C^{JM}_{m_1 m_2} f_h(k_h) f_h(k_h') f_e(k_e) \times \psi(k_h m_1; k_h' m_2; k_e \sigma_e) \quad , \tag{3}$$

where $\psi(k_h m_1; k_h' m_2; k_e \sigma_e)$ is a Slater determinant with the valence-band states (k_h, m_1) and $(k_h' m_2)$ empty and the conduction-band state $(k_e \sigma_e)$ occupied. Here m_1 and m_2 label the four hole states degenerate at the valence-band maximum, σ_e labels electron spin, J is the total hole spin with projection M in the BE, the coefficients C are closely related to Clebsch-Gordan coefficients,[6] and f_h and f_e are the amplitudes that a given hole and electron state are contained in the BE wave function. Taking the BE envelope function as a product form in Eq. (3) is equivalent to neglecting correlation in the BE. Correlation must be included in binding-energy calculations for the BE in order to have a stable complex. But no cancellations, such as the large cancellations between kinetic and potential energy terms which occur in binding-energy calculations, occur in the transition rates calculated here. Thus the simple product form should be adequate to give a reasonable estimate of the dependence of the transition rates on band gap and acceptor binding energy.

For Auger decay of the BE, the final state contains a free hole and an ionized acceptor. The Coulomb interaction between carriers is responsible for the Auger transition. The transition matrix element has the same structure in direct-band-gap materials as for indirect-band-gap materials discussed previously[6]

$$\langle F|v|I\rangle = \sum_{k_h k_h' k_e m_1 m_2} f_h(\vec{k}_h) f_h(\vec{k}_h') f_e(\vec{k}_e) U_{k_h m_1; k_f \sigma_f} U'_{k_h' m_2; k_e \sigma_e} \frac{e^2(2\pi)^3 \delta(\vec{k}_f + \vec{k}_e - \vec{k}_h - \vec{k}_h')}{\epsilon |k_f - k_h|^2} \left| C^{JM}_{m_1 m_2} - C^{JM}_{m_2 m_1} \right| \quad . \tag{4}$$

Here ϵ is the dielectric function and the overlap integrals U have the form[17]

$$U_{k_h m_1; k\sigma} = \frac{1}{\Omega} \int d^3r \, u^*_{k_h m_1}(r) u_{k\sigma}(r) \quad , \tag{5}$$

where Ω is the sample volume and $u_{k\sigma}$ is the periodic part of the Bloch function.

We use the same approximations for the envelope functions f here as in the indirect case.[6] The impurity potential is taken to be that of a negative point charge screened by the static dielectric function plus a short-range square well of variable strength. The square well is used to account for short-range differences in the potential of different impurities. As a first approximation, the envelope functions f_h and f_e are assumed to have a $1S$ hydrogenic form with the electron and hole Bohr radii determined by a variational calculation. Corrections to the hole envelope functions, due primarily to nonparabolic valence-band structure at large k, are taken into account by iterating the Hartree equation for the holes in the acceptor BE. The iterated envelope function is close to the hydrogenic one at small k, but drops off more slowly at large k.[6] The integral in Eq. (4) is simplified by the fact that the function $f_e(k_e)$ is sharply peaked at the zone center. We replace $f_e(k_e)$ by a normalized δ function

$$f_e(k_e) \approx \frac{(2\pi)^3}{(\pi b^3)^{1/2}} \delta(k_e) \quad , \tag{6}$$

where b is the electron Bohr radius.

For the overlap integrals U, we use the results of Kane obtained from degenerate $\vec{k} \cdot \vec{p}$ perturbation theory.[14,18] The discrete sums in the matrix element (m_1 and m_2), the sum over final hole spins and bands, and the average over initial states (labeled by J, M, and σ_e) can be performed in a straightforward but tedious fashion; the result becomes

$$\frac{1}{\tau_A} = \frac{2\pi}{\hbar} \sum_{k_f} \left[\tfrac{1}{3} I_h(k_f) \delta(E_I - E_h(k_f)) + \tfrac{1}{6} I_l(k_f) \delta(E_I - E_l(k_f)) + \tfrac{1}{6} I_S(k_f) \delta(E_I - E_S(k_f)) \right] \quad , \tag{7}$$

where h, l, and S refer to transitions in which this final state hole is in the heavy hole, light hole, and split-off bands, respectively.

The integrals I are given by

$$I_h(k_f)=\left[\frac{1}{\pi b^3}\right]\left|\sum_{k'}\frac{f_h(k_f-k')f_h(k')}{\epsilon|k'|^2}a_{v_2}(k')(\hat{k}_f\cdot\hat{k}')\right|^2 . \tag{8a}$$

$$I_l(k_f)=\left[\frac{1}{\pi b^3}\right]\left|\sum_{k'}\frac{f_h(k_f-k')f_h(k')}{\epsilon|k'|^2}a_{v_2}(k')(\hat{k}_f\cdot\hat{k}')\left[a_{v_2}(k_f-k')a_{v_2}(k_f)+b_{v_2}(k_f-k')b_{v_2}(k_f)+c_{v_2}(k_f-k')c_{v_2}(k_f)\right]\right|^2 . \tag{8b}$$

$$I_S(k_f)=\left[\frac{1}{\pi b^3}\right]\left|\sum_{k'}\frac{f_h(k_f-k')f_h(k')}{\epsilon|k'|^2}a_{v_2}(k')(\hat{k}_f\cdot\hat{k}')\left[a_{v_2}(k_f-k')a_{v_3}(k_f)+b_{v_2}(k_f-k')b_{v_3}(k_f)+c_{v_2}(k_f-k')c_{v_3}(k_f)\right]\right|^2 . \tag{8c}$$

Here $\hat{k}_f$ and $\hat{k}'$ are unit vectors, and the functions a_{v_i}, b_{v_i}, and c_{v_i} are those defined by Kane.[14]

The form for the iterated hole envelope function is the same as that used for the Auger transitions in direct-band-gap materials[6]

$$f_h(k)=\frac{e^2}{\epsilon}\frac{4\pi}{(\pi a^3)^{1/2}}\left[\frac{1}{E(k)+E_B}\right]\left[\frac{1}{k^2+9/a^2}+\frac{6}{a^2(k^2+9/a^2)^2}+\frac{VR^3}{6e^2/\epsilon}\right] . \tag{9}$$

where a is the hole Bohr radius, E_B is the BE localization energy, V is the depth of the short-range square well, and R is the radius of the short-range square well (taken to be half the nearest-neighbor distance). The one-hole energy $[E(k)]$ was taken as a spherical average of the heavy hole band from a tight-binding band-structure calculation joined continuously to the parabolic effective-mass result at small k. The tight-binding parameters for HgTe and CdTe were taken from Ref. 19; those for GaAs are from Ref. 20. The band structure for the HgCdTe alloy was calculated in a virtual crystal approximation. The integrations in the matrix elements of Eq. (8) were evaluated numerically. The final state integral in Eq. (7) was evaluated numerically; the final state hole energies were taken from a tight-binding band-structure calculation. The input parameters used in the calculation are summarized in Table I.

In radiative recombination of the acceptor BE, the final state is the neutral acceptor with a wave function of the form

$$|F\rangle=\sum_k F(k)\psi(kn) , \tag{10}$$

where $\psi(kn)$ is a Slater determinant with the valence-band state labeled by (k,n) not occupied and $F(k)$ is the hole envelope function. The radiative decay rate can be expressed in terms of oscillator strengths by

$$\frac{1}{\tau_R}=\left[\frac{g_{BE}}{g_A}\right]\frac{e^2 2\omega^2 n}{c^3 m}f , \tag{11}$$

where g_{BE} is the degeneracy of the BE (12), g_A is the degeneracy of the acceptor (4), $\hbar\omega$ is the photon energy, n is the index of refraction, and the oscillator strength is given as

$$f=\frac{2}{\hbar\omega m}|\langle I|P_Z|F\rangle|^2 . \tag{12}$$

Here Eq. (12) is to be summed over the 12 degenerate BE states and averaged over the 4 degenerate acceptor states. To evaluate the oscillator strength we use hydrogenic envelope functions

$$F(k)=\left[\frac{\pi}{a_A}\right]^{1/2}\frac{8}{(k^2+1/a_A^2)^2} . \tag{13}$$

TABLE I. Parameters used in the calculation. All symbols are defined in the text.

	$Hg_{1-x}Cd_xTe$	GaAs
P^2	$18+3x$ eV[a,b]	25.7 eV[b]
ϵ	$15.1-4.5x$[c]	12.53[d]
m_h	$0.45\ m$[e]	$0.36\ m$[h]
m_e		$0.067\ m$[b]
Δ	$1.00-0.24x$ eV[a,f]	0.35 eV[g]
E_g	$1.79x-0.26$ eV[a,f]	1.51 eV[g]

[a]Linearly interpolated between the HgTe and CdTe values.
[b]P. Lawaetz, Phys. Rev. B 4, 3460 (1971).
[c]J. J. Dubowski, Phys. Status Solidi B 85, 663 (1978).
[d]K. G. Hambleton, C. Hilson, and B. R. Holeman, Proc. Phys. Soc London 77, 1147 (1961).
[e]A. Jedrzejczak and T. Dietl, Phys. Status Solidi B 79, 691 (1977).
[f]Reference 15.
[g]J. R. Chelikowsky and M. L. Cohen, Phys. Rev. B 14, 556 (1976).
[h]Fit to Zn acceptor binding energy $E_A=31$ meV.

where a_A is the acceptor Bohr radius, and similar forms with Bohr radii b and a, for the electron and the holes in the BE. The radiative rate is not sensitive to the large k part of the hole envelope function so it is not necessary to use the iterated form for the hole envelope function to calculate radiative rates. The calculation of the oscillator strength from Eq. (12) is straightforward and the result is

$$f = \frac{2}{\hbar\omega m}|\langle S|P_z|Z\rangle|^2\left[\frac{8}{(1+a_A/a)^3}\left[\frac{a_A}{a}\right]^{3/2}\right]^2 \times\left[\frac{8}{(1+b/a)^3}\left[\frac{b}{a}\right]^{3/2}\right]^2. \quad (14)$$

The results of the calculation for Auger and radiative lifetimes in HgCdTe as a function of band gap (composition) are shown in Fig. 1. The solid curves correspond to hydrogenic acceptors ($VR^3=0$) and the dashed curve to a deeper acceptor modeled by $VR^3=16.5$ eV Å^3. The binding energy of the acceptors depends somewhat on the composition because of the compositional dependence of ϵ. For the hydrogenic acceptor the binding energy goes from $E_B=31$ meV in the smallest gap case considered to $E_B=46$ meV in the largest gap case; the binding energy of the deeper acceptor varies between $E_B=38$ meV and $E_B=59$ meV. The Auger lifetime has a local minimum at $E_g\approx 0.2$ eV; it increases for smaller E_g because the density of final hole states and the electron-hole overlap in space becomes small. The increase in the Auger lifetime for $E_g > 0.2$ eV is due to the larger values of k_f and the decreased amplitude for the BE wave function to contain these larger wave vectors. The sudden decrease in the Auger lifetime at $E_g\approx 0.9$ eV is due to the fact that transitions in which the final state hole is in the split-off band first become possible at this point. The Auger lifetime for the deeper acceptor is shorter than that for the hydrogenic acceptor because of the greater spread of the BE wave function in k space for the deeper acceptor. The results for the radiative lifetimes in the HgCdTe case are also shown in Fig. 1. The radiative lifetime decreases monotonically as the band gap is increased because of the larger density of photon states and increased electron-hole overlap in the larger gap material. The radiative lifetime is larger for the deeper acceptor than the hydrogenic acceptor because the electron-hole overlap is greater for the shallow acceptor. For band gap greater than

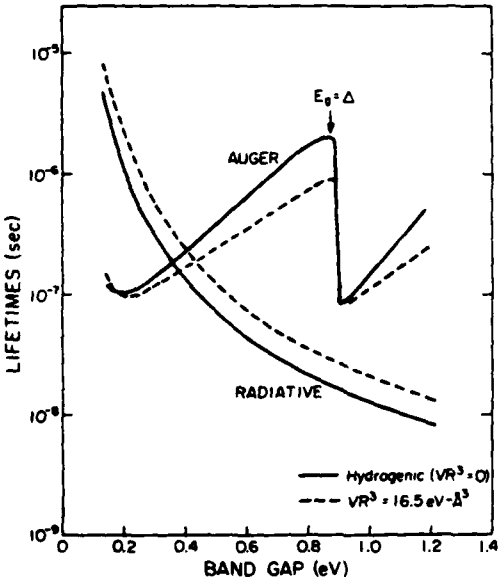

FIG. 1. Auger and radiative acceptor bound-exciton lifetimes as a function of band gap (composition) in the HgCdTe alloy system. The solid curves are for hydrogenic acceptors and the dashed curves are for a deeper acceptor where the impurity potential is taken to be that of a screened point charge plus a short-range attractive (for holes) square well. The radius of the square well (R) was taken to be half the nearest-neighbor distance and V is the depth of the square well.

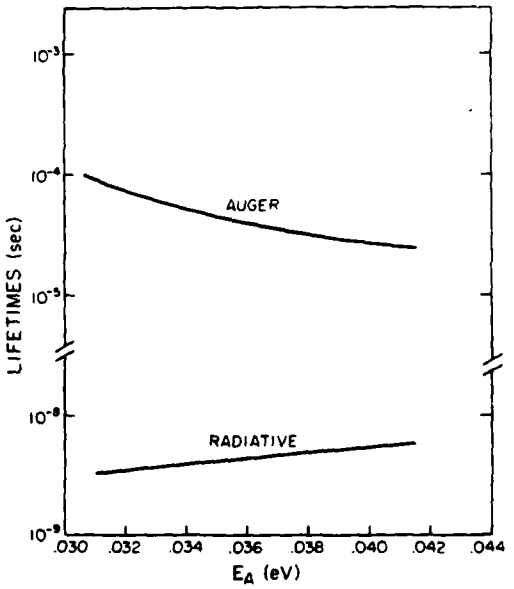

FIG. 2. Auger and radiative acceptor bound-exciton lifetimes as a function of acceptor binding energy in GaAs. The acceptor binding energy was varied by adjusting the strength of a short-range square well added to a screened point charge to form the acceptor potential. A binding energy of 31 meV corresponds to a hydrogenic acceptor (no square well).

about 0.35 eV for the hydrogenic acceptor and greater than about 0.43 eV for the deeper acceptor, the lifetime is dominated by radiative recombination; for smaller gaps, the lifetime is dominated by Auger recombination.

The results for the Auger and radiative lifetimes in GaAs as a function of impurity binding energy are shown in Fig. 2. The hydrogenic acceptor in this case has a binding energy of 31 meV (corresponding to the experimental value for the Zn acceptor in GaAs).[21] The radiative lifetime increases as the acceptor binding energy increases because the electron-hole overlap is decreased with increasing acceptor binding energy. The Auger lifetime decreases with increasing acceptor binding energy because of an increased spread of the BE wave function in k space for the deeper impurities. The radiative transition rate is much faster than the Auger rate for reasonably shallow impurities. The calculated value of the acceptor BE radiative lifetime for the hydrogenic acceptor is 3.1 nsec; experimentally a value of 1.6 ± 0.6 nsec (Ref. 12) is found for an exciton bound to a shallow acceptor in GaAs.

IV. SUMMARY AND CONCLUSIONS

We have presented a calculation of Auger and radiative transition rates for acceptor BE in HgCdTe and GaAs. The purpose of the work was to investigate the dependence of the Auger and radiative transition rates of acceptor BE in direct gap materials on acceptor binding energy and semiconductor band gap. For HgCdTe we find that the radiative lifetimes decrease with increasing energy gap, while the Auger lifetimes increase with energy gap except for $E_g \gtrsim \Delta$, where the split-off band first becomes accessible to the final state hole; and at $E_g \lesssim 0.2$ eV where the electron-hole overlap and density of final states becomes small. The Auger and radiative lifetimes cross for hydrogenic acceptors in HgCdTe at $E_g = 0.35$ eV; radiative decay dominates for larger band gaps and Auger decay dominates for smaller gaps. As the acceptor binding energy increases, the cross over point between the two rates moves to higher band gaps. For GaAs, the radiative rate is much faster than the Auger rate. As the acceptor binding energy is increased, the radiative rate decreases and the Auger rate increases. It is possible that the Auger rate could become dominant for very deep acceptors, but for reasonably shallow acceptors the Auger rate makes a negligible contribution to the BE lifetime in GaAs.

ACKNOWLEDGMENTS

The authors gratefully acknowledge the support of the Air Force Office of Scientific Research under Grant No. AFOSR-77-3216. One of us (D.L.S.) acknowledges support from the Alfred P. Sloan Foundation. We thank J. N. Schulman and T. C. McGill for providing us with their HgCdTe tight-binding parameters prior to publication.

[1]P. T. Landsberg, Phys. Status Solidi 41, 457 (1970).
[2]P. T. Landsberg and M. J. Adams, J. Lumin. 7, 3 (1973).
[3]D. F. Nelson, J. D. Cuthbert, P. J. Dean, and G. D. Thomas, Phys. Rev. Lett. 17, 1262 (1962).
[4]P. J. Dean, R. A. Faulkner, S. Kimura, and M. Ilegems, Phys. Rev. B 4, 1926 (1971).
[5]S. A. Lyon, G. C. Osbourn, D. L. Smith, and T. C. McGill, Solid State Commun. 23, 425 (1977).
[6]G. C. Osbourn and D. L. Smith, Phys. Rev. B 16, 5426 (1977).
[7]W. Schmid, Phys. Status Solidi B 84, 529 (1977).
[8]E. I. Rashba and G. E. Gurgenishvili, Fiz. Tverd. Tela (Leningrad) 4, 1029 (1962) [Sov. Phys. Solid State 4, 759 (1962)].
[9]E. I. Rashba, Fiz. Tekh. Poluprovodn. 8, 1241 (1974) [Sov. Phys. Semicond. 8, 807 (1974)].
[10]C. H. Henry and K. Nassau, Phys. Rev. B 1, 1628 (1970).
[11]C. J. Hwang and L. R. Dawson, Solid State Commun. 10, 443 (1972).
[12]C. J. Hwang, Phys. Rev. B 8, 646 (1973).
[13]G. C. Osbourn, S. A. Lyon, K. R. Elliott, D. L. Smith, and T. C. McGill, Solid State Electron. 21, 1339 (1978).
[14]E. O. Kane, J. Phys. Chem. Solids 1, 249 (1957).
[15]C. T. Elliott, I. Melngailis, T. C. Harmon, and A. G. Foyt, J. Phys. Chem. Solids 33, 1527 (1972).
[16]We treat the alloy in the virtual-crystal approximation and neglect phonon-assisted Auger recombination.
[17]We neglect umklapp terms in Eq. (4). Such terms will give a negligible contribution to the Auger rate because the wave-vector match ups will be very unfavorable.
[18]In the simple model calculation of Ref. 13, we used nondegenerate $\vec{k} \cdot \vec{p}$ perturbation theory for the electron-hole overlap integral. The nondegenerate result is not valid for small gap materials and leads to an overestimate of the Auger rate.
[19]J. N. Schulman and T. C. McGill (unpublished).
[20]D. J. Chadi, Phys. Rev. B 16, 790 (1977).
[21]W. Schairer and T. O. Yep, Solid State Commun. 9, 421 (1971).

Near-band-gap photoluminescence of $Hg_{1-x}Cd_xTe$

A. T. Hunter, D. L. Smith, and T. C. McGill
California Institute of Technology, Pasadena, California 91125

(Received 2 January 1980; accepted for publication 1 May 1980)

The results of photoluminescence studies of $Hg_{1-x}Cd_xTe$ with $x = 0.32$ and 0.48 for temperatures between 5 and 30 K are described. In the $x = 0.32$ and $x = 0.48$ material, band-to-band, band-to-acceptor, and donor-to-acceptor luminescence lines are observed. We report the first observation of bound-exciton luminescence in HgCdTe, which we observe in the samples with $x = 0.48$.

PACS numbers: 72.80.Ey, 78.55. – m, 78.55.Ds

The results of a series of photoluminescence experiments on $Hg_{1-x}Cd_xTe$ for samples with $x = 0.32$ and 0.48 are presented. We report the first observation of the luminescence from a bound exciton in $Hg_{1-x}Cd_xTe$. Other lines due to band-to-band, band-to-acceptor, and donor-to-acceptor transitions are also observed.

While $Hg_{1-x}Cd_xTe$ is an important material for infrared applications,[1] its luminescence properties have not been extensively investigated. Photo- and cathodo[2]-luminescence spectra have been measured by other groups for samples with $x = 0.3$. They observed two broad luminescence lines which they attributed to band-to-band and band-to-impurity transitions.[2,3] The impurity was thought to be Hg vacancies.[3] Recently, Osbourn and Smith[4] have suggested that radiative recombination should dominate nonradiative Auger recombination of bound excitons for $x > 0.4$. These results suggest that it should be easier to observe bound-exciton luminescence in high-x samples than in low-x samples.

Our luminescence experiments have been carried out on samples of two compositions, one of $x = 0.32$ with a band gap near 0.25 eV, and the other of $x = 0.48$, with band gap

 0003-6951/80/140200-04$00.50

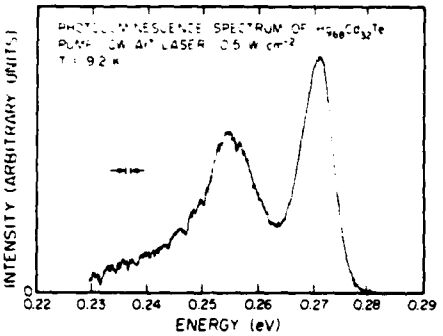

FIG. 1. Photoluminescence intensity vs energy of emitted photon for $Hg_{.68}Cd_{.32}Te$. The high-energy peak is attributed to a band-to-band transition. The low-energy peak is attributed primarily to donor-to-acceptor luminescence below ~ 10 K, and band-to-acceptor luminescence at higher temperature. The fine structure seen on the low-energy peak is due to absorption by water vapor.

near 0.5 eV. Spectra were measured for temperatures between 5 and 30 K and average pump power, provided by a mechanically chopped cw Ar^+ laser with 50% duty cycle, of between 0.5 and 14 W/cm^2. Laser light was focused onto the sample, mounted in a Janis liquid-helium research dewar. A heater and temperature sensor mounted near the sample in the sample arm of the dewar allowed temperature control. The luminescence from the sample was dispersed with a monochrometer and detected with either an InSb (for $x = 0.32$ material) or an InAs detector (for $x = 0.48$ material). The detector output was analyzed with a lock-in amplifier.

In the $x = 0.32$ samples, two broad luminescence bands are observed, as shown in Fig. 1. Two lightly p-type samples were studied, each grown by float-zone-refining polycrystalline HgCdTe, annealed in Hg vapor to reduce Hg vacancies, and doped with 10^{15} cm^{-3} Au atoms.[8] The composition of these samples was determined by measuring the photoconductivity cutoff wavelength for a sample cut from the same boule adjacent to the sample we studied.[8] The results of our experiments are similar for both our $x = 0.32$ samples.

The higher-energy line can be identified as a band-to-band transition by the variation in intensity with pump power, and energy shift with temperature. The peak intensity of the line divided by pump power increases as pump power is increased. As pump power is increased by a factor of 5, the ratio of intensity to pump power increases by 30% at 30 and by 100% at 4.8 K. The peak of the line shifts to higher energy as the temperature is increased. At all pump powers, the energy shift is 7.5 meV in going from ~ 5 to ~ 30 K, of which only ~ 4.5 meV is due to band-gap shift.[1] These observed properties are consistent with the interpretation of the line originating in a band-to-band transition.[5] The ratio of intensity to pump power increases with pump power because of the saturation of centers that bind carriers. The energy shift with temperature (over that caused by band-gap shift) comes about because higher-lying free-electron and hole states are filled as the temperature increases.

The lower-energy line in Fig. 1 has a different appearance and behavior from the higher-energy line. It is distinctly asymmetric, having a long low-energy tail. While the asymmetry is not particularly evident in the 9.2-K spectrum given in Fig. 1, the asymmetry is evident in lower-temperature spectra ($T \sim 5$ K) where the band-to-band line is less intense. This line is also wider than the higher-energy line, having a full width at half maximum of 13 as opposed to 7 meV. The intensity of this line does not increase with pump power as rapidly as the band-to-band line. The peak energy shifts like the band gap from 5 to 10 K, then shifts 2 to 4 meV (depending on pump power) more than band gap from 10 to 30 K.

These properties suggest that the lower-energy line is due to donor-to-acceptor luminescence[6] at low temperatures and is produced by a free electron recombining with a bound hole[7] at higher temperatures when the donors are ionized. The observed intensity variation with pump power supports the interpretation of the line as involving a bound hole: as the centers become saturated, both donor-to-acceptor and free-to-bound line intensities should decrease in relation to a free-to-free line intensity. The observed shift in energy of the line indicates a change from a transition involving only bound carriers at low temperature to one involving a free carrier at the higher temperatures studied. This change is indicated because, if the lower energy line is produced only by donor-to-acceptor luminescence, the line peak would shift at approximately the same rate as the band-gap energy as temperature is increased, for the entire temperature range.

In the $x = 0.48$ material, three luminescence lines (a spectrum is shown in Fig. 2) are observed in two of our samples. One of these samples is lightly p type, with 10^{16} cm^{-3} Au atoms.[8] The other is lightly n type, with 10^{15} cm^{-3} donors.[8] In the third $x = 0.48$ sample studied, only the low-and high-energy lines are observed. This sample is p type, with 10^{15} cm^{-3} Au atoms.[8] All three samples were grown using the solid-state recrystallization method, and were annealed in Hg vapor to reduce the concentration of Hg vacancies.[8] The composition of these samples was determined by the amount of the constituents put into the melt before it was quenched.[8]

The high-energy line is qualitatively similar to the corresponding line in the $x = 0.32$ material. The peak of the line shifts about 7 meV between 4.7 and 30 K in all samples of $x = 0.48$ material studied. As pump power is increased from

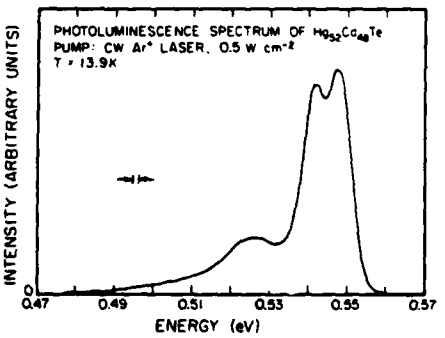

FIG. 2. Photoluminescence intensity vs energy of emitted photon for $Hg_{.52}Cd_{.48}Te$. The high-energy peak is attributed to a band-to-band transition. The low-energy peak is attributed primarily to donor-to-acceptor luminescence below ~ 10 K, and to band-to-acceptor luminescence at higher temperature. The intermediate-energy line is interpreted as bound-exciton recombination luminescence.

2 to 5 W cm^{-2}, the intensity of the line divided by the pump intensity increases by 30 to 100% (depending on temperature). This ratio of line intensity to pump intensity then stays the same, or decreases slightly as the pump power is increased to the highest pump power studied, 14 W cm^{-2}. These properties indicate that the line is produced by a band-to-band transition, for the same reasons given earlier for identifying the corresponding line in the $x = 0.32$ material.

The low-energy line in the $x = 0.48$ material is also similar to its counterpart in the $x = 0.32$ material. The line peak shifts to higher energy with increasing temperature above ~ 10 K, shifting 10 meV between 9.2 and 30 K at the lowest pump power, 2 W cm^{-2}. The peak does not shift with temperature below ~ 10 K, except for a small shift at the highest pump power studied. The ratio of the intensity of the low-energy line to the intensity of the high-energy line decreases with pump power, except that at 20 and 30 K the ratio increases as pump power is raised from 5 to 14 W cm^{-2}. Using the same argument given above for $x = 0.32$ material, we identify this line as donor-to-acceptor luminescence at low temperature, and free-to-bound luminescence at the higher temperature studied.

The intermediate-energy line appears only in some samples of the $x = 0.48$ material. The line peak does not shift with temperature to within 1 meV (the experimental uncertainty of the peak positions) between 4.6 and 18.8 K. Since the band gap for material of this composition shifts by less than 1 meV in this temperature range (Ref. 1, p. 29), the peak position is fixed with respect to the band gap for these temperatures. The line intensity falls off more rapidly with increasing temperature than either of the other lines, and is not visible in the spectra taken above 18.8 K. As pump power is increased, the line intensity increases at a rate that is slightly less than linear. The characteristics of this line suggests that it is produced by bound-exciton recombination. Since both the hole and electron are bound, the peak position should not change relative to the band gap with temperature. Also, the intensity should fall off rapidly with temperature as the centers are depopulated by thermal excitation of the excitons. Finally, the variation of intensity with pump power is also consistent with a bound-exiton interpretation, because the centers binding the exciton should saturate as the pump power is increased.

The position of this line is approximately that of donor–valence-band luminescence. There are several pieces of evidence that indicate that this is not the origin of the line. The most compelling argument is that donor–valence-band luminescence should shift to higher energies as the temperature is increased, and higher-energy hold states are occupied. Furthermore, the width is appropriate to a bound-exciton line. A donor–valence-band line should have a width of about 1 meV, while the observed line width is 6 meV, which is closer to the 4-meV width expected for a bound-exciton line.

The positions of the various lines provide donor and acceptor ionization energies. The difference in energy between the band-to-band line and the donor-acceptor line at zero temperature is a lower limit on the sum of the donor and acceptor energies. The acceptor energy is the difference between the band-to-band line and the band-to-acceptor line extrapolated to zero temperature. The overlap between the band-to-acceptor and donor-acceptor lines and errors associated with extrapolated to zero temperature cause some uncertainty in the procedure, but some limits may be estimated for the ionization energies. For the $x = 0.32$ material, the acceptor energy is 14.0 $\pm$ 1.5 meV, and for the donor, the ionization energy is less than 2 meV. For the $x = 0.48$ material, the two ionization energies are 15.5 $\pm$ 2 and 4.5 $\pm$ 2 meV, respectively. For comparison, the authors of Ref. 2 estimate values of acceptor ionization energy for $x \sim 0.3$ material of 13 meV from the luminescence data and 20 meV from the temperature dependence of the Hall data. For $x = 0.5$ material, they estimate 25 meV from luminescence measurements. While the agreement is not particularly good, the results are consistent with one another in light of the uncertainty involved.

In summary, we have shown spectra of near-band-gap photoluminescence from $Hg_{1-x}Cd_xTe$ with $x = 0.32$ and $x = 0.48$, and presented our interpretation of the origin of the lines. The $x = 0.32$ material shows two lines. The properties of the high-energy line are consistent with those for a band-to-band transition, and those of the low-energy line with donor-to-acceptor luminescence at low temperature and free-electron to bound-hole luminescence above ~ 10 K. The $x = 0.48$ material shows both these bands, which we interpret similarly, plus an additional line which we attribute to bound-exciton recombination.

The presence of the bound-exciton luminescence in the $x = 0.48$ material is consistent with the Osbourn-Smith calculation showing a radiative efficiency of 90% for the bound exciton in HgCdTe of this composition. The absence of a corresponding line in the $x = 0.32$ samples cannot be taken as conclusive evidence that bound-exciton luminescence does not occur in this material, since we do not observe bound-exciton luminescence in one of the $x = 0.48$ samples we have studied. It is therefore possible that other mechanisms are responsible for the absence of bound-exciton luminescence, such as overlap of the bound exciton with too many impurities. This overlap would be more likely in $x = 0.32$ than in $x = 0.48$ material, because the exciton radius is larger in the $x = 0.32$ material. However, the absence of the bound-exciton luminescence in the $x = 0.32$ samples is consistent with the Osbourn-Smith estimate of a much lower radiative efficiency of 20% for the bound exciton in that material.

We wish to acknowledge the valuable help of Dr. Peter Bratt of Santa Barbara Research Center, who provided us with samples, and Dr. L. H. DeVaux of the Hughes Research Laboratories, who gave us a number of useful suggestions on working with HgCdTe. This work was supported in part by AFOSR under Grant No. 77-3216.

[1]See, for example, R. Dornhaus, and G. Nimitz, in *Springer Tracts in Modern Physics, Vol. 78*, edited by G. Höhler (Springer, Berlin, 1976), pp. 1–112.
[2]C. T. Elliot, I. Melnagailis, T. C. Harman, and A. G. Foyt, J. Phys. Chem. Solids 33, 1527 (1972).
[3]V. I. Ivanov-Omskii, V. A. Mattseva, A. D Britov, and S. D. Sivachenko, Phys. Status Solidi (a) 46, 77 (1978).

[4]G. C. Osbourn and D. L. Smith, Phys. Rev. B 20, 1556 (1979).
[5]See, for example, R. J. Elliott, Phys. Rev. 108, 1384 (1957).
[6]See, for example, J. J. Hopfield, D. G. Thomas, and M. Gershenzon, Phys. Rev. Lett. 10, 162 (1963); D. G. Thomas, J. J. Hopfield, and W. M. Augustyniak, Phys. Rev. 140, A202 (1965); M. R. Lorentz, T. N. Morgan, and A. P. Pettet, in *Proceedings of the International Conference on the Physics of Semiconductors*, edited by S. M. Ryvkin (Nauka, Leningrad, 1968), p. 495.
[7]See, for example, D. M. Eagles, J. Phys. Chem. Solids 16, 76 (1960).
[8]Sample characterization and preparation were carried out at the Santa Barbara Research Center, Santa Barbara, Calif. [P. Bratt and R. Cole (private communication)].

Luminescence from HgCdTe alloys

A. T. Hunter, and T. C. McGill
California Institute of Technology, Pasadena, California 91125

(Received 9 February 1981; accepted for publication 28 May 1981)

We report the observation in $Hg_{1-x}Cd_xTe$ of band-to-band, band-to-acceptor, and donor-acceptor luminescence for material of $x = 0.32$ and 0.48, and bound exciton recombination luminescence, for material of 0.48. The band-to-band line shape and variation in intensity with pump power is appropriate to an electron-hole plasma with recombination proceeding without wave vector conservation. From line shape separations, we estimate acceptor binding energies of 14.0 ± 1.0 and 15.5 ± 2.0 meV in $x = 0.32$ and 0.48 material, respectively, and donor binding energies of 1.0 ± 1.0 and 4.5 ± 2.0 meV, respectively. Shifts in luminescence energy across the sample imply a change in composition across the sample of 0.03 cm^{-1}.

PACS numbers: 78.55.Ds, 71.45.Nt

I. INTRODUCTION

We have carried out a series of photoluminescence experiments on the important infrared detector material HgCdTe[1] as a probe of the near band-gap electronic states of the material. While these experiments can yield important information about the electronic and optical properties of HgCdTe, few experiments of this type have been reported in the literature.

Previous work on HgCdTe included both photoluminescence[2,3] and cathodoluminescence.[3] Two broad luminescence bands were observed, which were attributed to band-to-band and band-to-impurity transitions.[2,3] The impurity was thought to be Hg vacancies.[3] Acceptor ionization energies were estimated from luminescence and Hall data.[2] Temperature dependence of Hall measurements for $x = 0.32$ material indicated an acceptor with an activation energy of about 20 meV, but luminescence line separations gave acceptor ionization energies of 25 meV in the $x = 0.5$ material, and as low as 10 meV in $x \sim 0.3$ material.[2] Another group has done some additional Hall work, taking compensation into account, and checked their resulting acceptor energies by doing far IR photoconductivity.[4] These measurements yield an acceptor binding energy $E_A = 14.0 \pm 1.0$ meV for material with $x = 0.4$.[4] Previous theoretical work relevant to our experiments includes a calculation of the radiative efficiency of bound exciton luminescence in HgCdTe by Osbourn and Smith.[5] Their calculation suggests radiative decay of bound excitons should dominate nonradiative Auger decay in HgCdTe material with x greater than ~ 0.4.

In our experiments, which we have summarized elsewhere,[6] we observed band-to-band, band-to-acceptor and donor-to-acceptor, and bound exciton recombination luminescence. Our experiments were performed on samples of $x = 0.32$ and 0.48, for temperatures less than 30 K, and for excitation densities between 0.3 and 14.0 W cm^{-2}. Three samples of $x = 0.48$ material were studied, two p type and one n type, and two samples of $x = 0.32$ material were studied, both p type.

In this paper, we present a complete description of our data, and the results of our analysis of the data. We analyze line shapes and line shifts with temperature and pump power, which provide us with information on the exact nature of the transitions, and on the densities of initial and final state.

The remainder of this paper is organized as follows. The experimental apparatus and samples are discussed in Sec. II. Next, the results and analysis are presented in Sec. III. Finally, a summary of the results is presented in Sec. IV.

II. EXPERIMENT

The experiment will be described briefly. Samples were immersed in liquid helium or cold helium gas in a Janis research Dewar. A temperature sensor and heater mounted near the sample on the sample arm allowed temperature control. Excitation was provided by a mechanically chopped cw Ar^+ ion laser (the chopping produced a duty factor of $\sim 50\%$), focused onto the sample with a spot diameter of about 1 mm. The average power densities for the data presented here varied between 0.3 and 14.0 W cm^{-2}, although we were able to get power densities of up to 2 KW cm^{-2} by increasing the laser power and focusing the laser spot down to a few tenths of a millimeter. Luminescence from the sample was collected by BaF_2 lenses and analyzed with a Spex 1269 or 1400 spectrometer. The slit width of the spectrometer was chosen to give energy resolution of about 1 meV in the photoluminescence spectra. The signal was detected with an InAs detector for the $x = 0.48$ material, and an InSb detector for the $x = 0.32$ material. The signal was processed with a lock-in amplifier.

Characterizing the sample impurity concentrations is important because some of the observed luminescence is impurity related. The samples were obtained from Santa Barbara Research Center, and we report the sample descriptions they furnished us.[7] Both $x = 0.32$ samples were grown by float zone refining of polycrystalline HgCdTe. After the crystals were sliced, they were gold plated and annealed in Hg vapor. This process doped the crystals with Au and reduced the number of Hg vacancies. The acceptor concentration in both of the processed crystals is about 10^{15} Au cm^{-3}. The $x = 0.48$ crystals were grown by the solid-state recrystallization method. Two of the samples were treated as described above, and have an acceptor concentration of 10^{15} and 10^{16} Au cm^{-3}, respectively. The third was not gold plated before it was annealed in Hg vapor, and the result is an n-

 0021-8979/81/095779-07$01.10

type sample with 10^{15} cm^{-3} residual donors. For the p-type samples, the acceptors are either Au substitutional atoms or Hg vacancies.

III. RESULTS AND DISCUSSION

A. Band-to-band line

The highest energy line in both the $x = 0.48$ and $x = 0.32$ material is attributed to a band-to-band transition. The peak at the highest energy in Fig. 1 shows this line in the 0.48 material, for several temperatures, and the peak at the highest energy in Fig. 2 presents similar data for $x = 0.32$ material. The qualitative features that characterize the line are the shift of the line to higher energy as temperature is increased, and the superlinear increase in intensity of the line as pump power is increased. The shift as temperature is increased implies that free carriers are involved in the transition. The superlinear increase in line intensity with pump power comes about because the band-to-band transition probability depends on the product of hole and electron concentrations, both of which increase as pump power is increased. Another factor suggesting that this transition is band-to-band is that no luminescence is observed with higher photon energy. In the remainder of this section we will first describe these observations in detail, then we will discuss a model for the transition that explains most of the data.

Figures 1 and 2 both clearly show the high-energy luminescence band shifts toward higher energy as temperature is increased. This information is summarized for several pump powers in Figs. 3 and 4. In both figures, energy of the line peak is plotted against temperature, with the points for a given luminescence band at one pump power connected as an aid to the eye. Figure 3 shows this data for $x = 0.48$ material. The top three curves, labeled band-to-band, show the behavior of this line for three different pump powers. The

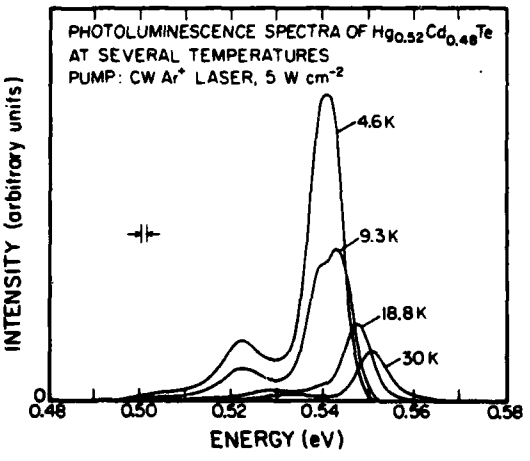

FIG. 1. Spectra of $Hg_{0.52}Cd_{0.48}Te$ showing photoluminescence intensity vs photon energy with the sample at 4.6, 9.3, 18.8, and 30 K, respectively. The high-energy peak is due to band-to-band recombination, the low-energy peak is due to donor-acceptor recombination at low temperature, and to band-to-acceptor luminescence above ~ 10 K. The intermediate energy line (shown most clearly in the 9.3 K spectrum) is due to bound exciton recombination. The sample was p type, with $N_A - N_D \sim 10^{16}$ cm^{-3}.

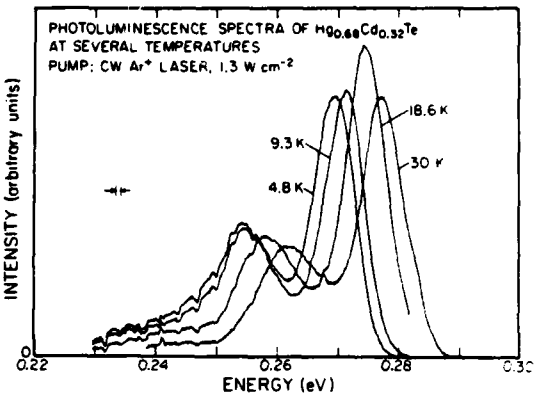

FIG. 2. Spectra of $Hg_{0.68}Cd_{0.32}Te$ showing photoluminescence intensity vs photon energy with the sample at 4.8, 9.3, 18.6, and 30 K, respectively. The high-energy peak is due to band-to-band recombination, and the low-energy peak is due to donor-acceptor recombination at low temperatures, and to band-to-acceptor recombination above ~ 10 K. The structure seen mostly on the lower-energy peak is due to atmospheric water vapor absorption. The sample was p type, with $N_A - N_D \sim 10^{15}$ cm^{-3}.

slope of each of these curves is approximately $3\,k_B$, where k_B is Boltzmann's constant, 0.0862 meV K^{-1}. The top three lines in Fig. 4 also yield a slope of approximately $3\,k_B$, for the shift of the band-to-band line in $x = 0.32$ materials.

The band-to-band intensity increases rapidly as pump power increases. In material of both compositions, the rate of increase is faster than linear at most temperatures and pump powers for which measurements were made. In the $x = 0.48$ material at 30 K (where the results are not complicated by overlap with the bound exciton line), the band-to-band intensity increases by a factor of 4 when pump power is increased by ~2.5. In the $x = 32\%$ material, the intensity at 5 K increases by a factor of 9 when pump power is increased by a factor of 5. (Although at 30 K in this sample, the increase is down to slightly sublinear with pump power.) So over the range of temperatures and pump powers for which we took data, the rate of increase of the band-to-band line intensity ranged from slightly sublinear to superlinear, but always less rapidly than the square of the pump power.

The model for the transition that best accounts for the

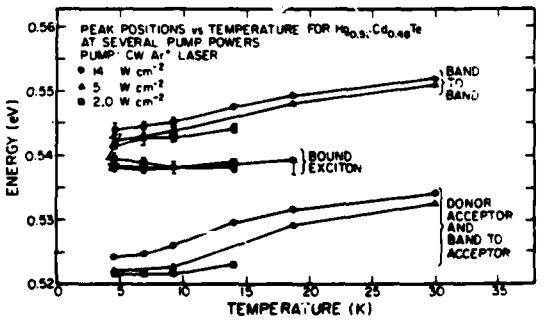

FIG. 3. Summary of luminescence-band peak energies vs temperature of $Hg_{0.52}Cd_{0.48}Te$ at three different pump powers for the sample of Fig. 1. The lines between data points are drawn as a visual aid, and connect points measured at different temperatures for one type of luminescence band at one pump power. Error bars are given where significant; the uncertainty is due to overlap between bands.

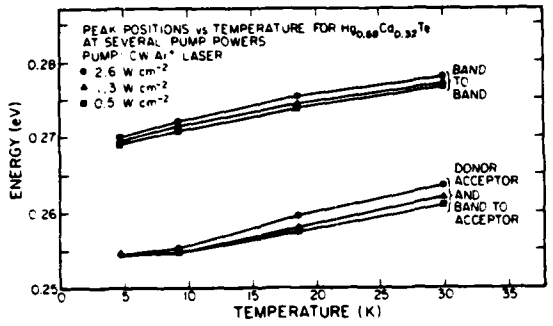

FIG. 4. Summary of luminescence-band peak energies vs temperature of $Hg_{0.68}Cd_{0.32}Te$ at three different pump powers for the sample of Fig. 2. The lines between data points are drawn as a visual aid, and connect points measured at different temperatures for one type of luminescence band at one pump power.

shape, peak shift, and intensity variation of the line, is that the free carriers act as an electron-hole plasma, with recombination proceeding without wave-vector conservation. Under the assumptions of our model, an electron-hole droplet like line shape[8] results:

$$I(\hbar\omega)\alpha\int_0^{(\hbar\omega - E_g)} d\epsilon \times \frac{\epsilon^{1/2}(\hbar\omega - \epsilon - E_g)^{1/2}}{[1+e^{(\hbar\omega - \epsilon - E_g - \mu_h)/k_BT}][1+e^{(\epsilon-\mu_e)/k_BT}]}, \quad (1)$$

where $I(\hbar\omega)$ is luminescence intensity at photon energy $\hbar\omega$, E_g is band-gap energy, μ_e and μ_h are electron and hole chemical potentials, respectively, and k_BT is Boltzmann's constant times the sample temperature. This equation fits the high-energy line fairly well at 20 and 30 K, although it is somewhat too narrow for the data at lower temperatures. However, the width of the lines observed at lower temperatures is approximately that which would be produced by compositional variation across the width of the pump beam. This compositional broadening was not included in the theoretical line shapes; however, if it were included, the line shape predicted by the model would probably agree with the data over the entire temperature range.

Figure 5 shows the result of a fit at 30 K for one spectrum of the $x = 0.48$ material. Band-gap energy and carrier density were varied to obtain the fit, with inputs being temperature ($T = 30$ K, the bath temperature in the experiment) and electron and hole effective masses ($m_e = 0.04$, $m_h = 0.5$, from Ref. 1). The agreement between theory and data, while not exact, is much better than could be obtained for different models, such as for an exciton gas, or an electron-hole plasma in which recombination proceeds with wave-vector conservation. Furthermore, the carrier density, which is the only variable that affects the shape of the predicted line, is not an entirely free parameter, since it can be estimated from the pump-laser power density. The accuracy of the fit is not seriously diminished for any carrier density within the range consistent with pump power. Therefore, the agreement in shape shown in Fig. 5 is almost entirely due to the model and measured material and experimental parameters.

The model can account for most of the large peak shift that is observed in the data as temperature is changed. In the nondegenerate limit (high temperature and low density, which is approximately valid for this experiment), Eq. (1) can be integrated analytically to give

$$I(\hbar\omega) = \tfrac{1}{4}(\hbar\omega - E_g)^2 e^{-(\hbar\omega - E_g)/k_BT} e^{(\mu_e + \mu_h)/k_BT}. \quad (2)$$

The maximum of this line shape occurs at $\hbar\omega = E_g + 2k_BT$, so as temperature is increased, the maximum shifts to higher energies at a rate equal to $2k_B$. This shift is smaller than the $3k_B$ observed experimentally, but there are several mechanisms which can provide additional peak shift.

The first source of additional shift is that the band gap may shift slightly in the temperature range covered. Above 20 K, the shift has been measured by other groups to be linear with temperature, and is ~ 0.2 meV K^{-1} for the $x = 0.32$ material, and less than 0.05 meV K^{-1} for $x = 0.48$ material.[1,9,10] Data are not available for lower temperatures; hence, we have had to estimate the shift at temperatures below 20 K. For many semiconductors, the rate of band-gap shift with temperature decreases below 20 K.[11] Therefore, the high-temperature values for the rate of shift are likely to be either reasonable approximations to the band-gap shift, or upper limits to it. Using the values at 20 K we estimate a band-gap shift between 5 and 30 K (the range over which we took data) of less than 4.5 meV for the $x = 0.32$ material, and less than 1 meV for the $x = 0.48$ material. While band-gap shift and line shift as predicted by Eq. (2) could account for all the observed shift of the line-peak energy with temperature in $x = 0.32$ material, we need to account for an additional 2 meV of shift in the 0.48 material. Since this remaining discrepancy is probably larger than the error bars on the measurement, we suggest one final source of additional shift. The peak shift of $2k_B$ assumes a constant carrier density as temperature is changed. This, however, is not quite true since the hole density increases as acceptor atoms become thermally ionized. This increase in free-carrier density can contribute a small shift of the band-to-band line to higher energy. However, while these two mechanisms, together

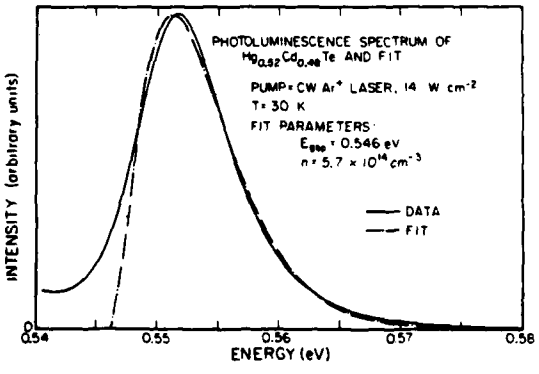

FIG. 5 Photoluminescence spectrum of the high-energy peak of $Hg_{0.52}Cd_{0.48}Te$ for the sample of Fig. 1, and a fit to the data. The fit is appropriate to an electron-hole plasma recombining without wave-vector conservation. Three parameters, the carrier density, band-gap energy, and peak intensity, were varied to obtain the fit. The temperature used in the expression for the line shape was 30 K, and electron and hole masses used were $0.04m_e$ and $0.5m_e$, respectively.

with the peak shift predicted by our model, can account for all the peak shift observed in $x = 0.32$ material, they may predict a shift slightly smaller than the shift observed in the $x = 0.48$ material.

The superlinear increase of line intensity provides additional evidence for a band-to-band transition of the type discussed earlier, which can be seen by some simple rate equation arguments. The band-to-band transition probability can be written as $n_e \cdot n_h \cdot A$, where n_e and n_h are the free-electron and hole concentrations, respectively, and A is a constant independent of temperature and pump power. Since both n_e and n_h increase with pump power, a superlinear increase of the product is expected. In contrast, recombination in an exciton gas would display at most a linear dependence on pump power.

All of the models for the transition considered assume parabolic band edges, which in turn predict a sharply defined absorption edge. It is possible that the band-edge electronic states are not well defined by this simple model, however, because the absorption edge for HgCdTe is fit by a modified Urbach tail in HgCdTe with a composition of $x \sim 0.2$.[12] This exponential turn on may be a reflection of compositional inhomogeneities on the macroscopic scale discussed earlier or, if the fluctuations are on a scale small enough that electric field gradients are significant on a microscopic scale, an entirely different calculation of band-to-band recombination should be considered.[13] These processes were not included in any of our attempted fits of the band-to-band line shape.

B. Electron-to-bound hole band

The low-energy peak, observed in all the spectra at all temperatures, is produced by electrons recombining with holes bound to acceptors, processes which have been extensively investigated in other materials.[14,15] The leftmost band in Fig. 1 shows this luminescence in $x = 0.48$ material, at several temperatures, and Fig. 2 shows similar data for $x = 0.32$ material. The same qualitative behavior is demonstrated in material of each composition. The peak position does not change in going from ~ 5 to ~ 10 K, then shifts substantially from 10 to 30 K. At the lowest temperatures studied, the electrons are bound to donor atoms, but at higher temperatures (above about 10 K), most of the donors are thermally ionized (donor binding energies are estimated to be approximately 2 and 3.5 meV for $x = 0.32$ and 0.48 material, respectively, from the hydrogenic model[1]) and the luminescence is caused by conduction-band electrons recombining with bound holes. The presence of a significant donor-acceptor luminescence line indicates the material is compensated, although the degree of compensation is difficult to estimate.

The shape of the line is similar in both materials, with a long tail on the low-energy side. On spectra taken at lower pump power, in which the band-to-band line is not as prominent, the low-energy line clearly appears asymmetric, with the high-energy edge falling off much more sharply than the low-energy side. This impurity related line is somewhat broader than the higher-energy band-to-band line. There are several reasons for the breadth. The first is that the energy of luminescence depends on the distance between the impurities, since part of the line is due to donor-acceptor recombination. The second is the Urbach tail behavior mentioned earlier for the absorption edge in HgCdTe, which can also produce tails on band related luminescence lines. This is probably the origin of the long low-energy tail seen in all the spectra. Finally, the impurities see a distribution of environments since, instead of being in a perfect lattice, they are in an alloy. Smith[16] has calculated that this would give a width of about 10 meV to an acceptor level. (The corresponding broadening for a donor level would be much smaller, simply because the donor binding energy itself is so small.) These broadening mechanisms are responsible for the fact that the low-energy threshold of the bands is not $E_g - E_A - E_D$ (E_A and E_D are the acceptor and donor binding energies, respectively), corresponding to luminescence produced by donor-acceptor pairs at infinite separation. The luminescence tail extends much farther to low energy than could be accounted for by reasonable estimates of the impurity ionization energies. Because of this long low-energy tail, and the overlap with the band-to-band line on the high-energy edge, we did not attempt a fit of this line.

The shift of the peak with temperature provides most of the information needed to understand the origin of the luminescence, however. The shift in the peak position of this line is caused by somewhat different mechanisms than for the band-to-band line. Figures 3 and 4 show the shift in the peak position of this line as a function of temperature for several pump powers. The most important feature of this shift is that it is not uniform with temperature, and does not shift significantly below 10 K, for any pump power. The peak position then shifts rapidly above 10 K. This sudden shift is consistent with a change from a transition involving mostly bound electrons recombining with the bound hole to a transition involving free electrons. The band-to-acceptor line by itself should shift with $\sim \frac{1}{2} kT$ in addition to band-gap shift,[15] since in this case the shift is caused by the thermal excitation of only one of the particles, the electron. The lower curves on Figs. 3 and 4 indicate it may shift somewhat more than this, but much of the excess shift is probably explained by the ionization of the electron.

Since this low-energy line is impurity related, it should decrease in intensity relative to the higher-energy band-to-band line as pump power is increased. This can be seen by again referring to our simple rate equation model. As mentioned earlier, the band-to-band probability goes as $n_e \cdot n_h \cdot A$. The band-to-acceptor probability goes as $n_e \cdot N_A^* \cdot B$, where N_A^* is the number of neutral acceptors and B is another constant. At the low temperatures of this experiment, with the ~ 15 meV acceptor ionization energy, almost all of the acceptors are neutral: from model rate equation calculations we estimate N_A^* does not change by more than 10% in the temperature range studied. Therefore, the ratio of band-to-band to band-to-acceptor intensity should go as $\sim$ constant n_h, which increases with pump power. This is the behavior observed in the experiment. For $x = 0.32$, the ratio increases by 25–100% (depending on temperature) as pump power is increased by a factor of 5. For $x = 0.48$, the situation is complicated by overlap with the bound exciton line, but the re-

sults are qualitatively similar.

Donor and acceptor ionization energies can be estimated from the separation between the peaks of the luminescence lines. Overlap between lines and low-energy tails make it impractical to use the low-energy thresholds for determination of these energies. However, allowing for the estimated linewidths, we can give limits for the donor and acceptor binding energies. We have estimated the donor binding energy to be 1.0 ± 1.0 meV in $x = 0.32$ material, and 4.5 ± 2.0 meV in $x = 0.48$ material. For acceptors, the corresponding energies are 14.0 ± 1.5 meV and 15.5 ± 2.0 meV. This agrees approximately with the values listed in Ref. 2: the authors estimate values of the acceptor ionization energy for $x \sim 0.3$ material of 13 meV from the luminescence data and 20 meV from Hall data. For $x = 0.5$ material, they estimate 25 meV from luminescence measurements. Our values agree very closely with a more recent estimate of E_A from temperature dependence of Hall data which included the effect of compensation.[4] They checked their estimate of E_A by doing far infrared photoconductivity measurements, and deduced 14.0 ± 1.0 meV for $x = 0.4$ material.[4]

C. Bound exciton

The last luminescence line we observe has the characteristics of bound exciton luminescence. The 9.3-K spectrum in Fig. 1 shows this third line fairly clearly. On the 4.6 K spectrum, it overlaps the band-to-band line and is difficult to identify. Also, the intensity has dropped sufficiently to make it difficult to resolve on the 18.8 K sample. This intermediate energy line was seen only in two out of three $x = 0.48$ samples, the p-type 10^{16} cm^{-3} sample and the n-type 10^{15} cm^{-3} sample. It was not seen in the other $x = 0.48$ sample (p-type, 10^{15} cm^{-3}), nor in either of the $x = 0.32$ samples.

Since the line was not seen in all of the $x = 0.48$ samples studied, composition was not the only factor that determined whether or not the line was observed in the luminescence spectrum. However, there are two reasons to expect a bound exciton line should be easier to observe in material of higher composition. The first involves the lifetime expected for bound excitons in this material. Osbourn and Smith[5] have performed a calculation showing that for material of low x (small Cd concentration), the Auger lifetime is shorter than the radiative lifetime for bound excitons, and therefore the radiative efficiency of the excitons should be low. On the other hand, for material of high x, the opposite is true, and bound excitons in high x material should have a high radiative efficiency. The crossover point occurs at $x \sim 0.4$. According to their calculation, the radiative efficiency for a bound exciton in $x = 0.48$ material is 90%, compared to an efficiency of 20% in $x = 0.32$ material, for which we observe no bound exciton luminescence. A second factor which would also make it less likely to observe a bound exciton in $x = 0.32$ material is that the exciton bohr radius is somewhat larger in this material than in the $x = 0.48$ material. This means that, for a fixed impurity concentration, the exciton would overlap more impurities in the $x = 0.32$ material than in the $x = 0.48$ material.

Figure 3 shows the shift in the peak position of the bound exciton as a function of temperature for several different pump powers. As can be seen from the spectra shown in Fig. 1, the bound exciton line is difficult to resolve from the band-to-band line. Although it is more clearly resolved at other pump powers and temperatures, it was necessary to use a fitting routine to determine the position of the lines when they overlapped substantially. For this purpose, we used a two Gaussian fitting routine, and did not attempt to fit the tails of the lines. Although this procedure obviously did not reproduce the exact shape of the lines, it did allow us to obtain reasonable estimates of the position of the lines. The error bars reflect a range of positions for the peaks that gave reasonable fits. To within the accuracy of our measurements, then, the line does not shift as either pump power or temperature is changed. This is an important piece of evidence indicating the line is a bound exciton line, since the carriers must be bound if the energy of the luminescence does not shift as temperature is raised.

The width of the line also supports the bound exciton interpretation of the luminescence. Figure 6 shows spectra taken on a different $x = 0.48$ sample in which the bound-exciton line was much more intense than the band-to-band line at the lowest temperature studied. In this case, the impurity concentration was high enough, and pump power low enough, that most available electrons and holes could become bound to impurity centers before recombination, rather than recombine as free carriers. These data, therefore, allow an unambiguous determination of the linewidth. We determined the width to be 6 meV from the 4.8-K spectrum shown in Fig. 6. This agrees with the width of ~ 5 meV for bound-exciton recombination luminescence calculated by Smith[16] taking into account the broadening induced by the distribution of environments around the acceptors.

Finally, the drop in intensity and position of this intermediate energy line are characteristic of a weakly bound state. At low temperatures, the line is only 2- or 3-meV below the band-to-band line, indicating an ionization energy of this magnitude. The rapid decrease in intensity of the line with respect to both of the other lines also indicate that the ioniza-

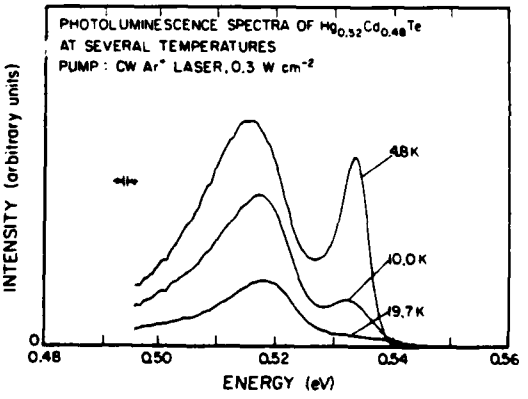

FIG. 6. Spectra of $Hg_{0.52}Cd_{0.48}Te$ showing photoluminescence intensity vs photon energy with the sample at 4.8, 10.0, and 19.7 K, respectively. These spectra are for a different sample (n type, $N_D - N_A \sim 10^{15}$ cm^{-3}), and were taken at lower pump power than the spectra in Fig. 1. The band-to-band line is not visible at these temperatures, and the high-energy line is due entirely to bound exciton recombination luminescence.

tion energy is small. The only other possibility beside the bound exciton is a free hole recombining with a weakly bound electron. This possibility is eliminated by the lack of shift of the line with temperature mentioned above.

D. Laser-induced damage

High intensity laser irradiation was found to damage one of the samples. Surface damage occurred while irradiating the sample with an estimated 2 kW cm^{-2} continuous laser beam, while the sample was in contact with a sample block at 5 K. The damage occurred suddenly, as indicated by a sudden loss of luminescence signal. The sample so damaged had a small pit of approximately the same size as the laser beam (about 0.1-mm radius) with a depth of about 0.1 mm.

E. Spatial variations in band gap

The samples we studied showed a concentration gradient from one side of the wafer to the other. Since the concentration determines the band gap, the change in concentration was reflected in a shift of the luminescence lines in energy. Figure 7 shows typical luminescence data for a sample of $x = 0.32$ material. The three different spectra were collected under identical conditions, except that the sample was moved with respect to the pump laser and spectrometer, so that the luminescence came from a different part of the sample in each case. Assuming that all of the shift in luminescence energy was caused by band-gap shift, and using published fits relating band-gap energy to composition,[1] a change in composition of 0.03 cm^{-1} is implied. This means that luminescence experiments can provide a fairly sensitive means of monitoring compositional changes across the surface of HgCdTe wafers. The position of the luminescence lines in our spectra can be determined to within about $\pm$ 1.0 meV, which would allow a resolution of $\pm$ 0.0006 for measurement in a compositional change from one point to another. Some additional uncertainty would be added to the measurement because of uncertainty in the relationship between composition and band gap. The formulas compiled in Ref. 1 give a spread of 15% in the compositional changes implied by a given band-gap shift.

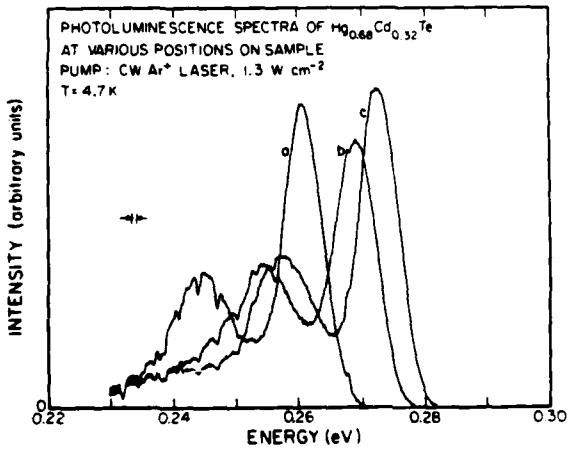

FIG. 7. Spectra of $Hg_{0.68}Cd_{0.32}Te$ showing photoluminescence intensity vs photon energy for the sample of Fig. 2. For spectrum b, the pump laser was 0.04 in. above its position for spectrum a, and for c, 0.10 in. above its position for spectrum a. The shift in energy between a and c implies a shift in composition of 0.03 cm^{-1}.

The compositional gradient may have contributed to the width of the luminescence lines, since the spot size of the pump laser was several millimeters in diameter. A 2-mm spot causes a 4-meV linewidth because of the gradient alone. This should be regarded as a lower limit on the width, however, since the gradient was measured over a distance of many millimeters and implies nothing about local, but still macroscopic, fluctuations in composition, which could contribute even more to the linewidth.

IV. SUMMARY

In this paper we have described our observations of luminescence spectra of $Hg_{1-x}Cd_xTe$, for $x = 0.32$ and 0.48. We observed band-to-band, band-to-acceptor, donor-acceptor, and bound exciton recombination luminescence.

The band-to-band line shape, and variation of intensity with pump power, implies an electron-hole plasma in which recombination proceeds without wave-vector conservation. This model for band-to-band recombination has been used successfully to explain the gain spectrum of GaAs,[17,18] where free-carrier and impurity scattering are large enough to relax the wave-vector selection rules. The model should apply to HgCdTe, but perhaps for slightly different reasons. The impurity and carrier concentrations are somewhat lower in the HgCdTe samples than in the GaAs lasers considered in Refs. 17 and 18. In the alloy the random fluctuations in concentration can also act as scattering centers for electrons,[19] and so lead to relaxation of the wave-vector selection rules. However, the major justification for invoking recombination without wave-vector conservation is that it helps to explain the large shift of this line with temperature, and can fit the shape of the line for the higher-temperature spectra. Other mechanisms, not considered in this paper, may also fit the available data. Therefore, the analysis presented here, especially the detailed model proposed, should be regarded as somewhat tentative until the assumptions can be checked against further data.

We have estimated donor and acceptor ionization energies from our luminescence data. For E_A, we estimate 14.0 ± 1.5 meV for $x = 0.32$ material and 15.5 ± 2.0 for $x = 0.48$ material. The acceptor is probably either a Au substitutional atom or alloy vacancy. This agrees well with values obtained from IR photoconductivity data and temperature dependence of Hall measurements in which compensation was taken into account.[4] We estimate $E_D = 1.0 \pm 1.0$ and 4.5 ± 2.0 meV in $x = 0.32$ and $x = 0.48$ material, respectively, which is consistent with values calculated in the hydrogenic model.[1] The identity of the donor is unknown. The presence of the donor-acceptor luminescence band indicates our samples are compensated.

The observation of the bound exciton luminescence in the $x = 0.48$ material is consistent with the calculation by Osbourn and Smith[5] showing a radiative efficiency of 90% for the bound exciton in HgCdTe of this composition. We did not observe the line in $x = 0.32$ material, although this

does not mean bound excitons do not occur in this material, since we did not see the bound exciton line in one of the $x = 0.48$ samples. However, the absence of the line in $x = 0.32$ material is consistent with the Osbourn–Smith estimate of a much lower radiative efficiency of 20% for bound exciton recombination in that material.

Finally, luminescence could be utilized as an easy, nondamaging means of monitoring compositional changes across the surface of a HgCdTe wafer. The area sampled can be made essentially as small as the spot size of the pump laser. Unlike an absorption measurement, it can be made on a sample of any thickness. Finally, the technique yields very reasonable signals at laser pump power densities two or three orders-of-magnitude below a power density that would damage the material. This is not necessarily true for techniques that use electron beams as a probe of Hg and Cd concentrations.

ACKNOWLEDGMENTS

We would like to acknowledge the valuable help of Dr. P. Bratt of the Santa Barbara Research Center, who provided us with samples, Dr. L. H. De Vaux of the Hughes Research Laboratories, who gave us a number of useful suggestions on working with HgCdTe, and D. L. Smith, who aided us with numerous discussions on the interpretation of our data. This work was supported in part by AFOSR under Grant No. 77-3216.

[1]See, for example, R. Dornhaus, and G. Nimtz in *Springer Tracts in Modern Physics*, edited by G. Höhler (Springer, Berlin, 1976), Vol. 78, pp 1–112.
[2]C. T. Elliot, I. Melngailis, T. C. Harman, and A. G. Foyt, J. Phys. Chem. Solids **33**, 1527 (1972).
[3]V. I. Ivanov-Omskii, V. A. Mattseva, A. D. Britov, and S. D. Sivachenko, Phys. Status Solidi A **46**, 77 (1978).
[4]W. Scott, E. L. Stelzer, and R. J. Hager, J. Appl. Phys. **47**, 1408 (1976).
[5]G. C. Osbourn and D. L. Smith, Phys. Rev. B **20**, 1556 (1979).
[6]A. T. Hunter, D. L. Smith, and T. C. McGill, Appl. Phys. Lett. **37**, 200 (1980).
[7]P. Bratt and R. Cole (private communication).
[8]Ya. E. Pokrovsky, Phys. Status Solidi A **11**, 385 (1972).
[9]M. W. Scott, J. Appl. Phys. **40**, 4077 (1969).
[10]J. L. Schmit and E. L. Stelzer, J. Appl. Phys. **40**, 4865 (1969).
[11]Y. P. Varshni, Physica (Utrecht) **34**, 149 (1967).
[12]E. Finkman and Y. Nemirovsky, J. Appl. Phys. **50**, 4356 (1979).
[13]J. D. Dow and D. Redfield, Phys. Rev. B **1**, 3358 (1970).
[14]See, for example, J. J. Hopfield, D. G. Thomas, and M. Gershenzon, Phys. Rev. Lett. **10**, 162 (1963); D. G. Thomas, J. J. Hopfield, and W. M. Augustyniak, Phys. Rev. A **140**, 202 (1965); M. R. Lorentz, T. N. Morgan, and A. P. Pettet, in *Proceedings on the Physics of Semiconductors*, edited by S. M. Ryvkin (Nauka, Leningrad, 1968), p. 495.
[15]See, for example, D. M. Eagles, J. Phys. Chem. Solids **16**, 76 (1960).
[16]D. L. Smith (private communication).
[17]G. Lasher and F. Stern, Phys. Rev. A **133**, 553 (1964).
[18]E. Göbel, Appl. Phys. Lett. **24**, 492 (1974).
[19]L. Makowski and M. Glicksman, J. Phys. Chem. Solids **34**, 487 (1973).

Experimental investigation of the infrared absorption saturation in p-type germanium and silicon

R. B. James,[a] Edgard Schweig, D. L. Smith,[b] and T. C. McGill
California Institute of Technology, Pasadena, California 91125

(Received 12 October 1981; accepted for publication 17 November 1981)

We investigate the room-temperature absorption saturation of p-Ge and p-Si for several samples over a range of doping densities for light having wavelengths of 10.6 and 9.6 μm. The transmission data can be fairly well described using an intensity dependent absorption coefficient characteristic of an inhomogeneously broadened two-level system. Measurements of the saturation intensity of p-Ge show that I_s increases monotonically with increasing hole concentration, and that the resonant transition is significantly easier to saturate in p-Ge than in p-Si for the samples we examined.

PACS numbers: 42.65.Bv, 78.20.Dj, 78.20. – e

In this letter we study the dependence of the absorption saturation in p-type germanium and silicon on the doping density for wavelengths in the 10-μm region. It has previously been observed that the absorption of light saturates in p-Ge[1-5] and p-Si[1] at CO_2 laser wavelengths. This nonlinear behavior in p-Ge has been exploited for generating passively mode-locked CO_2 laser pulses of subnanosecond duration,[6-8] and to provide interstage isolation of high-power oscillator-amplifier stage of CO_2 laser systems.[2] The main advantages of using a p-type semiconductor, such as Ge, over other saturable absorbers are the picosecond recovery time and the broadband performance under saturation conditions.

The dominant absorption mechanism in p-Ge at room temperature for light having a wavelength of about 10 μm has been shown to be direct transitions between the heavy- and light-hole bands.[9] For p-Si, the spin orbit splitting is less than the photon energy for $\lambda \sim 10\,\mu$m so that direct intervalence-band transitions are energetically allowed between the heavy- and light-hole bands, the heavy- and split-off hole bands, and the light- to split-off hole bands. In addition, the absorption of light by the creation of phonons is much larger in Si than Ge for the wavelengths we consider, consequently, the residual or nonsaturable absorption is much larger in Si than Ge.

The absorption due to the direct intervalence-band transitions is saturable, where the decrease in the absorption coefficient with increasing intensity is approximately given by an inhomogeneously broadened two-level model, where

$$\alpha(I,\omega) = \frac{\alpha_0(\omega)}{[1 + I/I_s(\omega)]^{1/2}}. \tag{1}$$

Here, $\alpha_0(\omega)$ is the absorption coefficient due to the intervalence-band transitions at low intensity and $I_s(\omega)$ is the saturation intensity. This intensity dependence in the absorption has been found to be well satisfied experimentally for p-Ge, and values of the saturation intensity have been reported.[2-4] In these papers, the saturation intensity was determined for rather low doping densities ($N_A \lesssim 3\times10^{15}$ cm^{-3}). Here we present a systematic study of the dependence of I_s on the doping density in p-Ge.

A theory describing the absorption saturation of p-Ge has been presented which realistically accounts for the anisotropic and nonparabolic valence bands and which is in close agreement with experiments.[10] In the calculation only the carrier-phonon scattering was included in determining the modification of the hole distribution by the high intensity light. For those temperatures and hole densities for which carrier-phonon scattering dominated the carrier relaxation ($N_A \lesssim 3\times10^{15}$ cm^{-3} at room temperature), the calculated values for I_s were independent of the hole concentration. In a subsequent paper,[11] the theory was modified to include the interaction of the hole carriers with ionized impurities and other free holes. The results of the calculation were that for hole concentrations such that hole-impurity and hole-hole scattering rates were non-negligible compared to hole-phonon scattering (i.e., $N_A \gtrsim 3\times10^{15}$ cm^{-3} at room temperature), the saturation intensity increases monotonically with increasing doping density. A similar dependence of I_s on the doping density is expected for p-Si; however, due to the larger hole-phonon scattering rate in Si, the dependence of I_s on N_A would most likely require more heavily doped samples to be observable. In this letter we experimentally investigate the saturation behavior of p-Ge and p-Si for several samples with different hole concentrations for light at 10.6 and 9.6 μm.

The transmission experiment is shown schematically in Fig. 1. The saturating laser was a transversely excited CO_2 laser at atmospheric pressure operating with a TEM_{00} output. The wavelength was controlled by an internal grating which allows a tunable output over the 9–11-μm region. The output energy of about 0.6 J was reproducible to within 1–2% from shot to shot. The output pulse has about 50% of the energy in the form of a spike with a pulse width full width at half-maximum (FWHM) of about 40 ns. The remainder of the energy is in a long tail of relatively low power density which lasts about 0.4 μs (depending on the N_2 mix). An iris was used to isolate the central portion of the Gaussian beam in order to minimize the spatial variation of the beam. The

[a]Present address: Solid State Division, Oak Ridge National Laboratory, Oak Ridge, TN 37830.
[b]Present address: Honeywell Systems and Research Center, Minneapolis, MN 55413.

 0003-6951/82/030231-03$01.00

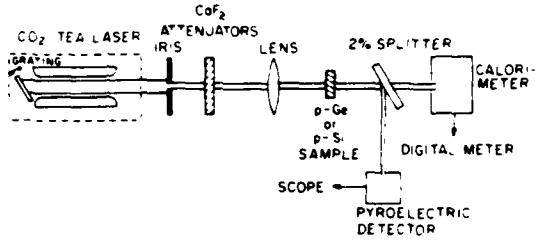

FIG. 1. Experimental setup for the absorption saturation measurements.

power density was controlled by using calibrated CaF_2 attenuators, a ZnSe optical lens for focusing, and by adjustment of the high voltage power supply. The p-Ge and p-Si samples were broadband antireflection coated for 10-μm radiation and normal incidence. In this way we were able to obtain transmission data as a function of incident intensity for pulses with approximately uniform spatial variation and high energy reproducibility from shot to shot. The maximum peak intensity used in the experiment was about 50 MW/cm^2, at which point the antireflection coatings began to exhibit optical damage.

A pyroelectric detector with 500-ps rise time was used to measure the time dependence of the pulses and a volume absorbing calorimeter was used to provide a measurement of the energy transmission. The calorimeter was accurate to within 3% according to specifications. Burn patterns on Polaroid films were used to determine the cross-sectional area of the beam at the position of the Ge or Si sample. The AR-coated ZnSe lenses used were of relatively large focal length to avoid any significant focusing as the beam propagated through the sample. Self-focusing effects were negligible for the power levels used in this experiment. Using the burn patterns, calorimeter output, and pyroelectric detector display, we were able to measure the intensity after passage through the sample. Due to the high reproducibility of the pulse energy from shot to shot, we could separately measure the intensity incident on the sample in the same way as shown in Fig. 1 but with the sample removed.

Using the transmission data of the energy incident on the sample (E_{in}) and the energy at the exit of the sample (E_{out}), we determine the linear absorption coefficient for $I_{peak} \ll I_s$ by

$$e^{-\alpha_0 L} = E_{out}/E_{in}, \tag{2}$$

where L is the sample thickness. We measure a cross section of about 7×10^{-16} cm^2 for 10.6-μm radiation and room-temperature conditions. The measured value of the cross section is consistent with other measurements given the uncertainty in N_A for the different samples. For larger intensities ($I_{peak} \gtrsim I_s$), we consider that only the spike of the laser pulse sees a nonlinear absorption coefficient. The spike is described by a rectangular pulse of 40-ns width containing 50% of the total incident energy. The remainder of the energy in the low intensity tail of the pulse is linearly absorbed according to Eq. (2). We subtract from our transmission data the contribution due to the linear absorption in the tail and obtain the average intensity in the spike incident on the sample (I_{in}) and at the exit of the sample (I_{out}). We numerically fit I_s and α_0 to satisfy

$$(I_{in} - I_{out}) = -\int_{\substack{\text{sample}\\\text{thickness}}} \left(\frac{\alpha_0(\omega)}{[1 + I/I_s]^{1/2}} + \alpha_p \right) I\, dz, \tag{2}$$

and we determine the value of the saturation intensity for the different samples. Here, α_p is the residual or nonsaturable absorption due to phonon absorption and indirect intravalence-band transitions. The absorption coefficient from multiphonon absorption at 10.6 μm is 0.030 cm^{-1} for Ge (Ref. 12) and 1.30 cm^{-1} for Si.[13] The corresponding values for 9.6-μm radiation are 0.025 cm^{-1} for Ge (Ref. 12) and 0.40 cm^{-1} for Si.[13] The intravalence-band absorption cross section, estimated from Drude–Zener theory, is about 1×10^{-17} cm^2 for Ge and 3×10^{-17} cm^2 for Si. Thus, for the hole densities we consider in this letter, $\alpha_p \ll \alpha_0$ for p-Ge and $\alpha_p \lesssim \alpha_0$ for the p-Si samples.

The measured values of I_s for p-Ge are shown in Fig. 2 for 10.6- and 9.6-μm radiation. Also shown are the calculated values for the dependence of the saturation intensity on the doping density. The calculated values of I_s vs N_A at 10.6 μm (solid line) are reproduced from Ref. 11 and values of I_s at 9.6 μm (dotted line) are calculated in the same manner as discussed in Ref. 11.

The experimental values of I_s at 10.6 μm indicate that the saturation intensity increases monotonically with increasing hole concentration for the Ge:Ga samples we studied. For the samples with larger hole concentrations, the scattering rates due to hole-impurity and hole-hole scattering are larger. The result of increasing the scattering rate is that higher intensities are required to reduce the free-hole population in the heavy-hole band at the resonant region, since the excited holes can relax at a faster rate. We also note that the experimental values for I_s vs N_A are in fair agreement with theory, with the experimental values consistently larger than the calculated values by about 20%. Previous measurements of I_s on lightly doped samples ($N_A \lesssim 3\times10^{15}$ cm^{-3}) have reported values of 3.2 (Ref. 2), 4.5 (Ref. 3), and 4 (Ref. 4) MW/cm^2 for $\lambda = 10.6\,\mu$m and 6.8 MW/cm^2 (Ref. 2) for $\lambda = 9.6\,\mu$m.

The measured values of I_s for p-Ge at 9.6 μm show a weaker fractional dependence on the hole concentration for

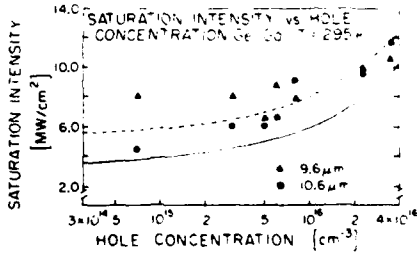

FIG. 2. Experimental and calculated values of the saturation intensity I_s vs the hole concentration for p-Ge. The circles (triangles) show the experimental values of I_s for light having a wavelength of 10.6 μm (9.6 μm). The solid line in the figure shows a calculation of I_s vs N_A taken from Ref. 11 for 10.6-μm radiation, and the dashed line shows the calculation of I_s vs N_A for 9.6-μm radiation.

the samples considered. For light having a wavelength of 9.6 μm, the direct transition between the heavy- and light-hole bands occurs at larger values in k space, and thus, for larger heavy- and light-hole energies. Phonon scattering was calculated on the basis of the deformation potential model, where the scattering rates have a square root dependence on the energy of the hole carrier.[14] The scattering rate for a hole with energy ϵ due to ionized impurities and other hole carriers has approximately an $\epsilon^{-3/2}$ dependence.[15,16] Consequently, the effect of increasing the heavy- and light-hole energies in the resonant region by going from 10.6 to 9.6-μm radiation is to increase the effect of phonon scattering and to decrease the contribution of hole-impurity and hole-hole scattering. Since I_s is substantially independent of the hole density in the region where hole-phonon scattering is dominant, we expect a weaker fractional dependence of I_s on N_h. A discussion of the wavelength dependence of I_s over the CO_2 laser spectrum has previously been presented.[17]

The measured values of I_s for p-Si at 10.6 and 9.6 μm are shown in Table I. The first three samples were doped with boron, and the fourth sample was doped with aluminum. We see that I_s is considerably larger for Si than Ge, which is primarily due to the larger hole-phonon scattering rate and the smaller excitation rate in Si. In addition, lattice absorption is much larger in Si than Ge for the wavelengths of interest. This larger nonsaturable absorption must be included in the analysis and creates a larger uncertainty in the values for the saturation intensities. Absorption saturation in p-Si has previously been observed[1]; however, the range of intensities considered was smaller and the data was interpreted in terms of a homogeneously broadened two-level model with $I_s \gtrsim 50$ MW/cm^2. We find that the data to be better approximated by an inhomogeneously broadened two-level model, where the deviation between the two functional forms for the intensity dependence of the absorption coefficient becomes apparent for $I \gtrsim I_s$.

A calculation of the nonlinear absorption of p-type semiconductors with small spin-orbit splittings, such as Si, has recently been presented.[18] In the calculation, the depletion of the hole distribution function in the three resonant regions for transitions between the heavy- and light-hole bands, heavy- and split-off hole bands, and light- to split-off hole bands were assumed to be decoupled so that the modification of the distribution due to one resonant transition does not strongly affect the population of occupied hole states in the resonant region for another direct intervalence-band transition. Using this approximation, values of I_s for p-Si were calculated to range from 140 to 180 MW/cm^2 for wavelengths in the 9–11-μm region. Although the calculated values of I_s are somewhat larger than the experimental values, the calculation does predict that p-Si is significantly more difficult to saturate than p-Ge, which is in agreement with our data.

TABLE I. Saturation intensities for uncompensated crystalline p-Si samples. N_h is the concentration of free holes and λ is the wavelength of the light.

N_h (cm^{-3})	λ (μm)	I_s (MW/cm^2)
7×10^{15}	10.6	55
3×10^{16}	10.6	71
7×10^{15}	9.6	43
2×10^{16}	9.6	36

In summary, we have experimentally examined the room-temperature absorption saturation of p-Ge and p-Si for several samples of varied doping density for light having a wavelength of 10.6 and 9.6 μm. We find that the transmission data can be fairly well understood by an inhomogeneously broadened two-level model for the range of intensities considered. We find that the saturation intensity for p-Ge monotonically increases with increasing hole concentration, in agreement with the calculations of Ref. 11. Thus, depending on the application of the saturable absorber, one can get more efficient nonlinear behavior by using lightly doped material, where hole-phonon scattering dominates the carrier relaxation. The data for p-Si indicates that the material is significantly more difficult to saturate than p-Ge, and is probably not as useful in the applications of saturable absorbers to CO_2 laser systems as Ge.

This work was supported by the Air Force Office of Scientific Research under Grant No. AFOSR-77-3216 and the U. S. Dept. of Energy under contract W-7405-eng-26 operated by Union Carbide Corporation. One of us (R.B.J.) wants to gratefully thank the Director of the Oak Ridge National Laboratory for financial support through the Eugene P. Wigner Fellowship fund, and one of us (D.L.S.) acknowledges support from the Alfred P. Sloan Foundation.

[1] A. F. Gibson, C. A. Rosito, C. A. Raffo, and M. F. Kimmitt, Appl. Phys. Lett. 21, 356 (1972).
[2] C. R. Phipps, Jr. and S. J. Thomas, Optics Lett. 1, 93 (1977).
[3] R. L. Carlson, M. D. Montgomery, J. S. Ladish, and C. M. Lockhart, IEEE J. Quantum Electron. QE-13, 35D (1977).
[4] F. Keilmann, IEEE J. Quantum Electron. QE-12, 592 (1976).
[5] P. J. Bishop, A. F. Gibson, and M. F. Kimmitt, J. Phys. D 9, L101 (1976).
[6] A. J. Alcock and A. C. Walker, Appl. Phys. Lett. 25, 299 (1974).
[7] B. J. Feldman and J. F. Figueira, Appl. Phys. Lett. 25, 301 (1974).
[8] A. C. Walker and A. J. Alcock, Opt. Commun. 12, 430 (1974).
[9] W. Kaiser, R. J. Collins, and H. Y. Fan, Phys. Rev. 91, 1342 (1953).
[10] R. B. James and D. L. Smith, Phys. Rev. Lett. 42, 1495 (1979).
[11] R. B. James and D. L. Smith, Solid State Commun. 33, 395 (1980).
[12] S. J. Fray, F. A. Johnson, J. E. Quarrington, and N. Williams, Proc. Phys. Soc. 85, 153 (1965).
[13] F. A. Johnson, Proc. Phys. Soc. (London) 73, 265 (1959).
[14] D. M. Brown and R. Bray, Phys. Rev. 127, 1593 (1962).
[15] H. Brooks, in *Advances in Electronics and Electron Physics*, edited by L. Marton (Academic, New York, 1955), Vol. 7, p. 85.
[16] I. N. Yassievich and I. D. Yaroshetskii, Fiz. Tekh. Poluprovodn 9, 857 (1975) [Sov. Phys. Semicond. 9, 565 (1975)].
[17] R. B. James and D. L. Smith, Phys. Rev. B 21, 2836 (1980).
[18] R. B. James and D. L. Smith, J. Appl. Phys. 52, 4238 (1981).

VOLUME 42, NUMBER 22 PHYSICAL REVIEW LETTERS 28 MAY 1979

Theory of Nonlinear Infrared Absorption in p-Type Germanium

R. B. James and D. L. Smith
California Institute of Technology, Pasadena, California 91125
(Received 22 March 1979)

We present a theory of the saturation of inter-valence-band absorption in p-type Ge by high-intensity light with a wavelength near 10 μm. The absorption coefficient decreases with intensity in a manner closely approximated by an inhomogeneously broadened two-level model. The saturation intensity is calculated as a function of excitation wavelength and temperature and found to be in good agreement with measured values.

Free-hole transitions between the heavy- and light-hole bands in p-type Ge are primarily responsible for the absorption of light with wavelengths in the 11- to 9-μm range. Absorption due to this process has been found to saturate at high light intensities.[1-4] Thus p-type Ge can be used as a saturable absorber to passively mode lock CO_2 lasers. In this Letter, we present a theory of the saturation of heavy-hole band to light-hole band transitions in p-type Ge at high light intensities.

Previously saturable absorption in p-type Ge has been analyzed by modeling the Ge valence bands as an ensemble of two-level systems whose level populations approach one another at high light intensities.[2-5] This model predicts that the dependence of the absorption coefficient as a function of intensity is given by

$$\alpha(I,\omega)=\alpha_0(\omega)[1+I/I_s(\omega)]^{-1/2}, \tag{1}$$

where $\alpha_0(\omega)$ is the absorption coefficient at low intensity, and $I_s(\omega)$ is the saturation intensity. This behavior was found to be reasonably well satisfied experimentally.[2-4] However, attempts to calculate $I_s(\omega)$ as a function of photon energy using the two-level model and a multistep cascade relaxation produced results that were in qualitative disagreement with experiment.[2,5] There has also been a theoretical discussion of the saturation based on a spherical, parabolic band model,[6] but this study produced a result for the absorption coefficient which was quite different from that of Eq. (1) and which is in qualitative disagreement with experimental results. Here we describe the Ge valence bands using degenerate $\vec{k}\cdot\vec{p}$ perturbation theory. This is the first time the saturable absorption has been discussed in a model which realistically accounts for the anisotropic and nonparabolic Ge valence bands. Our calculated results are in close numerical agreement with Eq. (1) and for the first time give results for $I_s(\omega)$ as a function of photon energy which are in good agreement with the experimental values. There are no adjustable parameters in the theory.

Both energy and wave vector are conserved in the inter-valence-band optical transition. Thus only holes in a narrow region of the heavy-hole band can directly participate in the absorption. As the light intensity becomes large, the population of these states in the heavy-hole band is decreased and the absorption coefficient is reduced. The absorption coefficient is given by

$$\alpha(I,\omega)=\frac{4\pi^2}{\epsilon^{1/2}m^2\omega c}\frac{Ne^2}{3}\sum_{\vec{k}}[f_h(\vec{k})-f_l(\vec{k})]\times|\vec{P}_{hl}(\vec{k})|^2\frac{1/\hbar\pi T_2(\vec{k})}{[\Omega(\vec{k})-\omega]^2+[1/T_2(\vec{k})]^2}, \tag{2}$$

where the subscripts h (l) designate the heavy- (light-) hole band, N is the density of holes, ϵ is the dielectric constant, m is the free-electron mass, $\hbar\omega$ is the photon energy, $f_i(\vec{k})$ is the probability that a hole state with wave vector $\vec{k}$ is occupied in band i, $|\vec{P}_{hl}(\vec{k})|^2$ is the squared momentum matrix element between the Bloch states in the heavy- and light-hole bands (summed over the two degenerate states in each band), and $\Omega(\vec{k})$ is the angular frequency associated with the energy difference $[\epsilon_h(\vec{k})-\epsilon_l(\vec{k})]$ where $\epsilon_i(\vec{k})$ is the energy of the hole with wave vector $\vec{k}$ in band i. The phase relaxation time $T_2(\vec{k})$ is given by

$$\frac{2}{T_2(\vec{k})}=\sum_{c\vec{k}'}[R_{h\vec{k}\to c\vec{k}'}+R_{l\vec{k}\to c\vec{k}'}], \tag{3}$$

where $R_{a\vec{k}\to b\vec{k}'}$ is the rate at which a hole in band a with wavevector $\vec{k}$ is scattered into a state in band b with wave vector $\vec{k}'$.

In p-type Ge the scattering rate of holes occurs on a subpicosecond time scale. Since the experimental studies use lasers with nanosecond pulse durations, transient effects are damped out. Hence, we calculate the steady-state distribution functions which are determined by the following

equations:

$$\beta(\vec{k}, I)[f_h(\vec{k}) - f_l(\vec{k})] = -\sum_{c\vec{k}'}[R_{h\vec{k}\to c\vec{k}'} f_h(\vec{k}) - R_{c\vec{k}'\to h\vec{k}} f_c(\vec{k})], \quad (4a)$$

$$\beta(\vec{k}, I)[f_h(\vec{k}) - f_l(\vec{k})] = \sum_{c\vec{k}'}[R_{l\vec{k}\to c\vec{k}'} f_l(\vec{k}) - R_{c\vec{k}'\to l\vec{k}} f_c(\vec{k}')], \quad (4b)$$

where

$$\beta(\vec{k}, I) = \frac{2\pi^2}{\epsilon^{1/2} m^2 \omega c} \frac{e^2 I}{3\hbar\omega} |\vec{P}_{hl}(\vec{k})|^2 \times \frac{1/\hbar\pi T_2(\vec{k})}{[\Omega(\vec{k}) - \omega]^2 + [1/T_2(\vec{k})]^2}. \quad (4c)$$

These equations state that the rate of optical excitation out of (into) a state is equal to the net rate of scattering into (out of) the state. The left-hand sides of Eqs. (4a) and (4b) give the net rate of optical excitation out of a state with wave vector $\vec{k}$ in the heavy-hole band into a state with wave vector $\vec{k}$ in the light-hole band. Here $\beta(\vec{k}, I)$ describes the strength of the optical interaction.

Using Eqs. (4), we obtain an expression for the steady-state difference in occupation probabilities,

$$f_h(\vec{k}) - f_l(k) = \frac{f_h^0(\vec{k}) - f_l^0(\vec{k})}{1 + \beta(\vec{k}, I)[T_h(\vec{k}) + T_l(\vec{k})]} + \frac{T_h(\vec{k})F(\vec{k}, I) - T_l(\vec{k})G(\vec{k}, I)}{1 + \beta(\vec{k}, I)[T_h(\vec{k}) + T_l(\vec{k})]}, \quad (5)$$

where $f_l^0(\vec{k})$ is the equilibrium value for the distribution function,

$$\frac{1}{T_h(\vec{k})} = \sum_{c\vec{k}'} R_{h\vec{k}\to c\vec{k}'}, \quad (6a)$$

$$F(\vec{k}, I) = \sum_{c\vec{k}'} R_{c\vec{k}'\to h\vec{k}}[f_c(\vec{k}') - f_c^0(\vec{k}')], \quad (6b)$$

and $T_l(\vec{k})$ and $G(\vec{k}, I)$ are defined for the light-hole band analogous to Eqs. (6a) and (6b), respectively. The function $F(\vec{k}, I)$ is the difference in the feeding rate of free holes from the equilibrium feeding rate for the state with wave vector $\vec{k}$ in the heavy-hole band. The first term in Eq. (5) gives the population difference that would occur for the states at $\vec{k}$ if the populations of the states that feed those at $\vec{k}$ were given by their equilibrium values. The second term in Eq. (5) accounts for the change in the populations of the states that feed those at $\vec{k}$. For those values of $\vec{k}$ which are important in the integral in Eq. (2), the first term in Eq. (5) is found to be significantly greater than the second.

For the hole concentrations and temperatures at which most saturable absorption measurements have been performed (room temperature, $N \lesssim 10^{16}$ cm^{-3}), phonon scattering is the dominant scattering mechanism. Phonon scattering was calculated on the basis of the deformable potential model, where the deformation parameters were taken from the mobility fits of Brown and Bray.[7] Following Ref. 7 we neglect angular dependence in the phonon scattering matrix elements and take the scattering rates to be the same function of energy for the heavy- and light-hole bands. Energy relaxation of the excited holes is determined by optical-phonon scattering. The optical-phonon spectrum is relatively flat for small k with an average energy of about 0.037 eV. We neglect the energy of the acoustic phonons; this is a reasonable approximation for the region of interest (small k). Acoustic-phonon scattering mixes states with approximately the same energy but different values of $\vec{k}$. The effect of acoustic-phonon scattering is not negligible because of the anisotropy of the valence bands.

If there is no angular dependence in the phonon scattering matrix elements, the functions $F(\vec{k})$ and $G(\vec{k})$ depend only on $\epsilon_h(\vec{k})$ and $\epsilon_l(\vec{k})$, respectively. We use Eq. (4) to write one-dimensional integral equations for these functions. If we take the optical-phonon energy as discrete and neglect the acoustic-phonon energy, these integral equations can be reduced to a set of algebraic equations which we solve numerically. Once these functions are determined, the absorption coefficient is calculated by numerically integrating Eq. (2). The one-hole energies and the momentum matrix elements are found from degenerate $\vec{k}\cdot\vec{p}$ perturbation theory.[8] The cyclotron-resonance parameters of Hensel and Suzuki[9] were used.

The calculated values of $\alpha(I, \omega)$ were compared with the expression in Eq. (1). The numerical results could be fitted by this expression to an accuracy of about 5% for intensities less than $25I_s$. (This is the range of intensities which has been explored experimentally.) If only the first term in Eq. (5) is retained, the calculated $\alpha(I, \omega)$ has precisely the form of Eq. (1). The second term in Eq. (1) is smaller than the first; it leads to the small deviations of the calculated $\alpha(I, \omega)$ from the expression in Eq. (1).

For those temperatures and hole densities for which hole-impurity and hole-hole scattering is small compared to phonon scattering, the calculated I_s is independent of hole concentration. At room temperature, I_s has been found experimen-

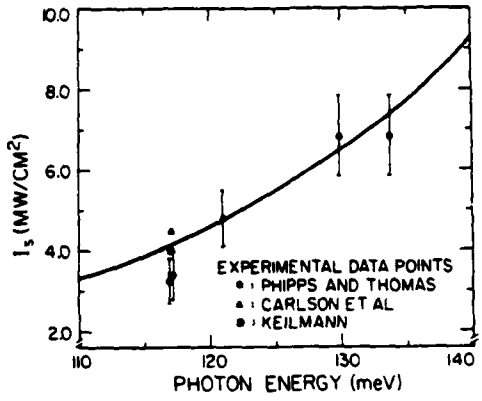

FIG. 1. Saturation intensity vs photon energy for p-type Ge at 295°K. The experimental data are from Refs. 2, 3, and 4. Error bars are given only in Ref. 2.

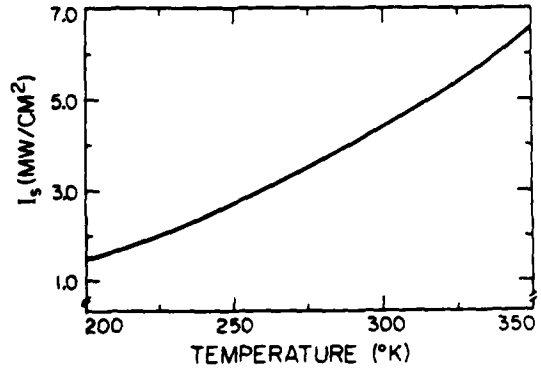

FIG. 2. Calculated saturation intensity vs temperature for p-type Ge and light with a wavelength of 10.6 μm.

tally to be independent of hole concentration for concentrations less than about 4×10^{15} cm^{-3}.[1]

Measurements of saturable absorption in p-type Ge have been interpreted in terms of the inhomogeneously broadened two-level model which produces Eq. (1), and values of $I_s(\omega)$ are reported.[2-4] In Fig. 1, we compare measured values of $I_s(\omega)$ at room temperature as a function of photon energy with the calculated values. In the range of photon energies considered, $I_s(\omega)$ was found to increase monotonically with photon energy. The increase in $I_s(\omega)$ with increasing ω is primarily a result of the larger density of states in the heavy-hole band for the higher-energy holes involved in the optical transition. There is good agreement between theory and experiment. There are no adjustable parameters in the theory.

In Fig. 2, we present the results of a calculation of the temperature dependence of $I_s(\omega)$ for light with a wavelength of 10.6 μm. I_s increases monotonically with temperature. This increase in I_s with temperature is due to the increased rate of phonon scattering at higher temperature. Because of the rather strong dependence of I_s on temperature, it should be possible to tune the saturation behavior of p-type Ge with temperature.

Many semiconductors have a valence-band structure which is similar to that of Ge, and saturation of inter-valence-band absorption should be observable in these materials. In addition to Ge, the effect has also been observed in p-GaAs.[1] The theory presented here should apply for these materials as well as for Ge.

Using this theory, we can determine the hole distribution as a function of laser intensity and frequency. Knowledge of the hole distribution function allows an interpretation of "pump-probe" experiments. In these experiments the absorption of a low-intensity light beam (probe) is measured as a function of frequency in the presence of a high-intensity laser (pump) of fixed frequency.[4,10-12]

In conclusion, we have presented a theory of the saturation of inter-valence-band absorption in p-type Ge. We have found that the saturation is closely approximated by an inhomogeneously broadened two-level model. We have calculated the saturation intensity as a function of photon energy and found good agreement with experimental values. We have predicted the dependence of the saturation intensity on temperature.

The authors thank R. N. Silver for many useful discussions. The authors gratefully acknowledge the support of the Air Force Office of Scientific Research under Grant No. AFOSR-77-3216. One of us (D.L.S.) acknowledges support from the Alfred P. Sloan Foundation.

[1]A. F. Gibson, C. A. Rosito, C. A. Raffo, and M. F. Kimmitt, Appl. Phys. Lett. 21, 356 (1972).

[2]C. R. Phipps, Jr., and S. J. Thomas, Opt. Lett. 1, 93 (1977).

[3]R. L. Carlson, M. D. Montgomery, J. S. Ladish, and C. M. Lockhart, IEEE J. Quantum Electron. 13, 85D (1977).

[4]F. Keilmann, IEEE J. Quantum Electron. 12, 592 (1976).

[5]M. Sargent, III, Opt. Commun. 20, 298 (1977).
[6]V. L. Komolov, I. D. Yaroshetskii, and I. N. Yassievich, Fiz. Tekh. Poluprovodn. 11, 85 (1977) [Sov. Phys. Semicond. 11, 48 (1977)].
[7]D. M. Brown and R. Bray, Phys. Rev. 127, 1593 (1962).
[8]E. O. Kane, J. Phys. Chem. Solids 1, 82 (1956).
[9]J. C. Hensel and K. Suzuki, Phys. Rev. B 9, 4219 (1974).
[10]P. J. Bishop, A. F. Gibson, and M. F. Kimmett, J. Phys. D 9, L101 (1976).
[11]F. Keilmann, Appl. Phys. 14, 29 (1977).
[12]F. Keilmann and J. Kuhl, IEEE J. Quantum Electron. 14, 203 (1978).

PHYSICAL REVIEW B VOLUME 21, NUMBER 8 15 APRIL 1980

Saturation of intervalence-band transitions in p-type semiconductors

R. B. James and D. L. Smith
California Institute of Technology, Pasadena, California 91125
(Received 15 October 1979)

We present a theory of the saturation of heavy-hole to light-hole band absorption in p-type semiconductors with the diamond or zinc-blende crystal structure by high-intensity light with a wavelength near 10 μm. The absorption coefficient is found to decrease with intensity in a manner closely approximated by an inhomogeneously broadened two-level model. For temperatures and hole concentrations where hole-phonon scattering dominates hole-impurity and hole-hole scattering, the saturation intensity is independent of the hole concentration. We calculate the saturation intensity as a function of excitation wavelength and temperature for p-Ge and p-GaAs. We find that the saturation intensity increases with photon energy and with temperature. The calculated results are compared with the available experimental data and good agreement is found.

I. INTRODUCTION

In many p-type semiconductors, direct free-hole transitions between the heavy- and light-hole bands are primarily responsible for the absorption of light with wavelengths near 10 μm. At high light intensities, absorption due to these transitions has been found to saturate in p-Ge (Refs. 1–4) and p-GaAs.[1] This saturation property allows a means of passively mode locking a CO_2 laser by inserting a slice of p-Ge or p-GaAs into the optical path of the cavity. Experiments have demonstrated that a CO_2 laser with p-Ge used as a saturable absorber can generate passively mode-locked pulses of subnanosecond duration.[5–7] In this paper, we present a theory of the saturation behavior of heavy-hole band to light-hole band transitions in p-type semiconductors at high light intensities. We present detailed numerical results for p-Ge and p-GaAs (the materials in which the effect has been experimentally observed). In a recent letter, we made a preliminary report of the results for p-Ge.[8]

In previous work, saturable absorption in p-type semiconductors has been described by modeling the valence bands as an ensemble of two-level systems whose level populations approach one another at high light intensities.[2–4,9] This two-level model predicts that the dependence of the absorption coefficient as a function of intensity is given by

$$\alpha(I,\omega)=\frac{\alpha_0(\omega)}{[1+I/I_s(\omega)]^{1/2}}, \tag{1}$$

where $\alpha_0(\omega)$ is the absorption coefficient at low intensity, and $I_s(\omega)$ is the saturation intensity. The behavior described in Eq. (1) was found to be reasonably well satisfied experimentally, and values of $I_s(\omega)$ were determined.[2–4] However, attempts to calculate $I_s(\omega)$ as a function of photon energy using the two-level model and a multistep cascade relaxation[9] gave results that disagree with experiment.[2] A theoretical discussion of saturable absorption in p-type Ge based on a spherical-parabolic-band model has also been presented.[10] However, the results of that discussion are qualitatively different than that of Eq. (1) and are in disagreement with experiment.

In this paper we present a theoretical analysis of the saturable absorption by considering the initial- and final-hole states in the optical transition to form a continuum with the valence-band structure determined by degenerate $\vec{k}\cdot\vec{p}$ perturbation theory.[11] Our calculated results are in close agreement with Eq. (1), and the values of $I_s(\omega)$ deduced from the calculation are in good agreement with experiment. We also determine the dependence of $I_s(\omega)$ on temperature. We present detailed results for p-Ge and p-GaAs; however, the theory should be applicable to other semiconductors with the zinc-blende crystal structure as well.

The paper is organized in the following way: in Sec. II we present our theoretical approach, in Sec. III we give the results for p-Ge, in Sec. IV we give the results for p-GaAs, and in Sec. V we summarize our conclusions. Calculational details are included in the Appendices.

II. THEORETICAL APPROACH

In semiconductors with the diamond or zinc-blende crystal structure, the valence-band maximum occurs at the zone center.[12] There are six bands (three sets of twofold degenerate bands) near the valence maximum. Four of the bands are degenerate at $k=0$ and the other two bands (degenerate) are split off to lower energy by the spin-orbit interaction. Away from the zone center, the bands degenerate at $k=0$ split into 2 twofold

$$F(\vec{k}) = \sum_{c\vec{k}'} R_{c\vec{k}'\to b\vec{k}} [f_c(\vec{k}') - f_c^0(\vec{k}')], \tag{13c}$$

and

$$G(\vec{k}) = \sum_{c\vec{k}'} R_{c\vec{k}'\to l\vec{k}} [f_c(\vec{k}') - f_c^0(\vec{k}')], \tag{13d}$$

where $f_c^0(\vec{k})$ is the equilibrium value for the distribution function. The function $F(\vec{k})$ is the difference in the feeding rate of free holes from the equilibrium feeding rate for the state with wave vector $\vec{k}$ in the heavy-hole band. The function $G(\vec{k})$ is analogously defined for the light-hole band. [Scattering into the light-hole band is small because of the small density of light-hole states. Thus the function $G(\vec{k})$ is less important than $F(\vec{k})$.] In terms of the auxiliary functions, the distribution functions can be written as

$$f_h(\vec{k}) = f_h^0(\vec{k}) - \frac{\beta(\vec{k})T_h(\vec{k})[f_h^0(\vec{k}) - f_l^0(\vec{k})]}{1+\beta(\vec{k})[T_h(\vec{k}) + T_l(\vec{k})]} + \frac{F(\vec{k})T_h(\vec{k}) + \beta(\vec{k})T_h(\vec{k})T_l(\vec{k})[F(\vec{k}) + G(\vec{k})]}{1+\beta(\vec{k})[T_h(\vec{k}) + T_l(\vec{k})]} \tag{14a}$$

and

$$f_l(\vec{k}) = f_l^0(\vec{k}) + \frac{\beta(\vec{k})T_l(\vec{k})[f_h^0(\vec{k}) - f_l^0(\vec{k})]}{1+\beta(\vec{k})[T_h(\vec{k}) + T_l(\vec{k})]} + \frac{G(\vec{k})T_l(\vec{k}) + \beta(\vec{k})T_h(\vec{k})T_l(\vec{k})[F(\vec{k}) + G(\vec{k})]}{1+\beta(\vec{k})[T_h(\vec{k}) + T_l(\vec{k})]} . \tag{14b}$$

The difference in occupation probabilities which appears in the expression for the absorption coefficient is given by

$$f_h(\vec{k}) - f_l(\vec{k}) = \frac{f_h^0(\vec{k}) - f_l^0(\vec{k})}{1+\beta(\vec{k})[T_h(\vec{k}) + T_l(\vec{k})]} + \frac{T_h(\vec{k})F(\vec{k}) - T_l(\vec{k})G(\vec{k})}{1+\beta(\vec{k})[T_h(\vec{k}) + T_l(\vec{k})]} . \tag{15}$$

The first term in Eq. (15) gives the population difference that would occur for the states at $\vec{k}$ if the populations of the states that feed those at $\vec{k}$ were given by their equilibrium values. The second term in Eq. (12) accounts for the change in the population of the states that feed those at $\vec{k}$. For those values of $\vec{k}$ which are important in the integral in Eq. (11), the first term in Eq. (15) is found to be significantly greater than the second.

Using Eq. (12) and the definition of the auxiliary functions, one can write equations which determine $F(\vec{k})$ and $G(\vec{k})$. If there is no angular dependence in the phonon scattering matrix elements which go into the scattering rates, the functions $F(\vec{k})$ and $G(\vec{k})$ depend on $E_h(\vec{k})$ and $E_l(\vec{k})$, respectively. Thus, one-dimensional (rather than three-dimensional) equations must be solved to determine these functions. Our treatment of these functions is included in Appendix D.

III. CALCULATION AND RESULTS FOR *p*-Ge

In order to calculate the difference in occupation probabilities for the heavy- and light-hole bands, it is necessary to know the free-hole scattering rates. We consider the region of temperature and impurity densities for which hole-phonon scattering is the dominant scattering mechanism. Optical-phonon scattering is the dominant energy relaxation mechanism. The optical-phonon spectrum is relatively flat for small k with an average energy of 0.037 eV. For the small k region in which we are interested, the acoustic phonon energy is quite small, and we neglect it. Although acoustic phonon scattering does not contribute significantly to energy relaxation, it can change the wave vector of the hole. The valence bands of Ge are rather anisotropic and an acoustic phonon scattering event can take a hole from a region in which $\beta(\vec{k})$ is small to one in which it is large. Thus, although acoustic phonon scattering is less important than optical phonon scattering in determining the distribution functions, it is not negligible because of the anisotropy of the valence bands. We take the scattering rates to be given by[10]

$$R_{a\vec{k}\to b\vec{k}'} = \frac{2\pi}{\hbar}|M_{op}^+|^2(E_a(\vec{k}) - E_b(\vec{k}') + \hbar\omega_0) + \frac{2\pi}{\hbar}|M_{op}^-|^2\delta(E_a(\vec{k}) - E_b(\vec{k}') - \hbar\omega_0) + \frac{2\pi}{\hbar}|M_{ac}|^2\delta(E_a(\vec{k}) - E_b(\vec{k}')), \tag{16a}$$

where

$$|M_{op}^+|^2 = \frac{E_{op}^2\hbar\omega_0}{2V\rho\omega_l^2}(N_0 + 1), \tag{16b}$$

$$|M_{op}^-|^2 = \frac{E_{op}^2\hbar\omega_0}{2V\rho\omega_l^2}N_0, \tag{16c}$$

and

$$|M_{ac}|^2 = \frac{E_{ac}^2 k_B T}{2V\rho\omega_l^2} . \tag{16d}$$

Here $|M_{op}^{+}|^2$ is the squared matrix element for optical phonon emission, $|M_{op}^{-}|^2$ is the squared matrix element for optical phonon absorption, and $|M_{ac}|^2$ is the squared acoustic phonon scattering matrix element (summed over both absorption and emission processes). In Eq. (16), E_{op} (E_{ac}) is the deformation potential for optical (acoustical) phonon scattering, $\hbar\omega_0$ is the zone-center optical phonon energy, ρ is the density, u_l is the longitudinal sound velocity, N_q is the optical phonon Bose factor, and V is the sample volume. Following Ref. 19, we have neglected angular dependence in the phonon scattering matrix element and taken the scattering rates to be the same for the heavy- and light-hole bands. The numerical value for the constants appearing in the squared matrix elements were taken from the mobility fits of Ref. 20; they are listed in Table I. The scattering times $T_2(\vec{k})$, $T_h(\vec{k})$, and $T_l(\vec{k})$ are computed from Eqs. (6c), (13a), and (13b) using these scattering rates. Optical phonon scattering (primarily emission) dominates in the results for $T_2(\vec{k})$ and $T_l(\vec{k})$ for the states of interest. For $T_h(\vec{k})$ in the resonant region, optical phonon emission is typically not possible and acoustic phonon scattering makes a significant contribution to $T_h(\vec{k})$.

The free-hole energies $E_h(\vec{k})$ and $E_l(\vec{k})$ and the momentum matrix elements $|\vec{P}_{hl}(\vec{k})|^2$ are determined by degenerate $\vec{k}\cdot\vec{p}$ perturbation theory.[11] The cyclotron resonance parameters of Hensel and Suzuki[21] are used.

TABLE I. Valence-band deformation potentials used in the calculation of phonon scattering rates.

	E_{ac} (eV)	E_{op} (eV)
Ge	3.5[a]	6.8[a]
GaAs	3.6[b]	6.5[b]

[a]Reference 20.
[b]Reference 23.

A. First approximation for $f_h(\vec{k}) - f_l(\vec{k})$

As a first approximation for the population difference $f_h(\vec{k}) - f_l(\vec{k})$, we neglect the auxiliary functions $F(\vec{k})$ and $G(\vec{k})$ and include only the first term in Eq. (15). This approximation is equivalent to assuming that the rate at which free holes are scattered into the states involved in the optical transition is given by the equilibrium value. For optical phonon scattering, the energy of the initial-hole state in the scattering event differs from that of the final-hole state by the optical phonon energy. As a result, hole states that can scatter into a resonant optical transition region by optical phonon scattering are, for the most part, themselves out of the resonant region. Thus, the population of these states is not directly depleted by the optical transitions. The population of these states is indirectly depleted by the optical transition because there is a decrease in the feeding rate of these states owing to the decrease in population of hole states in the resonant region. However, this decreased feeding from the resonant region is partially compensated for by an increased feeding from the rerouting of optically excited holes.

For acoustic phonon scattering, the energy of the initial-hole state in the scattering event is essentially the same as that of the final-hole state. As a result, hole states that can scatter into a resonant optical transition region by acoustic phonon scattering are, for the most part, in the resonant region themselves. Thus, the population of these states is directly depleted by the optical transitions. Including only the first term in Eq. (15), therefore, overestimates the importance of acoustic phonon scattering. At this level of approximation, it is better to ignore acoustic phonon scattering. We will see that this first approximation for $f_h(\vec{k}) - f_l(\vec{k})$ ignoring acoustic phonon scattering produces results close to that of our more complete calculation.

Using only the first term in Eq. (15) to determine the population difference, the absorption coefficient becomes

$$\alpha^1(I,\omega) = \frac{4\pi^2}{\sqrt{\epsilon_\infty}\, m^2\omega c}\frac{N_h e^2}{3}\sum_{\vec{k}}\left[f_h^0(\vec{k}) - f_l^0(\vec{k})\right]|\vec{P}_{hl}(\vec{k})|^2\frac{1/[\hbar\pi T_2(\vec{k})]}{[\Omega(\vec{k})-\omega]^2 + [1/T_2(\vec{k})]^2[1+I/I(\vec{k})]}, \tag{17a}$$

where

$$I(k) = \frac{3\hbar^2 c\sqrt{\epsilon_\infty}\, m^2\omega^2}{[T_h(\vec{k}) + T_l(\vec{k})]T_2(\vec{k})2\pi e^2|\vec{P}_{hl}(\vec{k})|^2}. \tag{17b}$$

Transforming to an integration over surfaces of constant $\Omega(\vec{k})$, and assuming that the power-broadened Lorentzian is sharply peaked, Eq. (17a) can be written as

$$\alpha^1(I,\omega) = \frac{4\pi^2}{\sqrt{\epsilon_\infty}\, m^2\omega c}\frac{N_h e^2}{3\hbar}\left(\frac{1}{2\pi}\right)^3\int_{\Omega(\vec{k})=\omega}\frac{ds}{|\nabla_{\vec{k}}\Omega(\vec{k})|}\frac{|\vec{P}_{hl}(\vec{k})|^2[f_h^0(\vec{k}) - f_l^0(\vec{k})]}{[1+I/I(\vec{k})]^{1/2}}. \tag{18}$$

Here the integral is over a surface of constant $\Omega(\vec{k})$. Integrating Eq. (18) numerically, we find that the absorption coefficient satisfies Eq. (1) to high accuracy. Indeed, if $I(\vec{k})$ were independent of $\vec{k}$ over the region of the surface integral, Eq. (18) would reduce to Eq. (1) exactly.

For hole densities and temperatures such that hole-phonon scattering dominates the hole-impurity and hole-hole scattering events, values of $I_s(\omega)$ deduced from Eq. (18) are independent of the hole density. Experimentally $I_s(\omega)$ has been found to be independent of hole density for densities less than 4×10^{15} cm^{-3} at room temperature.[1]

B. Higher-order approximation for $f_h(\vec{k})-f_l(\vec{k})$

The auxiliary functions $F(\vec{k})$ and $G(\vec{k})$ are computed numerically as discussed in Appendix D. The distribution function computed from these auxiliary functions for $\vec{k}$ in the [111] and [100] directions together with their equilibrium values are shown in Fig. 1. The dominant dip in the heavy-hole distribution function and corresponding peak in the light-hole distribution function is due to direct optical transitions. Additional dips in the heavy-hole distribution function occur because of the discrete energy of the optical phonons. The increase in the heavy-hole distribution compared to the equilibrium value at large values of k is due to scattering of the photoexcited holes in the light-hole band into the heavy-hole band.

The absorption coefficient is calculated numerically. The calculated result for $\lambda=10.6$ μm and $T=295$ °K is compared with the expression in Eq. (1) in Fig. 2. The value of I_s used in Eq. (1) was determined by fitting the calculated result for $\alpha(I,\omega)$. The numerical results could be fit to an accuracy of about 5% for intensities less than 25 times I_s. (This is the range of intensities which has been most frequently explored experimentally.) If only the first term in Eq. (15) is retained, the calculated $\alpha(I,\omega)$ has almost exactly the form of Eq. (1). The second term in Eq. (15) is smaller than the first and leads to the small deviations seen in Fig. 2.

Measurements of the saturable absorption in p-type Ge have been interpreted in terms of the inhomogeneously broadened two-level model which produces Eq. (1), and the values of $I_s(\omega)$ have been reported. In Fig. 3, we compare measured values of $I_s(\omega)$ at room temperature as a function of photon energy with our theoretical values. The theoretical values of $I_s(\omega)$ are determined by fitting the expression in Eq. (1) to the calculated results for $\alpha(I,\omega)$ for intensities between zero and 100 MW/cm^2. In the range of photon energies considered, $I_s(\omega)$ was found to increase monotonically with photon energy. There

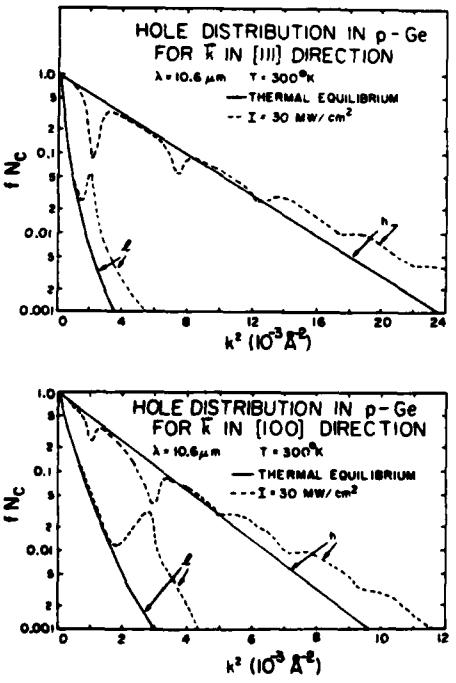

FIG. 1. Calculated hole distribution functions in p-Ge as a function of k^2 for $\vec{k}$ in the [111] and [100] directions. The calculations were performed for $\lambda=10.6$ μm, $T=300$ °K, and $I=30$ MW/cm^2. The equilibrium distribution functions are shown for comparison. N_v is the effective density of states.

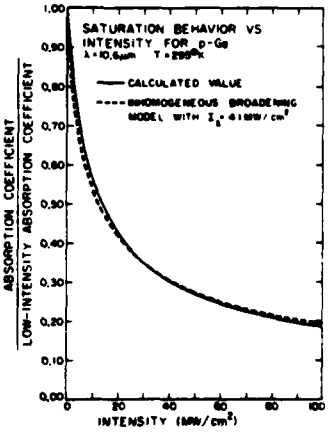

FIG. 2. Calculated absorption coefficient normalized to its low intensity value as a function of intensity for p-Ge. The calculations were performed for $\lambda=10.6$ μm and $T=295$ °K. The inhomogeneously broadened two-level model result with $I_s=4.1$ MW/cm^2 is also shown.

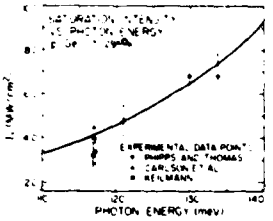

FIG. 3. Calculated saturation intensity as a function of photon energy for p-Ge at 295 °K. The experimental results are from Refs. 2–4. Error bars are only given in Ref. 2.

is good agreement between theory and experiment. There are no adjustable parameters in the theory.

The calculated results shown in Fig. 3 were attained using the higher-order approximation for $f_h(\vec{k}) - f_l(\vec{k})$. The results for the first-order approximation are qualitatively similar to those of the more complete calculation; the numerical values of the two calculations differ by an approximately constant factor. At $\lambda = 10.6\ \mu$m and $T = 295$ °K, the more complete calculation gives a value of I_s of 4.1 MW/cm^2, the first-order calculation including acoustic phonon scattering gives a result of 5.8 MW/cm^2, and the first-order calculation neglecting acoustic phonon scattering gives a result of 3.5 MW/cm^2. Thus the first-order calculation neglecting acoustic phonon scattering is within about 15% of the more complete calculation. This result is interesting because the first-order calculation is much easier and less expensive to perform than the more complete calculation.

The increase in $I_s(\omega)$ with increasing ω is due both to the behavior of the scattering rates and the optical matrix elements. The relative contribution of the scattering rates and the optical matrix elements can be most easily seen in the first-order calculation. At this level of approximation, $I_s(\omega)$ is given by a weighted average of $l(\vec{k})$ [see Eq. (18)]. The values of $l(\vec{k})$ are proportional to ω^2, $T_2^{-1}(\vec{k})$, $[T_h(\vec{k}) + T_l(\vec{k})]^{-1}$, and $|\vec{P}_{hl}(\vec{k})|^{-2}$. In Fig. 4, the variation of these factors is illustrated as a function of photon energy for $\vec{k}$ in the [100] and [111] directions.

Since the usefulness of p-Ge as a saturable absorber in CO_2 laser systems is determined by its saturation characteristics, it is of interest to be able to control the saturation behavior. Since optical phonon scattering is the dominant relaxation mechanism, and the optical phonon occupation is temperature dependent, it is clear that $I_s(\omega)$ will depend on temperature. In Fig. 5, we present the results of a calculation of the temperature

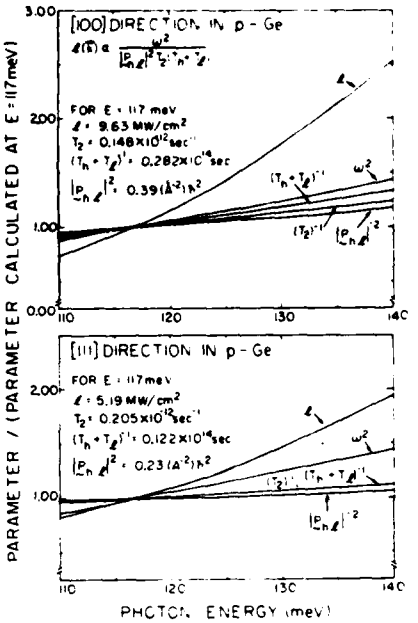

FIG. 4. Variation of the factors which contribute to the photon energy dependence of $I_s(\omega)$ in our first approximation for the absorption coefficient in p-Ge. The values of the factors are normalized to their value at $\hbar\omega = 117$ meV ($\lambda = 10.6\ \mu$m). The factors were computed for $T = 295$ °K.

dependence of $I_s(\omega)$ in p-Ge for light with a wavelength of 10.6 μm. $I_s(\omega)$ increases monotonically with temperature. This increase is due to the increased rate of phonon scattering at higher temperatures. Because of the rather strong dependence of $I_s(\omega)$ on temperature, it should be possible to tune the saturation behavior of p-Ge with temperature.

IV. CALCULATION AND RESULTS FOR p-GaAs

The dependence of the absorption coefficient on intensity in p-GaAs can be described by the same theory as in p-Ge. We use the cyclotron reso-

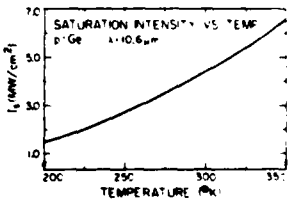

FIG. 5. Calculated saturation intensity as a function of temperature for p-Ge and light with a wavelength of 10.6 μm.

nance parameters of Lawaetz[22] to determine the GaAs valence-band structure. (We neglect the small terms linear in k which appear in the $\vec{k}\cdot\vec{p}$ perturbation theory for zinc-blende cyrstals.) Hole-phonon scattering is described as in Ge; the deformation potential parameters are taken from Ref. 23 and are listed in Table I. We neglect the small splitting between the zone-center LO and TO phonons and take an average optical phonon energy of 34.3 meV. The input parameters that we use for GaAs are not as accurately known as those for Ge.

Our calculations of the intensity dependence of the absorption coefficient give a result that is numerically close to the inhomogeneously broadened two-level model result of Eq. (1).[24] In Fig. 6, we compare the calculated result for $\lambda = 10.6\ \mu$m and $T = 295$ °K with Eq. (1). As for Ge, the small difference between the calculated result and inhomogeneously broadened two-level model result comes from the second term in Eq. (15).

In Fig. 7, we show the theoretical results for $I_s(\omega)$ as a function of photon energy at room temperature. The theoretical results are determined by fitting the expression in Eq. (1) to the calculated results for $\alpha(I, \omega)$ for intensities between zero and 100 MW/cm^2. The results for $I_s(\omega)$ are qualitatively similar to those for Ge except that $I_s(\omega)$ is uniformly larger in GaAs than in Ge. The values of $I_s(\omega)$ are larger in GaAs than in Ge primarily because the hole-phonon scattering times are shorter in GaAs. The scattering times are shorter in GaAs because the heavy-hole effective mass is larger in GaAs, and as a result the density of final scattering states is larger in GaAs.

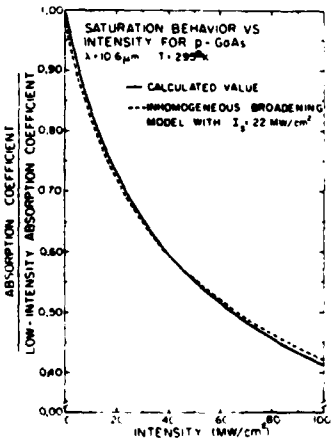

FIG. 6. Calculated absorption coefficient normalized to its low-intensity value as a function of intensity for p-GaAs. The calculations were performed for $\lambda = 10.6$ μm and $T = 295$ °K. The inhomogeneously broadened two-level model result with $I_s = 22$ MW/cm^2 is also shown.

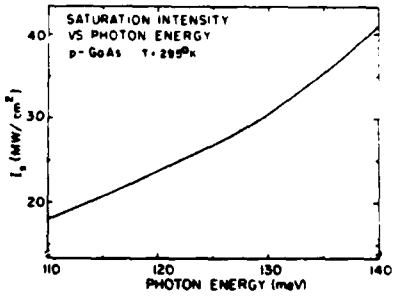

FIG. 7. Calculated saturation intensity as a function of photon energy for p-GaAs at 295 °K.

Saturation of intervalence-band absorption in p-GaAs has been observed in one experiment in p-GaAs.[1] A saturation intensity of $I_s = 20 \pm 5$ MW/cm^2 at $\lambda = 10.6\ \mu$m and room temperature was reported. However, these measurements were performed over a relatively small range of incident intensities and were interpreted in terms of a homogeneously (rather than an inhomogeneously) broadened two-level model. If the results had been interpreted in terms of the inhomogeneously broadened two-level model (which we believe would have been more correct), a smaller value of I_s would most likely have been attained.

In Fig. 8, we present the results of a calculation of the temperature dependence of the saturation intensity at $\lambda = 10.6\ \mu$m in p-GaAs. As for Ge, I_s is an increasing function of temperature owing to the increased phonon scattering rates at higher temperature.

V. SUMMARY AND CONCLUSIONS

We have presented a theory of saturation of heavy- to light-hole band transitions in p-type semiconductors with the diamond or zinc-blende crystal structure. Detailed calculations have

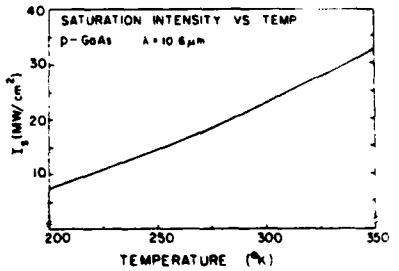

FIG. 8. Calculated saturation intensity as a function of temperature for p-GaAs and light with a wavelength of 10.6 μm.

been presented for p-type Ge and GaAs. We found that the intensity dependence of the absorption coefficient is closely approximated by an inhomogeneously broadened two-level model. For the temperature and concentration range where hole-phonon scattering dominates hole-impurity and hole-hole scattering, I_s is found to be independent of the hole density. This behavior is consistent with experimental results. The dependence of the saturation intensity on photon energy has been computed and compared with available experimental results. Good agreement between theory and experiment was found. We have predicted the dependence of the saturation intensity on temperature.

ACKNOWLEDGMENTS

The authors thank R. N. Silver and T. C. McGill for many useful discussions. We thank P. G. James, G. C. Osbourn, and M. S. Daw for assistance with the numerical calculations. We gratefully acknowledge the support of the Air Force Office of Scientific Research under Grant No. AFOSR-77-3216. One of us (D. L. S.) acknowledges support from the Alfred P. Sloan Foundation.

APPENDIX A: FREE-HOLE DENSITY MATRIX

In this appendix we outline the derivation of Eqs. (6a)–(6c) for the hole density matrix. We consider the low-hole density limit and take the Hamiltonian to be given by Eq. (2). The density matrix $\rho(t)$ satisfies

$$\frac{d\rho}{dt} = \frac{-i}{\hbar}[H, \rho]. \tag{A1}$$

We assume that ρ can be approximated by

$$\rho(t) \approx \sigma(t) P_L, \tag{A2}$$

where $\sigma(t)$ is the free-hole density matrix, and P_L describes the lattice in thermal equilibrium. Using standard approximations,[25] one finds

$$\frac{d\sigma_I(t)}{dt} \approx \frac{-i}{\hbar}[\gamma_I(t), \sigma_I(t)] - \frac{1}{\hbar^2}\int_0^\infty dt' \, \mathrm{Tr}_L\{[V_I(t), [V_I(t'), \sigma_I(t)P_L]]\}. \tag{A3}$$

Here the subscript I signifies that an operator is in the interaction representation, and Tr_L signifies a trace over lattice modes.

From Eq. (A3), one can see that $\sigma(t)$ is diagonal in wave vector. Prior to laser excitation, $\sigma(t)$ has the equilibrium value which is diagonal in wave vector. Taking matrix elements of Eq. (A3), we see that the time derivative of any matrix element of $d\sigma_I(t)/dt$ which is off-diagonal in $\vec{k}$ is equal to a sum of terms, all of which are proportional to a matrix element of $\sigma_I(t)$, which is off-diagonal in $\vec{k}$. Thus when the equation is integrated in time, all off-diagonal in $\vec{k}$ matrix elements of $\sigma_I(t)$ vanish. This result is to be expected since the electromagnetic field leads to transitions between states with the same wave vector. Taking matrix elements of Eq. (A3), dropping nonresonant terms and returning to the Schrödinger representation gives Eq. (6).

APPENDIX B: EQUATIONS OF MOTION FOR $\vec{J}(\vec{k})$

In this appendix we derive Eq. (7). Multiplying Eq. (6b) by $\vec{P}'$, taking the time derivative and tracing over bands gives

$$\frac{d^2}{dt^2}\mathrm{Tr}_b[\sigma(\vec{k},t)\vec{P}'] + \frac{1}{T_2(\vec{k})}\frac{d}{dt}\mathrm{Tr}_b[\sigma(\vec{k},t)\vec{P}'] = -\frac{i}{\hbar}\mathrm{Tr}_b\left(\frac{d\sigma(\vec{k},t)}{dt}[\vec{P}', H_e]\right). \tag{B1}$$

We have used the facts that σ, $\vec{P}'$, γ, and H_e are all diagonal in $\vec{k}$ and hence can be cyclically permuted in the trace on bands and that $[\vec{P}', \gamma]$ vanishes. Using Eq. (6b), we can write

$$\frac{1}{\hbar}\mathrm{Tr}_b\left(\frac{d\sigma(\vec{k},t)}{dt}[\vec{P}', H_e]\right) = -\frac{i}{\hbar^2}\mathrm{Tr}_b\{\sigma(\vec{k},t)[(H_e+\gamma), [H_e, \vec{P}']]\} - \frac{i}{T_2(\vec{k})}\frac{d}{dt}\mathrm{Tr}_b[\sigma(\vec{k},t)\vec{P}'] - \frac{i}{[T_2(\vec{k})]^2}\mathrm{Tr}_b[\sigma(\vec{k},t)\vec{P}']. \tag{B2}$$

Thus Eq. (B1) becomes

$$\frac{d^2}{dt^2}\mathrm{Tr}_b[\sigma(\vec{k},t)\vec{P}'] + \frac{2}{T_2(\vec{k})}\frac{d}{dt}\mathrm{Tr}_b[\sigma(\vec{k},t)\vec{P}'] + \left(\frac{1}{T_2(\vec{k})}\right)^2\mathrm{Tr}_b[\sigma(\vec{k},t)\vec{P}'] = -\frac{1}{\hbar^2}\mathrm{Tr}_b\{\sigma(\vec{k},t)[(H_e+\gamma), [H_e, \vec{P}']]\}. \tag{B3}$$

Evaluating the trace on the right-hand side, multiplying by $(N_h e/m)$, and neglecting $[1/T_2(\vec{k})]^2$ compared with $[\Omega(\vec{k})]^2$ gives Eq. (7).

APPENDIX C: EQUATIONS OF MOTION FOR THE DISTRIBUTION FUNCTIONS

In this appendix we derive the equations for the distribution functions $f_h(\vec{k})$ and $f_l(\vec{k})$. Multiplying Eq. (6b) by $(N_h e\vec{P}'/m)$ and taking the trace over bands gives

$$i\frac{d}{dt}\vec{J}(\vec{k})+\frac{i}{T_2(\vec{k})}\vec{J}(\vec{k})=\frac{N_h e}{m}\Omega(\vec{k})\sum_{\substack{b \text{ in } h\\ b' \text{ in } l}}[\sigma_{bb'}(\vec{k},t)\vec{P}_{b'b}(\vec{k})-\sigma_{b'b}(\vec{k},t)\vec{P}_{bb'}(\vec{k})]. \tag{C1}$$

Using Eq. (C1) and neglecting $[1/T_2(\vec{k})]$ compared with ω, Eq. (6a) can be written as (with b in the heavy-hole band)

$$\frac{df_h(\vec{k},t)}{dt}=-\frac{1}{2N_h c\hbar\Omega(\vec{k})}\left(\frac{d}{dt}\vec{J}(\vec{k})\cdot\vec{A}\right)-\sum_{c\vec{k}'}[R_{h\vec{k}-c\vec{k}'}f_h(\vec{k},t)-R_{c\vec{k}'-h\vec{k}}f_c(\vec{k}',t)]. \tag{C2}$$

With b in the light-hole band, Eq. (6a) can be written as

$$\frac{df_l(\vec{k},t)}{dt}=\frac{1}{2N_h c\hbar\Omega(\vec{k})}\left(\frac{d}{dt}\vec{J}(\vec{k})\cdot\vec{A}\right)-\sum_{c\vec{k}'}[R_{l\vec{k}-c\vec{k}'}f_l(\vec{k},t)-R_{c\vec{k}'-l\vec{k}}f_c(\vec{k}',t)]. \tag{C3}$$

Assuming $\vec{J}(\vec{k})$ and $\vec{A}$ have sinusoidal time dependence and averaging over many cycles, one gets the steady-state rate equations of Eq. (12).

APPENDIX D: AUXILIARY FUNCTIONS $F(\vec{k})$ AND $G(\vec{k})$

In this appendix we describe our treatment of the auxiliary functions $F(\vec{k})$ and $G(\vec{k})$. From the definition of these functions, we see that when the phonon scattering matrix elements are approximated as independent of the scattering angle, $F(\vec{k})$ depends on $E_h(\vec{k})$, and $G(\vec{k})$ depends on $E_l(\vec{k})$. Using the definitions of $F(\vec{k})$ and $G(\vec{k})$ and Eqs. (12a)–(12c) for the distribution functions, $F(E_h(\vec{k}))$ is seen to be determined by

$$\begin{aligned}F(E_h(\vec{k}))=\sum_{\vec{k}'}\{&-R_{h\vec{k}'-h\vec{k}}T_h(\vec{k}')+R_{l\vec{k}'-h\vec{k}}T_l(\vec{k}')\}\{[f_h^0(\vec{k}')-f_l^0(\vec{k}')]+F(E_h(\vec{k}'))T_h(\vec{k}')\\&-G(E_l(\vec{k}'))T_l(\vec{k}')\}\frac{\beta(\vec{k}')}{\beta(\vec{k}')[T_h(\vec{k}')+T_l(\vec{k}')]+1}\\&+\sum_{\vec{k}'}R_{h\vec{k}'-h\vec{k}}F(E_h(\vec{k}'))T_h(\vec{k}')+\sum_{\vec{k}'}R_{l\vec{k}'-h\vec{k}}G(E_l(\vec{k}))T_l(\vec{k}'),\end{aligned} \tag{D1}$$

and $G(E_l(\vec{k}))$ is determined by a similar equation where $(h\vec{k})$ in the scattering rates is replaced by $(l\vec{k})$. The function $G(\vec{k})$ describes the increased (from the equilibrium value) scattering into the light-hole band states. Because of the small density of light-hole band states, the magnitude of this function is much smaller than that of $F(\vec{k})$. In addition $T_h(\vec{k})$ is much greater than $T_l(\vec{k})$. Thus in Eq. (D1), we neglect $T_l(\vec{k})G(\vec{k})$ compared with $T_h(\vec{k})F(\vec{k})$. We have explicitly checked the self-consistency of this approximation at the end of the calculation.

Equation (D1) is an inhomogeneous, linear integral equation. Because of the energy conserving δ functions in the phonon scattering rates, it reduces to algebraic equations relating $F(E_h(\vec{k}))$ at different values of $E_h(\vec{k})$. The term proportional to $R_{l\vec{k}'-h\vec{k}}F(E_h(\vec{k}'))$, however, is responsible for coupling the equation for $F(E_h(\vec{k}))$ to those for all other values of $E_h(\vec{k}')$. [In other terms, the equation for $F(E_h(\vec{k}))$ is only coupled to those for $F(E_h(\vec{k})+\hbar\omega_0)$ and $F(E_h(\vec{k})-\hbar\omega_0)$]. To overcome this difficulty, we approximate the first term on the right-hand side of Eq. (D1), which can be written as

$$\sum_{\vec{k}'}[-R_{h\vec{k}'-h\vec{k}}T_h(\vec{k}')+R_{l\vec{k}'-h\vec{k}}T_l(\vec{k}')]\times\beta(\vec{k}')[f_h(\vec{k}')-f_l(\vec{k}')],$$

by

$$X\sum_{\vec{k}'}[-R_{h\vec{k}'-h\vec{k}}T_h(\vec{k}')+R_{l\vec{k}'-h\vec{k}}T_l(\vec{k}')]\times\beta(\vec{k}')[f_h(\vec{k}')-f_l(\vec{k}')]^1, \tag{D2}$$

where $[f_h(\vec{k}')-f_l(\vec{k}')]^1$ is the first approximation to $f_h(\vec{k}')-f_l(\vec{k}')$; that is, the first term in Eq. (15). Here X is a function of $\hbar\omega$, T, and l, but is as-

sumed independent of $E_h(k)$. We determine X by requiring

$$\sum_{\vec{k}'} \beta(\vec{k}')[f_h(\vec{k}') - f_l(\vec{k}')] = X \sum_{\vec{k}'} \beta(\vec{k}')[f_h(\vec{k}') - f_l(\vec{k}')]^1 . \quad \text{(D3)}$$

Since scattering to the light-hole band is much slower than scattering to the heavy-hole band (owing to the small density of states in the light-hole band);

$$\sum_{\vec{k}'} R_{h\vec{k}'-h\vec{k}} T_h(\vec{k}') \approx \sum_{\vec{k}'} R_{l\vec{k}'-h\vec{k}} T_l(\vec{k}') \approx 1 . \quad \text{(D4)}$$

Thus Eq. (D3) assures that the integral of the positive and negative parts of Eq. (D2) are separately satisfied. We solve the equation

$$F(E_h(\vec{k})) = X \sum_{\vec{k}'} [-R_{h\vec{k}'-h\vec{k}} T_h(\vec{k}') + R_{l\vec{k}'-h\vec{k}} T_l(\vec{k}')] \times \beta(\vec{k}')[f_h(\vec{k}') - f_l(\vec{k}')]^1 + \sum_{\vec{k}'} R_{h\vec{k}'-h\vec{k}} F(E_h(\vec{k}')) T_h(\vec{k}') , \quad \text{(D5)}$$

which is a series of inhomogeneous linear algebraic equations. We truncate the series for $E_h(\vec{k}) > 400$ meV. [$F(E_h(\vec{k}))$ is negligible for these high energies.] We first find the solution for $X = 1$. Calling the result of this calculation F', F is given by XF'. We determine X from Eq. (D3) which reduces to

$$X = 1 + \frac{X\left[\int_{\Omega(\vec{k})=\omega} \frac{ds\,|\vec{P}_{hl}(\vec{k})|^2 T_h(k) F^1(E_h(\vec{k}))}{|\nabla_{\vec{k}}\Omega(\vec{k})|[1 + l/l(\vec{k})]^{1/2}}\right]}{\left[\int_{\Omega(\vec{k})=\omega} \frac{ds[f_h^0(\vec{k}) - f_l^0(\vec{k})]\,|\vec{P}_{hl}(\vec{k})|^2}{|\nabla_{\vec{k}}\Omega(\vec{k})|[1 + l/l(\vec{k})]^{1/2}}\right]} . \quad \text{(D6)}$$

In order to limit the numerical expense, we approximate the surface integrals in Eq. (D6) using the four-point prescription suggested by Kane.[11]

From Eqs. (11) and (D3), we see that the function X relates the absorption coefficient calculated in the first approximation to the result of the more complete calculation by

$$\alpha(I, \omega) = X \alpha^1(I, \omega) , \quad \text{(D7)}$$

where $\alpha^1(I, \omega)$ is given by Eq. (18).

[1] A. F. Gibson, C. A. Rosito, C. A. Raffo, and M. F. Kimmitt, Appl. Phys. Lett. 21, 356 (1972).
[2] C. R. Phipps, Jr. and S. J. Thomas, Opt. Lett. 1, 93 (1977).
[3] R. L. Carlson, M. D. Montgomery, J. S. Ladish, and C. M. Lockhart, IEEE J. Quantum Electron. 13, 35D (1977).
[4] F. Keilmann, IEEE J. Quantum Electron. 12, 592 (1976).
[5] A. J. Alcock and A. C. Walker, Appl. Phys. Lett. 25, 299 (1974).
[6] B. J. Feldman and J. F. Figueria, Appl. Phys. Lett. 25, 301 (1974).
[7] A. F. Gibson, M. F. Kimmitt, and B. Norris, Appl. Phys. Lett. 24, 306 (1974).
[8] R. B. James and D. L. Smith, Phys. Rev. Lett. 42, 1495 (1979).
[9] M. Sargent III, Opt. Commun. 20, 298 (1977).
[10] V. L. Komolov, I. D. Yaroshetskii, and I. N. Yassievich, Fiz. Tekh. Poluprovodn. 11, 85 (1977) [Sov. Phys. Semicond. 11, 48 (1977)].
[11] E. O. Kane, J. Phys. Chem. Solids 1, 82 (1956).
[12] We neglect the small terms linear in k which appear in the $\vec{k}\cdot\vec{p}$ perturbation theory for zinc-blende crystals.
[13] H. B. Briggs and R. C. Fletcher, Phys. Rev. 91, 1342 (1953).
[14] A. H. Kahn, Phys. Rev. 97, 1647 (1955).
[15] W. Kaiser, R. J. Collins, and H. Y. Fan, Phys. Rev. 91, 1342 (1953).
[16] R. Braunstein, J. Phys. Chem. Solids 8, 280 (1959).
[17] A. J. Bishop and A. F. Gibson, Appl. Opt. 12, 2549 (1973).
[18] We neglect off-diagonal terms that can appear in the nonlinear susceptibility tensor for polarized light and we average over polarizations. That is, we consider the case of unpolarized light.
[19] E. Conwell, J. Phys. Chem. Solids 8, 236 (1959).
[20] D. M. Brown and R. Bray, Phys. Rev. 127, 1593 (1962).
[21] J. C. Hensel and K. Suzuki, Phys. Rev. B 9, 4219 (1974).
[22] P. Lawaetz, Phys. Rev. B 4, 3460 (1971).
[23] J. D. Wiley, Solid State Commun. 8, 1865 (1970).
[24] The first-order calculation for $\lambda = 10.6$ μm and $T = 295$ °K, neglecting acoustical phonon scattering, gives a value of 18 MW/cm^2 for I_s.
[25] See, for example, A. Abragam, *The Principles of Nuclear Magnetism* (Clarendon, Oxford, England, 1961), p. 272ff.

Solid State Communications, Vol.33, pp.395-398.
Pergamon Press Ltd. 1980. Printed in Great Britain.

DEPENDENCE OF THE SATURATION INTENSITY OF p-TYPE GERMANIUM ON IMPURITY CONCENTRATION AND RESIDUAL ABSORPTION AT 10.59 μm

R. B. James and D. L. Smith
California Institute of Technology
Pasadena, California 91125

(Received 5 November 1979 by H. Suhl)

We present a calculation of the saturation intensity I_s of p-Ge at 10.59 μm as a function of the impurity concentration. The effect of residual absorption is calculated and found to be important in the interpretation of experiments for intensities much greater than I_s.

The absorption of light in p-type Ge has been shown to saturate at sufficiently high intensities at wavelengths near 10 μm.[1-3] This behavior has been analyzed by modeling the Ge valence band structure as an ensemble of two-level absorbers[4]. Recently, the saturation characteristics of p-Ge were described by the authors in a way which realistically accounts for the anisotropic and nonparabolic valence bands and which is in close agreement with experiment[5-6]. Both calculations are valid only over a restricted range of impurity concentrations. In this letter, we extend the range of doping concentrations by including the effects of hole-impurity and hole-hole scattering. We also investigate the effects of residual absorption.

The dominant absorption mechanism at room temperature for light having a wavelength of 10.59 μm has been shown to be direct transitions between the heavy-hole band and the light-hole band[7]. Absorption due to this process is saturable, and the decrease in the absorption coefficient with increasing intensity is approximately given by[2-4]

$$\alpha_D(I,\omega) = \frac{\alpha_o(\omega)}{\sqrt{1+I/I_s(\omega)}} \quad , \tag{1}$$

where α_o is the absorption coefficient at low intensity due to direct free-hole transitions, $\alpha_D(I,\omega)$ is the absorption due to direct transitions as a function of intensity, and $I_s(\omega)$ is the saturation intensity.

The theory of the saturable absorption of p-Ge previously presented by the authors includes only the carrier-phonon scattering mechanism in determining the energy and phase relaxation of the hole carriers[5-6]. We now present a calculation of the saturation behavior which also allows for the interaction of the excited holes with ionized impurities and with other free holes. We consider only uncompensated samples of p-Ge where the acceptors are all shallow and ionized at room temperature conditions.

The scattering rate for a hole with energy ε by singly ionized impurities is given by

$$V_I = \frac{\pi e^4}{K^2\sqrt{2m^*}\varepsilon^{3/2}} N_I\left[\ln(1+\beta^2) - \frac{\beta^2}{1+\beta^2}\right] \quad , \tag{2a}$$

where

$$\beta^2 = \frac{2Km^*k_BT}{\pi N_I e^2\hbar^2}\varepsilon \quad , \tag{2b}$$

K is the dielectric constant, m^* is the free-carrier effective mass, k_B is the Boltzmann constant, and N_I is the total concentration of ionized impurities[8].

Following Ref. (9), the rate of hole-hole scattering for a hole with energy ε is given by

$$V_{hh} = \frac{2\sqrt{2}\,\pi\, N_h e^4 \lambda}{K^2\,\varepsilon^{3/2}\sqrt{m^*}} \tag{3a}$$

where

$$\lambda = 1 + \ln\left(\frac{\varepsilon}{2\hbar}\left(\frac{K m^*}{2\pi N_h e^2}\right)^{1/2}\right). \tag{3b}$$

The calculation of I_s at different impurity concentrations is performed using the theory presented in Ref. (6), where the calculation of scattering rates is modified to include hole-impurity and hole-hole scattering in addition to carrier-phonon scattering[10]. The inclusion of hole scattering by ionized impurities and other holes causes an increase in the scattering rate of the free holes and introduces a concentration dependence in the saturation intensity. The result of increasing the scattering rates is that higher intensities are required to reduce the free-hole population in the heavy-hole band at the resonant region, since the excited holes can re-route at a faster rate.

The calculated values of I_s as a function of the impurity concentration are given in Fig. (1) for 250, 300 and 350°K. We note that I_s is substantially independent of hole concentrations for concentrations less than about 3×10^{15}cm^{-3}, that is, in the region where the hole-phonon scattering mechanism is dominant. For hole concentrations greater than about 3×10^{15}cm^{-3}, the saturation intensity begins to increase monotonically with increasing hole concentration due

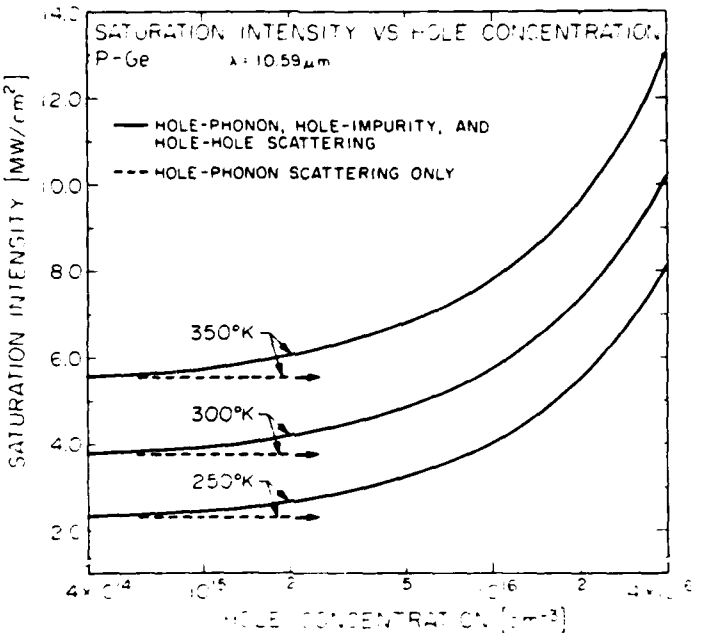

Figure 1. Calculated values of the saturation intensity I_s vs the hole concentration for p-Ge with light having a wavelength of 10.59 μm. Values of I_s vs N_h are shown for 250, 300 and 350°K. The dashed line in the figure represents a calculation of I_s assuming hole-impurity and hole-hole scattering to be negligible compared to hole-phonon scattering. The solid line in the figure represents a calculation of I_s which includes hole-impurity, hole-hole, and hole-phonon scattering mechanisms.

to the increased scattering rate of the free holes participating in the optical interaction. For hole concentrations less than about 3.5×10^{15} cm^{-3}, measured values of I_s at room temperature have been found to be independent of hole concentrations[1] with a value of about 4 MW/cm^2,[2-4] which is consistent with our calculation.

For a fixed impurity density, we find that I_s increases with increasing temperature. This increase is predominantly due to the increase in the hole-phonon scattering rate at the higher temperatures[5-6]. The fractional increase in I_s with increasing impurity density is smaller for the larger temperatures. The decrease in the impurity concentration dependence at higher temperatures occurs because the hole-impurity and hole-hole scattering mechanisms become less important compared to hole-phonon scattering as the temperature is increased.

Thus, depending on the intended application of the saturable absorber, we predict that at a fixed temperature one can control the saturation characteristics by controlling the doping concentration. In addition, knowledge of the effect of the doping concentration on the saturation intensity is useful in interpreting independent experimental results where the transmission experiments are performed in samples of different resistivities.

The effect of the residual absorption produces deviations of $\alpha(I)/\alpha(I=0)$ from the form given in Eq. (1). This deviation may be significant for $I >> I_s$ owing to the decrease in the direct intervalence band absorption compared to the nonsaturable absorption. The important residual (nonsaturable) absorption mechanisms are lattice absorption and indirect free-hole transitions. Measured values of the lattice absorption yield $\alpha_p = 0.013$ cm^{-1} at room temperature[11]. The absorption coefficient $\alpha_I(\omega)$ due to indirect free-hole transitions is approximated by

$$\alpha_I(\omega) = \frac{4\pi}{nc} \frac{N_h e^2 \tau}{m^*(1+\omega^2\tau^2)} , \qquad (4)$$

where ω is the frequency of the light, n is the refractive index, and τ is the average scattering time of the carriers determined by mobility data [12]. The intravalence band absorption cross section estimated from Eq. (4) is about 10^{-17} cm^2.

The total absorption coefficient at 10.59 μm can be written as:

$$\alpha(I) = \alpha_p + \alpha_I + \frac{\alpha_o}{\sqrt{1+I/I_s}} \quad , \qquad (5)$$

where I_s has a calculated value of about 4 MW/cm^2 for a hole concentration of 2×10^{15}cm^2 (5-6). The effect of a nonzero α_p and α_I in Eq. (4) is illustrated in Fig. (2) for $N_h = 2\times10^{15}$cm^{-3}, where values of $\alpha(I)/\alpha(I=0)$ are plotted as a function of intensity. Values of $\alpha(I)/\alpha(I=0)$ are shown for intensities ranging up to 1 GW/cm^2, which corresponds to the estimated optical damage threshold(3). For this value of N_h, α_o=1.20 cm^{-1}, α_I=0.02 cm^{-1}, and α_p=0.013 cm^{-1}. The values of $\alpha(I)/\alpha(I=0)$ for $\alpha_p = \alpha_I = 0$ are also shown for comparison. The inclusion of residual absorption effects becomes important for $I >> I_s$ and produces significant deviations of $\alpha(I)/\alpha(I=0)$ from the form of Eq. (1). A deviation has been measured for $I \geq 200$ MW/cm^2, which is consistent with our predictions; however, other effects may also be contributing to the deviation as discussed in Ref. (6).

In conclusion, we have calculated the saturation intensity as a function of the doping concentration. We have presented the results of the dependence of the residual absorption on the calculation of the absorption coefficient and found that the effect is important for intensities greater than about 30 times I_s.

Acknowledgement- The authors gratefully acknowledge the support of the Air Force Office of Scientific Research under Grant No. AFOSR-77-3216. One of us (DLS) acknowledges support from the Alfred P. Sloan Foundation.

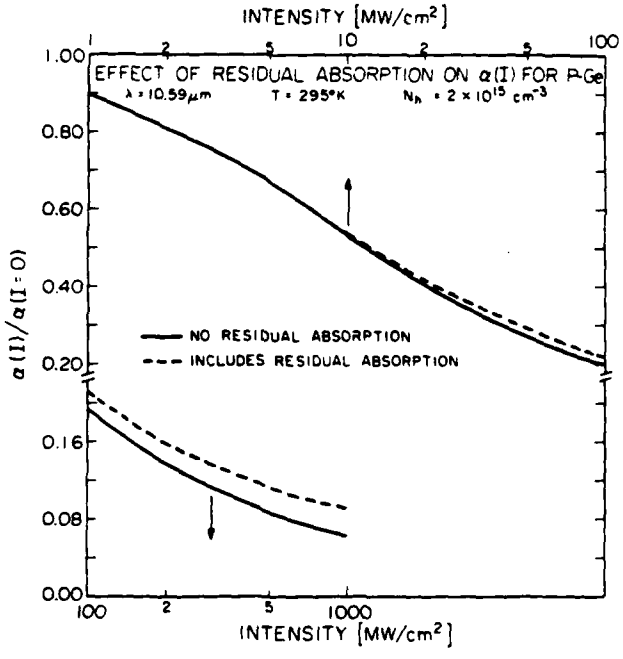

Figure 2. Calculated values of the absorption coefficient $\alpha(I)/\alpha(I=0)$ vs intensity for a hole concentration of 2×10^{15}cm^{-3} and light having a wavelength of 10.59 μm. The solid line in the figure represents the calculated values assuming no residual absorption. The dashed line in the figure represents the calculated values assuming a residual (non-saturable) absorption due to lattice absorption and indirect free-hole transitions. The upper curves show values of $\alpha(I)/\alpha(I=0)$ for intensities in the range of 1 - 100 MW/cm^2, and the lower curves are for intensities ranging from 100-1000 MW/cm^2.

REFERENCES

1. GIBSON, A. F., ROSITO, C. A., RAFFO, C. A., and KIMMITT, M. F., Appl. Phys. Lett. 21, 356 (1972).
2. PHIPPS, C. R., Jr. and THOMAS, S. J., Optics Lett. 1, 93 (1977).
3. CARLSON, R. L., MONTGOMERY, M. D., LADISH, J. S., and LOCKHART, C. M., IEEE J. Quant. Electron. QE-13, 35D (1977).
4. KEILMANN, F., IEEE J. Quant. Electron. QE-12, 592 (1976).
5. JAMES, R. B. and SMITH, D. L., Phys. Rev. Lett. 42, 1495 (1979).
6. JAMES, R. B. and SMITH, D. L., Phys. Rev. to be published.
7. KAISER, N., COLLINS, R. J., and FAN, H. Y., Phys. Rev. 91, 1380 (1953).
8. BROOKS, H., Advances in Electronics and Electron Physics (L. Marton, ed.), Vol. 7, p. 85. Academic Press, New York (1955).
9. YASSIEVICH, I. N. and YAROSHETSKII, I. D., Fiz. Tekh. Poluprovodn. 9, 857 (1975) [Sov. Phys. Semicond. 9, 565 (1975)].
10. We use the first order approximation discussed in Ref. (6). This approximation was shown to produce results for I_s within 15% of the more complete calculations in Ref. (5) and (6).
11. BISHOP, A. J. and GIBSON, A. F., Appl. Optics 12, 2549 (1973).
12. KAHN, A. H., Phys. Rev. 97, 1647 (1955).

Absorption of high-intensity CO_2 laser light in p-type semiconductors with small spin-orbit splittings

R. B. James and D. L. Smith
California Institute of Technology, Pasadena, California 91125

(Received 30 June 1980; accepted for publication 16 December 1980)

We present the results of a theory describing the saturation behavior of p-type semiconductors, such as Si, with small spin-orbit splittings by high intensity light with a wavelength near 10 μm. We consider absorption due to direct intervalence-band transitions between the heavy-hole and light-hole, heavy-hole and split-off, and light-hole and split-off bands. The functional form for the saturation of each transition is given and values for the saturation intensity as a function of photon energy and temperature are reported.

PACS numbers: 78.50.Ge, 42.10.Ke

I. INTRODUCTION

In a previous publication[1] we presented the results of a theory describing the saturable absorption of several p-type semiconductors for light having a wavelength in the 9–11 μm region, which corresponds to the CO_2 laser spectrum. The dominant absorption mechanism is intervalence-band transitions where a free-hole in the heavy-hole band absorbs a photon and makes a direct transition to the light-hole band. The absorption due to this mechanism has been shown to be saturable in Ge[2–5] and GaAs.[2] Results of the theory have been presented for most of the Group IV and III-V semiconductors for which the spin-orbit splitting was large compared to the energy of the incident photon. However, for materials such as Si, where the spin-orbit splitting is less than the photon energy, one must generalize the theory to include transitions from the heavy-hole to light-hole band, the heavy-hole to split-off band, and the light-hole to split-off band. In this paper, we consider the saturation properties of Si and InP, GaP and AlP which also have small spin-orbit splittings.

The absorption coefficient for these materials in the 9–11 μm region can be written as

$$\alpha = \alpha_p + \alpha_{h\to l} + \alpha_{h\to s} + \alpha_{l\to s}, \tag{1}$$

where α_p is the residual absorption due to phonons, $\alpha_{h\to l}$ ($\alpha_{h\to s}$) is the absorption coefficient due to direct heavy-hole to light-hole (split-off) band transitions, and $\alpha_{l\to s}$ is the absorption coefficient due to direct light-hole to split-off band transitions. The effect of lattice absorption depends on the wavelength of the light and the temperature of the material. Lattice absorption at 9.6 μm requires the cooperation of at least three phonons to conserve energy and is therefore small. In Si, two-phonon absorption is energetically possible for a wavelength of 10.6 μm. The absorption of light by the creation of phonons can be included in a straightforward way, since this process is nonsaturable and just adds a residual absorption term.[6] In this paper, we analyze the saturable absorption due to the direct intervalence-band transitions.

The paper is organized in the following way: in Sec. II we describe the theoretical approach, in Sec. III we present the results of the calculation, and in Sec. IV we summarize our conclusions.

II. THEORETICAL APPROACH

In previous work we have given an expression to determine the decrease in the absorption coefficient with increasing intensity when only the heavy-hole and light-hole bands were involved in the optical transition.[1,7,8] Analogous expressions can be written for direct transitions between the heavy-hole and split-off bands and between the light-hole and split-off bands. In order to numerically integrate the expressions for $\alpha_{h\to l}$, $\alpha_{h\to s}$ and $\alpha_{l\to s}$, we must calculate the steady-state distribution functions in each band as a function of intensity for each wave vector $\mathbf{k}$. If we assume that the three direct optical transitions are uncoupled, then the absorption due to each resonant transition can be independently analyzed. That is, we can determine the saturation characteristics for $\alpha_{h\to l}$, $\alpha_{h\to s}$, and $\alpha_{l\to s}$ independently using the theory previously presented. Here, we assume that the modification in the distribution function of free holes due to one particular resonant transition between two valence bands in $\mathbf{k}$ space does not strongly affect the distribution of free holes in the resonant regions for the other transitions. This assumption is made in order to limit the numerical expense involved in the calculation of the distribution functions for each band; however, a more exact calculation can be performed provided new experimental evidence becomes available to justify the additional complexity in the calculation. We present the calculation to qualitatively characterize the saturation behavior of these materials and determine if the saturation properties are of sufficient interest to warrant additional experimental investigation.

In Ref. 8 we find that $\alpha_{h\to l}$ is given by

$$\alpha_{h\to l} = \frac{4\pi^2}{(\epsilon_\infty)^{1/2}m^2\omega c}\frac{N_h e^2}{3\hbar}\left(\frac{1}{2\pi}\right)^3 \times\left(\int_{\Omega_{hl}(\mathbf{k})=\omega}\frac{dS}{|\nabla_{\mathbf{k}}\Omega_{hl}(\mathbf{k})|}\frac{|\mathbf{p}_{hl}(\mathbf{k})|^2[f_h^o(\mathbf{k})-f_l^o(\mathbf{k})]}{[1+I/\xi_{hl}(\mathbf{k})]^{1/2}}\right), \tag{2}$$

where

$$\xi_{hl}(\mathbf{k}) = \frac{3\hbar^2 c(\epsilon_\infty)^{1/2}m^2\omega^2}{[T_h(\mathbf{k})+T_l(\mathbf{k})]T_{hl}(\mathbf{k})2\pi e^2|\mathbf{p}_{hl}(\mathbf{k})|^2}, \tag{3a}$$

$$\frac{2}{T_{hl}(\mathbf{k})} = \sum_{\mathbf{k}'}(R_{h\mathbf{k}\to c\mathbf{k}'} + R_{l\mathbf{k}\to c\mathbf{k}'}), \tag{3b}$$

 0021-8979/81/064238-03$01.10

$$\frac{1}{T_h(\mathbf{k})} = \sum_{\mathbf{k}'} (R_{h\mathbf{k}\to c\mathbf{k}'}), \tag{3c}$$

and

$$\frac{1}{T_l(\mathbf{k})} = \sum_{\mathbf{k}'} (R_{l\mathbf{k}\to c\mathbf{k}'}). \tag{3d}$$

Here, $R_{a\mathbf{k}\to b\mathbf{k}'}$ is the rate at which a hole in band a with wave vector $\mathbf{k}$ is scattered into a state in band b with wave vector $\mathbf{k}'$, I is the intensity of the light, N_h is the density of holes, the subscripts h (l) designate the heavy- (light-) hole band, m is the free-electron mass, $\hbar\omega$ is the photon energy, ϵ_∞ is the high-frequency dielectric constant, $|p_{hl}(\mathbf{k})|^2$ is the squared momentum matrix element between the Bloch states in the heavy- and light-hole bands (summed over the two degenerate states in each band), $\Omega_{hl}(\mathbf{k})$ is the angular frequency associated with the energy difference $(\epsilon_h(\mathbf{k})\epsilon_l(\mathbf{k}))$, where $\epsilon_i(\mathbf{k})$ is the energy of the hole with wave vector $\mathbf{k}$ in band i, and $f_i^*(\mathbf{k})$ is the probability that a hole state with wave vector $\mathbf{k}$ is occupied in band i in thermal equilibrium. The integral in Eq. (2) is calculated over a surface of constant $\Omega_{hl}(\mathbf{k})$. Analogous expressions are written for $\alpha_{h\to s}$ and $\alpha_{l\to s}$. The method used for determining the momentum matrix elements $|p_{hl}(\mathbf{k})|^2$, $|p_{hs}(\mathbf{k})|^2$, and $|p_{ls}(\mathbf{k})|^2$ is described by Kane.[9] The one-hole energies are determined by degenerate $\mathbf{k}\cdot\mathbf{p}$ perturbation theory.[9]

We consider hole densities such that hole-phonon scattering is the dominant scattering mechanism. If we assume that the mobility data can be explained by acoustic and nonpolar optical phonon scattering, then the valence-band deformation potential parameters can be chosen so that the temperature dependence of the mobility agrees with the experimental results. Using the results of Ref. (10), we write the mobility μ as

$$\mu = \frac{2^{3/2}\pi^{1/2}e\hbar^4}{3m_0^{5/2}k_B^{3/2}}\left(\frac{r+r^{3/2}}{1+r^{3/2}}\right)\left[\left(\frac{m_h^*}{m_0}\right)^{5/2}\xi\right]^{-1} \times S(\theta,\eta,T)T^{-3/2}, \tag{4}$$

where

$$r = m_h^*/m_l^*, \tag{5a}$$

$$\eta = (E_{op}/E_{ac})^2, \tag{5b}$$

$$\xi = E_{ac}^2/(\rho\bar{u}^2), \tag{5c}$$

and

$$S(\theta,\eta,T) = \int_0^\infty \frac{xe^{-x}dx}{1+\frac{1}{2}\eta(\theta/T)(e^{\theta/T}-1)^{-1}(1+\theta/xT)^{1/2}+e^{\theta/T}(1-\theta/xT)^{1/2}}. \tag{5d}$$

Here, $m_h^*(m_l^*)$ is the effective heavy-hole (light-hole) mass, ρ is the material density, $\bar{u}$ is the average speed of sound, $k_B\theta$ is the energy of the zone-center longitudinal optical phonon, and $E_{ac}(E_{op})$ is the deformation potential for the acoustic (nonpolar optical) mode. The values of ξ for the materials considered are given in Table I. The values are obtained by assuming $\eta = 4$ and fitting the magnitude of the mobility at room temperature.[10] Given the values for the deformation potential parameters, we can write expressions for the scattering rates for acoustical and nonpolar optical phonon scattering following Conwell.[11] For the case of lightly doped material near room-temperature, ionized impurity scattering and hole-hole scattering can be neglected.[6] For heavier doped material, the effect of these scattering mechanisms can be included in analogy with the results of Ref. 6.

TABLE I. Parameters used in determining the valence-band deformation potential parameters. The hole mobility is given at room temperature in units of cm^2/V sec. Values of ξ are given in units of eV^2 cm sec^2/gm.

Material	μ	m_h^*/m_0	m_l^*/m_0	θ	Cyclotron resonance parameters	Δ (meV)	ξ ($\times 10^{-11}$)
Si	480[a]	0.53[b]	0.16[b]	730[c]	Ref. 13	44.0[d]	3.71
InP	154[e]	0.85[b]	0.089[b]	498[c]	Ref. 13	130.0[f]	2.52
GaP	150[g]	0.79[b]	0.14[b]	582[c]	Ref. 13	80.0[h]	3.59
AlP	450[i]	0.63[b]	0.20[b]	719[c]	Ref. 13	50.0[h]	2.53

[a]Reference 12.
[b]Reference 13.
[c]Reference 14.
[d]Reference 15.
[e]Reference 16.
[f]Reference 17.
[g]Reference 18.
[h]Reference 19.
[i]Reference 20.

III. RESULTS AND DISCUSSION

We numerically integrate the expressions for $\alpha_{h\to l}$, $\alpha_{h\to s}$, and $\alpha_{l\to s}$, and find that the intensity dependence of the absorption due to each direct transition can be fit to high accuracy by the functional form

$$\alpha_i(I) = \frac{\alpha_{oi}}{[1+I/(I_s)_i]^{1/2}}, \tag{6}$$

where α_{oi} is the low-intensity absorption coefficient and $(I_s)_i$ is the saturation intensity of the i^{th} intervalence-band transition. Values of $(I_s)_{hl}$, $(I_s)_{hs}$, and $(I_s)_{ls}$ at $\lambda = 9.6\,\mu$m and $T = 295$ are given in Table II for the materials considered.

Most measurements of the saturable absorption in p-type semiconductors are interpreted in terms of an inhomogeneously broadened two-level model in which the reduction in the absorption coefficient is given by

$$\alpha(I) = \frac{\alpha_0}{(1+I/I_s)^{1/2}}, \tag{7}$$

where α_0 is the low-intensity absorption coefficient. The absorption coefficient from the sum of the three intervalence-band processes can be reasonably well approximated by this form for intensities in the range in which most saturable absorption experiments have been performed ($I \lesssim 100$ MW/cm^2). For intensities low enough that the square roots in Eqs. (6) and (7) can be power series expanded, one has

TABLE II. Parameters describing the saturation characteristics for heavy-hole to light-hole band transitions, heavy-hole to split-off band transitions, and light-hole to split-off band transitions for $T_0 = 295$ K and $E_0 = 129.8$ meV. Values of the saturation intensity are given owing to the cumulative effect of all three direct intervalence-band transitions. Also included are the first derivatives of the saturation intensity with respect to photon energy and temperature. All intensities are given in units of MW/cm².

Material	$(I_s)_{hl}$	$(I_s)_{hs}$	$(I_s)_{ls}$	I_s	$\left.\frac{\partial I_s}{\partial E}\right\|_{E_0}\left(\frac{\text{MW}}{\text{cm}^2}\frac{1}{\text{meV}}\right)$	$\left.\frac{\partial I_s}{\partial T}\right\|_{T_0}\left(\frac{\text{MW}}{\text{cm}^2}\frac{1}{^\circ\text{K}}\right)$
Si	301	127	161	175	3.3	1.7
InP[a]	745	...	97	159	8	1.0
GaP	1900	161	332	229	0.9	2.3
AlP	104	190	215	122	3.1	1.0

[a]The $h \rightarrow s$ transition in InP is not energetically allowed for this photon energy.

$$\frac{1}{I_s} = \frac{1}{\alpha_0}\sum_j \frac{\alpha_{oj}}{(I_s)_j}. \tag{8}$$

The values of α_{oj}/α_0 for each of the three resonant transitions are listed in Table III. We have taken I_s to fit the result for the sum of the three processes for intensities up to 100 MW/cm². We find the saturation intensity to have a smooth behavior near room temperature and $\lambda = 9.6\,\mu$m ($E_0 = 129.8$ meV). This allows one to describe the saturation near room temperature and near E_0 by giving the values of I_s (at $E_0 = 129.8$ meV and $T = 295$ K) and the slopes $\partial I_s/\partial E|_{E_0}$ and $\partial I_s/\partial T|_{T_0}$. The values of I_s, $\partial I_s/\partial E|_{E_0}$, and $\partial I_s/\partial T|_{T_0}$ are given in Table II.

Values of the saturation intensities in the materials with small spin-orbit splittings are generally larger than the values in materials with larger spin-orbit splittings such as Ge and GaAs. This difference is primarily due to the relatively slow splitting between the valence bands with increasing $|k|$. As a result, the resonant optical transitions occur at larger values of $|k|$. As discussed in Ref. 1, this leads to larger scattering rates for the states involved in the transitions and thus large values for the saturation intensity. The deformation potentials and the values of the optical matrix elements also play an important role in determining the value of the saturation intensity.

There has been one experimental attempt to observe saturable absorption in Si[2]. In this experiment only a small degree of saturation was observed and a lower limit of 50 MW/cm² was set for the saturation intensity.

IV. CONCLUSIONS

The calculated values for the saturation intensity indicate that Si, InP, GaP, and AlP are more difficult to saturate than several other p-type semiconductors.[1] Thus it seems likely that these materials will not be as useful in the applications of saturable absorbers to CO_2 laser systems as other p-type semiconductors such as Ge. In addition the residual (nonsaturable) absorption is larger for the materials considered in this paper owing to their larger longitudinal optical-phonon energy, which is undesirable.

TABLE III. Values of α_{oj}/α_0 for transitions between the heavy- and light-hole bands, the heavy-hole and split-off bands, and the light-hole and split-off bands. All values are given for a photon energy of 129.8 meV ($\lambda = 9.6$ μm) and room-temperature conditions.

Material	$\frac{(\alpha_0)_{h\rightarrow l}}{\alpha_0}$	$\frac{(\alpha_0)_{h\rightarrow s}}{\alpha_0}$	$\frac{(\alpha_0)_{l\rightarrow s}}{\alpha_0}$
Si	0.37	0.39	0.24
InP[a]	0.39	...	0.61
GaP	0.14	0.58	0.28
AlP	0.71	0.19	0.10

[a]The $h \rightarrow s$ transition in InP is not energetically allowed for this photon energy.

ACKNOWLEDGMENTS

The authors gratefully acknowledge the support of the Air Force Office of Scientific Research under Grant No. AFOSR-77-3216. One of us (D.L.S) acknowledges support from the Alfred P. Sloan Foundation.

[1] R. B. James and D. L. Smith, J. Appl. Phys. 51, 2836 (1980).
[2] A. F. Gibson, C. A. Rosito, C. A. Raffo, and M. F. Kimmitt, Appl. Phys. Lett. 21, 356 (1972).
[3] C. R. Phipps, Jr. and S. J. Thomas, Opt. Lett. 1, 93 (1977).
[4] R. L. Carlson, M. D. Montgomery, J. S. Ladish, and C. M. Lockhart, IEEE J. Quantum Electron. 13, 35 (1977).
[5] F. Keilmann, IEEE J. Quantum Electron. 12, 592 (1976).
[6] R. B. James and D. L. Smith, Solid State Commun. 33, 395 (1980).
[7] R. B. James and D. L. Smith, Phys. Rev. Lett. 42, 1495 (1979).
[8] R. B. James and D. L. Smith, Phys. Rev. B 21, 3502 (1980).
[9] E. O. Kane, J. Phys. Chem. Solids 1, 82 (1956).
[10] J. D. Wiley and M. DiDomenico, Jr., Phys. Rev. B 2, 427 (1970).
[11] E. M. Conwell, J. Phys. Chem. Solids 8, 236 (1959).
[12] J. I. Pankove, *Optical Processes in Semiconductors* (Dover, New York, 1971), Appendix II.
[13] P. Lawaetz, Phys. Rev. B 4, 3460 (1971).
[14] W. Richter, *Springer Tracts in Modern Physics* 78, *Solid-State Physics*, edited by G. Hohler (Springer-Verlag, Berlin, 1976), p. 174.
[15] S. Zwerdling, K. J. Button, B. Lax, and L. M. Roth, Phys. Rev. 118, 975 (1960).
[16] M. Glicksman and K. Weiser, J. Phys. Chem. Solids 10, 337 (1959).
[17] M. Cardona, K. L. Shaklee, and F. H. Pollack, Phys. Rev. 154, 696 (1967).
[18] R. J. Cherry and J. W. Allen, J. Phys. Chem. Solids 23, 163 (1962).
[19] P. J. Dean, G. Kaminsky, and R. B. Zettersirom, J. Appl. Phys. 38, 3551 (1967).
[20] J. D. Wiley, *Semiconductors and Semimetals*, edited by R. K. Willardson and A. C. Beer (Academic, New York, 1975), p. 141.

Absorption of high-intensity CO_2 laser light in p-type semiconductors with small spin-orbit splittings

R. B. James and D. L. Smith
California Institute of Technology, Pasadena, California 91125

(Received 30 June 1980; accepted for publication 16 December 1980)

We present the results of a theory describing the saturation behavior of p-type semiconductors, such as Si, with small spin-orbit splittings by high intensity light with a wavelength near 10 μm. We consider absorption due to direct intervalence-band transitions between the heavy-hole and light-hole, heavy-hole and split-off, and light-hole and split-off bands. The functional form for the saturation of each transition is given and values for the saturation intensity as a function of photon energy and temperature are reported.

PACS numbers: 78.50.Ge, 42.10.Ke

I. INTRODUCTION

In a previous publication[1] we presented the results of a theory describing the saturable absorption of several p-type semiconductors for light having a wavelength in the 9–11 μm region, which corresponds to the CO_2 laser spectrum. The dominant absorption mechanism is intervalence-band transitions where a free-hole in the heavy-hole band absorbs a photon and makes a direct transition to the light-hole band. The absorption due to this mechanism has been shown to be saturable in Ge[2–5] and GaAs.[2] Results of the theory have been presented for most of the Group IV and III-V semiconductors for which the spin-orbit splitting was large compared to the energy of the incident photon. However, for materials such as Si, where the spin-orbit splitting is less than the photon energy, one must generalize the theory to include transitions from the heavy-hole to light-hole band, the heavy-hole to split-off band, and the light-hole to split-off band. In this paper, we consider the saturation properties of Si and InP, GaP and AlP which also have small spin-orbit splittings.

The absorption coefficient for these materials in the 9–11 μm region can be written as

$$\alpha = \alpha_p + \alpha_{h\to l} + \alpha_{h\to s} + \alpha_{l\to s}, \tag{1}$$

where α_p is the residual absorption due to phonons, $\alpha_{h\to l}$ ($\alpha_{h\to s}$) is the absorption coefficient due to direct heavy-hole to light-hole (split-off) band transitions, and $\alpha_{l\to s}$ is the absorption coefficient due to direct light-hole to split-off band transitions. The effect of lattice absorption depends on the wavelength of the light and the temperature of the material. Lattice absorption at 9.6 μm requires the cooperation of at least three phonons to conserve energy and is therefore small. In Si, two-phonon absorption is energetically possible for a wavelength of 10.6 μm. The absorption of light by the creation of phonons can be included in a straightforward way, since this process is nonsaturable and just adds a residual absorption term.[6] In this paper, we analyze the saturable absorption due to the direct intervalence-band transitions.

The paper is organized in the following way: in Sec. II we describe the theoretical approach, in Sec. III we present the results of the calculation, and in Sec. IV we summarize our conclusions.

II. THEORETICAL APPROACH

In previous work we have given an expression to determine the decrease in the absorption coefficient with increasing intensity when only the heavy-hole and light-hole bands were involved in the optical transition.[1,7,8] Analogous expressions can be written for direct transitions between the heavy-hole and split-off bands and between the light-hole and split-off bands. In order to numerically integrate the expressions for $\alpha_{h\to l}$, $\alpha_{h\to s}$ and $\alpha_{l\to s}$, we must calculate the steady-state distribution functions in each band as a function of intensity for each wave vector k. If we assume that the three direct optical transitions are uncoupled, then the absorption due to each resonant transition can be independently analyzed. That is, we can determine the saturation characteristics for $\alpha_{h\to l}$, $\alpha_{h\to s}$, and $\alpha_{l\to s}$ independently using the theory previously presented. Here, we assume that the modification in the distribution function of free holes due to one particular resonant transition between two valence bands in k space does not strongly affect the distribution of free holes in the resonant regions for the other transitions. This assumption is made in order to limit the numerical expense involved in the calculation of the distribution functions for each band; however, a more exact calculation can be performed provided new experimental evidence becomes available to justify the additional complexity in the calculation. We present the calculation to qualitatively characterize the saturation behavior of these materials and determine if the saturation properties are of sufficient interest to warrant additional experimental investigation.

In Ref. 8 we find that $\alpha_{h\to l}$ is given by

$$\alpha_{h\to l} = \frac{4\pi^2}{(\epsilon_\infty)^{1/2}m^2\omega c}\frac{N_h e^2}{3\hbar}\left(\frac{1}{2\pi}\right)^3 \times\left(\int_{\Omega_{hl}(\mathbf{k})=\omega}\frac{dS}{|\nabla_{\mathbf{k}}\Omega_{hl}(\mathbf{k})|}\frac{|\mathbf{p}_{hl}(\mathbf{k})|^2[f_h^s(\mathbf{k})-f_l^s(\mathbf{k})]}{[1+I/\xi_{hl}(\mathbf{k})]^{1/2}}\right), \tag{2}$$

where

$$\xi_{hl}(\mathbf{k}) = \frac{3\hbar^2 c(\epsilon_\infty)^{1/2}m^2\omega^2}{[T_h(\mathbf{k})+T_l(\mathbf{k})]T_{hl}(\mathbf{k})2\pi e^2|\mathbf{p}_{hl}(\mathbf{k})|^2}, \tag{3a}$$

$$\frac{2}{T_{hl}(\mathbf{k})} = \sum_{\mathbf{k}'}(R_{h\,\mathbf{k}\to\mathbf{k}'} + R_{l\,\mathbf{k}\to\mathbf{k}'}), \tag{3b}$$

 0021-8979/81/064238-03$01.10

$$\frac{1}{T_h(\mathbf{k})} = \sum_{\mathbf{k}'} (R_{h\mathbf{k}\to c\mathbf{k}'}), \tag{3c}$$

and

$$\frac{1}{T_l(\mathbf{k})} = \sum_{\mathbf{k}'} (R_{l\mathbf{k}\to c\mathbf{k}'}). \tag{3d}$$

Here, $R_{a\mathbf{k}\to b\mathbf{k}'}$ is the rate at which a hole in band a with wave vector $\mathbf{k}$ is scattered into a state in band b with wave vector $\mathbf{k}'$, I is the intensity of the light, N_h is the density of holes, the subscripts h (l) designate the heavy- (light-) hole band, m is the free-electron mass, $\hbar\omega$ is the photon energy, ϵ_∞ is the high-frequency dielectric constant, $|\mathbf{p}_{hl}(\mathbf{k})|^2$ is the squared momentum matrix element between the Bloch states in the heavy- and light-hole bands (summed over the two degenerate states in each band), $\Omega_{hl}(\mathbf{k})$ is the angular frequency associated with the energy difference $(\epsilon_h(\mathbf{k})\epsilon_l(\mathbf{k}))$, where $\epsilon_i(\mathbf{k})$ is the energy of the hole with wave vector $\mathbf{k}$ in band i, and $f_i^e(\mathbf{k})$ is the probability that a hole state with wave vector $\mathbf{k}$ is occupied in band i in thermal equilibrium. The integral in Eq. (2) is calculated over a surface of constant $\Omega_{hl}(\mathbf{k})$. Analogous expressions are written for $\alpha_{h\to s}$ and $\alpha_{l\to s}$. The method used for determining the momentum matrix elements $|\mathbf{p}_{hl}(\mathbf{k})|^2$, $|\mathbf{p}_{hs}(\mathbf{k})|^2$, and $|\mathbf{p}_{ls}(\mathbf{k})|^2$ is described by Kane.[9] The one-hole energies are determined by degenerate $\mathbf{k}\cdot\mathbf{p}$ perturbation theory.[9]

We consider hole densities such that hole-phonon scattering is the dominant scattering mechanism. If we assume that the mobility data can be explained by acoustic and nonpolar optical phonon scattering, then the valence-band deformation potential parameters can be chosen so that the temperature dependence of the mobility agrees with the experimental results. Using the results of Ref. (10), we write the mobility μ as

$$\mu = \frac{2^{3/2}\pi^{1/2}e\hbar^4}{3m_0^{5/2}k_B^{3/2}}\left(\frac{r+r^{3/2}}{1+r^{3/2}}\right)\left[\left(\frac{m_h^*}{m_0}\right)^{5/2}\xi\right]^{-1} \times S(\theta,\eta,T)T^{-3/2}, \tag{4}$$

where

$$r = m_h^*/m_l^*, \tag{5a}$$

$$\eta = (E_{op}/E_{ac})^2, \tag{5b}$$

$$\xi = E_{ac}^2/(\rho\bar{u}^2), \tag{5c}$$

and

$$S(\theta,\eta,T) = \int_0^\infty \frac{xe^{-x}dx}{1+\tfrac{1}{2}\eta(\theta/T)(e^{\theta/T}-1)^{-1}(1+\theta/xT)^{1/2}+e^{\theta/T}(1-\theta/xT)^{1/2}}. \tag{5d}$$

Here, $m_h^*(m_l^*)$ is the effective heavy-hole (light-hole) mass, ρ is the material density, $\bar{u}$ is the average speed of sound, $k_B\theta$ is the energy of the zone-center longitudinal optical phonon, and $E_{ac}(E_{op})$ is the deformation potential for the acoustic (nonpolar optical) mode. The values of ξ for the materials considered are given in Table I. The values are obtained by assuming $\eta = 4$ and fitting the magnitude of the mobility at room temperature.[10] Given the values for the deformation potential parameters, we can write expressions for the scattering rates for acoustical and nonpolar optical phonon scattering following Conwell.[11] For the case of lightly doped material near room-temperature, ionized impurity scattering and hole-hole scattering can be neglected.[6] For heavier doped material, the effect of these scattering mechanisms can be included in analogy with the results of Ref. 6.

TABLE I. Parameters used in determining the valence-band deformation potential parameters. The hole mobility is given at room temperature in units of cm^2/V sec. Values of ξ are given in units of eV^2 cm sec^2/gm.

Material	μ	m_h^*/m_0	m_l^*/m_0	θ	Cyclotron resonance parameters	Δ (meV)	ξ ($\times 10^{-11}$)
Si	480[a]	0.53[a]	0.16[b]	730[c]	Ref. 13	44.0[d]	3.71
InP	154[e]	0.85[b]	0.089[b]	498[c]	Ref. 13	130.0[f]	2.52
GaP	150[g]	0.79[b]	0.14[b]	582[c]	Ref. 13	80.0[h]	3.59
AlP	450[i]	0.63[b]	0.20[b]	719[c]	Ref. 13	50.0[h]	2.53

[a]Reference 12.
[b]Reference 13.
[c]Reference 14.
[d]Reference 15.
[e]Reference 16.
[f]Reference 17.
[g]Reference 18.
[h]Reference 19.
[i]Reference 20.

III. RESULTS AND DISCUSSION

We numerically integrate the expressions for $\alpha_{h\to l}$, $\alpha_{h\to s}$, and $\alpha_{l\to s}$, and find that the intensity dependence of the absorption due to each direct transition can be fit to high accuracy by the functional form

$$\alpha_i(I) = \frac{\alpha_{oi}}{[1+I/(I_s)_i]^{1/2}}, \tag{6}$$

where α_{oi} is the low-intensity absorption coefficient and $(I_s)_i$ is the saturation intensity of the i^{th} intervalence-band transition. Values of $(I_s)_{hl}$, $(I_s)_{hs}$, and $(I_s)_{ls}$ at $\lambda = 9.6\,\mu$m and $T = 295$ are given in Table II for the materials considered.

Most measurements of the saturable absorption in p-type semiconductors are interpreted in terms of an inhomogeneously broadened two-level model in which the reduction in the absorption coefficient is given by

$$\alpha(I) = \frac{\alpha_0}{(1+I/I_s)^{1/2}}, \tag{7}$$

where α_0 is the low-intensity absorption coefficient. The absorption coefficient from the sum of the three intervalence-band processes can be reasonably well approximated by this form for intensities in the range in which most saturable absorption experiments have been performed ($I \lesssim 100$ MW/cm^2). For intensities low enough that the square roots in Eqs. (6) and (7) can be power series expanded, one has

TABLE II. Parameters describing the saturation characteristics for heavy-hole to light-hole band transitions, heavy-hole to split-off band transitions, and light-hole to split-off band transitions for $T_0 = 295$ K and $E_0 = 129.8$ meV. Values of the saturation intensity are given owing to the cumulative effect of all three direct intervalence-band transitions. Also included are the first derivatives of the saturation intensity with respect to photon energy and temperature. All intensities are given in units of MW/cm².

Material	$(I_s)_{hl}$	$(I_s)_{hs}$	$(I_s)_{ls}$	I_s	$\left.\frac{\partial I_s}{\partial E}\right\|_{E_0}\left(\frac{\text{MW}}{\text{cm}^2}\frac{1}{\text{meV}}\right)$	$\left.\frac{\partial I_s}{\partial T}\right\|_{T_0}\left(\frac{\text{MW}}{\text{cm}^2}\frac{1}{^\circ\text{K}}\right)$
Si	301	127	161	175	3.3	1.7
InP[a]	745	...	97	159	8	1.0
GaP	1900	161	332	229	0.9	2.3
AlP	104	190	215	122	3.1	1.0

[a]The $h \rightarrow s$ transition in InP is not energetically allowed for this photon energy.

$$\frac{1}{I_s} = \frac{1}{\alpha_0}\sum_j \frac{\alpha_{oj}}{(I_s)_j}. \tag{8}$$

The values of α_{oj}/α_0 for each of the three resonant transitions are listed in Table III. We have taken I_s to fit the result for the sum of the three processes for intensities up to 100 MW/cm². We find the saturation intensity to have a smooth behavior near room temperature and $\lambda = 9.6\,\mu$m ($E_0 = 129.8$ meV). This allows one to describe the saturation near room temperature and near E_0 by giving the values of I_s (at $E_0 = 129.8$ meV and $T = 295$ K) and the slopes $\partial I_s/\partial E|_{E_0}$ and $\partial I_s/\partial T|_{T_0}$. The values of I_s, $\partial I_s/\partial E|_{E_0}$, and $\partial I_s/\partial T|_{T_0}$ are given in Table II.

Values of the saturation intensities in the materials with small spin-orbit splittings are generally larger than the values in materials with larger spin-orbit splittings such as Ge and GaAs. This difference is primarily due to the relatively slow splitting between the valence bands with increasing $|k|$. As a result, the resonant optical transitions occur at larger values of $|k|$. As discussed in Ref. 1, this leads to larger scattering rates for the states involved in the transitions and thus large values for the saturation intensity. The deformation potentials and the values of the optical matrix elements also play an important role in determining the value of the saturation intensity.

There has been one experimental attempt to observe saturable absorption in Si[2]. In this experiment only a small degree of saturation was observed and a lower limit of 50 MW/cm² was set for the saturation intensity.

IV. CONCLUSIONS

The calculated values for the saturation intensity indicate that Si, InP, GaP, and AlP are more difficult to saturate than several other p-type semiconductors.[1] Thus it seems likely that these materials will not be as useful in the applications of saturable absorbers to CO_2 laser systems as other p-type semiconductors such as Ge. In addition the residual (nonsaturable) absorption is larger for the materials considered in this paper owing to their larger longitudinal optical-phonon energy, which is undesirable.

TABLE III. Values of α_{oj}/α_0 for transitions between the heavy- and light-hole bands, the heavy-hole and split-off bands, and the light-hole and split-off bands. All values are given for a photon energy of 129.8 meV ($\lambda = 9.6$ μm) and room-temperature conditions.

Material	$\frac{(\alpha_0)_{h\rightarrow l}}{\alpha_0}$	$\frac{(\alpha_0)_{h\rightarrow s}}{\alpha_0}$	$\frac{(\alpha_0)_{l\rightarrow s}}{\alpha_0}$
Si	0.37	0.39	0.24
InP[a]	0.39	...	0.61
GaP	0.14	0.58	0.28
AlP	0.71	0.19	0.10

[a]The $h \rightarrow s$ transition in InP is not energetically allowed for this photon energy.

ACKNOWLEDGMENTS

The authors gratefully acknowledge the support of the Air Force Office of Scientific Research under Grant No. AFOSR-77-3216. One of us (D.L.S) acknowledges support from the Alfred P. Sloan Foundation.

[1] R. B. James and D. L. Smith, J. Appl. Phys. 51, 2836 (1980).
[2] A. F. Gibson, C. A. Rosito, C. A. Raffo, and M. F. Kimmitt, Appl. Phys. Lett. 21, 356 (1972).
[3] C. R. Phipps, Jr. and S. J. Thomas, Opt. Lett. 1, 93 (1977).
[4] R. L. Carlson, M. D. Montgomery, J. S. Ladish, and C. M. Lockhart, IEEE J. Quantum Electron. 13, 35 (1977).
[5] F. Keilmann, IEEE J. Quantum Electron. 12, 592 (1976).
[6] R. B. James and D. L. Smith, Solid State Commun. 33, 395 (1980).
[7] R. B. James and D. L. Smith, Phys. Rev. Lett. 42, 1495 (1979).
[8] R. B. James and D. L. Smith, Phys. Rev. B 21, 3502 (1980).
[9] E. O. Kane, J. Phys. Chem. Solids 1, 82 (1956).
[10] J. D. Wiley and M. DiDomenico, Jr., Phys. Rev. B 2, 427 (1970).
[11] E. M. Conwell, J. Phys. Chem. Solids 8, 236 (1959).
[12] J. I. Pankove, *Optical Processes in Semiconductors* (Dover, New York, 1971), Appendix II.
[13] P. Lawaetz, Phys. Rev. B 4, 3460 (1971).
[14] W. Richter, *Springer Tracts in Modern Physics* 78, *Solid-State Physics*, edited by G. Hohler (Springer-Verlag, Berlin, 1976), p. 174.
[15] S. Zwerdling, K. J. Button, B. Lax, and L. M. Roth, Phys. Rev. 118, 975 (1960).
[16] M. Glicksman and K. Weiser, J. Phys. Chem. Solids 10, 337 (1959).
[17] M. Cardona, K. L. Shaklee, and F. H. Pollack, Phys. Rev. 154, 696 (1967).
[18] R. J. Cherry and J. W. Allen, J. Phys. Chem. Solids 23, 163 (1962).
[19] P. J. Dean, G. Kaminsky, and R. B. Zetterstrom, J. Appl. Phys. 38, 3551 (1967).
[20] J. D. Wiley, *Semiconductors and Semimetals*, edited by R. K. Willardson and A. C. Beer (Academic, New York, 1975), p. 141.

Solid State Communications, Vol.37, pp.379-381.
Pergamon Press Ltd. 1981. Printed in Great Britain.

CALCULATION OF 3 μm PROBE TRANSMISSION IN p-Ge EXCITED BY A CO_2 LASER

R. B. James and D. L. Smith
California Institute of Technology
Pasadena, California 91125

(Received 23 July 1980; in revised form 3 October 1980 by H. Suhl)

We present a theory to describe the enhanced transmission of a weak tunable probe laser with a wavelength near 3 μm in the presence of a high-intensity saturating beam with a wavelength near 10 μm. The mechanism responsible for the increased transmission is the depletion of holes in the heavy-hole band by the saturating beam.

At room temperature, the absorption spectrum of p-Ge in the wavelength region of 2-25 μm is determined by direct intervalence-band transitions [1]. For light with a wavelength between 5 and 25 μm, the dominant transition occurs between the heavy- and light-hole bands, for wavelengths between 4 and 5 μm the dominant transition occurs between the light- and split-off hole bands; and for wavelengths between 2 and 4 μm the dominant transition occurs between the heavy- and split-off hole bands. For sufficiently high intensities, the heavy- to light-hole transitions have been shown to saturate due to a depletion of the population of holes in the resonant region of the heavy-hole band [2-5]. With a high-intensity pump laser saturating the heavy- to light-hole band transition, the transmission of a low intensity probe resonant between the heavy- and split-off hole bands is altered. If the wavelength of the pump laser is fixed and the wavelength of the probe is tuned, there is a spectral region for the probe in which the two optical transitions are coupled due to their sharing of common initial states in the heavy-hole band. These features have been experimentally observed in p-Ge by Keilmann and Kuhl [6]. In this experiment, the wavelength of the pump laser was fixed at 9.6 μm and the probe was tuned in wavelength near 3 μm. In this communication, we present a theory describing the enhanced transmission of the 3 μm probe in the presence of the 10 μm pump in p-Ge.

We consider single quantum transitions between the heavy- and light-hole bands due to the pump laser and between the heavy- and split-off hole bands due to the probe. The absorption coefficient of the probe is given by

$$\alpha(I,\omega_2) = \frac{4\pi^2}{\sqrt{\varepsilon_m}^2\omega_2 c}\frac{N_h e^2}{3}\sum_{\underset{\sim}{k}}[f_h(\underset{\sim}{k})-f_s(\underset{\sim}{k})]|P_{hs}(\underset{\sim}{k})|^2 \frac{1/(\pi[T_2(\underset{\sim}{k})]_{hs})}{[\Omega_{hs}(\underset{\sim}{k})-\omega_2]^2+[1/T_2(\underset{\sim}{k})]^2_{hs}}, \quad (1)$$

where the subscripts h(s) designate the heavy- (split-off) hole band, N_h is the density of holes, I is the intensity of the pump, $\hbar\omega_2$ is the photon energy of the probe beam, ε is the dielectric constant, $f_i(\underset{\sim}{k})$ is the probability that a hole state with wavevector $\underset{\sim}{k}$ is occupied in band i, $\Omega_{hs}(\underset{\sim}{k})$ is the angular frequency associated with the energy difference $[\varepsilon_h(\underset{\sim}{k}) - \varepsilon_s(\underset{\sim}{k})]$ where $\varepsilon_i(\underset{\sim}{k})$ is the one-hole energy for a state with wavevector $\underset{\sim}{k}$ in band i, and $|P_{hs}(\underset{\sim}{k})|^2$ is the squared momentum matrix element between the Bloch states in the heavy- and split-off hole bands (summed over the two degenerate states in each band). Here, $[T_2(\underset{\sim}{k})]_{hs}$ is defined by

$$\frac{2}{[T_2(\underset{\sim}{k})]_{hs}} = \sum_{\underset{\sim}{ck'}}[R_{hk\to ck'} + R_{sk\to ck'}], \quad (2)$$

where $R_{ak\to bk'}$ is the rate at which a hole in band a with wavevector $\underset{\sim}{k}$ is scattered into a state in band b with wavevector $\underset{\sim}{k'}$.

The dependence of the absorption coefficient on the intensity of the pump laser occurs through the distribution function in the heavy-hole band, $f_h(\underset{\sim}{k})$. We consider the case in which the probe is of sufficiently low intensity that it cannot saturate the transition [7]. Thus we take the distribution in the split-off hole band to be given by the equilibrium value. We calculate the distribution function for the heavy-hole band as a function of the intensity of the pump in the manner of Ref. (8).

The valence band structure of Ge has been calculated by several investigators to various degrees of accuracy [9-11]. The more exact of these calculations is given by Fawcett [9] where the interactions between the valence band and the two neighboring conduction bands are treated exactly rather than by perturbation methods. The result of the calculation indicates that for small k the heavy- and light-hole bands can be adequately described by a simpler calculation given by Kane [10], and that the split-off band is better approximated by a simpler calculation given by Dresselhaus, et al [11]. We calculate the dispersion curves for the heavy- and light-hole bands and the momentum matrix elements following Kane [10]. The dispersion curve for the split-off band was taken to be

$$\varepsilon_s(k) = -\Delta - Ak^2 - Dk^4[\sin^4\theta\cos^2\phi\sin^2\phi + \sin^2\theta\cos^2\theta], \quad (3)$$

where Δ is the spin-orbit splitting (.044 meV), A is a cyclotron resonance parameter, θ and φ are the polar and azimuthal angles relative to a [100] axis, respectively, and Γ is determined by fitting to the results of Ref. (9) (12). The angular dependence of the K^7 term in Eq. (3) is suggested by symmetry. The value of Γ used was 5×10^{6} meV-$Å^4$. For the small K region of interest, the fit of Eq. (3) to the results of Ref. (9) is very good. Of course, this result cannot be extended to large values of K. The cyclotron resonance parameters of Hensel and Suzuki (13) were used.

For room temperature conditions, the dominant scattering mechanism is phonon scattering for hole concentrations less than about $3\times10^{15}cm^{-3}$. For larger concentrations, one should also include the effect of hole-impurity and hole-hole scattering. Here we consider two cases; the low concentration case and the case of a hole concentration of $1.3\times10^{16}cm^{-3}$ (which corresponds to the experimental conditions in Ref. (6)). The phonon scattering rates are treated as in Ref. (8) and hole-impurity and hole-hole scattering are treated as in Ref. (14).

The calculated values for the absorption coefficient of the probe as a function of the photon energy of the probe are presented in Fig. (1) for a pump wavelength of 9.6 μm. All values of the absorption coefficient at a given photon energy are given relative to the small-signal absorption $\alpha_o(\omega_2)$ at that energy. To indicate the dependence of the absorption of the probe on the intensity of the pump, we plot $\alpha(I)/\alpha_o$ for I=20, 40, 60, and 80 MW/cm². We note that the transmission of the probe is further enhanced as the pump intensity is increased due to the further depletion of the hole distribution in the resonant region of the heavy-hole band. We also note that for a given intensity and probe energy, values of α/α_o are larger for more heavily doped samples. This occurs because an increase in the hole concentration increases the hole-impurity and hole-hole scattering rates. Thus higher intensities are required to deplete the heavy-hole band population in the more heavily doped material.

The quantity that is presented by the authors of Ref. (6) is

$$\bar{\alpha}/\alpha_o \equiv \ln T/\ln T_o \quad , \tag{4}$$

where T is the transmission with the pump and T_o is the transmission without the pump. Because the intensities of the pump and probe beams change in space on a scale which is long compared with the wavelengths of the beams and the carrier mean free paths, this ratio can be written as

$$\bar{\alpha}/\alpha_o = \frac{\ln\left[\dfrac{\int I_{in}(\rho)\, e^{-\int_0^{\ell}\alpha(I(\rho,z))dz}\, d^2\rho}{\int I_{in}(\rho)\, d^2\rho}\right]}{(-\alpha_o \ell)} \quad . \tag{5}$$

Here z is the direction of propagation of the probe, ρ is the axial dimension of the probe, $I_{in}(\rho)$ is the incident intensity of the probe and ℓ is the sample length. The quantity which we calculate is α(I) (normalized to α_o which is separately calculated). If the experimental geometry was accurately known, it would be straightforward to perform the spatial integrals and make a direct comparison with the experiment but the experimental conditions were not accurately enough defined to make this practical. However, the calculated values of $\alpha(I)/\alpha_o$ account for the main qualitative features of the experimental results.

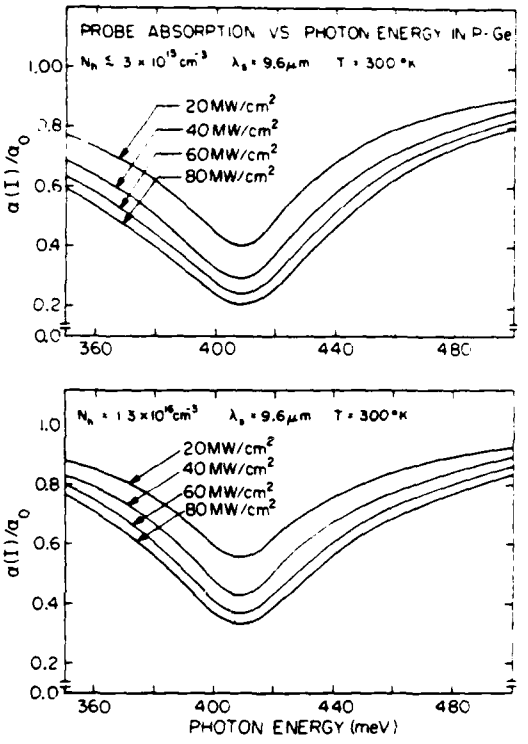

Figure 1. Calculated spectral response for the absorption of a weak tunable probe in the presence of a saturating pump laser with a wavelength of 9.6 μm in p-Ge at room temperature. Curves are shown for pump intensities of 20, 40, 60 and 80 MW/cm². The top figure illustrates the probe absorption for hole concentrations such that hole-hole and hole-impurity scattering can be neglected compared with hole-phonon scattering. The bottom figure illustrates the probe absorption for a hole concentration of $1.3\times10^{16}cm^{-3}$.

The experiments of Ref. (6) were done at room temperature with a pump laser at λ = 9.6 μm and a sample with $N_h = 1.3\times10^{16}cm^{-3}$. The intensity of the pump laser was estimated by the authors of Ref. (6) to vary between 80 MW/cm² and 7 MW/cm² as the beam passed through the absorbing sample. The pump was focused to a Gaussian spot size of 2w = 0.7 mm. The probe entered the sample from the opposite surface and was characterized by an elliptical cross section with 2w = 1.6 mm in the plane of incidence and 0.4 mm perpendicular to it. In addition the pump and probe beams were

not colinear. Thus much of the probe was outside of the pumped region. Ideally one would like to have the spot size of the probe to be considerably less than the spot size of the pump. Under these experimental conditions, a dip in α/α_o was observed. The dip was centered at a probe energy of 417 meV, the minimum value of α/α_o was 0.8, and the FWHM of the dip was about 13 meV.

The calculated values of $\alpha(I)/\alpha_o$ predict the location of the saturation dip center to be at 410 meV, in close agreement with the experimental measurement of 417 meV. The location of the dip can be shifted to higher (lower) probe energies by adjusting the pump to higher (lower) photon energies. This allows a means to tune the maximum transmission of the probe by controlling the wavelength of the pump laser. It has been previously noted that the band structure results of Ref. (9) could account for the position of the dip [15].

Comparing the magnitude of the calculated dip in α/α_o with the experimental results, we see that the calculated values of the dip are larger than was measured. This is to be expected because, as we have previously noted, much of the probe passed through unpumped regions of the sample in the experiment.

The calculated value of the FWHM of the dip in α/α_o varies from about 70 to 110 meV for intensities in the 20-80 MW/cm^2 range. The lineshape is non-Lorentzian (there is an inner dip in the curve) owing to the convolution of the Lorentzian lineshape of the probe with the hole distribution function in the heavy-hole band. The experimental results indicate a somewhat broader FWHM of about 130 meV. The experimental lineshape is approximately Lorentzian. Some of the discrepancy could be understood if the presence of the calculated inner dip was not experimentally observed owing to the broad frequency settings [16] of the probe used in measuring α/α_o.

In Ref. (6), it was suggested that a homogeneous linewidth of about 80 meV for the heavy to split-off band transitions is required to account for the measured width of the dip in α/α_o. This large width requires a hole lifetime in the split-off band of about 0.008 psec. We believe that this is an unphysically small value for the lifetime and it is inconsistent by almost an order of magnitude with previous estimates [17]. Theoretically, we find a value of about 0.06 psec.[7] In our calculations the width of the dip in α/α_o results primarily from band structure effects.[8] Because of anisotropy in the band structure, the energy of the initial heavy-hole state resonant with the pump laser varies with the direction in k-space from about 30 to 60 meV. The energy of the initial heavy-hole state resonant with the probe laser also varies with direction in k-space. As a result, the value of the probe frequency for which the same heavy-hole states are resonant with both optical transitions will change with the particular direction in k-space. Thus anisotropy broadens the dip in α/α_o compared with the result one would find in a spherical model for the band structure. In addition, the distribution of holes not directly depleted by the pump laser can be depleted by scattering into the depleted regions [18]. Also the curvature of the split-off hole band is greater than that of the heavy-hole band which further broadens the dip.

For semiconductors with the diamond or zincblende crystal structure, the valence band is similar to that of Ge and enhanced transmission of a probe in the presence of a saturating pump should be observable in these materials as well. Such measurements could provide useful information on the valence band structure for materials in which the cyclotron resonance parameters are not as well known as those for Ge.

In conclusion, we have presented a theory describing the enhanced transmission of a probe due to the presence of a saturating pump. Detailed calculations for p-Ge with a pump laser wavelength of 9.6 μm and probe energies between 350 and 500 meV have been shown. The results of the calculation are qualitatively consistent with existing experimental measurements; however, more experimental information is required for a detailed quantitative comparison.

The authors gratefully acknowledge the support of the Air Force Office of Scientific Research under Grant No. AFOSR-77-3216. One of us (TJS) acknowledges support from the Alfred P. Sloan Foundation.

REFERENCES

1. KAISER, W., COLLINS, R. J. and FAN, H. Y., Phys. Rev. 91, 1342 (1953).
2. GIBSON, A. F., ROSITO, C. A., RAFFO, C. A. and KIMMETT, M. F., Appl. Phys. Lett. 21, 356 (1972).
3. PHIPPS, C. R., Jr., and THOMAS, S. J., Opt. Lett. 1, 93 (1977).
4. CARLSON, R. L., MONTGOMERY, M. D., LADISH, J. S. and LOCKHART, C. M., IEEE J. Quantum Electron. 13, 35D (1977).
5. KEILMANN, F., IEEE J. Quantum Electron. 12, 592 (1976).
6. KEILMANN, F. and KUHL, J., IEEE J. Quantum Electron. 14, 203 (1978).
7. For probe energies in the 360 to 480 meV range, we calculate a saturation intensity at room temperature which varies with photon energy between 35 and 55 MW/cm^2.
8. JAMES, R. B. and SMITH, D. L., Phys. Rev. B21, 3502 (1980).
9. FAWCETT, W., Proc. Phys. Soc. 85, 931 (1965).
10. KANE, E. O., J. Phys. Chem. Solids 1, 82 (1956).
11. DRESSELHAUS, G., KIP, A. F., and KITTEL, C., Phys. Rev. 98, 368 (1955).
12. Using the theory in Ref. (11) to describe the split-off hole band yields Eq. (3) with D=0.
13. HENSEL, J. C. and SUZUKI, K., Phys. Rev. B9, 4219 (1974).
14. JAMES, R. B. and SMITH, D. L., Solid State Commun. 33, 395 (1980).
15. KEILMANN, F., Solid State Commun. 25, 451 (1978).
16. The difference between photon energy settings of the probe is about 28 meV in the vicinity of the dip minimum.
17. ARTHUR, J. B., BAYNHAM, A. C., FAWCETT, W., and PAIGE, E. G. S., Phys. Rev. 152, 740 (1966).

PHYSICAL REVIEW B VOLUME 23, NUMBER 8 15 APRIL 1981

Theoretical description of intervalence-band photoconductivity of p-Ge at 10.6 μm

R. B. James and D. L. Smith
California Institute of Technology, Pasadena, California 91125
(Received 18 August 1980)

The absorption of CO_2 laser radiation alters the distribution of free holes in p-Ge due to optical transitions between the heavy- and light-hole bands. The modification of the hole distribution function leads to a change in the conductivity. We present a calculation of the linear photoconductive response at 10.6 μm as a function of hole density at room temperature and as a function of temperature for fixed hole density. We also describe the photoconductivity for high light intensities for which the effects of saturation of the intervalence-band transitions are important.

I. INTRODUCTION

The absorption of light in the 10-μm region by p-type germanium is determined by direct intervalence-band transitions in which a free hole in the heavy-hole band absorbs a photon and is excited to the light-hole band.[1] Since the absorption of light modifies the distribution of free holes, one expects a change in the sample conductivity upon illumination. Because the density of states in the heavy-hole band is much greater than that in the light-hole band, the photoexcited holes primarily scatter into high-energy states in the heavy-hole band. Thus the dominant change in the distribution function is an increase in the average energy of occupied states in this band. For temperatures and doping levels for which phonon scattering dominates the momentum relaxation, the conductivity decreases upon illumination because the rate of phonon scattering increases with increasing hole energy. For lower temperatures or higher doping levels where ionized-impurity scattering dominates the momentum relaxation, the conductivity increases with illumination because ionized-impurity scattering decreases with increasing hole energy. These photoconductive effects have been observed experimentally[2-7] and have been shown to influence the performance of p-Ge photon drag detectors.[8-10] In this paper we present a calculation of the photoconductive response of p-Ge upon illumination by 10.6-μm light as a function of doping level, temperature, and intensity.

Previous calculations of this photoconductive response have been based on idealized models in which the Ge valence bands have been replaced by a set of discrete energy levels, each characterized by an effective mobility.[6,7] In addition, the effects of saturation of the intervalence-band transitions were not included, so that the results could only be applied for low intensities. Here we describe the Ge valence band using degenerate $\vec{k}\cdot\vec{p}$ perturbation theory. We calculate the hole distribution as a function of the laser intensity in both the linear and nonlinear regimes. Using the calculated hole distribution, we determine the photoconductive response. We find reasonable agreement with experimental results. There are no adjustable parameters in the theory.

The paper is organized in the following way: In Sec. II we present our theoretical approach, in Sec. III we give our results for the change in the conductivity, and in Sec. IV we summarize our conclusions.

II. THEORETICAL APPROACH

The valence bands of Ge consist of three twofold degenerate bands: the heavy-hole, the light-hole, and the split-off hole bands. In thermal equilibrium the occupied hole states are in the heavy- and light-hole bands only. We consider the intervalence-band photoconductivity of p-Ge when the sample is pumped by a CO_2 laser. Since the laser does not couple free holes to states in the split-off hole band, only the heavy- and light-hole bands need to be considered. The dc current density owing to free holes is given by

$$\vec{J}=\left(\frac{1}{2\pi}\right)^3 N_h e \sum_b \int f_b(\vec{k})\vec{v}_{b\vec{k}}\,d^3k\,, \tag{1}$$

where N_h is the density of holes, b labels the band index, $\vec{k}$ is the wave vector, $f_b(\vec{k})$ is the one-hole distribution function, and $\vec{v}_{b\vec{k}}$ is the group velocity of the carrier with wave vector $\vec{k}$ in band b.

In order to calculate the current density and thus determine the conductivity, it is necessary to find the distribution function in the presence of the exciting laser and a small applied dc electric field. The distribution functions in the heavy- and light-hole bands are determined by solving the following equations[11,12]:

$$\beta(\vec{k})[f_h(\vec{k})-f_l(\vec{k})]+\frac{e}{\hbar}\vec{E}\cdot\nabla_{\vec{k}}f_h(\vec{k})$$
$$=-\sum_{c\vec{k}'}[R_{h\vec{k}\to c\vec{k}'}f_h(\vec{k})-R_{c\vec{k}'\to h\vec{k}}f_c(\vec{k}')]\,, \tag{2a}$$

and

$$\beta(\vec{k})[f_h(\vec{k}) - f_l(\vec{k})] - \frac{e}{\hbar}\vec{E}\cdot\nabla_{\vec{k}} f_l(\vec{k}) = \sum_{c\vec{k}'}[R_{l\vec{k}\to c\vec{k}'} f_l(\vec{k}) - R_{c\vec{k}'\to l\vec{k}} f_c(\vec{k}')], \quad (2b)$$

where $\beta(\vec{k})$ is given by

$$\beta(\vec{k}) = \frac{2\pi^2}{\sqrt{\epsilon}\, m^2 \omega c}\frac{e^2 I}{3\hbar\omega}|\vec{P}_{hl}(\vec{k})|^2 \frac{1/\pi\hbar T_2(\vec{k})}{[\Omega(\vec{k}) - \omega]^2 + [1/T_2(\vec{k})]^2}, \quad (3)$$

and

$$\frac{2}{T_2(\vec{k})} = \sum_{c\vec{k}'}(R_{h\vec{k}\to c\vec{k}'} + R_{l\vec{k}\to c\vec{k}'}). \quad (4)$$

Here, I is the light intensity, $\hbar\omega$ is the photon energy, $|\vec{P}_{hl}(\vec{k})|^2$ is the squared momentum matrix element between the Bloch states in the heavy- and light-hole bands (summed over the two degenerate states in each band), $R_{a\vec{k}\to b\vec{k}'}$ is the rate in which a hole in band a with wave vector $\vec{k}$ is scattered into band b with wave vector $\vec{k}'$, and $\Omega(\vec{k})$ is the angular frequency associated with the energy difference $[\epsilon_h(\vec{k}) - \epsilon_l(\vec{k})]$, where $\epsilon_i(\vec{k})$ is the energy of the hole in band i with wave vector $\vec{k}$. The proportional to β in Eqs. (2a) and (2b) describes the change in the distribution due to optical excitation, the term proportional to E describes the acceleration of the holes by the electric field, and the terms proportional to R describe the scattering of the holes. The one-hole energies and momentum matrix elements in Eq. (3) are determined by degenerate $\vec{k}\cdot\vec{p}$ perturbation theory.[13] The cyclotron resonance parameters of Ref. 14 are used in the calculation. The hole-phonon contribution to the scattering rates appearing in Eqs. (2a) and (2b) are treated in the manner of Ref. 11. The hole-hole and hole-ionized-impurity scattering rates are included following Ref. 15.

In small dc electric fields, the distribution of carriers can be described by the sum of a small drift term and the distribution function without an electric field. Thus in small electric fields, we write

$$f_b(\vec{k}) = f_b^0(\vec{k}) + g_b(\vec{k}), \quad (5)$$

where $f_b^0(\vec{k})$ is the distribution function subject to the high-intensity laser but with no external electric field, and $g_b(\vec{k})$ is the modification of $f_b(\vec{k})$ due to the presence of the electric field. Here, it is assumed that $g_b(\vec{k}) \ll f_b^0(\vec{k})$. The function $f_b^0(\vec{k})$ is computed as in Ref. 11. Using Eq. (5), we write Eqs. (2) to first order in the electric field

$$\beta(\vec{k})[g_h(\vec{k}) - g_l(\vec{k})] + \frac{e}{\hbar}\vec{E}\cdot\nabla_{\vec{k}} f_h^0(\vec{k}) = -\sum_{c\vec{k}'}[R_{h\vec{k}\to c\vec{k}'} g_h(\vec{k}) - R_{c\vec{k}'\to h\vec{k}} g_c(\vec{k}')], \quad (6a)$$

and

$$\beta(\vec{k})[g_h(\vec{k}) - g_l(\vec{k})] - \frac{e}{\hbar}\vec{E}\cdot\nabla_{\vec{k}} f_l^0(\vec{k}) = \sum_{c\vec{k}'}[R_{l\vec{k}\to c\vec{k}'} g_l(\vec{k}) - R_{c\vec{k}'\to l\vec{k}} g_c(\vec{k}')]. \quad (6b)$$

We assume that a relaxation time approximation can be made for the low dc field; that is, the rate of change of $g_h(\vec{k})$ due to collisions can be approximated by

$$\sum_{c\vec{k}'}[R_{h\vec{k}\to c\vec{k}'} g_h(\vec{k}) - R_{c\vec{k}'\to h\vec{k}} g_c(\vec{k}')] = \frac{g_h(\vec{k})}{\tau_h(\vec{k})}, \quad (7)$$

and a similar expression for the effect of collisions on $g_l(\vec{k})$. Here, $\tau_h(\vec{k})$ $[\tau_l(\vec{k})]$ is the momentum relaxation time due to scattering of holes with wave vector $\vec{k}$ in the heavy- (light-) hole band by phonons and ionized impurities.[16]

Using Eqs. (6) and the relaxation time approximation, we write expressions for $g_b(\vec{k})$ in terms of the functions $f_b^0(\vec{k})$. Taking the dc electric field to be in the z direction, we have

$$g_h(\vec{k}) = \frac{-e}{\hbar}\tau_h|E|\frac{\partial f_h^0}{\partial k_z}\left(\frac{1 + \beta\tau_l[(\partial f_l^0/\partial k_z)/(\partial f_h^0/\partial k_z) + 1]}{1 + \beta(\tau_h + \tau_l)}\right), \quad (8a)$$

$$g_h(\vec{k}) = \frac{-e}{\hbar}\tau_l|E|\frac{\partial f_l^0}{\partial k_z}\left(\frac{1 + \beta\tau_h[(\partial f_h^0/\partial k_z)/(\partial f_l^0/\partial k_z) + 1]}{1 + \beta(\tau_h + \tau_l)}\right). \quad (8b)$$

Since $\vec{v}_b(\vec{k}) = -\vec{v}_b(-\vec{k})$ and $f_b^0(\vec{k}) = f_b^0(-\vec{k})$, we can write

$$J_z = 2\left(\frac{1}{2\pi}\right)^3 eN_h \sum_b \int g_b(\vec{k}) v_{bz}(\vec{k}) d^3k. \quad (9)$$

Integrating Eq. (9) by parts the conductivity is given by

$$\sigma = 2\left(\frac{1}{2\pi}\right)^3\frac{e^2}{\hbar}N_h\int d^3k f_h^0(\vec{k})\frac{\partial}{\partial k_z}\left[\tau_h v_{hz}\left(\frac{1 + \beta\tau_l[(\partial f_l^0/\partial k_z)/(\partial f_h^0/\partial k_z) + 1]}{1 + \beta(\tau_h + \tau_l)}\right)\right]$$
$$+ 2\left(\frac{1}{2\pi}\right)^3\frac{e^2}{\hbar}N_h\int d^3k f_l^0(\vec{k})\frac{\partial}{\partial k_z}\left[\tau_l v_{lz}\left(\frac{1 + \beta\tau_h[(\partial f_h^0/\partial k_z)/(\partial f_l^0/\partial k_z) + 1]}{1 + \beta(\tau_h + \tau_l)}\right)\right]. \quad (10)$$

The factor

$$Z_h = \frac{1+\beta\tau_l\left[(\partial f_l^0/\partial k_z)/(\partial f_h^0/\partial k_z)+1\right]}{1+\beta(\tau_h+\tau_l)} \tag{11}$$

appearing in the heavy-hole band contribution to the conductivity, and the analogous factor Z_l present some numerical difficulties owing to the peaked nature of the terms involved. This factor differs significantly from unity only if $\beta\tau_h \gtrsim 1$.[17] We note that β is sharply peaked in the resonant region of the optical transition and negligibly small outside of this region. Thus we need only evaluate $\partial f^0/\partial k_z$ in the vicinity of the resonant region. At low light intensities where saturation of the optical transitions does not occur ($I \leq 1$ MW/cm^2), $\beta\tau_h$ is small compared to unity even in the resonant region, and Z_h is essentially one. At high intensities where saturation does occur, Z_h differs from unity in the resonant region. However, for the range of intensities considered in this paper ($I \leq 10$ MW/cm^2), this difference still does not make a large contribution to the integral in Eq. (10) because of limited range over which it occurs.

To estimate the value of Z_h, we only need to know the distribution function in the resonant region. We have previously found that these functions can be reasonably approximated by a simple analytical form for states in the resonant region[11]

$$f_h^0(\bar{k}) \approx f_h^e(\bar{k}) - \frac{\beta(\bar{k})T_h^{op}\left[f_h^e(\bar{k})-f_l^e(\bar{k})\right]}{1+\beta(\bar{k})(T_h^{op}+T_l)} \tag{12a}$$

and

$$f_l^0(\bar{k}) \approx f_l^e(\bar{k}) + \frac{\beta(\bar{k})T_l(\bar{k})\left[f_h^e(\bar{k})-f_l^e(\bar{k})\right]}{1+\beta(\bar{k})(T_h^{op}+T_l)}, \tag{12b}$$

where $f^e(\bar{k})$ is the equilibrium distribution,

$$\frac{1}{T_l(\bar{k})} = \sum_{\bar{k}'} R_{l\bar{k}\to l\bar{k}'}, \tag{13}$$

and T_h^{op} is defined for the heavy-hole band analogous to Eq. (13) except that only optical-phonon scattering is included.

In the resonant region, the distribution functions in Eqs. (12a) and (12b) have a peaked structure owing to the Lorentzian factor contained in β. Taking the other factors in Eqs. (12) to be slowly varying in the resonant region, we approximate

$$\frac{\partial f^0}{\partial k_z} \approx \frac{\partial f^0}{\partial \beta}\frac{\partial \beta}{\partial k_z}. \tag{14}$$

With this approximation we have

$$\frac{\partial f_l^0/\partial k_z}{\partial f_h^0/\partial k_z} \approx \frac{T_l}{T_h^{op}}, \tag{15}$$

and thus a simple analytical expression for Z_h. To calculate the conductivity we must also evaluate the derivative of Z_h with respect to k_z. In evaluating this derivative, we take the factors other than β to be slowly varying in the resonant region and take the change in β to occur primarily through the Lorentzian factor which depends on $\Omega(\bar{k})$; that is, we approximate

$$\frac{\partial Z_h}{\partial k_z} \approx \frac{\partial Z_h}{\partial \beta}\frac{\partial \beta}{\partial \Omega}\frac{d\Omega}{dk_z}. \tag{16}$$

With this approximation, we have

$$\frac{\partial Z_h}{\partial k_z} = \left[\tau_h + \tau_l\left(\frac{T_l}{T_h^{op}}\right)\right]\frac{d\Omega}{dk_z}\frac{2\beta}{\left[1+\beta(\tau_h+\tau_l)\right]^2} \times \frac{\Omega-\omega}{(\Omega-\omega)^2+(1/T_2)^2}. \tag{17}$$

We treat the factor Z_l, which appears in the light-hole contribution to the conductivity in a similar way. We note that the expression in Eq. (17) is vanishingly small outside of the resonant region and changes sign as $\Omega(\bar{k})$ crosses ω. As a result this term tends to cancel in the $\bar{k}$-space integration. The inclusion of the terms containing $\partial Z_h/\partial k_z$ and $\partial Z_l/\partial k_z$ makes a contribution of less than 20% to the calculation of the photoinduced change in the conductivity at the highest intensities we consider.

III. RESULTS OF $\Delta\sigma(I)$

We compute the conductivity due to free holes by numerically integrating Eq. (10). For very lightly doped (near intrinsic) samples, we also include a term due to free electrons. We assume that the electron contribution is not much modified by illumination because the absorption cross section for electrons is nearly 2 orders of magnitude smaller than that for holes.[18]

In Fig. 1 we show the calculated results for $(-\Delta\sigma/\sigma I)$ vs N_h in the low-intensity regime where $\Delta\sigma$ is proportional to I. The calculation was done for room-temperature Ge illuminated by $\lambda = 10.6$ μm light. The conductivity has decreased upon illumination. The primary effect of illumination on the hole distribution is to increase the population of high-energy holes in the heavy-hole band. At room temperature and for the doping levels considered here, hole-phonon scattering limits the conductivity. Since hole-phonon scattering rates increase with increasing hole energy, the conductivity decreases with illumination. For hole densities between about 10^{14} and 4×10^{15} cm^{-3}, $(-\Delta\sigma/\sigma I)$ is essentially independent of N_h. In this region hole-impurity scattering makes a negligible contribution to the scattering rates. For hole densities greater than about 4×10^{15} cm^{-3}, $(-\Delta\sigma/\sigma I)$ decreases with increasing N_h. In this regime, hole-impurity scattering begins to play a role in limiting the mobility. Hole-impurity scattering

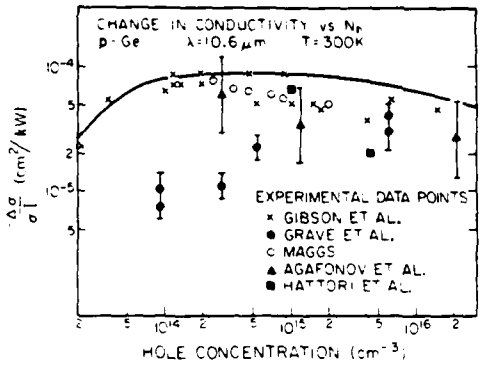

FIG. 1. Values of $(-\Delta\sigma/\sigma I)$ versus the hole concentration in p-Ge for CO_2 laser excitation at 10.6 μm, room temperature, and low light intensities. The calculated values of $(-\Delta\sigma/\sigma I)$ are shown by the solid curve. The experimental data are taken from ×, Ref. 4; ▲, Ref. 5; ■, Ref. 6; ●, Ref. 7; and c, Ref. 9. Error bars are reported only in Refs. 5 and 7.

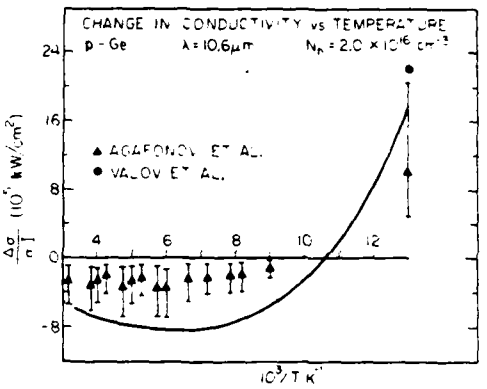

FIG. 2. Calculated values of the normalized change in the conductivity of p-Ge versus temperature for light at 10.6 μm, a hole concentration of 2.0×10^{16} cm^{-3}, and low-intensity excitation. The experimental data are taken from: ▲, Ref. 5 and ●, Ref. 3. Error bars are only reported in Ref. 5.

rates decrease with increasing hole energy. As a result the fractional increase in the total scattering rate (hole-phonon plus hole-impurity) does not increase as much with increasing hole energy in the more heavily doped samples. In addition, the hole distribution is not as strongly modified by illumination of a given intensity in the more heavily doped samples due to the increase in hole-ionized-impurity and hole-hole scattering which tends to maintain the equilibrium distribution. For hole densities less than about 10^{14} cm^{-3}, $(-\Delta\sigma/\sigma I)$ decreases with decreasing hole density. This decrease is due to the increased contribution to the conductivity of free electrons whose distribution is not strongly modified by illumination. (In Ge at 300 K, the intrinsic density is about 2×10^{13} cm^{-3}.)

Also shown in Fig. 1 are the available experimental results. There is considerable variation in the results reported by the various authors. Our calculated values are in fairly good agreement with the data of Gibson *et al.*[4] and those of Maggs.[9]

In Fig. 2 we present our results for the temperature dependence of $(\Delta\sigma/\sigma I)$ for a hole concentration of 2×10^{16} cm^{-3}. We choose this value for the hole density since experimental measurements exist and the change in the conductivity was observed to change sign over the temperature range that was reported.[5] We note that the change in the conducitivity is negative for temperatures greater than about 100 K and becomes positive for lower temperatures. In the higher-temperature regime, hole-phonon scattering plays a greater role in determining the momentum relaxation than hole-impurity scattering, and thus the conductivity decreases upon illumination. In the lower-temperature regime hole-ionized-impurity scattering dominates the momentum relaxation and the conducitivity increases upon illumination. The temperature at which $\Delta\sigma$ changes sign depends on the doping level. At lower doping levels, the sign change in $\Delta\sigma$ occurs at lower temperatures. This effect has been observed experimentally.[5] In addition, we note that the magnitude of $|\Delta\sigma/\sigma I|$ decreases as the temperature increases from about 150K. This decrease is due to an increase in the rate of phonon scattering at the higher temperatures. As a result of the increased scattering rate, the hole distribution is less strongly modified by a given light intensity at the higher temperatures. The experimental results of Refs. 3 and 5 are included in Fig. 2. The data show the same qualitative features as the calculated results. The calculation gives somewhat larger values for $|\Delta\sigma/\sigma I|$ than were observed in Ref. 5. From Fig. 1 we note that the room-temperature results reported in Ref. 5 are systematicallly smaller than those of Refs. 4 and 9.

Because of interest in the performance of photon-drag detectors at high laser intensities,[8-10] we also examine the photoconductive response of p-Ge at intensities for which saturation effects are important. In Fig. 3 we present the results of our calculation of $(-\Delta\sigma/\sigma I)$ as a function of N_A for different light intensities. The curve for 0.05 MW/cm^2 is in the linear regime. At the higher intensities, $(-\Delta\sigma/\sigma)$ increases with increasing intensity at a rate which is slower than

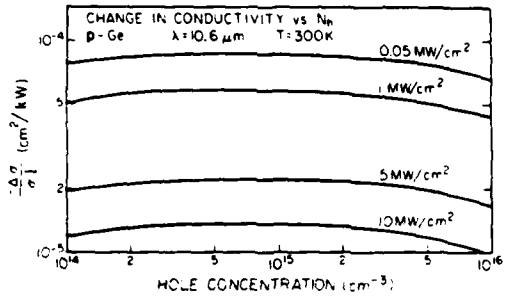

FIG. 3. Values of $(-\Delta\sigma/\sigma I)$ versus the hole concentration in p-Ge for $\lambda = 10.6$ μm and $T \approx 300$ K. The solid curves are our calculated values for intensities of 0.05 (linear regime), 1, 5, and 10 MW/cm².

linear. The nonlinear behavior is due to saturation of the intervalence-band transitions. The shapes of the curves at any given intensity are similar. We are not aware of any direct measurements of $(\Delta\sigma/\sigma I)$ at these high intensities; however, both saturable absorption[19,20] and nonlinear photon-drag voltages[9,10] have been seen experimentally. It is possible that this saturation effect could account for some of the variation in the experimental results shown in Fig. 1.

IV. SUMMARY AND CONCLUSIONS

We have presented a theory of the photoconductive response of p-Ge for light with a wavelength of 10.6 μm. Values of $(\Delta\sigma/\sigma I)$ are calculated as a function of doping level in the low-intensity regime at room temperature. We have also reported the temperature dependence of $(\Delta\sigma/\sigma I)$ at a fixed hole concentration in the low-intensity regime. The effect of saturation at high light intensities was investigated. The theory presented can be applied to other p-type semiconductors with a valence-band structure similar to that of Ge.

ACKNOWLEDGMENTS

The authors gratefully acknowledge the support of the Air Force Office of Scientific Research under Grant No. AFOSR-77-3216. One of us (D.L.S.) acknowledges support from the Alfred P. Sloan Foundation.

[1] W. Kaiser, R. J. Collins, and H. Y. Fan, Phys. Rev. 91, 1342 (1953).
[2] A. M. Danishevskii, A. A. Kastal'skii, B. S. Ryvkin, S. M. Ryvkin, and I. D. Yaroshetskii, Zh. Eksp. Teor. Fiz. Pis'ma Red. 10, 470 (1969) [JETP Lett. 10, 302 (1969)].
[3] P. M. Valov, I. D. Yaroshetskii, and I. N. Yassievich, Zh. Eksp. Teor. Fiz. Pis'ma Red. 20, 448 (1974) [JETP Lett. 20, 204 (1974)].
[4] A. F. Gibson and P. N. D. Maggs, J. Phys. D 7, 292 (1974).
[5] V. G. Agafonov, P. M. Valov, B. S. Ryvkin, and I. D. Yarosketskii, Sov. Phys. Semicond. 9, 571 (1975)
[6] H. Hattori, O. Fujitani, and M. Umeno, J. Phys. Soc. Jpn. 36, 485 (1974).
[7] T. Grave and F. Keilmann, Z. Phys. B 32, 347 (1979).
[8] A. F. Gibson, M. F. Kimmitt, P. N. D. Maggs, and B. Norris, J. Appl. Phys. 46, 1413 (1975).
[9] P. J. Bishop, A. F. Gibson, and M. F. Kimmitt, IEEE J. Quantum Electron. QE-9, 1007 (1973). Values of $\Delta\sigma/\sigma I$ quoted in this paper were measured by P. Maggs.
[10] T. Kamibayashi, S. Yonemochi, and T. Miyakawa, Appl. Phys. Lett. 22, 119 (1973).
[11] R. B. James and D. L. Smith, Phys. Rev. B 21, 3502 (1980).
[12] We have assumed that there exist no impact ionization processes in which a hole is sufficiently energetic ($\gtrsim$ the band gap) to relax by an electron-hole pair production. This energy relaxation mechanism may be important at very high intensities; however, the experiments of Ref. 19 indicate that this process is negligible over the range of intensities presented in this paper.
[13] E. O. Kane, J. Phys. Chem. Solids 1, 82 (1956).
[14] J. C. Hensel and K. Suzuki, Phys. Rev. B 9, 4219 (1974).
[15] R. B. James and D. L. Smith, Solid State Commun 33, 395 (1980).
[16] Hole-hole scattering is included in the calculation of the distribution f^0, but it is not included in the momentum relaxation rates. For hole-hole scattering, the total momentum is not changed, thus, it has little influence on the mobility.
[17] For p-Ge and hole states in the resonant region, τ_h is much greater than τ_l.
[18] P. J. Bishop and A. F. Gibson, Appl. Opt. 12, 2549 (1973).
[19] C. R. Phipps, Jr. and S. J. Thomas, Opt. Lett. 1, 93 (1977).
[20] A. F. Gibson, C. A. Rosito, C. A. Raffo, and M. F. Kimmitt, Appl. Phys. Lett. 21, 356 (1972).

PHYSICAL REVIEW B VOLUME 23, NUMBER 8 15 APRIL 1981

Laser-induced changes in the dispersive properties of p-Ge due to intervalence-band transitions

R. B. James and D. L. Smith
California Institute of Technology, Pasadena, California 91125
(Received 25 August 1980)

We present a theory describing the laser-induced change in the real part of the complex dielectric constant in p-Ge that results from saturation of the intervalence-band transitions. Calculations are performed for room temperature and for light with a wavelength of 10.6 μm. The real part of the dielectric constant is found to increase monotonically with increasing intensity. The magnitude of the increase is directly proportional to the density of free holes. The intervalence-band contribution to the first-order modification of the real part of the dielectric constant equals the intrinsic contribution at a doping level of about 3×10^{15} cm^{-3}.

I. INTRODUCTION

There is considerable theoretical and experimental interest in nonlinear optical phenomena in semiconductors, particularly with those effects which are connected with the dependence of the complex dielectric constant on the intensity of the light. For example, the saturable absorption properties of p-type Ge have been used to achieve interstage isolation of high-power CO_2 laser amplifiers[1] and to passively mode-lock CO_2 lasers.[2-4] Saturable absorption is described by the intensity dependence of the imaginary part of the dielectric constant (ϵ_2). There is in addition an intensity dependence in the real part of the dielectric constant (ϵ_1). These laser-induced changes in the real part of the dielectric constant alter the dispersive properties of the media and thus modify the spatial and temporal behavior of the laser pulse. Since the laser-pulse shape is important in many applications of CO_2 laser systems, one needs to understand the changes in the dispersive properties induced by the high-intensity beam. An intensity dependence of the real part of the dielectric constant can be exploited for phase conjugation. Phase conjugation in the CO_2 laser frequency regime using Ge as the nonlinear medium is of current interest.[5]

For light with a wavelength near 10 μm, the dominant absorption mechanism in p-Ge is due to direct free-hole transitions between the heavy- and light-hole bands. These resonant transitions also contribute to the real part of the dielectric constant (ϵ_1). At high intensities, the absorption due to these transitions saturates[1,6-8] owing to a modification of the free-hole distribution function. This intensity-dependent modification of the distribution function also changes the contribution of the free-hole transitions to ϵ_1.[9] In addition to the intensity dependence of ϵ_1 from the resonant intervalence-band transitions, there is an intrinsic contribution due to a field modification of the virtual electron-hole pair creation processes.[10] The magnitude of the resonant intervalence-band contribution depends on the doping level. Both contributions lead to an increase in ϵ_1 with increasing intensity. In this paper we present a theory of the resonant intervalence-band contribution to the intensity dependence of ϵ_1 in p-Ge for light with a wavelength of 10.6 μm. We find that the magnitude of the resonant intervalence-band contribution to the first-order modification of ϵ_1 equals measured values[11] of the intrinsic contribution at a doping level of about 3×10^{15} cm^{-3}. The paper is organized in the following way: in Sec. II we present our theoretical approach, in Sec. III we give the results for p-Ge, and in Sec. IV we summarize our conclusions.

II. THEORETICAL APPROACH

In p-Ge, light with a wavelength in the CO_2 laser spectrum induces hole transitions between the heavy- and light-hole bands. The rate of transitions is proportional to the population of free holes in the heavy-hole band which can participate in the absorption process. For even lightly doped p-Ge samples ($N_A \geq 10^{14}$ cm^{-3}), these direct intervalence-band transitions dominate the absorptive loss for wavelengths near 10 μm.[12,13]

Since both energy and wave vector are conserved in the direct heavy- to light-hole band transitions, only holes in a narrow region of $\vec{k}$ space directly participate in the absorption. At low intensities, the population of the heavy-hole states involved in the optical transitions is maintained close to the equilibrium value by the various scattering mechanisms. However, at sufficiently large intensities, the population of the pertinent heavy-hole states is depleted. This modification of the free-hole distribution is responsible for laser-induced changes in the complex dielectric constant.

The qualitative dependence of the free-hole contribution to ϵ_1 on the excitation intensity can easily be anticipated. Holes in states whose resonant optical transition energy $[\epsilon_b(\vec{k}) - \epsilon_l(\vec{k})]$ is greater

than the photon energy ($\hbar\omega$) lead to positive contributions to ϵ_1, whereas holes in states whose resonant energy is less than the photon energy lead to negative contributions to ϵ_1.[14] As the intensity of the light beam is increased, the holes are excited to higher energy states (on the average) which have larger resonant transition energies. Thus the positive contribution to ϵ_1 from holes with $[\epsilon_h(\vec{k})-\epsilon_l(\vec{k})]>\hbar\omega$ is increased, while the magnitude of the negative contribution to ϵ_1 from holes with $[\epsilon_h(\vec{k})-\epsilon_l(\vec{k})]<\hbar\omega$ is decreased which leads to a monotonic increase of ϵ_1 with increasing intensity. At large intensities, the population of the heavy-hole states whose transition energy is resonant with the photon energy becomes depleted so that heating of the hole distribution saturates at large intensities. Thus ϵ_1 increases with intensity, but the rate of increase saturates at high intensities.

The current density owing to the intervalence-band transitions is given by[15]

$$\vec{J}=\frac{N_h e^2}{2m^2 c\hbar}\sum_{\vec{k}}[f_h(\vec{k})-f_l(\vec{k})]\times\sum_{b\,\text{in}\,h;c\,\text{in}\,l}\frac{\vec{A}\cdot\vec{P}_{bc}\vec{P}_{cb}+\vec{A}\cdot\vec{P}_{cb}\vec{P}_{bc}}{[\Omega(\vec{k})-\omega]-i/T_2(\vec{k})}, \tag{1}$$

where $\vec{k}$ labels the wave vector, the subscripts h (l) designate the heavy- (light-) hole band, N_h is the density of free holes, $\hbar\omega$ is the photon energy, m is the free-electron mass, $f_i(\vec{k})$ is the probability that a hole state with wave vector $\vec{k}$ is occupied in band i, $\Omega(\vec{k})$ is the angular frequency associated with the energy difference $[\epsilon_h(\vec{k})-\epsilon_l(\vec{k})]$, where $\epsilon_i(\vec{k})$ is the energy of a hole with wave vector $\vec{k}$ in band i, and $\vec{P}_{bc}(\vec{k})$ is the momentum matrix element between the Bloch states in the bands b and c. Here, $T_2(\vec{k})$ is defined as

$$\frac{2}{T_2(\vec{k})}=\sum_{c\vec{k}'}(R_{a\vec{k}\to c\vec{k}'}+R_{l\vec{k}\to c\vec{k}'}), \tag{2}$$

where $R_{a\vec{k}\to b\vec{k}'}$ is the rate at which a hole in band a with wave vector $\vec{k}$ is scattered into a state in band b with wave vector $\vec{k}'$.

Using Eq. (1), we write the susceptibility as a second-rank tensor given by

$$\underline{\chi}(\omega,I)=\frac{N_h e^2}{2m^2\omega^2\hbar}\sum_{\vec{k}}[f_h(\vec{k})-f_l(\vec{k})]\times\sum_{b\,\text{in}\,h;c\,\text{in}\,l}\frac{\vec{P}_{cb}\vec{P}_{bc}+\vec{P}_{bc}\vec{P}_{cb}}{[\Omega(\vec{k})-\omega]-i/T_2(\vec{k})}. \tag{3}$$

The imaginary part of $\underline{\chi}$ describes the changes in the absorptive properties of the semiconductor, whereas the real part of $\underline{\chi}$ describes the changes in the dispersive properties. We define

$$\underline{\chi}=\underline{\chi}'+i\underline{\chi}'', \tag{4}$$

where $\underline{\chi}'$ and $\underline{\chi}''$ are assumed to be real. Thus, we find

$$\underline{\chi}'(\omega,I)=\frac{N_h e^2}{2m^2\omega^2\hbar}\sum_{\vec{k}}[f_h(\vec{k})-f_l(\vec{k})]\times\sum_{b\,\text{in}\,h;c\,\text{in}\,l}(\vec{P}_{cb}\vec{P}_{bc}+\vec{P}_{bc}\vec{P}_{cb})\times\frac{\Omega(\vec{k})-\omega}{[\Omega(\vec{k})-\omega]^2+[1/T_2(\vec{k})]^2}. \tag{5}$$

Here, the intensity dependence is contained in the distribution functions $f_h(\vec{k})$ and $f_l(\vec{k})$. At low light intensities, $\underline{\chi}$ is a scalar because of the cubic symmetry of Ge. For high-intensity polarized light, the cubic symmetry is reduced and $\underline{\chi}$ is described by a second-rank tensor.

In order to determine the intensity dependence of χ', we must calculate the distribution function for free holes in the heavy- and light-hole bands. In Ge, the scattering rate for free holes occurs on a subpicosecond time scale. But for typical experimental situations, laser beams of nanosecond pulse widths are used. Thus, transient effects are damped out. Using the results of Ref. 16, the steady-state difference in the occupation probabilities which appear in the expression for $\chi'(\omega,I)$ is given by

$$f_h(\vec{k})-f_l(\vec{k})=\frac{f_h^0(\vec{k})-f_l^0(\vec{k})}{1+\beta(\vec{k})[T_h(\vec{k})+T_l(\vec{k})]}+\frac{T_h(\vec{k})F(\vec{k})-T_l(\vec{k})G(\vec{k})}{1+\beta(\vec{k})[T_h(\vec{k})+T_l(\vec{k})]}, \tag{6}$$

where we have introduced the auxiliary functions

$$\frac{1}{T_h(\vec{k})}=\sum_{c\vec{k}'}R_{h\vec{k}\to c\vec{k}'}, \tag{7a}$$

$$\frac{1}{T_l(\vec{k})}=\sum_{c\vec{k}'}R_{l\vec{k}\to c\vec{k}'}, \tag{7b}$$

$$F(\vec{k})=\sum_{c\vec{k}'}R_{c\vec{k}'\to h\vec{k}}[f_c(\vec{k}')-f_c^0(\vec{k}')], \tag{7c}$$

$$G(\vec{k})=\sum_{c\vec{k}'}R_{c\vec{k}'\to l\vec{k}}[f_c(\vec{k}')-f_c^0(\vec{k}')], \tag{7d}$$

and $f_c^0(\vec{k})$ is the equilibrium value for the distribution in band c with wave vector $\vec{k}$. The function $\beta(\vec{k})$ is defined as

$$\beta(\vec{k})=\frac{2\pi^2}{\sqrt{\epsilon_0}m^2\omega c}\frac{e^2 I}{\hbar\omega}\sum_{b\,\text{in}\,h;c\,\text{in}\,l}|\vec{\eta}\cdot\vec{P}_{bc}(\vec{k})|^2\times\frac{1/[\pi\hbar T_2(\vec{k})]}{[\Omega(\vec{k})-\omega]^2+[1/T_2(\vec{k})]^2}, \tag{8}$$

where I is the light intensity, $\vec{\eta}$ is the polarization of the light, and ϵ_0 is the intrinsic material dielec-

tric constant. The definition of $\beta(\vec{k})$ in Eq. (8) differs slightly from that of Ref. 16 because we have not averaged over polarizations. As a result the distribution function which we calculate here depends on the polarization of the light and does not have cubic symmetry. The calculational approach however is the same as that of Ref. 16. Some of the results we present here are for unpolarized light. In this case we average Eq. (8) over polarizations.[17]

III. CALCULATION AND RESULTS

We calculate the intensity dependence of the real part of the susceptibility due to resonant intervalence-band transitions. The results quoted in this section for $\Delta n(I)$ or $\Delta\epsilon_1(I)$ refer to only this contribution. There is an additional intrinsic contribution which is to be added to our results. There may also be heating effects in any particular experiment. One can determine the contribution from thermal effects using measured values of dn/dT. The thermal effects can be eliminated by using short laser pulses.

In order to calculate the occupation probability that a hole state is occupied, it is necessary to know the free-hole scattering rates. For the hole concentrations and temperatures at which most saturable absorption experiments have been performed, phonon scattering is the dominant scattering mechanism. The phonon scattering rates were treated in the manner of Ref. 15. The one-hole energies and momentum matrix elements are determined by degenerate $\vec{k}\cdot\vec{p}$ perturbation theory.[18] The cyclotron resonance parameters of Henzel and Suzuki[19] were used. Using the steady-state solution for the difference in the occupation probabilities, we integrate Eq. (5) to determine the laser-induced changes in the real part of the susceptibility.

The real part of the susceptibility is calculated numerically for $\lambda = 10.6$ μm and $T = 300$ K. Using Eq. (5) we can calculate $\underline{\chi}'(I)$ for any polarization of the light. Explicit values of $\underline{\chi}'(I)$ are calculated for the case of unpolarized light and for the polarization along the [100] and [110] directions.

For unpolarized light the second-rank tensor $\underline{\chi}'$ becomes a scalar, since any orientational dependence has been averaged out when we averaged over the directions of the vector potential.[17] The values of $\chi'(I)$ increase monotonically with increasing intensity due to changes in the distribution of free holes. Room-temperature values of $\chi'(I)/\chi'(I=0)$ are given in Fig. 1 for intensities between 0 and 60 MW/cm^2. At low intensities $[\chi'(I=0)/N_a]$ is equal to 1.4×10^{-20} cm^3 $[\chi'(I=0)$ is proportional to $N_a]$.

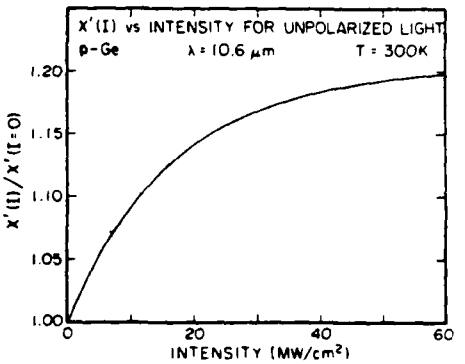

FIG. 1. Calculated values of $\chi'(I)/\chi'(I=0)$ as a function of intensity for unpolarized light in p-Ge. The calculation was done for light with a wavelength of 10.6 μm and a temperature of 300 K.

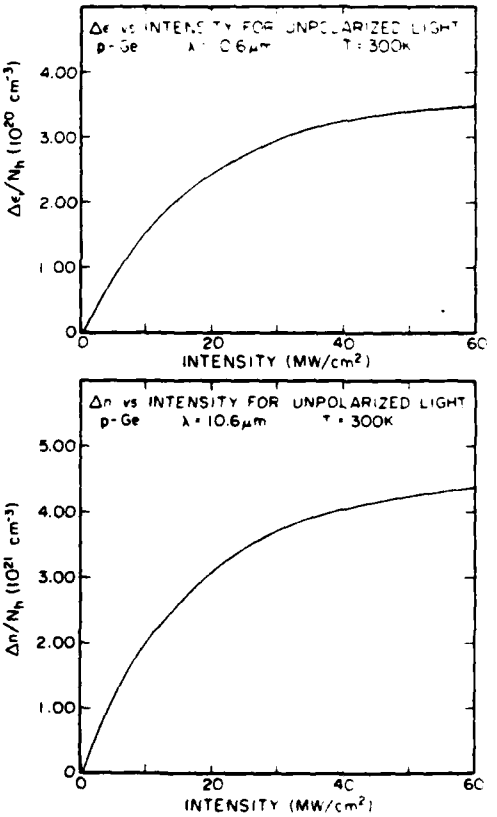

FIG. 2. The top panel gives the calculated values of the change in the real part of the dielectric constant (divided by the density of free holes) as a function of intensity for p-Ge at $\lambda = 10.6$ μm, $T = 300$ K, and for unpolarized light. The corresponding values for the change in the index of refraction are given in the lower panel.

Laser-induced changes in $\underline{\chi}'(\omega)$ can be measured by observing changes in the real part of the dielectric constant, which determine the dispersive properties of the medium. The real part of the complex dielectric constant $\underline{\epsilon}_1$ is given by

$$\underline{\epsilon}_1 = \epsilon_0 + 4\pi\underline{\chi}'. \tag{9}$$

Values for the change in $\underline{\epsilon}_1$ can be measured by studying threshold values for self-focusing (for $d\epsilon_1/dI$ positive). In Fig. 2 we show the calculated results for $\Delta\epsilon_1$ and the corresponding results for the change in the index of refraction, Δn, for unpolarized light with a wavelength of 10.6 μm at 300 K. The changes in ϵ_1 and in n are directly proportional to the free-hole density. We find that ϵ_1 and n are increasing functions of intensity.

The intrinsic contribution to dn/dI in Ge has recently been measured to be about 1×10^{-6} cm^2/MW.[11] The resonant intervalence-band contribution to dn/dI is intensity dependent. In the lower-intensity region the change in n is linear in I. For hole densities greater than about 3×10^{15} cm^{-3}, the resonant intervalence-band contribution is larger than the intrinsic contribution at the lower intensities.

In Fig. 3 we show the calculated results for the diagonal components of $(\Delta\underline{\epsilon}_1/N_h)$ as a function of intensity for light polarized in the [100] and [110] directions. For the case of [100] polarization the coordinate axes are chosen to be the crystal axis of the sample. In this coordinate system, the off-diagonal components of $\underline{\epsilon}_1$ vanish as at low intensities. There is a small difference in the values of $(\epsilon_1)_{zz}$ and $(\epsilon_1)_{xx}$ [$(\epsilon_1)_{yy} = (\epsilon_1)_{xx}$ in this case] due to the polarization dependence of $\beta(\vec{k})$ in determining the distribution of holes in the heavy- and light-hole bands. For the case of [110] polarization, the x axis is taken in the [110] direction, the y axis in the [1$\bar{1}$0] direction, and the z axis in the [001] direction. In this coordinate system $\underline{\epsilon}_1$ is diagonal. There is a small difference in the values of the three diagonal components. Overall, from Fig. 3 we see that the effects of polarization on $\Delta\underline{\epsilon}_1$ are rather small.

The change in $\underline{\epsilon}_1$ with intensity is due to the change in the distribution of hole states. The diagonal components of $\underline{\epsilon}_1$ increase monotonically with increasing intensity. From Eq. (5), we see that values of $\vec{k}$ for which $\Omega(\vec{k}) > \omega$ lead to a positive contribution to $\underline{\chi}'$ and thus to $\underline{\epsilon}_1$, whereas values of $\vec{k}$ for which $\Omega(\vec{k}) < \omega$ lead to a negative contribution to $\underline{\chi}'$. Under optical excitation, the holes occupy higher-energy states than in equilibrium. Thus for the higher-energy states with $\Omega(\vec{k}) > \omega$, the difference in occupation probabilities $[f_a(\vec{k}) - f_i(\vec{k})]$ is on the average enhanced compared to the equilibrium value, whereas for states

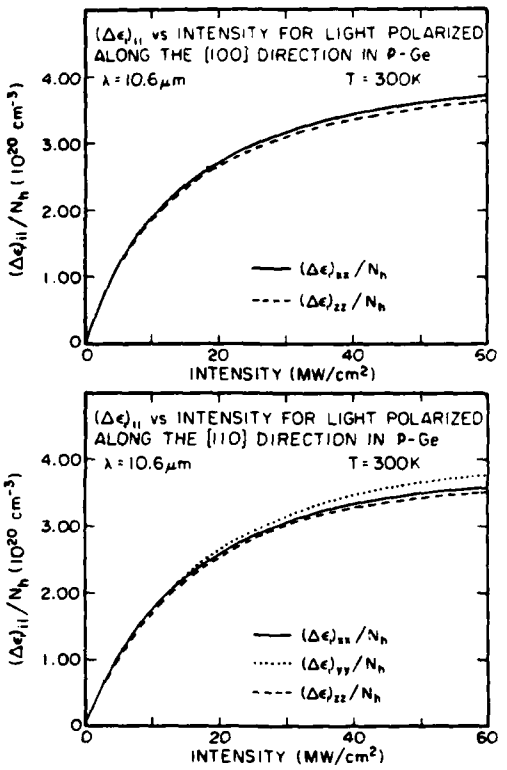

FIG. 3. Calculated values of the diagonal elements of $\Delta\epsilon_1$ (divided by the free-hole density) as a function of intensity on p-Ge at 300 K for light with a wavelength of 10.6 μm. In the top panel the result for [100] polarization is shown. The coordinate system is chosen to be the crystal axis; ϵ_1 is diagonal in this coordinate system. In the lower panel the result for [110] polarization is shown. For this panel, the x axis is in the [110] direction, the y axis is in the [1$\bar{1}$0] direction, and the z axis is in the [001] direction. In this coordinate system ϵ_1 is diagonal.

with $\Omega(\vec{k}) < \omega$ the difference in occupation probabilities is decreased compared to the equilibrium value. Hence the positive contributions to $\underline{\epsilon}_1$ from terms with $\Omega(\vec{k}) > \omega$ is increased by illumination, and the magnitude of the negative contribution to $\underline{\epsilon}_1$ from terms with $\Omega(\vec{k}) < \omega$ is decreased by illumination. Consequently, $\underline{\epsilon}_1$ monotonically increases with increasing intensity. As the intensity increases, the increase in $\underline{\epsilon}_1$ is slower than linear due to saturation of the intervalence-band transitions. That is, $d\epsilon_1/dI$ decreases with intensity (but it is always positive) because the population of the heavy-hole states in the resonant region of the heavy-hole band becomes depleted at high intensities and thus the heating of the hole distribution saturates with intensity.

From the results for $\Delta\underline{\epsilon}_1(I)$, together with the

intrinsic contribution, one can determine the effect of self-focusing actions in nonlinear optics experiments using p-Ge. The importance of self-focusing in any given experimental situation must be independently analyzed since it depends on the doping level, the intensity range, the sample thickness, and the beam profile.

For two laser beams incident on a Ge sample, as in a pump-probe experiment, the light intensity is modulated in space and time due to the interference of the two beams. Since the index of refraction is a function of intensity, it is modulated by the oscillating intensity. The periodic variation of the index of refraction leads to a coupling of the two beams. This coupling can influence the transmission of the beams which may be important in the analysis of a pump-probe experiment.

Many semiconductors have a valence-band structure which is similar to that of Ge and an intensity dependence in χ' should be present in these materials. The theory presented here should apply for these materials as well as for Ge.

IV. SUMMARY AND CONCLUSIONS

We have presented a theory describing the intensity dependence of the real part of the dielectric constant in p-Ge due to modifications of the free-hole distribution function by the high-intensity CO_2 laser light. We find that the high-intensity light alters the optical isotropy, and the susceptibility becomes a second-rank tensor with elements which depend on both the intensity and the polarization of the saturating beam. These changes in the susceptibility are directly proportional to the concentration of free holes in the sample. The diagonal components of the susceptibility increase monotonically with increasing intensity. At high light intensities, the increase in χ' is slower than linear due to saturation of the intervalence-band transitions. The magnitude of the resonant intervalence-band contribution to the first-order modification of n equals measured values of the intrinsic contribution at a doping level of about 3×10^{15} cm^{-3}.

ACKNOWLEDGMENTS

The authors gratefully acknowledge the support of the Air Force Office of Scientific Research under Grant No. AFOSR-77-3216. One of us (D.L.S.) acknowledges support from the Alfred P. Sloan Foundation.

[1] C. R. Phipps, Jr. and S. J. Thomas, Opt. Lett. 1, 93 (1977).
[2] A. J. Alcock and A. C. Walker, Appl. Phys. Lett. 25, 299 (1974).
[3] B. J. Feldman and J. F. Figueria, Appl. Phys. Lett. 25, 301 (1974).
[4] A. F. Gibson, M. F. Kimmitt, and B. Norris, Appl. Phys. Lett. 24, 306 (1974).
[5] See, for example, E. Bergmann, I. Bigio, B. Feldman, and R. Fisher, Opt. Lett. 3, 82 (1978).
[6] A. F. Gibson, C. A. Rosito, C. A. Raffo, and M. F. Kimmitt, Appl. Phys. Lett. 21, 356 (1972).
[7] R. L. Carlson, M. D. Montgomery, J. S. Ladish, and C. M. Lockhart, IEEE J. Quantum Electron. 13, 35D (1977).
[8] F. Kellmann, IEEE J. Quantum Electron. 12, 592 (1976).
[9] One cannot use the Kramers-Kronig dispersion relation to relate the nonlinear behavior of ϵ_1 and ϵ_2 because this dispersion relation only applies for linear systems.
[10] J. Wynne, Phys. Rev. 178, 1295 (1969).
[11] D. E. Watkins, C. R. Phipps, Jr., and S. J. Thomas, Opt. Lett. 5, 248 (1980).
[12] A. H. Kahn, Phys. Rev. 97, 1647 (1955).
[13] W. Kaiser, R. J. Collins, and H. Y. Fan, Phys. Rev. 91, 1342 (1953).
[14] This is completely analogous to the contribution to ϵ_1 from a group of harmonic oscillators, some with resonant frequencies greater and some with resonant frequencies less than the driving frequency.
[15] R. B. James and D. L. Smith, Phys. Rev. B 21, 3502 (1980).
[16] R. B. James and D. L. Smith, Phys. Rev. Lett. 42, 1495 (1979).
[17] We average the vector potential over all angles.
[18] E. O. Kane, J. Phys. Chem. Solids 1, 82 (1956).
[19] J. C. Hensel and K. Suzuki, Phys. Rev. B 9, 4219 (1974).

Luminescence studies of HgCdTe alloys [a)]

A. T. Hunter [b)] and T. C. McGill

California Institute of Technology, Pasadena, California 91125

(Received 13 November 1981; accepted 10 February 1982)

We report the observation in $Hg_{1-x}Cd_xTe$ of band-to-band, band-to-acceptor, and donor–acceptor luminescence for material of $x = 0.32$ and 0.5, and bound exciton recombination luminescence, for material of $x = 0.5$. The band-to-band lineshape and variation in intensity with pump power are appropriate to an electron-hole plasma with recombination proceeding without wave vector conservation. Differences between the spectra among the four 0.5 samples studied are attributed to variations in the Hg vacancy concentration. Shifts in luminescence energy across one of the $x = 0.32$ samples imply a change in composition across the surface of the sample of 0.03 cm^{-1}. The absence of bound exciton luminescence in the $x = 0.32$ samples is consistent with theoretical calculations by Osbourn and Smith showing a radiative efficiency of 20% for bound excitons in material of this composition and 90% for $x = 0.48$ material. From line shape separations, we estimate acceptor binding energies of 14.0 ± 1.0 and 15.5 ± 2.0 meV in $x = 0.32$ and 0.48 materials, respectively, and donor binding energies of 1.0 ± 1.0 and 4.5 ± 2.0 meV, respectively.

PACS numbers: 78.55.Hx, 71.35. + x, 71.55.Dp

I. INTRODUCTION

Photoluminescence spectra have been widely used as a method for studying the properties of II–VI semiconductors.[1] However, the photoluminescence spectra for $Hg_{1-x}Cd_xTe$ has not been explored extensively.[2,3] Recently we have initiated a study of the photoluminescence spectra of HgCdTe with x values less than 0.5.[4]

In this manuscript we summarize a series of luminescence experiments that we have carried out on HgCdTe. Spectra were taken on bulk-grown samples of $x = 0.32$ and $x = 0.48$, and on an epitaxial sample with $x = 0.51$.

II. EXPERIMENTAL TECHNIQUE

Spectra were taken over the temperature range of 5 to 30 K for a wide range of pump-laser power densities. A mechanically chopped Ar^+ ion laser was used to create excited electrons and holes in the samples. The samples were mounted in a cryogenic dewar. The light emitted by the sample was focused onto the slits of a grating spectrometer and was detected with a solid-state detector. The slit width used for most of the spectra gave an energy resolution of ~1 meV. An InAs detector was used for the $x = 0.48$ and 0.51 material, and an InSb detector was used for the $x = 0.32$ material. The detector output was fed into a lock-in amplifier, with a signal from the mechanical chopper used as a reference signal.

III. RESULTS

Figure 1 is a spectrum showing luminescence intensity as a function of emitted photon energy for Sample 1 which has a composition of $x = 0.48$. This sample is n type, with $N_D - N_A = 10^{15}$ cm^{-3}.[5] This spectrum shows all of the different luminescence lines we have observed in the material. The line at the highest energy in the figure has the characteristics of band-to-band recombination luminescence. We attribute the line at the lowest energy to donor–acceptor recombination below ~10 K, and to free electron-to-bound hole recombination at higher temperatures where a substantial fraction of the donors are ionized. The line at the intermediate energy has the characteristics of bound exciton recombination luminescence.

The shift of the line peaks with temperature provides much of the information necessary to identify the mechanisms responsible for the luminescence. Figure 2 summarizes the peak positions for the sample of Fig. 1 for a variety of temperatures and pump powers. The points for a given

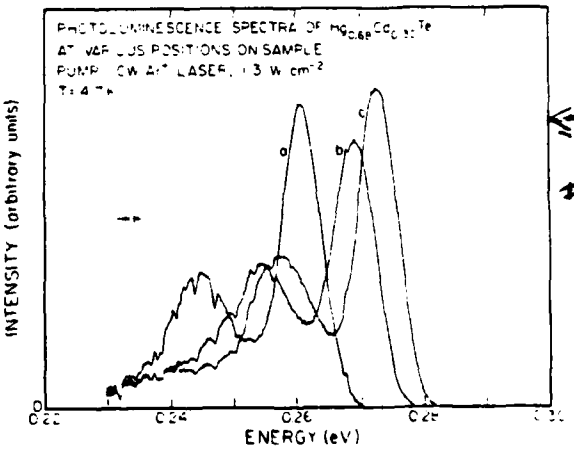

FIG. 1. Spectrum of $Hg_{0.52}Cd_{0.48}Te$ showing photoluminescence intensity vs photon energy with the sample at 13.9 K. The high energy peak is due to band-to-band recombination. The low energy peak is due to a combination of donor–acceptor and band-to-acceptor luminescence. The intermediate energy line is due to bound exciton luminescence. The sample was n-type, with $N_D - N_A \sim 10^{15}$ cm^{-3}.

(This caption is the correct caption for Figure 1.)

band at one pump power are connected together as an aid to the eye. The band-to-band peak shifts toward higher energy at a rate equal to 3 k_B, where k_B is Boltzmann's constant. The bound exciton, on the other hand, does not shift at all within the uncertainty of the measurement. The low energy impurity related line shifts very little below 10 K, especially at the two lowest pump powers. Then it shifts rapidly above 10 K.

The peak shift of the band-to-band line is consistent with an electron-hole plasma recombining without wave vector conservation. This mechanism predicts a line peak which shifts, in the nondegenerate limit, at a rate equal to 2 k_B. While this is not quite enough to match the shift observed, it is a better match than could be obtained with other mechanisms. For example, an electron-hole plasma in which the wave vector is conserved during recombination would shift at a rate of only $\frac{1}{2} k_B$. A shift of the band gap with temperature may explain some of the additional shift. Another piece of evidence for recombination without wave vector conservation is that the predicted lineshape fits the data reasonably well at 30 K. The carrier density was the only parameter varied which affected the shape and width of the fit, and the value of the carrier density needed to fit the observed width of the line was consistent with that estimated from the pump-laser power density.

The factors that identify the intermediate energy line as bound exciton luminescence are the lack of shift as temperature is varied and a rapid decrease in intensity as temperature is raised. Since the peak does not shift with temperature, the electron and hole involved in the recombination must be bound. However, the rapid decrease in intensity with respect to the other lines indicate that the binding energy is small. Both of these properties are characteristic of bound exciton recombination luminescence.

The lack of shift of the low energy peak at low temperatures again indicates that bound particles are involved in the recombination. However, the luminescence is deeper than for the bound exciton line, and the line width is much greater, pointing to donor–acceptor pair recombination. The rapid shift in energy of the line peak above 10 K comes about because the weakly bound donors become thermally ionized. The widths of the donor–acceptor luminescence and the free-electron to bound-hole luminescence lines are too broad compared to the donor binding energy to resolve each as a separate line.

Three other samples of $x = 0.5$ material were studied. The results of the luminescence experiments are similar for these samples as for the sample described above, but there are a few differences in some of the samples. Sample 2 was p type with $N_A - N_D \sim 10^{15}$ cm^{-3}, Sample 3 was p type with $N_A - N_D \sim 10^{16}$ cm^{-3}, and Sample 4 was an epitaxial sample grown on a CdTe substrate.[5] The bound exciton was observed in samples 2 and 4 but was not observed in sample 3. The other luminescence lines were observed in all the samples.

Sample 3, in addition to showing no bound exciton luminescence, also had a very weak band-to-band line in comparison to Sample 1, under similar pump-laser power densities and temperatures. This difference could be explained by a higher defect density in sample 3 than in sample 1. The added defects could directly cause the difference by being the acceptor responsible for the luminescence, or indirectly by reducing the free carrier lifetime by promoting nonradiative recombination. Hg vacancies are a likely candidate for the defect. Evidence for this explanation is provided by the evolution of the spectrum from sample 2. Originally, the sample showed a strong bound exciton line at low temperature. Prior to many of the luminescence experiments on the sample, its surface was etched briefly in a weak bromine–methanol solution, since this procedure was found to enhance the luminescence signal. After a period of several months, and several etchings, the bound exciton signal was no longer observed, and the luminescence signal resembled that observed from sample 3. All of the bulk grown samples were annealed in a Hg atmosphere after growth, which reduced the carrier concentration in a thin surface layer,[5] presumably by reducing the Hg vacancy concentration. Therefore, it is likely that the interior of sample 2 (and all of the other bulk-grown

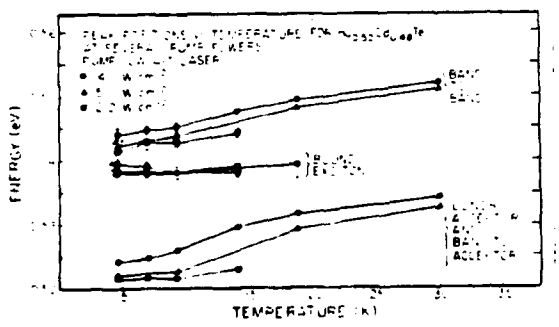

FIG. 2. Summary of luminescence band peak energies vs temperature of $Hg_{0.52}Cd_{0.48}Te$ at three different pump powers for the sample of Fig. 1. The line between data points are drawn as a visual aid, and connect points measured at different temperatures for one type of luminescence band at one pump power. Error bars are given where significant; the uncertainty is due to overlap between bands.

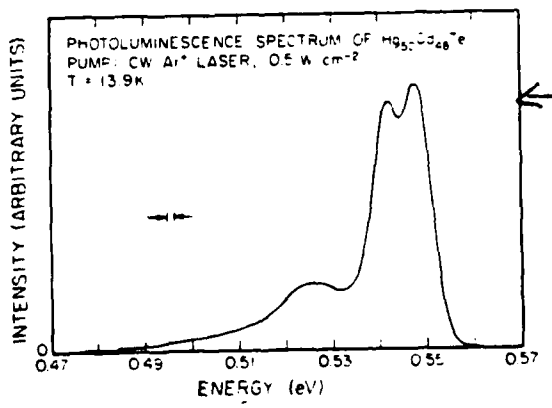

FIG. 3. Spectra of $Hg_{0.48}Cd_{0.52}Te$ showing photoluminescence intensity vs photon energy. For spectrum (b), the pump laser was 1.0 mm above its position for spectrum (a), and for (c), 2.5 mm above its position for spectrum (a). The shift in energy between (a) and (c) implies a shift in composition for 0.03 cm^{-1}.

(Note: this caption is the correct caption for figure 2)

samples) had a much higher Hg vacancy concentration, than the region near the surface. Therefore, the etchings gradually exposed material with a higher vacancy concentration, which changed the luminescence signal. The similarity between the spectra in sample 3 and the spectra in sample 2 after etching indicates that sample 3 had a higher vacancy concentration to begin with, which was responsible for the dominance of the defect related band.

The spectra observed from sample 4, the epitaxial sample, were similar to those observed from sample 1 and from sample 2 before etching. However, the band-to-band line was much more intense at comparable pump power densities than in the other two bulk-grown samples. This may indicate a much lower overall defect density for the epitaxial sample.

The data for the $x = 0.32$ material is shown in Fig. 3. The band-to-band and electron-to-bound hole lines are observed in this material. This figure shows luminescence spectra from a p-type $x = 0.32$ sample, with $N_A - N_D \sim 10^{15}\ \mathrm{cm}^{-3}$.[5] The three spectra shown in this figure were all taken at the same pump power and temperature. The only thing varied between the spectra was the position of the pump beam on the surface of the HgCdTe wafer. Using measured relationship between composition and band gap,[6] the composition gradient is estimated to be $0.03\ \mathrm{cm}^{-1}$ for this sample.

The major difference between the $x = 0.5$ samples and the $x = 0.32$ samples is that the bound exciton luminescence line was not seen in either of the two $x = 0.32$ samples studied. One possible explanation for this absence is provided by a calculation of the radiative efficiency of bound exciton luminescence.[7] This calculation shows that the radiative efficiency in $x = 0.32$ material is 20%, much smaller than the 90% radiative efficiency for bound exciton luminescence in $x = 0.48$ material.

The energy differences between the lines allow estimates of the donor and acceptor binding energy. From the separation between the band-to-band line and the band-to-bound-hole line, we estimate 14.0 ± 1.0 and 15.5 ± 2.0 meV in $x = 0.32$ and 0.48 material, respectively, for the acceptor binding energies. Values of 1.0 ± 1.0 and 4.5 ± 2.0, respectively, were obtained for the donor binding energies from the energy difference between the donor–acceptor and band-to-bound hole line positions.

IV. CONCLUSIONS

In summary, we have observed luminescence from band-to-band transitions, donor–acceptor transitions, and free electron-to-bound-hole transitions in $x = 0.32$ and $x = 0.5$ $Hg_{1-x}Cd_xTe$. We have observed bound exciton recombination luminescence in $x = 0.5$ material. The variation in composition across the surface of a sample was measured using photoluminescence. Finally, donor and acceptor binding energies were estimated from the data. A more extensive report of this work is contained in Ref. 4.

ACKNOWLEDGMENTS

We wish to acknowledge P. Bratt and K. Riley of the Santa Barbara Research Center for providing us with HgCdTe samples, and L. DeVaux of the Hughes Research Center for useful discussions on the properties of HgCdTe.

Laboratories

[a]Work supported in part by the Air Force Office of Scientific Research under Grant No. AFOSR-77-3216.

[b]Present address: Hughes Research Laboratories, 3011 Malibu Canyon Road, Malibu, CA 90265.

[1]See, for example, A. A. Bergh and P. J. Dean, *Light-Emitting Diodes* (Clarendon, Oxford, 1976), p. 245ff, and references therein.
[2]C. T. Elliot, I. Melngailis, T. C. Harman, and A. G. Foyt, J. Phys. Chem. Solids 33, 1527 (1972).
[3]V. I. Ivanov-Omskii, V. A. Mattseva, A. D. Britov, and S. D. Sivachenko, Phys. Status Solidi A: 46, 77 (1978).
[4]A. T. Hunter and T. C. McGill, J. Appl. Phys. 52, 5779 (1981).
[5]P. Bratt (private communication).
[6]R. Dornhaus and G. Nimtz, in *Springer Tracts in Modern Physics*, edited by G. Hohler (Springer-Berlin, 1976), Vol. 78, pp. 1–112.
[7]G. C. Osbourn and D. L. Smith, Phys. Rev. B 20, 1556 (1979).

(Springer-Verlag, Berlin, 1976)

Solid State Communications, Vol.36, pp.761-764.
Pergamon Press Ltd. 1980. Printed in Great Britain.

PHOTOIONIZATION OF SHALLOW ACCEPTORS IN Ge

M. B. Weimer and D. L. Smith
California Institute of Technology
Pasadena, California 91125

(Received 13 August 1980 by A. A. Maradudin)

We compute the cross section for the transition, induced by the absorption of light, of acceptor bound holes to states in the split-off valence band in Ge. We find good agreement with the available low temperature optical absorption data.

At low temperature in p-type Ge, holes are bound to shallow acceptors. Transitions from the bound acceptor levels to states in the split-off valence band determine the optical absorption in the spectral region from about 300 to 400 meV. The absorption due to this process has been observed in boron doped Ge at 4.2°K by Pokrovskii and Svistunova [1]. However, these authors interpreted their results in terms of a free hole picture. There was substantial discrepancy between the free hole calculation and the experimental data; the calculation predicted a much narrower absorption band than was observed.

In the free hole picture, the initial and final states are Bloch functions in the heavy and split-off hole bands, respectively. The transition conserves wavevector and hence only one final state is possible for a given initial state. At low temperature, only those levels very close to the zone center are populated, restricting transitions to a small region of the split-off band. The absorption spectrum is consequently predicted to be sharply peaked at the spin orbit splitting energy. By contrast, when the hole is initially bound it no longer has a unique wavevector. Rather, there is an amplitude, given by an envelope function, to occupy a range of Bloch states near the valence band edge. For a bound initial state there is a set of final states possible which span a range in energy. Thus, the spread in k space of the envelope function is reflected in an irreducible energy width for the absorption spectrum [2,3].

In this communication we present a calculation of the cross section for photoionizing acceptor bound holes to states in the split-off band.

The absorption cross section per hole is given by

$$\sigma(\omega) = \frac{4\pi^2 e^2}{n\omega m^2 c} \sum_F |\langle F|\hat{n}\cdot\vec{p}|I\rangle|\ \delta(E_F - E_I - \hbar\omega) \qquad (1)$$

where I and F represent the initial and final state wavefunctions with energies E_I and E_F, respectively; n is the index of refraction, $\hat{n}$ is the photon polarization vector and the other symbols have their usual meaning.

The evaluation of the acceptor eigenfunctions is complicated by the degenerate structure of the valence band in Ge. In the limit of large spin-orbit splitting only the four states at the top of the band need be considered to describe the bound hole. We take as basis functions at the zone center those multiplets which arise from diagonalizing the spin-orbit interaction among the Γ_{25} states [4] and denote by $\phi_j(o)$ this fourfold set degenerate at the band edge. Moving out into the Brillouin zone "pseudo-Bloch functions" [5,6] are defined as

$$\chi_j(k) = e^{i\vec{k}\cdot\vec{r}}\ \phi_j(k) \qquad (2a)$$

with

$$\phi_j(k) = \phi_j(o) - \frac{\hbar}{m}\sum_\ell \frac{|u_\ell\rangle\langle u_\ell|\vec{k}\cdot\vec{p}|\phi_j(o)\rangle}{\epsilon_\ell} \qquad (2b)$$

where $|u_\ell\rangle$ is a Bloch function at the zone center in band ℓ with energy ϵ_ℓ relative to the valence band edge. The hole wave function in this representation can be written as

$$|I^n\rangle = \sum_{k,j} C_j^n(k)\ \chi_j(k) \qquad (3)$$

where n is a label for the hole quantum numbers. The fourier transform of the expansion coefficients

$$F_j^n(r) = \sum_k C_j^n(k)\ e^{i\vec{k}\cdot\vec{r}} \qquad (4a)$$

satisfies

$$\sum_j \left[H_{ij}(-i\vec{\nabla}) - \frac{e^2}{\epsilon_o r}\delta_{ij}\right] F_j^n(r) = E_n\ F_i^n(r) \qquad (4b)$$

with H_{ij} the 4x4 effective mass Hamiltonian for the valence band and $e^2/\epsilon_o r$ the screened impurity potential.

To approximate the solutions of Eq. (4b) we use the spherical model of Baldereschi and Lipari [7]. The effective mass hamiltonian is split into a component with full rotational symmetry plus a small term invariant under the cubic point group. Only the spherically symmetric part is retained. The spectrum of eigenvalues is such

that the first excited level lies a significant fraction of the binding energy above the ground state. For $k_BT \ll E_B$ (E_B is the binding energy) only the ground state will be occupied with non-negligible probability. With appropriate phases for the $X_i(k)$, the ground state envelope function is given by

$$F_j^{F_z}(r) = f_o(r)\, Y_{00}(\theta,\phi) \times \langle L=0, M=0, J=3/2, j | L=0, J=3/2, F=3/2, F_z\rangle + g_o(r) \sum_M Y_{2M}(\theta,\phi) \times \langle L=2, M, J=3/2, j | L=2, J=3/2, F=3/2, F_z\rangle \quad (5)$$

The orbital angular momentum, L, is coupled with the "spin 3/2", J, of $\phi_j(o)$ (j=J) to form the total angular momentum $\vec{F} = \vec{L} + \vec{J}$, and $^2\langle LMJj|LJFF_z\rangle$ is a Clebsch-Gordon coefficient. The acceptor ground state has four degenerate solutions each with a definite value of F_z. The radial functions, f_o and g_o, satisfy a set of coupled differential equations [7] which must be solved variationally. Since we are interested only in the ground state we adopt as trial functions Slater orbitals (in contrast to Baldereschi and Lipari who use gaussians) possessing the correct asymptotic dependence at the origin and infinity:

$$f_o(r) = \sum_{i=1}^{10} A_i e^{-\alpha_i r} \quad \text{and} \quad g_o(r) = r \sum_{i=1}^{10} B_i e^{-\alpha_i r}$$

The α_i are a fixed set of exponents chosen to cover a wide range [8] and the coefficients A_i, and B_i are variationally determined. The energy eigenvalue obtained by this procedure is 9.72 meV (compared to 9.73 meV quoted in Ref. 7) and the experimental value for boron in Ge is 10.5 meV [9].

The final state pseudo-Bloch functions are given by

$$\xi_s(k) = e^{i\vec{k}\cdot\vec{r}}\, \psi_s(k) \quad (7a)$$

$$\psi_s(k) = \psi_s(o) - \frac{\hbar}{m} \sum_\ell \frac{|u_\ell\rangle\langle u_\ell|\vec{k}\cdot\vec{p}|\psi_s(o)\rangle}{\Delta+\epsilon_\ell} \quad (7b)$$

where Δ is the Γ_{25}' spin-orbit splitting (295 meV), s labels the two-fold degeneracy of the split-off band and the final state wave function is expanded as in Eq. (3). The fouriers transform, $G_s(r)$, of the expansion coefficients satisfies a relation identical to Eq. (4b) except that H is replaced by the appropriate effective mass hamiltonian. (The equations for the two bands decouple). The problem is identical to that of an electron in an attractive coulomb field (scaled by an effective Bohr radius) and the solution has bound as well as continuum levels. Focusing momentarily on the final state continuum, the solutions for $G_s(r)$ with boundary conditions for photoionization are the well-known coulomb wave functions. Neglecting the acceptor-hole interaction, $G_s(r)$ reduces to a plane wave.

The optical matrix element for a transition from the acceptor ground state to the split-off band continuum is

$$\langle F_s|\vec{\eta}\cdot\vec{p}|I^{F_z}\rangle = \sum_{j,\alpha} M_{\vec{\eta}}^{j,s,\alpha} \langle G_s(r)|p_\alpha|F_j^{F_z}(r)\rangle \quad (8a)$$

where the constants $M_{\vec{\eta}}^{j,s,\alpha}$ are defined by

$$\hbar \sum_\alpha M_{\vec{\eta}}^{j,s,\alpha} k_\alpha \equiv \langle\psi_s(k)|\vec{\eta}\cdot\vec{p}|\phi_j(k)\rangle \quad . \quad (8b)$$

The overlap of $\vec{\eta}\cdot\vec{p}$ between the periodic parts of the pseudo-Bloch functions is given by

$$\langle\psi_s(k)|\vec{\eta}\cdot\vec{p}|\phi_j(k)\rangle = -\frac{\hbar}{m}\sum_\ell \left[\frac{\langle\psi_s(o)|\vec{\eta}\cdot\vec{p}|u_\ell\rangle\langle u_\ell|\vec{k}\cdot\vec{p}|\phi_j(c)\rangle}{\epsilon_\ell} + \frac{\langle\psi_s(o)|\vec{k}\cdot\vec{p}|u_\ell\rangle\langle u_\ell|\vec{\eta}\cdot\vec{p}|\phi_j(o)\rangle}{\epsilon_\ell} + \left(\frac{\Delta}{\Delta+\epsilon_\ell}\right)\frac{\langle\psi_s(o)|\vec{k}\cdot\vec{p}|u_\ell\rangle\langle u_\ell|\vec{\eta}\cdot\vec{p}|\phi_j(o)\rangle}{\epsilon_\ell}\right] \quad (9)$$

The matrix elements appearing in Eq. (9) are evaluated in terms of the valence band effective mass parameters as determined by cyclotron resonance [10,11]. The first two terms combined are symmetric in the components η_α k_β and the additional contribution proportional to Δ may be rewritten as the sum of symmetric and antisymmetric parts. It arises because we take the states at the zone center to be approximated by the correct zero'th order linear combination of simple group ⊗ spinor basis functions which diagonalizes the spin-orbit interaction. We adopt this procedure because, owing to the weak acceptor binding and strong spin-orbit coupling in Ge, we are primarily interested in the small k region where the k·p perturbation is less than the spin-orbit perturbation. For consistency, the splitting of the Γ_{15} intermediate states is explicitly taken into account in the first two terms of Eq. (9).

We follow the usual procedure of restricting the sum in Eq. (9) to the nearest intermediate state of a given symmetry. The contribution proportional to $\left(\frac{\Delta}{\Delta+\epsilon_\ell}\right)$ is then calculable for the Γ_2' and Γ_{15} intermediate states whose energies [11] relative to the valence band are well known. Quantities second order in the spin orbit interaction are ignored, as is the small effect of the more remote Γ_{12}' and Γ_{25} bands.

AD-A119 264 CALIFORNIA INST OF TECH PASADENA F/G 20/5
OPTICAL PROPERTIES OF SMALL BAND GAP SEMICONDUCTORS SUBJECT TO --ETC(U)
1982 T C MCGILL, D L SMITH AFOSR-77-3216
UNCLASSIFIED AFOSR-TR-82-0678 NL

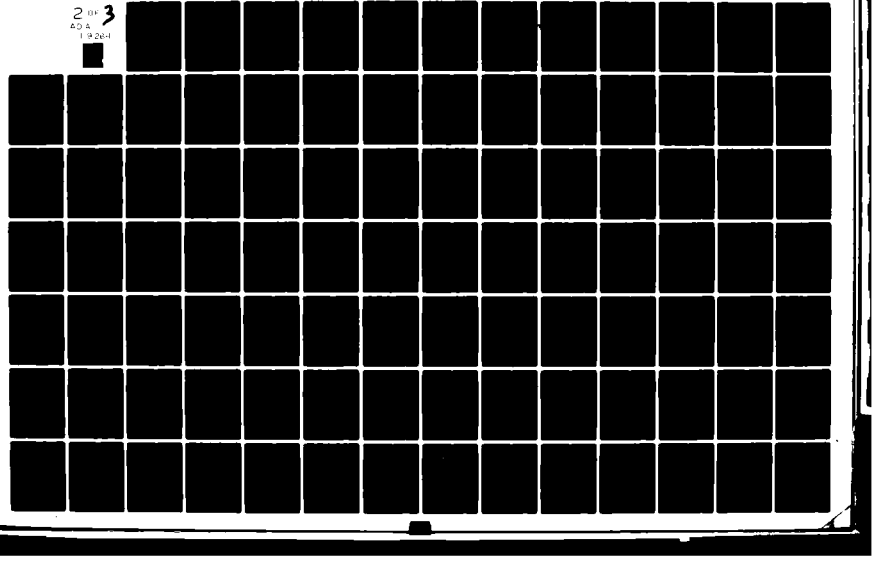

The dispersion relation for the final state energies obtained in the same order of approximation is

$$\epsilon_{so} = -(\Delta + \hbar^2 k^2/2m^*_{so}) \qquad (10a)$$

with

$$m/m^*_{so} = \gamma_1 + Fy + 2H_1 y' \qquad (10b)$$

where F and H_1 are the Dresselhaus-Kip-Kittel $\vec{k}\cdot\vec{p}$ parameters, $y^{-1} = \Delta/3(\epsilon_{\Gamma_2'}+\Delta)$[10] and $y' = \Delta/3(\epsilon_{\Gamma_{15}}+\Delta)$.

It is evident from Eq. (8a) that, in direct analogy with atomic processes, parity and angular momentum selection rules are determined by the transformation properties of $\vec{p}$ and the envelope functions. The initial state is a coherent sum of s and d waves; the final state contains all partial waves. Thus only transitions from s to p wave and d to p or f wave are allowed. The radial integrals which are encountered can be evaluated in closed form[12].

When averaged over the initial four-fold degeneracy and summed over the final states in the split-off band, the cross section is independent of the direction and polarization of the incident light owing to the cubic symmetry of the crystal. The results are illustrated in Fig. (1)[13]. For comparison, the cross section neglecting acceptor-hole interaction in the final state is also presented. The threshold

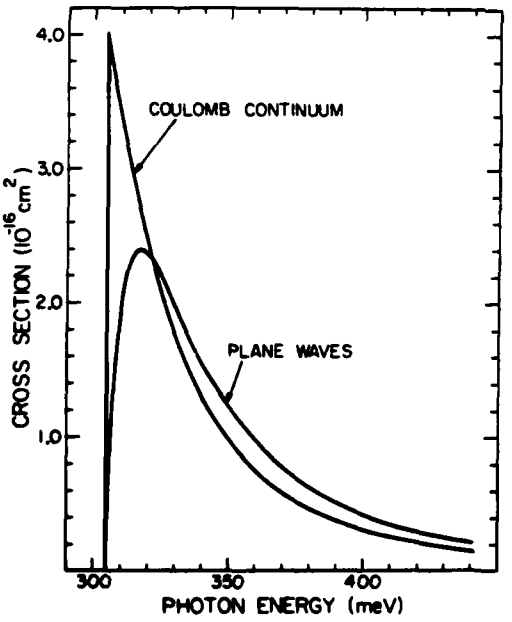

Figure 1. Calculated photoionization cross section vs. photon energy in Ge. Transitions are from bound acceptor levels to continuum states in the split-off valence band. Comparison of the two curves illustrates the effect of the acceptor-hole interaction in the final state.

value is finite when the impurity charge is included in the final state as is typical for a coulomb potential. Note that the coulomb curve is broader and its peak lower in relation to the plane wave curve than is the case in the analagous results for the photo-effect in hydrogen. The primary reasons for this are: (i) the smaller effective mass of the split-off band as compared to the heavy hole mass and (ii) the large value of the spin-orbit splitting relative to the acceptor ionization energy.

We now consider the effect of bound levels in the split-off band. The initial hole will couple to all such p and f states. The lowest of these, the 2p, lies roughly 1.3 meV below the continuum threshold. The finite hole lifetime in the split-off band introduces a Lorentzian broadening with a FWHM of about 8.6 meV[14]. Therefore, any fine structure produced by transitions to the bound levels will be washed out and only their integrated contribution to the cross section is of interest. A sum rule may be used to calculate this quantity. Specifically, multiplying Eq. (1) by ω and integrating over all frequencies one obtains the same result for both the complete set of coulomb solutions and plane wave final states. Thus,

$$\int \omega\sigma_B(\omega)\, d\omega = \int \omega\sigma_{pw}(\omega)\, d\omega - \int \omega\sigma_{cw}(\omega)\, d\omega \qquad (11)$$

where $\sigma_B(\omega)$ is the acceptor to bound, σ_{cw} is the acceptor to coulomb wave continuum and $\sigma_{pw}(\omega)$ is the acceptor to plane wave cross section, respectively. The photon energy is essentially constant over the range of $\sigma_B(\omega)$. One can therefore approximate

$$\sigma_B(\omega) \approx \left[\frac{\hbar\int\omega\sigma_B(\omega)d\omega}{\Omega}\right]\frac{1}{\pi}\frac{\Gamma}{\Gamma^2+(\hbar\omega-\hbar\Omega)^2} \qquad (12a)$$

with

$$\hbar\Omega = \Delta + E_B - \frac{1}{4}E_B' \qquad (12b)$$

Here E_B' is the binding energy of a hole in the split-off band and 2Γ is the FWHM of the Lorentzian. The energy integral of $\sigma_B(\omega)$ was found to be 10.2×10^{-16} meV cm^2.

In Fig. (2), we show the total lifetime broadened cross section. The experimental data is that of Pokrovskii and Svistunova for Ge at 4.2° K doped with 6.6×10^{16} cm^{-3} boron. The theory and data are in qualitative agreement sharing a similar broad shape. The calculated curve peaks somewhat above the experimental points near threshold falling slightly below them at higher energies. One expects this kind of behavior since the model hamiltonian somewhat underestimates the acceptor binding energy.

No parameters were adjusted in our calculation to improve agreement with experiment. The absolute normalization of the data was reported to only one significant figure and the impurity concentration, recalling the large spatial extent of acceptor states in Ge, was relatively high. There may be some uncertainty in the final hole

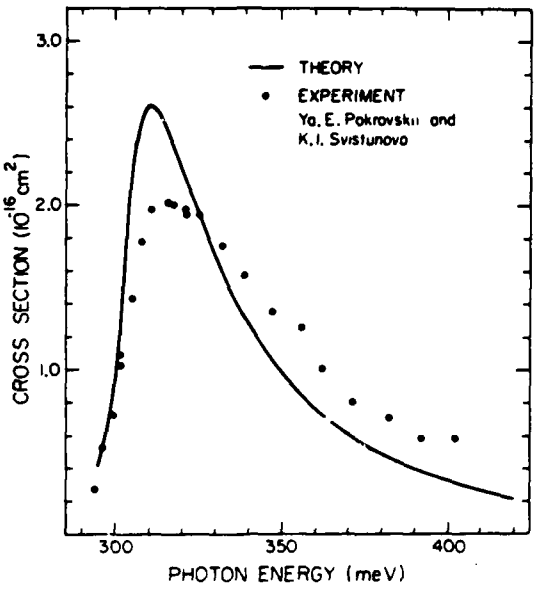

Figure 2. Photoionization cross section vs. photon energy in Ge. Theory includes transition to bound and continuum levels in the split-off valence band. Broadening due to finite hole lifetime is included. Experimental points are from Ref. (1).

lifetime broadening and in the precise value of the spin orbit energy which determines the position of the continuum threshold. In view of these considerations, theory and experiment are in reasonable quantitative agreement.

To conclude, we have calculated, in the spherical model [7] of shallow impurity states, the cross section for photoionization of acceptor bound holes in Ge and find that the dominant features of the observed low temperature optical absorption spectrum are well accounted for.

Acknowledgement- We thank Y. C. Chang for assistance with the variational calculation. We gratefully acknowledge the support of the Air Force Office of Scientific Research under Grant No. AFOSR-77-3216. One of us (D.L.S.) acknowledges support from the Alfred P. Sloan Foundation.

REFERENCES

1. POKROVSKII, Ya. E. and SVISTUNOVA, K. I., Fiz. Tverd. Tela 13, 2788 (1971). [Sov. Phys. - Solid State 13, 2334 (1972).]
2. SMITH, D. L., CHEN, M. and McGILL, T. C., Phys. Rev. B14, 3504 (1976).
3. SILVER, R. N. and ALDRICH, C. H., Phys. Rev. Letts. 41, 1249 (1978).
4. KANE, E. O., J. Phys. Chem. Solids 1, 82 (1956).
5. KITTEL C. and MITCHELL, A., Phys. Rev. 96, 1488 (1954).
6. LUTTINGER, J. M. and KOHN, W., Phys. Rev. 97, 869 (1955).
7. BALDERESCHI, A. and LIPARI, N. O., Phys. Rev. B8, 2697 (1973).
8. In units of inverse effective Bohr radii (defined in Ref. (7)) α_1 = 16.0, 7.0, 4.0, 2.0, 1.0, 2/3, 2/5, 1/5, 2/15, 1/15.
9. JONES, R. L. and FISHER, P., J. Phys. Chem. Solids 26, 1125 (1965).
10. HENSEL, J. C. and SUZUKI, K., Phys. Rev. B9, 4219 (1974).
11. LAWAETZ, P., Phys. Rev. B4, 3460 (1971).
12. See, e.g., Landau and Lifschitz, Quantum Mechanics 3rd ed. Appendix f; Pergamon (1977).
13. The initial state energy was taken to be the experimental value for boron in Ge (Ref. (9)).
14. ARTHUR, J. B., BAYNHAM, A. C., FAWCETT and PAIGE, E. G. S., Phys. Rev. 152, 740 (1966).

APPENDIX B

REVIEW ARTICLE

ON

NONLINEAR OPTICS

THEORY OF NONLINEAR OPTICAL ABSORPTION ASSOCIATED WITH FREE CARRIERS IN SEMICONDUCTORS

R. B. James
Solid State Division, Oak Ridge National Laboratory
Oak Ridge, Tennessee 37830

and

D. L. Smith*
California Institute of Technology
Pasadena, California 91125

ABSTRACT

We present calculations of the intensity dependence of the free carrier absorption in semiconductors by high intensity light with a wavelength near 10μm. The paper is divided into two sections: the first section examines the nonlinear absorptive and dispersive properties associated with free-hole transitions in semiconductors, and the second section presents calculations of the nonlinear absorption associated with free-electron intraband transitions in germanium. The dominant free hole absorption of CO_2 laser light for most p-type semiconductors with the diamond or zinc-blende crystal structure is direct intervalence-band transitions where a hole in the heavy- (or light-) hole band absorbs a photon and makes a direct transition to another band within the valence band structure. The absorption coefficient due to this mechanism is found to decrease with increasing intensity in a manner closely approximated by an inhomogeneously broadened two-level model. We present detailed results for the saturation behavior of germanium as a function of temperature, wavelength, and doping density. Calculated values for the intensity dependence of the index of refraction and low frequency conductivity are presented. Calculated values

*Present address: Honeywell Systems and Research Center, Mail Code: MN17-2328, 2600 Ridgway Parkway, Minneapolis, Minnesota 55413.

of the saturation intensity are also given for most of the other Groups IV and III-V semiconductors. In several *n*-type semiconductors, the dominant absorption for 10μm light is free-electron intraband absorption where an electron absorbs a photon and is excited to a state in the same band. The interaction of the electron distribution with the high-intensity light increases the average energy of the electrons and leads to an increase in the free-carrier cross section. For sufficiently high intensities, a significant fraction of the electron density in the interaction region can have an energy greater than the band gap (relative to the conduction band minimum) by successive one-photon intraband transitions. These hot electrons can relax by creating an electron-hole pair by an impact ionization process. This can lead to the formation of an optically induced plasma and an abrupt increase in the absorption coefficient for light well below the band gap of the material. Calculated threshold values for the formation of a laser-induced plasma by this impact ionization process are presented for germanium as a function of the lattice temperature and wavelength of the CO_2 laser light.

I. INTRODUCTION

There is considerable theoretical and experimental interest in nonlinear optical phenomena in semiconductors, particularly with those effects which are connected with the dependence of the complex dielectric constant on the intensity of the light. In this paper we present a theory describing the intensity dependence of the absorptive and dispersive properties associated with free carriers in semiconductors for light with wavelength in the 9-11μm region, which corresponds to the CO_2 laser spectrum.

When radiation at a given frequency interacts with a material with an electronic transition near that frequency, a resonant interaction occurs, and several nonlinear phenomena associated with the resonance may result. For materials in thermal equilibrium, the radiation is absorbed as it propagates through the medium, resulting in the attenuation of the wave. The decay of a wave propagating in the z-direction is given by

$$\frac{dI}{dz} = -\alpha I \ . \tag{1}$$

Here, I is the light intensity, and α is the absorption coefficient. At low light intensities (linear regime), the absorption coefficient is independent of the light intensity; however, at sufficiently high intensities, the absorption becomes a nonlinear function. We examine the intensity dependence of the complex dielectric constant associated with free electron and free hole transitions for below bandgap radiation. Detailed results of the calculation are presented for germanium for which nonlinear optical data at 10.6 μm is fairly extensive.

The absorption of CO_2 laser light by free carriers in germanium should be divided into two categories, the absorption associated with free hole carriers and the absorption associated with free electron carriers. Experimentally, it has been observed that the absorption of 10μm light by free holes decreases with increasing intensity,[1] and that the absorption of 10μm light by free electrons increases with increasing intensity.[2-3] Both of these nonlinear optical properties have practical uses.

The nonlinear infrared absorption exhibited by many p-type semiconductors, such as Ge, has several applications in the control of lasers to obtain large peak output powers. For example, the saturation of the intervalence-band absorption allows passive mode locking of a CO_2 laser by inserting a slice of a suitable p-type semiconductor into the optical path of the cavity. The saturable absorber causes the laser to oscillate in a pulsed fashion, since this mode of oscillation undergoes less loss than one in which the energy is spread more uniformly. That is, the loss is a minimum when the phases of the oscillating modes are locked and the energy distribution inside the resonator corresponds to a narrow traveling pulse with a period equal to the round trip transit time of the resonator. Experiments have demonstrated that a CO_2 laser with p-Ge as a saturable absorber can be used to generate passively mode-locked pulses of subnanosecond duration,[4-6] where the pulse duration is limited by the gain linewidth of the laser. Considerably shorter pulses should be possible by operating the laser at higher pressures.[6]

The saturable absorption characteristics of p-type semiconductors have also been used to achieve isolation of high power CO_2 oscillator-amplifier systems,[7-8] which is important for amplifier stabilization and the suppression

of spurious oscillations. Ideally, the isolation device would prevent spontaneous lasing in the high gain amplifiers and suppress retrodirected signals which can arise from windows and targets as well as other pulsed laser systems in a multiple beam irradiation experiment. Here, one would like the material to attenuate low-level oscillations and reflections, while the material would be transparent to the high intensity pulses which are to be amplified.

The saturable absorption property of p-Ge has also been used to temporally compress laser pulses.[9] The low intensity tail of a pulse sees a higher absorption coefficient while the peak of the pulse propagates relatively unattenuated, which leads to a pulse shortening effect. The long tail, characteristic of CO_2 TEA oscillators, can be removed by the larger linear absorption of the crystal.

The nonlinear absorption observed in n-type semiconductors, such as n-type germanium, has been used to amplify reflected CO_2 laser light via degenerate four-wave mixing in an optically induced free carrier plasma.[10] The laser heats the free carrier distribution to a point where the higher energy electrons can relax by creating an electron-hole pair by an impact ionization process. This process can lead to the formation of an optically induced plasma and to an abrupt increase in the absorption coefficient for light well below the bandgap of the material. The increase in the absorption coefficient associated with the free carriers is believed to have an important effect in limiting the efficiency of a spin-flip InSb laser at high pump intensities.[11] This nonlinear phenomena also presents a fundamental limitation to the usefulness of n-type semiconductors (such as Ge, Si, and GaAs) as optical grade components in the infrared.[2-3]

The paper is presented in the following way. We first discuss the intensity dependence of the absorption coefficient and index of refraction associated with free hole transitions in p-Ge, as well as other p-type semiconductors. Parts of this section will be a review of the authors' research results which have been previously published in other shorter papers. The second half of the paper presents new results for the nonlinear absorption associated with free electron intraband transitions in germanium. Both calculations require knowledge of the free carrier distribution function as a function of the light intensity; however, the excitation mechanisms are different for the two types of carriers.

II. SATURATION OF INTERVALENCE-BAND TRANSITIONS

In p-type germanium, direct free-hole transitions between the heavy- and light-hole bands are primarily responsible for the absorption of light in the 6-25μm region. At high light intensities, absorption due to these intervalence-band transitions has been found to saturate in p-Ge.[1,7-9,12] In this section we summarize a theory of the saturation behavior of heavy-hole band to light-hole band transitions in p-type semiconductors as a function of the light intensity. Detailed numerical results are presented for the intensity dependence of the absorption coefficient of p-Ge (the material in which the effect has been most frequently observed experimentally).

The theory is also used to describe the laser-induced change in the real part of the complex dielectric constant in p-Ge that results from saturation of the intervalence-band transitions. We find that the presence of a saturable beam alters the optical isotropy of p-Ge, where the changes in the dispersive properties depend on the intensity and polarization of

the beam. A nonlinearity of this form manifests itself in a dependence of the index of refraction on the light intensity. This causes beam self-focusing (de-focusing) in regions where a beam "sees" a higher (lower) index of refraction at the center of the Gaussian beam profile than at the tails. We show explicit values for the intensity dependence of the index of refraction for light at 10.6μm and room temperature conditions.

In previous work, saturable absorption in p-type semiconductors had been described by modeling the valence bands as an ensemble of two-level systems whose level populations approach one another at high light intensities.[12-14] This two-level model predicts that the dependence of the absorption coefficient as a function of intensity is given by

$$\alpha(I,\omega) = \frac{\alpha_0(\omega)}{\sqrt{1 + I/I_s(\omega)}} \quad , \tag{2}$$

where $\alpha_0(\omega)$ is the absorption coefficient at low intensity, and $I_s(\omega)$ is the saturation intensity. The behavior described in Eq. (2) was found to be reasonably well satisfied experimentally, and values of $I_s(\omega)$ were determined.[7-9,12] However, attempts to calculate $I_s(\omega)$ as a function of photon energy using the two-level model and a multistep cascade relaxation[14] gave results that disagree with experiment.[7] In section A, we review the results of a theory of saturable absorption in p-type semiconductors which realistically accounts for the anisotropic and nonparabolic band structure. Our calculated results are in good agreement with Eq. (2), and values of $I_s(\omega)$ deduced from the calculation are in good agreement with experiment.

A. Theoretical Approach

The valence band structure for small k is determined by degenerate $\underset{\sim}{k}\cdot\underset{\sim}{p}$ perturbation theory using a method developed by Kane[15] based on measured

values of the cyclotron resonance parameters.[16] In Figure 1 the valence band structure of germanium is shown for small $\underset{\sim}{k}$ in the [100] direction. There are three bands, each of which is two-fold degenerate. The six bands correspond to states constructed from the atomic p functions of the individual atoms times the two spin functions, spin up and spin down. The heavy- (h) and light- (ℓ) hole bands are degenerate at k=0, and the split-off hol band (s) is separated at k=0 from the heavy- and light-hole bands by the spin-orbit interaction. Here, the spin-orbit interaction lowers the two $j = 1/2$ bands with respect to the four $j = 3/2$ bands.

For a given direction in $\underset{\sim}{k}$-space, the heavy-hole band may be taken as parabolic, the light-hole band effective mass increases with energy, and the split-off hole band effective mass decreases with energy. These qualitative features also hold for the valence band structures of other semiconductors with the diamond or zincblende structure; however, the effective masses and spin-orbit splittings are different for the various materials.

We now consider the absorption processes in p-Ge at room temperature. At λ=10.6μm, the intervalence-band absorption cross section in Ge is 6.8×10^{-16} cm^2.[17] The intravalence-band absorption cross section, estimated from Drude-Zener theory is about 10^{-17} cm^2, and the absorption coefficient from multiphonon absorption is about 0.03 cm^{-1}.[18] Thus, for hole concentrations greater than 10^{15} cm^{-3}, intervalence-band absorption is 1 to 2 orders of magnitude greater than the other absorption processes. Similar intervalence-band absorption has been observed in several other p-type semiconductors as well;[19-24] however, the range of wavelengths which correspond to the three sets of intervalence-band transitions vary for the different materials.

Both energy and wavevector are conserved in the intervalence-band optical transitions. Thus, only holes in a narrow region of the heavy-hole band can directly participate in the absorption, and the absorption coefficient is governed by the population of these hole states. The optical transitions tend to deplete the population of the pertinent heavy-hole states. At low intensities, the population of heavy-hole states involved in the optical transition is maintained close to the equilibrium value by various scattering processes. However, as the intensity becomes large, scattering cannot maintain the equilibrium population of these heavy-hole states, and they become depleted. As a result the absorption saturates at high intensity. To determine the saturation characteristics of the intervalence-band transitions, it is necessary to set up rate equations for the hole distribution function in the heavy- and light-hole bands.

For the hole concentrations and temperatures at which most saturable absorption measurements have been performed (room temperature and $N_h \lesssim 4\times10^{15}$ cm^{-3}), hole-phonon scattering is the dominant relaxation mechanism. We first consider only hole-phonon scattering. (Hole-impurity and hole-hole scattering are later included so the theory can be applied to more heavily doped material.) The system can then be described by the Hamiltonian

$$H = H_o + V + \gamma(t) \quad , \tag{3a}$$

where

$$H_o = H_{el} + H_{ph} \quad , \tag{3b}$$

and

$$Y(t) = \frac{e}{mc} \underset{\sim}{A}(t) \cdot \underset{\sim}{P} \quad . \tag{3c}$$

Here H_{el} describes the free holes, H_{ph} describes the phonon system, V is the hole-phonon interaction, and Y(t) describes the interaction of the holes with the electromagnetic field. The electromagnetic field is described by the vector potential $\underset{\sim}{A}$; in the Coulomb gauge $\underset{\sim}{A}$ satisfies the wave equation

$$\nabla^2 \underset{\sim}{A} - \frac{\epsilon_\infty}{c^2} \frac{\partial^2 \underset{\sim}{A}}{\partial t^2} = - \frac{4\pi}{c} \underset{\sim}{J} \quad , \tag{4}$$

where $\underset{\sim}{J}$ is the current density induced by the intervalence-band transitions,

$$\underset{\sim}{J} = N_h \frac{e}{m} \mathrm{Tr} [\sigma \underset{\sim}{P}'] \quad . \tag{5}$$

Here N_h is the hole density, σ is the one-hole density matrix, and $\underset{\sim}{P}'$ is the off-diagonal (including only intervalence-band matrix elements) part of the hole momentum operator.

We consider the low-hole density limit and take the Hamiltonian to be given by Eq. (3). The density matrix of the whole system $\rho(t)$ satisfies

$$\frac{d\rho}{dt} = \frac{-i}{\hbar} [H, \rho] \quad . \tag{6}$$

We are interested in the electronic part of the problem. The lattice can be considered as a surrounding medium and regarded as large and dissipative. In general, to calculate the time evolution of physical observables, we would need to know the density matrix of the whole system $\rho(t)$. But since the effects of the interaction with the incident light on the free-holes are quickly dissipated by the lattice, and since the lattice (which acts as

a heat bath) is not significantly heated over the duration of the interaction, we write the density matrix $\rho(t)$ as the product of an operator $\sigma(t)$ describing the free-hole density matrix and an operator P_L describing the lattice in equilibrium. Then $\rho(t) \approx \sigma(t)P_L$. Using standard approximations,[25] one finds

$$\frac{d\sigma_I(t)}{dt} \approx \frac{-i}{\hbar}\left[V_I(t), \sigma_I(t)\right] - \frac{1}{\hbar^2}\int_0^\infty dt'\ Tr_L\left[V_I(t), \left[V_I(t'), \sigma_I(t)\ P_L\right]\right]. \tag{7}$$

Here the subscript I signifies that an operator is in the interaction representation, and Tr_L signifies a trace over lattice modes.

From Eq. (7), one can see that $\sigma(t)$ is diagonal in wavevector. Prior to laser excitation, $\sigma(t)$ has the equilibrium value which is diagonal in wavevector. Taking matrix elements of Eq. (7), we see that the time derivative of any matrix element of $d\sigma_I(t)/dt$ which is off-diagonal in $\underset{\sim}{k}$ is equal to a sum of terms, all of which are proportional to a matrix element of $\sigma_I(t)$ which is off-diagonal in $\underset{\sim}{k}$. Thus, when the equation is integrated in time, all off-diagonal in $\underset{\sim}{k}$ matrix elements of $\sigma_I(t)$ vanish. This result is to be expected since the electromagnetic field leads to transitions between states with the same wavevector.

We define

$$\langle b\underset{\sim}{k}|\sigma|b'\underset{\sim}{k}\rangle = \sigma_{bb'}(\underset{\sim}{k}) , \tag{8}$$

where $\underset{\sim}{k}$ labels the wavevector, and b is the band index. Taking matrix elements of Eq. (7), dropping nonresonant terms, and returning to the Schrodinger representation gives[26]

$$\frac{d}{dt}\sigma_{bb}(\underset{\sim}{k},t) = -\frac{i}{\hbar}[\gamma(\underset{\sim}{k},t), \sigma(\underset{\sim}{k},t)]_{bb}$$

$$-\sum_{c\underset{\sim}{k}'}[R_{b\underset{\sim}{k}\to c\underset{\sim}{k}'}\sigma_{bb}(\underset{\sim}{k},t) - R_{c\underset{\sim}{k}'\to b\underset{\sim}{k}}\sigma_{cc}(\underset{\sim}{k}',t)] \quad , \tag{9a}$$

for the band index diagonal matrix elements of σ, and

$$\frac{d}{dt}\sigma_{bb'}(\underset{\sim}{k},t) = -\frac{i}{\hbar}[H_{el}(\underset{\sim}{k}) + \gamma(\underset{\sim}{k},t), \sigma(\underset{\sim}{k},t)]_{bb'}$$

$$-\frac{1}{T_2(\underset{\sim}{k})}\sigma_{bb'}(\underset{\sim}{k},t) \quad , \tag{9b}$$

for the off-diagonal matrix elements. Here

$$\frac{2}{T_2(\underset{\sim}{k})} = \sum_{c\underset{\sim}{k}'}[R_{h\underset{\sim}{k}\to c\underset{\sim}{k}'} + R_{\ell\underset{\sim}{k}\to c\underset{\sim}{k}'}] \quad , \tag{9c}$$

where $R_{a\underset{\sim}{k}\to b\underset{\sim}{k}'}$ is the rate at which a hole in band a with wavevector $\underset{\sim}{k}$ is scattered into a state in band b with wavevector $\underset{\sim}{k}'$, h(ℓ) refers to the heavy- (light-) hole band, and $\gamma(\underset{\sim}{k})$ and $H_{el}(\underset{\sim}{k})$ are defined analogous to Eq. (8).

Using the equations for the time evolution of σ, the current density owing to intervalence-band transitions is found (see Ref. 26 for details) to be determined by

$$\frac{d^2}{dt^2}\underset{\sim}{J}(\underset{\sim}{k}) + \frac{2}{T_2(\underset{\sim}{k})}\frac{d}{dt}\underset{\sim}{J}(\underset{\sim}{k}) + \Omega^2(\underset{\sim}{k})\,\underset{\sim}{J}(\underset{\sim}{k})$$

$$= N_h\frac{e^2}{\hbar^2 m^2 c}\sum_{bc} f_b(\underset{\sim}{k})\,(\varepsilon_c(\underset{\sim}{k}) - e_b(\underset{\sim}{k}))$$

$$\times\,(\underset{\sim}{A}\cdot\underset{\sim}{P}_{bc}(\underset{\sim}{k})\,\underset{\sim}{P}_{cb}(\underset{\sim}{k}) + \underset{\sim}{P}_{bc}\underset{\sim}{A}\cdot\underset{\sim}{P}_{cb}(\underset{\sim}{k})) \quad . \tag{10}$$

Here $\varepsilon_b(\underset{\sim}{k})$ is the energy of a hole in band b with wavevector $\underset{\sim}{k}$, $\hbar\Omega(\underset{\sim}{k})$ is $(\varepsilon_h(\underset{\sim}{k}) - \varepsilon_\ell(\underset{\sim}{k}))$, we rename the diagonal elements of the hole density matrix $f_b(\underset{\sim}{k})$, and $\underset{\sim}{J}(\underset{\sim}{k})$ is the part of $\underset{\sim}{J}$ which includes only those terms in the trace with wavevector $\underset{\sim}{k}$ ($\sum_{\underset{\sim}{k}} \underset{\sim}{J}(\underset{\sim}{k}) = \underset{\sim}{J}$).

Eq. (10) is the basic equation describing the absorption and dispersion for the medium. We find that the current density acts as a harmonic oscillator of frequency Ω driven by the electric field through a coupling coefficient proportional to the population difference for a given state with wavevector $\underset{\sim}{k}$. One important conclusion is that the ability of the vector potential to drive the current density is decreased as the probability of occupation of states in the heavy- and light-hole bands become more nearly equal. This constitutes the physical basis for the observed nonlinear absorption. Another important point is that in the absence of the applied interaction, the current density will be damped because of the internal dephasing of the individual dipoles through the interaction with the lattice, given by the constant T_2.

Assuming both $\underset{\sim}{A}$ and $\underset{\sim}{J}(\underset{\sim}{k})$ oscillate in time with angular frequency ω, we have

$$\underset{\sim}{J} = \frac{N_h e^2}{m^2 c\hbar} \sum_{\underset{\sim}{k}} (f_h(\underset{\sim}{k}) - f_\ell(\underset{\sim}{k})) \sum_{bc} \frac{\underset{\sim}{A}\cdot\underset{\sim}{P}_{bc}\underset{\sim}{P}_{cb} + \underset{\sim}{A}\cdot\underset{\sim}{P}_{cb}\underset{\sim}{P}_{bc}}{(\Omega^2(\underset{\sim}{k})-\omega^2) - i\,2\omega/T_2(\underset{\sim}{k})} \Omega(\underset{\sim}{k}). \qquad (11)$$

Due to the peaked behavior of Eq. (11), the primary contribution to the current density is from states in the heavy- and light-hole bands with an energy difference $\hbar\Omega(\underset{\sim}{k})$ that does not differ greatly from the photon energy $\hbar\omega$; thus, we write

$$\underset{\sim}{J} = \frac{N_h e^2}{2m^2 c\hbar} \Sigma (f_h(\underset{\sim}{k}) - f_\ell(\underset{\sim}{k})) \sum_{bc} \frac{\underset{\sim}{A}\cdot\underset{\sim}{P}_{bc}\underset{\sim}{P}_{cb} + \underset{\sim}{A}\cdot\underset{\sim}{P}_{cb}\underset{\sim}{P}_{bc}}{(\Omega(\underset{\sim}{k}) - \omega) - i/T_2(\underset{\sim}{k})} \quad . \tag{12}$$

Using Eq. (12), we write the susceptibility as a second-rank tensor given by

$$\underset{\approx}{\chi}(\omega, I) = \frac{N_h e^2}{2m^2\omega^2\hbar} \sum_{\underset{\sim}{k}} (f_h(\underset{\sim}{k}) - f_\ell(\underset{\sim}{k})) \sum_{bc} \frac{\underset{\sim}{P}_{cb}\underset{\sim}{P}_{bc} + \underset{\sim}{P}_{bc}\underset{\sim}{P}_{cb}}{(\Omega(\underset{\sim}{k}) - \omega) - i/T_2(\underset{\sim}{k})} \quad . \tag{13}$$

The imaginary part of $\underset{\approx}{\chi}$ describes the changes in the absorptive properties of the semiconductor, and the real part of $\underset{\approx}{\chi}$ describes the changes in the dispersive properties. We define

$$\underset{\approx}{\chi} = \underset{\approx}{\chi}' + i\underset{\approx}{\chi}'' \ , \tag{14}$$

where $\underset{\approx}{\chi}'$ and $\underset{\approx}{\chi}''$ are real. Thus, we find

$$\underset{\approx}{\chi}'(\omega, I) = \frac{N_h e^2}{2m^2\omega^2\hbar} \Sigma (f_h(\underset{\sim}{k}) - f_\ell(\underset{\sim}{k})) \left(\sum_{bc} \underset{\sim}{P}_{cb}\underset{\sim}{P}_{bc} + c.c\right) \frac{\Omega(\underset{\sim}{k}) - \omega}{(\Omega(\underset{\sim}{k}) - \omega)^2 + (1/T_2(\underset{\sim}{k}))^2} \ , \tag{15}$$

and

$$\underset{\approx}{\chi}''(\omega, I) = \frac{N_h e^2}{2m^2\omega^2\hbar} \Sigma (f_h(\underset{\sim}{k}) - f_\ell(\underset{\sim}{k})) \left(\sum_{bc} \underset{\sim}{P}_{cb}\underset{\sim}{P}_{bc} + c.c.\right) \frac{1/T_2(\underset{\sim}{k})}{(\Omega(\underset{\sim}{k}) - \omega)^2 + (1/T_2(\underset{\sim}{k}))^2} . \tag{16}$$

Here, the intensity dependence in the susceptibility is contained in the distribution functions $f_h(\underset{\sim}{k})$ and $f_\ell(\underset{\sim}{k})$.

For a plane wave vector potential,

$$\underset{\sim}{A} = \underset{\sim}{A}_0 \, e^{i(\underset{\sim}{K}\cdot\underset{\sim}{r} - \omega t)} \ , \tag{17}$$

the absorption coefficient is given by[26]

$$\alpha(I,\omega) = \frac{4\pi^2}{\sqrt{\epsilon_\infty}\, m^2\, \omega c}\ \frac{N_h e^2}{3} \times \sum_{\underset{\sim}{k}} (f_h(\underset{\sim}{k}) - f_\ell(\underset{\sim}{k}))\left|\underset{\sim}{P}_{h\ell}(\underset{\sim}{k})\right|^2 \frac{1/(\hbar\pi\, T_2(\underset{\sim}{k}))}{(\Omega(\underset{\sim}{k})-\omega)^2 + (1/T_2(\underset{\sim}{k}))^2}\,, \tag{18}$$

where the squared momentum matrix element $\left|\underset{\sim}{P}_{h\ell}(\underset{\sim}{k})\right|^2$ is to be summed over the two degenerate states in both the heavy- and light-hole bands.

Eq. (18) is the usual expression for the absorption coefficient except that a normalized Lorentzian replaces the usual energy conserving delta function. The absorption coefficient is a function of the light intensity because the interaction of the holes with the laser radiation alters the distribution in the heavy- and light-hole bands. We want to solve this equation as a function of intensity to determine the saturation characteristics.

In order to determine the absorption coefficient, we must calculate the distribution functions for free holes in the heavy- and light-hole bands. In the semiconductors of interest, the scattering rate for free holes occurs on a subpicosecond time scale. For a saturating laser operating with nanosecond pulse widths (the typical experimental situation), transient effects are damped out. Thus, we are interested in the steady state values of the distribution functions. Using Eqs. (9) the steady state distribution functions are found to solve the rate equations[26-27]

$$\beta(\underset{\sim}{k})\ (f_h(\underset{\sim}{k}) - f_\ell(\underset{\sim}{k})) = -\sum_{c\underset{\sim}{k}'} \left[R_{h\underset{\sim}{k}\to c\underset{\sim}{k}'} f_h(\underset{\sim}{k}) - R_{c\underset{\sim}{k}'\to h\underset{\sim}{k}} f_c(\underset{\sim}{k}')\right], \tag{19a}$$

$$\beta(\underset{\sim}{k})\ (f_h(\underset{\sim}{k}) - f_\ell(\underset{\sim}{k})) = \sum_{c\underset{\sim}{k}'} \left[R_{\ell\underset{\sim}{k}\to c\underset{\sim}{k}'} f_\ell(\underset{\sim}{k}) - R_{c\underset{\sim}{k}'\to \ell\underset{\sim}{k}} f_c(\underset{\sim}{k}')\right], \tag{19b}$$

where

$$\beta(\underset{\sim}{k}) = \frac{2\pi^2}{\sqrt{\epsilon_\infty} m^2 \omega c} \frac{e^2 I}{3\hbar\omega} |P_{h\ell}(\underset{\sim}{k})|^2 \frac{1/(\pi\hbar T_2(\underset{\sim}{k}))}{(\Omega(\underset{\sim}{k})-\omega)^2 + (1/T_2(\underset{\sim}{k}))^2}. \quad (19c)$$

These equations state that the rate of optical excitation out of (into) a given state is equal to the net rate of scattering into (out of) the state when steady state is attained. The lefthand sides of Eqs. (19a) and (19b) give the net rate of optical excitation out of a state with wavevector $\underset{\sim}{k}$ in the heavy-hole band into a state with wavevector $\underset{\sim}{k}$ in the light-hole band. The righthand side of Eq. (19a) gives the net rate of scattering into the state with wavevector $\underset{\sim}{k}$ in the heavy-hole band, and the righthand side of Eq. (19b) gives the net rate of scattering out of the state with wavevector $\underset{\sim}{k}$ in the light-hole band.

To calculate the absorption coefficient as a function of intensity, we first solve Eq. (19) for the distribution functions and then integrate Eq. (18). In solving Eq. (19), it is convenient to introduce auxiliary functions defined by

$$\frac{1}{T_h(\underset{\sim}{k})} = \sum_{c\underset{\sim}{k}'} R_{h\underset{\sim}{k}\to c\underset{\sim}{k}'} , \quad (20a)$$

$$\frac{1}{T_\ell(\underset{\sim}{k})} = \sum_{c\underset{\sim}{k}'} R_{\ell\underset{\sim}{k}\to c\underset{\sim}{k}'} , \quad (20b)$$

$$F(\underset{\sim}{k}) = \sum_{c\underset{\sim}{k}'} \left[R_{c\underset{\sim}{k}'\to h\underset{\sim}{k}} (f_c(\underset{\sim}{k}') - f_c^e(\underset{\sim}{k}')) \right], \quad (20c)$$

and

$$G(\underset{\sim}{k}) = \sum_{c\underset{\sim}{k}'} \left[R_{c\underset{\sim}{k}'\to \ell\underset{\sim}{k}} (f_c(\underset{\sim}{k}') - f_c^e(\underset{\sim}{k}')) \right], \quad (20d)$$

where $f_c^e(\underset{\sim}{k})$ is the equilibrium value for the distribution function. The function $F(\underset{\sim}{k})$ is the difference in the feeding rate of free holes from the equilibrium feeding rate for the state with wavevector $\underset{\sim}{k}$ in the heavy-hole band. The function $G(\underset{\sim}{k})$ is analogously defined for the light-hole band. (Scattering into the light-hole band is small because of the small density of light-hole states. Thus, the function $G(\underset{\sim}{k})$ is less important than $F(\underset{\sim}{k})$). In terms of these auxiliary functions, the distribution functions can be written as

$$f_h(\underset{\sim}{k}) = f_h^e(\underset{\sim}{k}) - \frac{\beta(\underset{\sim}{k})\, T_h(\underset{\sim}{k})\, (f_h^e(\underset{\sim}{k}) - f_\ell^e(\underset{\sim}{k}))}{1 + \beta(\underset{\sim}{k})\, (T_h(\underset{\sim}{k}) + T_\ell(\underset{\sim}{k}))} + \frac{F(\underset{\sim}{k})\, T_h(\underset{\sim}{k}) + \beta(\underset{\sim}{k})\, T_h(\underset{\sim}{k})\, T_\ell(\underset{\sim}{k})\, (F(\underset{\sim}{k}) + G(\underset{\sim}{k}))}{1 + \beta(\underset{\sim}{k})\, (T_h(\underset{\sim}{k}) + T_\ell(\underset{\sim}{k}))} \quad . \tag{21a}$$

and

$$f_\ell(\underset{\sim}{k}) = f_\ell^e(\underset{\sim}{k}) + \frac{\beta(\underset{\sim}{k})\, T_\ell(\underset{\sim}{k})\, (f_h^e(\underset{\sim}{k}) - f_\ell^e(\underset{\sim}{k}))}{1 + \beta(\underset{\sim}{k})\, (T_h(\underset{\sim}{k}) + T_\ell(\underset{\sim}{k}))} + \frac{G(\underset{\sim}{k})\, T_\ell(\underset{\sim}{k}) + \beta(\underset{\sim}{k})\, T_h(\underset{\sim}{k})\, T_\ell(\underset{\sim}{k})\, (F(\underset{\sim}{k}) + G(\underset{\sim}{k}))}{1 + \beta(\underset{\sim}{k})\, (T_h(\underset{\sim}{k}) + T_\ell(\underset{\sim}{k}))} \quad . \tag{21b}$$

The difference in occupation probabilities which appears in the expression for the absorption coefficient is given by

$$f_h(\underset{\sim}{k}) - f_\ell(\underset{\sim}{k}) = \frac{(f_h^e(\underset{\sim}{k}) - f_\ell^e(\underset{\sim}{k}))}{1 + \beta(\underset{\sim}{k})\, (T_h(\underset{\sim}{k}) + T_\ell(\underset{\sim}{k}))} + \frac{T_h(\underset{\sim}{k})\, F(\underset{\sim}{k}) - T_\ell(\underset{\sim}{k})\, G(\underset{\sim}{k})}{1 + \beta(\underset{\sim}{k})\, (T_h(\underset{\sim}{k}) + T_\ell(\underset{\sim}{k}))} \quad . \tag{22}$$

The first term in Eq. (22) gives the population difference that would occur for the states at $\underset{\sim}{k}$ if the populations of the states that feed those at $\underset{\sim}{k}$ were given by their equilibrium values. The second term in Eq. (19) accounts for the change in the population of the states that feed those at $\underset{\sim}{k}$. For those values of $\underset{\sim}{k}$ which are important in the integral in Eq. (18), the first term in Eq. (22) is found to be significantly greater than the second.

Using Eq. (19) and the definition of the auxiliary functions, one can write equations which determine $F(\underset{\sim}{k})$ and $G(\underset{\sim}{k})$. If there is no angular dependence in the phonon scattering matrix elements which go into the scattering rates, the functions $F(\underset{\sim}{k})$ and $G(\underset{\sim}{k})$ depend on $\varepsilon_h(\underset{\sim}{k})$ and $\varepsilon_\ell(\underset{\sim}{k})$, respectively. Thus, one-dimensional (rather than three-dimensional) equations must be solved to determine these functions. A more complete discussion of the solution for the functions $F(\underset{\sim}{k})$ and $G(\underset{\sim}{k})$ is presented in Ref. 26.

In order to calculate the distribution of free holes as a function of intensity, it is necessary to know the hole scattering rates. We first consider the region of temperature and impurity densities for which hole-phonon scattering is the dominant scattering mechanism. (This condition is relaxed in a later section to also include the effect of hole-impurity and hole-hole scattering). Optical phonon scattering is the dominant energy relaxation mechanism. The optical phonon spectrum of Ge is relatively flat for small k with an average energy of 0.037 eV. For the small k region in which we are interested, the acoustic phonon energy is quite small, and we neglect it. Although acoustic phonon scattering does not contribute significantly to energy relaxation, it can change the wavevector of the hole.

The valence bands of Ge are rather anisotropic and an acoustic phonon scattering event can take a hole from a region in which $\beta(\underset{\sim}{k})$ is small to one in which it is large. Thus, although acoustic phonon scattering is less important than optical phonon scattering in determining the distribution functions, it is not negligible because of the anisotropy of the valence bands. We take the scattering rates to be given by

$$R_{\underset{\sim}{a}\underset{\sim}{k}\to\underset{\sim}{b}\underset{\sim}{k}'} = \frac{2\pi}{\hbar}|M_{op}^{+}|^2\,\delta(\varepsilon_a(\underset{\sim}{k}) - \varepsilon_b(\underset{\sim}{k}') + \hbar\omega_o)$$

$$+ \frac{2\pi}{\hbar}|M_{op}^{-}|^2\,\delta(\varepsilon_a(\underset{\sim}{k}) - \varepsilon_b(\underset{\sim}{k}') - \hbar\omega_o) \qquad (23)$$

$$+ \frac{2\pi}{\hbar}|M_{ac}|^2\,\delta(\varepsilon_a(\underset{\sim}{k}) - \varepsilon_b(\underset{\sim}{k}'))\,.$$

Here $|M_{op}^{+}|^2$ is the squared matrix element for optical phonon emission, $|M_{op}^{-}|^2$ is the squared matrix element for optical phonon absorption, and $|M_{ac}|^2$ is the squared acoustic phonon scattering matrix element (summed over both absorption and emission processes).

For spherical energy surfaces and acoustic mode scattering, the shift of the the band edge is given by

$$\delta E_v = E_{ac}\,(e_{xx} + e_{yy} + e_{zz}) = E_{ac}\Delta\ , \qquad (24)$$

where the e_{ii} are the diagonal components of the strain tensor, their sum being equal to the dilatation Δ, and E_{ac} is the shift of the band edge per unit dilatation. Only longitudinal lattice waves scatter the holes. The matrix element is given by[28]

$$|M_{ac}|^2 = \frac{E_{ac}^2 k_B T}{2V\rho u_\ell^2} \quad . \tag{25}$$

Here, T is the temperature, V is the sample volume, ρ is the material density, and u_ℓ is the longitudinal sound velocity.

For nonpolar crystals (as Ge) and spherical energy surfaces, the hole-optical phonon scattering can also be described by a deformation potential approach. In this case, the optical strain is proportional to the displacement of the sublattice containing one type of atom with respect to the sublattice containing the other, where the displacement is induced by the optical mode. Integration over the electron coordinates and lattice oscillator coordinates gives[28]

$$|M_{op}^{+}|^2 = \frac{E_{op}^2 \hbar\omega_o}{2V\rho u_\ell^2} \left[N_q + 1 \right] , \tag{26a}$$

and

$$|M_{op}^{-}|^2 = \frac{E_{op}^2 \hbar\omega_o}{2V\rho u_\ell^2} N_q \quad , \tag{26b}$$

where E_{op} is the deformation potential for optical phonon scattering, $\hbar\omega_o$ is the zone-center optical phonon energy, and N_q is the optical phonon Bose factor defined by

$$N_q = \frac{1}{\exp\left(\frac{\hbar\omega_o}{k_B T}\right) - 1} \quad . \tag{27}$$

Following Ref. 28, we have neglected angular dependence in the phonon scattering matrix element and taken the scattering rates to be the same for the heavy- and light-hole bands. The numerical value for the constants appearing in the squared matrix elements were determined from the mobility fits of Ref. 29, where E_{ac} was taken to be 3.5 eV and E_{op} to be 6.8 eV. The scattering times $T_2(\underset{\sim}{k})$, $T_h(\underset{\sim}{k})$ and $T_\ell(\underset{\sim}{k})$ are computed from Eqs. (9c) and (20a, b) using these scattering rates. Optical phonon scattering (primarily emission) dominates in the results for $T_2(\underset{\sim}{k})$ and $T_\ell(\underset{\sim}{k})$ for the states of interest. For states in the resonant region of the heavy-hole band, optical phonon emission is typically not possible and acoustic phonon scattering makes a significant contribution to $T_h(\underset{\sim}{k})$.

B. Calculation of the Hole Distribution

We calculate the distribution of holes in $\underset{\sim}{k}$-space allowing the holes to interact with the laser excitation and the phonon system. As a first approximation for the population difference $(f_h(\underset{\sim}{k})-f_\ell(\underset{\sim}{k}))$, we neglect the auxiliary functions $F(\underset{\sim}{k})$ and $G(\underset{\sim}{k})$ and include only the first term in Eq. (22). This approximation is equivalent to assuming that the rate at which free holes are scattered into the states involved in the optical transition is given by the equilibrium value. For optical phonon scattering, the energy of the initial hole state in the scattering event differs from that of the final hole by the optical phonon energy. As a result, hole states that can scatter into a resonant optical transition region by optical phonon scattering are themselves, for the most part, out of the resonant region. Thus, the population of these states is not directly depleted by the optical transitions. The population of these states is indirectly

depleted by the optical transition because there is a decrease in the feeding rate of these states owing to the decrease in population of hole states in the resonant region. However, this decreased feeding from the resonant region is partially compensated for by an increased feeding from the re-routing of optically excited holes. For acoustical phonon scattering, the energy of the initial-hole state in the scattering event is essentially the same as that of the final hole state. As a result, hole states that can scatter into a resonant optical transition region by acoustic phonon scattering are, for the most part, in the resonant region themselves. Thus, the population of these states is directly depleted by the optical transitions. Including only the first term in Eq. (22) therefore overestimates the importance of acoustic phonon scattering. At this level of approximation it is better to ignore acoustic phonon scattering. We find that this first approximation for $(f_h(\underset{\sim}{k}) - f_\ell(\underset{\sim}{k}))$ ignoring acoustic phonon scattering produces results close to those of our more complete calculation.

Using only the first term in Eq. (22) to determine the population difference, the absorption coefficient written in Eq. (18) becomes

$$\alpha^1(I,\omega) = \frac{4\pi^2}{\sqrt{\epsilon_\infty}\, m^2 \omega c} \frac{N_h e^2}{3} \sum_{\underset{\sim}{k}} (f_h^e(\underset{\sim}{k}) - f_\ell^e(\underset{\sim}{k})) \left| P_{\underset{\sim}{h\ell}}(\underset{\sim}{k}) \right|^2$$

$$\times \frac{1/(\hbar\pi\, T_2(\underset{\sim}{k}))}{(\Omega(\underset{\sim}{k}) - \omega)^2 + \left(\frac{1}{T_2(\underset{\sim}{k})}\right)^2 \left[1 + I/I_s(\underset{\sim}{k})\right]} \quad , \tag{28}$$

where

$$\ell(\underset{\sim}{k}) = \frac{3\hbar^2 c\,\sqrt{\epsilon_\infty}\,m^2\,\omega^2}{(T_h(\underset{\sim}{k}) + T_\ell(\underset{\sim}{k}))\,T_2(\underset{\sim}{k})\,2\pi\,e^2\left|P_{h\ell}(\underset{\sim}{k})\right|^2} \quad . \tag{29}$$

Transforming to an integration over surfaces of constant $\Omega(\underset{\sim}{k})$, and assuming that the power-broadened Lorentzian is sharply peaked, Eq. (29) can be written as

$$\alpha^1(I,\omega) = \frac{4\pi^2}{\sqrt{\epsilon_\infty}\,m^2\,\omega c}\,\frac{N_h e^2}{3\hbar}\left(\frac{1}{2\pi}\right)^3 \int_{\Omega(\underset{\sim}{k})=\omega} \frac{ds}{|\nabla_{\underset{\sim}{k}}\Omega(\underset{\sim}{k})|}\,\frac{|P_{h\ell}(\underset{\sim}{k})|^2\,(f_h^e(\underset{\sim}{k}) - f_\ell^e(\underset{\sim}{k}))}{\sqrt{1 + I/\ell(\underset{\sim}{k})}} \quad . \tag{30}$$

Here, the integral is over a surface of constant $\Omega(\underset{\sim}{k})$. Integrating Eq. (30) numerically, we find that the absorption coefficient satisfies Eq. (2) to high accuracy. Indeed, if $\ell(\underset{\sim}{k})$ were independent of $\underset{\sim}{k}$ over the region of the surface integral, Eq. (30) would reduce to Eq. (1) exactly.

The auxiliary functions $F(\underset{\sim}{k})$ and $G(\underset{\sim}{k})$ are computed numerically as discussed in Ref. 26. The distribution functions computed from these auxiliary functions for $\underset{\sim}{k}$ in the [111] and [100] directions together with their equilibrium values are shown in Fig. 2. The dominant dip in the heavy-hole distribution function and corresponding peak in the light-hole distribution function is due to direct optical transitions. Additional dips in the heavy-hole distribution function occur because of the discrete energy of the optical phonons. The increase in the heavy-hole distribution compared to the equilibrium value at large values of k is due to scattering of the photoexcited holes in the light-hole band into the heavy-hole band.

C. Intensity Dependence of the Absorption Properties of p-Ge

The absorption coefficient is calculated numerically. In Fig. 3 the calculated result for λ=10.6μm and T=295°K is compared with the expression in Eq. (2). The value of I_s used in Eq. (2) was determined by fitting the calculated result for $\alpha(I,\omega)$. The numerical results could be fit to an accuracy of about 5% for intensities less than 25 times I_s. (This is the range of intensities which has been most frequently explored experimentally.) If only the first term in Eq. (22) is retained, the calculated $\alpha(I,\omega)$ has almost exactly the form of Eq. (2). The second term in Eq. (22) is smaller than the first and leads to the small deviations seen in Fig. 3.

Measurements of the saturable absorption in p-type Ge have been interpreted in terms of the inhomogeneously broadened two-level model which produces Eq. (2), and the values of $I_s(\omega)$ have been reported. In Fig. 4, we compare measured values of $I_s(\omega)$ at room temperature as a function of photon energy with our theoretical values. The theoretical values of $I_s(\omega)$ are determined by fitting the expression in Eq. (2) to the calculated results for $\alpha(I,\omega)$ for intensities between zero and 100 MW/cm^2. In the range of photon energies considered, $I_s(\omega)$ was found to increase monotonically with photon energy. There is good agreement between theory and experiment. There are no adjustable parameters included in the theory.

The calculated results shown in Fig. 4 were attained using the higher order approximation for $(f_h(\underset{\sim}{k}) - f_\ell(\underset{\sim}{k}))$. The results for the first order approximation are qualitatively similar to those of the more complete calculation; the numerical values of the two calculations differ by an approximately constant factor. At λ=10.6μm and T=295K, the more complete

calculation gives a value of I_s of 4.1 MW/cm^2, the first order calculation including acoustic phonon scattering gives a result of 5.8 MW/cm^2, and the first order calculation neglecting acoustic phonon scattering gives a result of 3.5 MW/cm^2. Thus, the first order calculation neglecting acoustic phonon scattering is within about 15% of the more complete calculation. This result is interesting because the first order calculation is much easier and less expensive to perform than the more complete calculation.

The increase in $I_s(\omega)$ with increasing ω is primarily due to the behavior of the scattering rates and the optical matrix elements. The relative contribution of the scattering rates and the optical matrix elements can be most easily seen in the first order calculation. At this level of approximation, $I_s(\omega)$ is given by a weighted average of $\ell(\underset{\sim}{k})$ (see Eq. (28)). The values of $\ell(\underset{\sim}{k})$ are proportional to ω^2, $T_2^{-1}(\underset{\sim}{k})$, $(T_h(\underset{\sim}{k}) + T_\ell(\underset{\sim}{k}))$, and $|P_{h\ell}(\underset{\sim}{k})|^{-2}$. For wavelengths near 10μm and room temperature, values for ω^2, $T_2^{-1}(\underset{\sim}{k})$, and $|P_{h\ell}(\underset{\sim}{k})|^2$ increase with increasing photon energy and $(T_h(\underset{\sim}{k}) + T_\ell(\underset{\sim}{k}))$ decreases. We find that for the wavelengths of interest, $\ell(\underset{\sim}{k})$ increases monotonically with increasing photon energy.

Since the usefulness of p-Ge as a saturable absorber in CO_2 laser systems is determined by its saturation characteristics, it is of interest to be able to control the saturation behavior. Since optical phonon scattering is the dominant relaxation mechanism, and the optical phonon occupation is temperature dependent, it is clear that $I_s(\omega)$ will depend on temperature. In Fig. 5 we present the results of a calculation of the temperature dependence of $I_s(\omega)$ in p-Ge for light with a wavelength of

10.6μm. $I_s(\omega)$ increases monotonically with temperature. This increase is due to the increased rate of phonon scattering at higher temperatures. Because of the rather strong dependence of $I_s(\omega)$ on temperature, it should be possible to tune the saturation behavior of p-Ge with temperature.

We now consider the polarization dependence of the saturation characteristics. The polarization dependence of the momentum matrix elements increases the anisotropy of the hole distribution in $\underset{\sim}{k}$-space. Since the excitation rates depend on the direction in $\underset{\sim}{k}$-space (primarily through the $\underset{\sim}{n}\cdot\underset{\sim}{p}$ matrix elements), the saturation of the resonantly-coupled states by state-filling will be much larger for some directions in k-space than for other directions for polarized light. Using the first-order approximation for the hole distribution, we numerically calculate $\alpha(I)$ for light polarized along the [100], [110], and [111] directions. Values of I_s for the different directions of polarization and for the case of unpolarized light are given in Table 1. The experimental results of Ref. 7 indicate no significant variation of I_s with crystal orientation, which is consistent with our calculations in consideration of the uncertainty in the reported data.

D. Hole-Ionized Impurity and Hole-Hole Scattering

For those temperatures and hole densities for which hole-impurity and hole-hole scattering is small compared to phonon scattering, the calculated I_s is independent of hole concentration. At room temperature, I_s has been found experimentally to be roughly independent of hole concentration for concentrations less than about 4×10^{15} cm^{-3}.[1,30] We now extend the range of doping concentrations for which the theory is valid by including the effects of hole-impurity and hole-hole scattering. We consider uncompensated samples of p-type germanium where the acceptors are all shallow and ionized at room temperature conditions.

The scattering rate for a hole with energy ε by singly ionized impurities is given by

$$V_I = \frac{\pi e^4}{K^2 \sqrt{2m^*}\, \varepsilon^{3/2}} N_I \left[\ell n(1+\beta^2) - \frac{\beta^2}{1+\beta^2} \right] , \tag{31a}$$

where

$$\beta^2 = \frac{2Km^* k_B T}{\pi N_I e^2 \hbar^2} , \tag{31b}$$

K is the low frequency dielectric constant, m^* is the free-carrier effective mass, k_B is the Boltzmann constant, and N_I is the total concentration of ionized impurities.[31]

Following Ref. 32, the rate of hole-hole scattering for a hole with energy ε is given by

$$V_{hh} = \frac{2\sqrt{2}\,\pi N_h e^4 \lambda}{K^2 \varepsilon^{3/2} \sqrt{m^*}} , \tag{32a}$$

where

$$\lambda = 1 + \ell n \left[\frac{\varepsilon}{2\hbar} \left(\frac{K m^*}{2\pi N_h e^2} \right)^{1/2} \right] . \tag{32b}$$

The calculation of the saturation intensity I_s at different impurity concentrations is performed using the first-order approximation to $(f_h(\underset{\sim}{k}) - f_\ell(\underset{\sim}{k}))$, where the calculation of scattering rates is modified to include hole-impurity and hole-hole scattering in addition to carrier-phonon scattering.[26] The inclusion of hole scattering by ionized impurities and other holes causes an increase in the scattering rate of the free holes and introduces a concentration dependence in the saturation intensity. The

result of increasing the scattering rates is that higher intensities are required to reduce the free-hole population in the heavy-hole band at the resonant region, since the excited holes can re-route at a faster rate.

The calculated values of I_s as a function of the doping density for p-Ge at room temperature are shown in Fig. 6.[34] Also shown are the measured values for the dependence of the saturation intensity on the doping density.[30]

The experimental values of I_s at 10.6μm indicate that the saturation intensity increased monotonically with increasing hole concentration for the Ge:Ga samples we studied. We note that the experimental values for I_s vs N_h are in fair agreement with theory, with the experimental values consistently larger than the calculated values by about 20%.

The calculated and measured values of I_s for p-Ge at 9.6μm show a weaker fractional dependence on the hole concentration than the values of I_s at 10.6μm. For light having a wavelength of 9.6μm, the direct transition between the heavy- and light-hole bands occurs at larger values in $\underset{\sim}{k}$-space, and thus, for larger heavy- and light-hole energies. Phonon scattering was calculated on the basis of the deformation potential model, where the scattering rates have a square root dependence on the energy of the hole carrier.[29] The scattering rates for a hole with energy ε due to ionized impurity and other hole carriers has approximately an $\varepsilon^{-3/2}$ dependence.[31-32] Consequently, the effect of increasing the hole energies in the resonant region in going from 10.6μm to 9.6μm radiation is to increase the effect of phonon scattering and to decrease the contribution of hole-impurity and hole-hole scattering. Since I_s is substantially independent

of the hole density in the region where hole-phonon scattering is dominant, we find a weaker fractional dependence of I_s on N_h at 9.6μm than at 10.6μm.

For lower temperature or higher doping density, the effect of scattering by ionized impurities and other free carriers can dominate the scattering. In this region, the theory predicts a strong dependence of the saturation intensity on the hole density. In Fig. 7, we present the calculated values of I_s as a function of the hole density in p-Ge for hole concentrations in the 10^{14}-10^{16} cm^{-3} range and T = 77 K. The two curves shown are for λ = 10.6μm (solid curve) and λ = 9.5μm (dashed curve) laser radiation.

For those hole states in the resonant region of the light-hole band, the scattering rate is determined by hole-phonon scattering, in which the emission of optical phonons makes the dominant contribution. The rate for emission of optical phonons is not strongly dependent on temperature for $k_BT < \hbar\omega_0$, where $\hbar\omega_0$ is the zone-center longitudinal optical phonon energy. Consequently, the scattering rate for hole carriers in the resonant region of the light-hole band is not very sensitive to temperature. On the other hand, optical phonon emission is not energetically allowed for most states in the resonant region of the heavy-hole band. For these hole energies ($<\hbar\omega_0$), the rate at which holes are scattered out of (and into) the resonant region of the heavy-hole band is determined by the interaction of the hole carriers with acoustical phonons, ionized impurities and other free carriers. Thus, the scattering rates for these states depend strongly on temperature, because of hole-acoustical phonon scattering, and strongly on the hole density, because of hole-ionized impurity and hole-hole scattering. For temperatures and hole densities in which the scattering of holes in the resonant

region of the heavy-hole band is determined by hole-acoustical phonon interactions, we find the saturation intensity to be independent of the hole density, and for cases in which the scattering is dominated by hole-impurity and hole-hole scattering, we find the saturation intensity to be approximately linear with the hole density.

Experimental measurements of the saturable absorption at 77K[35] have been made, but the data was taken over a relatively small range of intensities, and the results were interpreted in terms of a homogeneously broadened two-level model, rather than an inhomogeneously broadened model, which we believe to be more correct. These measured values of I_s at 77K show a monotonic increase with increasing hole density, in qualitative agreement with our calculation. The experimental values for I_s at 9.5μm radiation and 77K are a little larger than the corresponding values at 10.6μm for the hole concentrations investigated, which is in agreement with our calculation.

E. Intensity Dependence of the Dispersive Properties of p-Ge

There is also an intensity dependence in the real part of the dielectric constant associated with the saturation of the intervalence-band transitions. These laser-induced changes in the real part of the dielectric constant alter the dispersive properties of the media and thus can modify the spatial and temporal behavior of the laser pulse. Since the laser pulse shape is important in many applications of CO_2 laser systems, one needs to understand the changes in the dispersive properties induced by the high-intensity beam. An intensity dependence of the real part of the dielectric constant can be exploited for phase conjugation. Phase conjugation

in the CO_2 laser frequency regime using Ge as the nonlinear medium is of current interest.[36]

As previously discussed, for light with a wavelength near 10μm, the dominant absorption mechanism in p-Ge is due to direct free-hole transitions between the heavy- and light-hole bands. These resonant transitions also contribute to the index of refraction. At high light intensities, the absorption due to these transitions saturates owing to a modification of the free-hole distribution function. This intensity dependent modification of the distribution function also changes the contribution of the free-hole transitions to the index of refraction.[37] In addition to the intensity dependence of the index of refraction from the resonant intervalence-band transitions, there is an intrinsic contribution due to a field modification of the virtual electron-hole pair creation processes.[38] The magnitude of the resonant intervalence-band contribution depends on the doping level. Both contributions lead to an increase in the index of refraction with increasing intensity. We find that the magnitude of the resonant intervalence-band contribution to the first order modification of the index of refraction equals measured values[39] of the intrinsic contribution at a doping level of about 3×10^{15} cm^{-3}. In this section we present a calculation of the resonant intervalence-band contribution to the intensity dependence of the real part of the dielectric constant in p-Ge for light with a wavelength of 10.6μm.

Using the equation for the current density owing to the intervalence-band transitions, the real part of the susceptibility is given by Eq. (15). Here, the intensity dependence is contained in the distribution functions $f_h(\underset{\sim}{k})$ and $f_\ell(\underset{\sim}{k})$. At low light intensities, $\underset{\approx}{\chi}$ is a scalar because of the

cubic symmetry of Ge. For high intensity polarized light, the cubic symmetry is reduced and $\underset{\approx}{\chi}$ is described by a second-rank tensor.

The function $\beta(\underset{\sim}{k})$ is defined as

$$\beta(\underset{\sim}{k}) = \frac{2\pi^2}{\sqrt{\epsilon_\infty} m^2 \omega c} \frac{e^2 I}{\hbar\omega} \sum_{\substack{b \text{ in } h \\ c \text{ in } \ell}} |\underset{\sim}{\eta}\cdot\underset{\sim}{P}_{bc}(\underset{\sim}{k})|^2 \frac{1/(\pi\hbar T_2(\underset{\sim}{k}))}{(\Omega(\underset{\sim}{k})-\omega)^2 + (1/T_2(\underset{\sim}{k}))^2}, \quad (33)$$

where I is the light intensity, $\underset{\sim}{\eta}$ is the polarization of the light, and ϵ_∞ is the intrinsic material dielectric constant. The definition of $\beta(\underset{\sim}{k})$ in Eq. (33) differs slightly from that of Eq. (19c) because we have not averaged over polarizations. As a result, the distribution function, which we calculate here, depends on the polarization of the light and does not have cubic symmetry. The calculational approach, however, is the same as previously discussed. Some of the results we present here are for unpolarized light. In this case we average the vector potential over all angles.

We calculate the intensity dependence of the real part of the susceptibility due to resonant intervalence-band transitions. The results quoted in this section for $\Delta n(I)$ and $\Delta\epsilon(I)$ refer to only this contribution. There is an additional intrinsic contribution which is to be added to our results. There may also be heating effects in any particular experiment. One can determine the contribution from thermal effects using measured values of $\frac{dn}{dT}$. The thermal effects can be eliminated by using sufficiently short laser pulses.

The real part of the susceptibility is calculated numerically for λ = 10.6μm and T=300K. We consider the case of lightly doped samples, where the relaxation is dominated by hole-phonon scattering. Using Eq. (15) we

can calculate $\underset{\sim}{\chi}'(I)$ for any polarization of the light. Explicit values of $\underset{\sim}{\chi}'(I)$ are calculated for the case of unpolarized light, and for the polarization along the [100] and [110] directions.

For unpolarized light the second-rank ransor $\underset{\sim}{\chi}'$ becomes a scalar, since any orientational dependence has been averaged out when we averaged over the directions of the vector potential.[39] We find that values of $\chi'(I)$ increase monotonically with increasing intensity due to changes in the distribution of free-holes. Room temperature values of $\chi'(I)/\chi'(I=0)$ are given in Fig. 8 for intensities between 0 and 60 MW/cm^2. At low intensities $(\chi'(I=0)/N_h)$ is equal to 1.4×10^{-20} cm^3 ($\chi'(I=0)$ is proportional to N_h).

Laser-induced changes in $\chi'(\omega)$ can be measured by observing changes in the real part of the dielectric constant, which determine the dispersive properties of the medium. The real part of the complex dielectric constant $\underset{\sim}{\epsilon}$ is given by

$$\underset{\sim}{\epsilon} = \underset{\sim}{\epsilon}_\infty + 4\pi\underset{\sim}{\chi}' \quad . \tag{34}$$

Values for the change in ϵ can be measured by studying threshold values for self-focusing (for $\frac{d\epsilon}{dI}$ positive). In Fig. 9 we show the calculated results for $\Delta\epsilon$ and the corresponding results for the change in the index of refraction, Δn, for unpolarized light with a wavelength of 10.6μm at 300K. The changes in ϵ and in n are directly proportional to the free-hole density. We find that ϵ and n are increasing functions of intensity.

The intrinsic contribution to dn/dI in Ge has recently been measured to be about 1×10^{-6} cm^2/MW.[40] The resonant intervalence-band contribution to dn/dI is intensity dependent. In the lower intensity region the change

in n is linear in I. For hole densities greater than about 3×10^{15} cm^{-3}, the resonant intervalence-band contribution is larger than the intrinsic contribution at the lower intensities.

In Fig. 10 we show the calculated results for the diagonal components of $(\Delta\underset{\sim}{\epsilon}/N_h)$ as a function of intensity for light polarized in the [100] and [110] directions. For the case of [100] polarization the coordinate axes are chosen to be the crystal axis of the sample. In this coordinate system, the off-diagonal components of $\underset{\sim}{\epsilon}$ vanish as at low intensities. There is a small difference in the values of ϵ_{xx} and ϵ_{zz} ($\epsilon_{yy} = \epsilon_{zz}$ in this case) due to the polarization dependence of $\beta(\underset{\sim}{k})$ in determining the distribution of holes in the heavy- and light-hole bands. For the case of [110] polarization, the X axis is taken in the [110] direction, the Y axis in the [1$\bar{1}$0] direction and the Z axis in the [001] direction. In this coordinate system $\underset{\sim}{\epsilon}$ is diagonal. There is a small difference in the values of the three diagonal components. Overall, from Fig. 10, we see that the effects of polarization on $\Delta\underset{\sim}{\epsilon}$ are rather small.

The change in ϵ with intensity is due to the change in the distribution of hole states. We find that the diagonal components of $\underset{\sim}{\chi}'$ increase monotonically with increasing intensity. From Eq. (15), we see that values of $\underset{\sim}{k}$ for which $\Omega(\underset{\sim}{k}) > \omega$ lead to a positive contribution to $\underset{\sim}{\chi}'$ and thus to ϵ, whereas values of $\underset{\sim}{k}$ for which $\Omega(\underset{\sim}{k}) < \omega$ lead to a negative contribution to $\underset{\sim}{\chi}'$. Under optical excitation, the holes occupy higher energy states than in equilibrium. Thus, for the higher energy states with $\Omega(\underset{\sim}{k}) > \omega$ the difference in occupation probabilities $(f_h(\underset{\sim}{k})-f_\ell(\underset{\sim}{k}))$ is on the average enhanced compared to the equilibrium value, whereas for states with $\Omega(\underset{\sim}{k}) < \omega$

the difference in occupation probabilities is decreased compared to the equilibrium value. Hence, the positive contributions to $\underset{\approx}{\epsilon}$ from terms with $\Omega(\underset{\sim}{k}) > \omega$ is increased by illumination, and the magnitude of the negative contribution to $\underset{\approx}{\epsilon}$ from terms with $\Omega(\underset{\sim}{k}) < \omega$ is decreased by illumination. Consequently, $\underset{\approx}{\epsilon}$ increases monotonically with increasing intensity. As the intensity increases, the increase in $\underset{\approx}{\epsilon}$ is slower than linear due to saturation of the intervalence-band transitions.

For two laser beams incident on a Ge sample, as in a pump-probe experiment, the light intensity is modulated in space and time due to the interference of the two beams. Since the index of refraction is a function of intensity, it is modulated by the oscillating intensity. The periodic variation of the index of refraction leads to a coupling of the two beams. This coupling can influence the transmission of the beams, which may be important in the analysis of a pump-probe experiment.

F. Saturation Behavior of Other Groups IV and III-VI Semiconductors

In this section, we present the results for the saturation characteristics for two different types of materials: semiconductors with a spin-orbit splitting large compared to the photon energy of the CO_2 laser (as is the case for Ge), and semiconductors with a small spin-orbit splitting compared to the photon energy (as Si). In the first case the split-off hole band is not involved in the optical excitation process. For materials with small spin-orbit splittings, the theory must be modified to include transitions between the heavy- and light-hole bands, the light- and split-off hole bands, and the heavy- and split-off hole bands.

We first present a calculation describing the saturation behavior of materials with spin-orbit splittings large compared to the energy of the incident radiation. Thus, the split-off band is not involved in the optical transition and can be ignored. Some of the materials with large spin-orbit splitting include p-type Ge, GaAs, GaSb, AlSb, InAs, and AlAs. Results for p-Ge have already been presented. In addition to Ge, saturable absorption has been observed in p-type GaAs.[1] The measurements were made over a smaller intensity range than for Ge and the results were interpreted in terms of a homogeneously broadened two-level model (rather than the inhomogeneously broadened two-level model which we believe would have been more correct). A saturation intensity of 20 MW/cm^2 was reported. We are not aware of any experimental measurements for p-type GaSb, AlSb, AlAs, or InAs; however, due to the similarities with p-Ge and p-GaAs, we also expect the absorption in these materials to saturate.

In order to limit the numerical expense involved in the calculation, we use the first-order calculation for the distribution of hole states in the resonant region of the heavy- and light-hole bands. The first-order calculation which neglects acoustical phonon scattering produces results which are within 15% of the more complete calculation of the saturation intensity for p-Ge and p-GaAs (for which the more complete calculation was also performed).

The calculated values of the saturation intensity at room temperature and a photon energy of 117 meV (λ=10.6μm) for the materials considered are given in Table II. We find that the dependence of I_s on temperature and incident photon energy are qualitatively similar to that for Ge. This

smooth behavior of I_s near room temperature and over the CO_2 laser spectrum allows one to characterize the saturation behavior by I_s (at E_0 = 117 meV and T_0 = 295°K) and the slopes $(\partial I_s/\partial E)_{E_0}$ and $(\partial I_s/\partial T)_{T_0}$. Values of the derivative of I_s with respect to photon energy and temperature are given in Table II. For completeness, we include the results for Ge.

From Table II, we note a large variation of the saturation intensity for the materials. This large variation of the saturation intensity I_s is due to two factors: (1) the deformation potential parameters, and (2) the valence band structures. A discussion of the systematic dependence of I_s on the material parameters is presented in Ref. 41.

In the previous discussion we presented the results of a theory describing the saturation of the intervalence-band transitions for most of the Group IV and III-V semiconductors for which the spin-orbit splitting was large compared to the energy of the incident photon. However, for materials such as Si, where the spin-orbit splitting is less than the photon energy, one must generalize the theory to include transitions from the heavy-hole to light-hole band, the heavy-hole to split-off band, and the light-hole to split-off band. We now consider the saturation properties of Si and InP, GaP, and AlP, which also have small spin-orbit splittings.

The absorption coefficient for these materials in the 9-11μm region can be written as

$$\alpha = \alpha_p + \alpha_{h\to\ell} + \alpha_{h\to s} + \alpha_{\ell\to s} , \tag{35}$$

where α_p is the residual absorption due to phonons, $\alpha_{h\to\ell}(\alpha_{h\to s})$ is the absorption coefficient due to direct heavy-hole to light-hole (split-off)

band transitions, and $\alpha_{\ell \to s}$ is the absorption coefficient due to direct light-hole to split-off band transitions. The effect of lattice absorption depends on the wavelength of the light and the temperature of the material. Lattice absorption at 9.6μm requires the cooperation of at least three phonons to conserve energy and is therefore small. In Si two-phonon absorption is energetically possible for a wavelength of 10.6μm. The absorption of light by the creation of phonons can be included in a straightforward way, since this process is nonsaturable and just adds a residual absorption term. Here, we consider the saturable absorption due to the direct intervalence-band transitions.

In Eq. (18) we have given an expression to determine the decrease in the absorption coefficient with increasing intensity when only the heavy-hole and light-hole bands were involved in the optical transition. Analogous expressions can be written for direct transitions between the heavy-hole and split-off bands and between the light-hole and split-off bands. In order to numerically integrate the expressions for $\alpha_{h \to \ell}$, $\alpha_{h \to s}$ and $\alpha_{\ell \to s}$, we must calculate the steady-state distribution functions in each band as a function of intensity for each wavevector $\underset{\sim}{k}$. If we assume that the three direct optical transitions are uncoupled, then the absorption due to each resonant transition can be independently analyzed. That is, we can determine the saturation characteristics for $\alpha_{h \to \ell}$, $\alpha_{h \to s}$, and $\alpha_{\ell \to s}$ independently using Eq. (18) for $\alpha_{h \to \ell}$ and the analogous expression for $\alpha_{h \to s}$ and $\alpha_{\ell \to s}$. Here, we assume that the modification in the distribution function of free-holes due to one particular resonant transition between two valence bands in $\underset{\sim}{k}$-space does not strongly affect the distribution of free-holes in the

resonant regions for the other transitions. A more complete discussion of the calculational approach is presented in Ref. 42.

We numerically integrate the expressions for $\alpha_{h\to\ell}$, $\alpha_{h\to s}$, and $\alpha_{\ell\to s}$, and find that the intensity dependence of the absorption due to each direct transition can be fit to high accuracy by the functional form

$$\alpha_i(I) = \frac{\alpha_{oi}}{\sqrt{1 + I/(I_s)_i}} , \tag{36}$$

where α_{oi} is the low-intensity absorption coefficient and $(I_s)_i$ is the saturation intensity of the i^{th} intervalence-band transition. Values of $(I_s)_{h\ell}$, $(I_s)_{hs}$, and $(I_s)_{\ell s}$ at λ=9.6μm and T=295K are given in Table III for the materials considered. For intensities low enough that the square root in Eq. (36) can be power series expanded, one has

$$\frac{1}{I_s} = \frac{1}{\alpha_o} \sum_j \frac{\alpha_{oj}}{(I_s)_j} \tag{37}$$

The values of α_{oj}/α_o for each of the three resonant transitions are listed in Table IV. We have taken I_s to fit the result for the sum of the three processes for intensities up to 100 MW/cm^2. We find the saturation intensity to have a smooth behavior near room temperature and λ=9.6μm (E_o=129.8 meV). This allows one to describe the saturation near room temperature and near E_o by giving the values of I_s (at E_o=129.8 meV and T_o=295K) and the slopes $\left.\frac{\partial I_s}{\partial E}\right|_{E_o}$ and $\left.\frac{\partial I_s}{\partial T}\right|_{T_o}$. The values of I_s, $\left.\frac{\partial I_s}{\partial E}\right|_{E_o}$, and $\left.\frac{\partial I_s}{\partial T}\right|_{T_o}$ are given in Table III.

The measured values of I_s for p-Si at 10.6μm and 9.6μm are shown in Table V.[30] We see that I_s is considerably larger for Si than Ge, which is primarily due to the larger hole-phonon scattering rates and the smaller excitation rates in Si. In addition, lattice absorption is much larger in Si than Ge for the wavelengths of interest. This larger nonsaturable absorption must be included in the numerical analysis and creates a larger uncertainty in the values for the saturation intensities. Absorption saturation in p-Si has previously been observed;[1] however, the range of intensities considered was smaller and the data was interpreted in terms of a homogeneously broadened two-level model with $I_s \gtrsim 50$ MW/cm^2. We find the data to be better approximated by an inhomogeneously broadened two-level model, where the deviation between the two functional forms for the intensity dependence of the absorption coefficient becomes apparent for $I \gtrsim I_s$.

Values of the saturation intensities in the materials with small spin-orbit splittings are generally larger than the values in materials with larger spin-orbit splittings such as Ge and GaAs. This difference is primarily due to the relatively slow splitting between the valence bands with increasing $|k|$. This leads to larger scattering rates for the states involved in the transitions and thus large values for the saturation intensity. The deformation potentials and the values of the optical matrix elements also play an important role in determining the value of the saturation intensity.

G. Intensity Dependence of the Conductivity

Since the absorption of light modifies the distribution of free holes, one expects a change in the sample conductivity upon illumination. Because the density of states in the heavy-hole band is much greater than that in the light-hole band, the photoexcited holes primarily scatter into high energy states in the heavy-hole band. Thus, the dominant change in the distribution function is an increase in the average energy of occupied states in this band. For temperatures and doping levels for which phonon scattering dominates the momentum relaxation, the conductivity decreases upon illumination because the rate of phonon scattering increases with increasing hole energy. For lower temperatures or higher doping levels where ionized impurity scattering dominates the momentum relaxation, the conductivity increases with illumination because ionized impurity scattering decreases with increasing hole energy. These photoconductive effects have been observed experimentally[43-47] and have been shown to influence the performance of p-Ge photon drag detectors.[48-50] In this section we present the results of a calculation of the photoconductive response of p-Ge upon illumination by 10.6μm light as a function of doping level, temperature and intensity.

Previous calculations of this photoconductive response have been based on idealized models in which the Ge valence bands have been replaced by a set of discrete energy levels, each characterized by an effective mobility.[46-47] In addition, the effects of saturation of the intervalence-band transitions

were not included, so that the results could only be applied for low intensities. Using the calculated hole distribution, we determine the photoconductive response in both the linear and nonlinear regimes. We find reasonable agreement with experimental results.

The intensity dependence of the conductivity is given by the following expression[51] for an electric field in the z-direction [52]

$$\sigma = 2\left(\frac{1}{2\pi}\right)^3 \frac{e^2}{\hbar} N_h \int d^3k\, f_h^o(\underset{\sim}{k}) \frac{\partial}{\partial k_z} \left[\tau_h\, v_{hz} \left[\frac{1 + \beta\tau_\ell \left(\frac{\partial f_\ell^o/\partial k_z}{\partial f_h^o/\partial k_z} + 1 \right)}{1 + \beta(\tau_h + \tau_\ell)} \right] \right] \tag{38}$$

$$+ 2\left(\frac{1}{2\pi}\right)^3 \frac{e^2}{\hbar} N_h \int d^3k\, f_\ell^o(\underset{\sim}{k}) \frac{\partial}{\partial k_z} \left[\tau_\ell\, v_{\ell z} \left[\frac{1 + \beta\tau_h \left(\frac{\partial f_h^o/\partial k_z}{\partial f_\ell^o/\partial k_z} + 1 \right)}{1 + \beta(\tau_h + \tau_\ell)} \right] \right].$$

Here, N_h is the hole density, $f_h^o(\underset{\sim}{k})$ is the distribution function in the heavy-hole band subject to the laser light but with no external electric field, v_{bz} is the group velocity of the carrier in band b for $\underset{\sim}{k}$ in the z-direction, $\tau_h(\underset{\sim}{k})$ $[\tau_\ell(\underset{\sim}{k})]$ is the momentum relaxation time due to scattering of holes with wavevector $\underset{\sim}{k}$ in the heavy- [light-] hole band by phonons and ionized impurities,[53] and $\beta(\underset{\sim}{k})$ is defined by Eq. (19c) and describes the excitation of the hole carrier by the high-intensity light.

In Fig. 11 we show the calculated results for $(-\Delta\sigma/\sigma I)$ vs N_h in the low intensity regime where $\Delta\sigma$ is proportional to I. The calculation was

done for room temperature Ge illuminated by λ=10.6μm light. The conductivity has decreased upon illumination. The primary effect of illumination on the hole distribution is to increase the population of high energy holes in the heavy-hole band. At room temperature and for the doping levels considered here, hole-phonon scattering limits the conductivity. Since hole-phonon scattering rates increase with increasing hole energy, the conductivity decreases with illumination. For hole densities between about 10^{14}-4×10^{15} cm^{-3}, $(-\Delta\sigma/\sigma I)$ is essentially independent of N_h. In this region hole-impurity scattering makes a negligible contribution to the scattering rates. For hole densities greater than about 4×10^{15} cm^{-3}, $(-\Delta\sigma/\sigma I)$ decreases with increasing N_h. In this regime, hole-impurity scattering begins to play a role in limiting the mobility. Hole-impurity scattering rates decrease with increasing hole energy. As a result the fractional increase in the total scattering rate (hole-phonon plus hole-impurity) does not increase as much with increasing hole energy in the more heavily doped samples. In addition, the hole distribution is not as strongly modified by illumination of a given intensity in the more heavily doped samples due to the increase in hole-ionized impurity and hole-hole scattering which tends to maintain the equilibrium distribution. For hole densities less than about 10^{14} cm^{-3}, $(-\Delta\sigma/\sigma I)$ decreases with decreasing hole density. This decrease is due to the increased contribution to the conductivity of free electrons whose distribution is not strongly modified by illumination. (In Ge at 300K, the intrinsic density is about 2×10^{13} cm^{-3}). Also shown in Fig. 11 are the available experimental results. There is considerable variation in the results reported by the various authors. Our calculated

values are in fairly good agreement with the data of Gibson et al.[44] and those of Maggs.[48]

In Fig. 12 we present our results for the temperature dependence of $(\Delta\sigma/\sigma I)$ for a hole concentration of 2×10^{16} cm^{-3}. We choose this value for the hole density since measurements exist and the change in the conductivity was observed to change sign over the temperature range that was reported.[45] We note that the change in the conductivity is negative for temperatures greater than about 100K and becomes positive for lower temperatures. In the higher temperature regime, hole-phonon scattering plays a greater role in determining the momentum relaxation than hole-impurity scattering and thus the conductivity decreases upon illumination. In the lower temperature regime, hole-ionized impurity scattering dominates the momentum relaxation and the conductivity increases upon illumination. The temperature at which $\Delta\sigma$ changes sign depends on the doping level. At lower doping levels, the sign change in $\Delta\sigma$ occurs at lower temperatures. This effect has been observed experimentally.[45] In addition, we note that the magnitude of $|\Delta\sigma/\sigma I|$ decreases as the temperature increases from about 150K. This decrease is due to a decrease in the rate of phonon scattering at the lower temperatures. As a result of the decreased scattering rate, the hole distribution is more strongly modified by a given light intensity at the lower temperatures. The experimental results of Refs. 43 and 45 are included in Fig. 12. The data show the same qualitative features as the calculated results. The calculation gives somewhat larger values for $|\Delta\sigma/\sigma I|$ than were observed in Ref. 45. From Fig. 11 we note that the room temperature results reported in Ref. 45 are systematically smaller than those of Refs. 44 and 48.

Because of interest in the performance of photon-drag detectors at high laser intensities,[48-50] we also examine the photoconductive response of p-Ge at intensities for which saturation effects start to become important. In Fig. 13 we present the results of our calculation of $(-\Delta\sigma/\sigma I)$ as a function of N_h for different light intensities. The curve for 0.05 MW/cm^2 is in the linear regime. At the higher intensities, $(-\Delta\sigma/\sigma)$ increases with increasing intensity at a rate which is slower than linear. The nonlinear behavior is due to saturation of the intervalence-band transitions. The shape of the curves at any given intensity are similar. We are not aware of any direct measurements of $(\Delta\sigma/\sigma I)$ at these high intensities; however, both saturable absorption[1,7-9] and nonlinear photon-drag voltages[48,50] have been seen experimentally. It is possible that this saturation effect could account for some of the variation in the experimental results shown in Fig. 11.

III. NONLINEAR ABSORPTION IN n-TYPE GERMANIUM

In this section we present a quantitative investigation of the formation of a laser-induced plasma in n-type or intrinsic germanium by absorption of 10μm light. For this spectral region the material is relatively transparent at low intensity and is often used as a window material for CO_2 lasers. Germanium has also been used as phase-conjugate mirrors at 10.6μm via degenerate four-wave mixing.[36] Recently, amplified reflection at 10.6μm has been observed via degenerate four-wave mixing in an optically induced free-carrier plasma in germanium.[10]

Experimentally, it is observed that n-germanium exhibits an increase in the absorption coefficient with increasing intensity.[2-3,9] This

laser-induced "opacity" has a decay time of about 100μsec, which is on the order of the electron-hole recombination time in germanium. The increase in the absorption coefficient at high intensities has been shown through photoconductivity measurements[2-3] to result from the formation of electron-hole pairs and subsequent free carrier absorption. Two mechanisms have been proposed to describe the generation of the electron-hole pairs by the below gap light. In one model,[3] multiphoton absorption is invoked. For absorption at the direct gap at least seven photons must be involved, absorption at the indirect gap requires six photons (and one phonon) at 10.6μm or five photons (and one phonon) at 9.6μm. In the second model, the excess electron-hole pairs are generated by impact ionization. That is, the high intensity light increases the average energy of the conduction electrons initially present (n-type material). When an electron (or hole) has an energy relative to its band minimum in excess of the band gap energy, the hot carrier is able to lose energy by creating an electron-hole pair. Here we consider the second model (which we believe to be the more likely). To describe the process, we set up and solve rate equations to determine the hot-electron distribution as a function of laser intensity. We then find the rate at which electron-hole pairs are generated. The absorption produced by the excess carriers is then found. We compare our results with the experimental results of Ref. 10 and of Refs. 2 and 3. The experimental results reported by these two groups are in disagreement. Our results are in good agreement with the results reported in Ref. 10 but cannot account for the much lower threshold intensities for electron-hole

pair generation which are reported in Refs. 2 and 3. There are no fitting parameters in our calculation. If the threshold intensities reported in Ref. 10 prove to be correct, our calculation strongly suggests that impact ionization is indeed the mechanism responsible for the observed generation of excess electron-hole pairs by high intensity CO_2 radiation in Ge. On the other hand, if the much lower threshold intensities reported in Refs. 2 and 3 prove to be correct, our calculation strongly suggests that impact ionization cannot be invoked to explain the electron-hole pair generation.

We consider n-type and intrinsic Ge. Thus, the initial electron density is greater than or equal to the initial hole density. We assume that impact ionization is larger for electrons than for holes and only include electron-hole pair generation via electron impact ionization in our calculations. There are two reasons for this assumption: the hole-optical phonon coupling is somewhat stronger than the electron-optical phonon coupling (thus the energy relaxation for the holes is somewhat stronger than for electrons) and the intravalence-band optical absorption cross sections are somewhat smaller than the intraconduction-band cross sections (thus the electrons are more easily optically excited). Note that the intervalence-band cross sections for free holes are large, but to excite a hole to an energy for which impact ionization is possible would require that many photons be absorbed. Direct intervalence-band absorption can only contribute at the low energy part of the hole distribution where the heavy and light hole bands are in resonance (that is, only the "first" photon will be absorbed via an intervalence-band process and the "other" photons must be absorbed via the intravalence-band process). If the hole impact ionization

were comparable to electron impact ionization our results would be only slightly modified, even for undoped material, because the impact ionization rates are a very strong function of intensity. Thus, if the electron-hole pair generation rates as a function of intensity were (say) doubled, the intensity required to produce a fixed generation rate would be only slightly modified. Of course, for n-type material there are initially few holes and the hole impact ionization process would have to significantly exceed the electron process to invalidate our procedure. In p-type material, impact ionization by holes may dominate (at least initially) because there are very few electrons present. Thus, we expect that the threshold intensity for electron-hole pair formation in p-type material should be somewhat larger than in n-type material.

A. Calculational Approach

Simplified rate-equation models have previously been presented in which the conduction band is divided into a discrete set of energy levels with an energy separation of the photon energy[11] or the longitudinal optical phonon energy.[54] These calculations have been applied to studying carrier multiplication in InSb, $Hg_{.77}Cd_{0.23}Te$ and InAs by 10.6μm light pulses. For these materials the relaxation of the energetic electrons is largely determined by polar optical phonon scattering, while for germanium, nonpolar optical phonon scattering dominates the energy relaxation of the energetic carriers. The rate equations to be solved for the distribution of free electrons have the following form

$$\frac{\partial f_{c\underset{\sim}{k}}}{\partial t} = \left.\frac{\partial f_{c\underset{\sim}{k}}}{\partial t}\right|_{\text{absorption}} - \sum_{c'\underset{\sim}{k}'} \left[R_{c\underset{\sim}{k}\rightarrow c'\underset{\sim}{k}'} \left(f_{c\underset{\sim}{k}} - f^{e}_{c\underset{\sim}{k}}\right)\right] \tag{39}$$

$$+ \sum_{c'\underset{\sim}{k}'} \left[R_{c'\underset{\sim}{k}'\rightarrow c\underset{\sim}{k}} \left(f_{c'\underset{\sim}{k}'} - f^{e}_{c'\underset{\sim}{k}'}\right)\right] \quad ,$$

where $f_{c\underset{\sim}{k}}$ is the one-electron occupation probability for a state with wavevector $\underset{\sim}{k}$ in band c, $f^{e}_{c\underset{\sim}{k}}$ is the thermal equilibrium value for the distribution $f_{c\underset{\sim}{k}}$, and $R_{c\underset{\sim}{k}\rightarrow c'\underset{\sim}{k}'}$ is the rate at which an electron with wavevector $\underset{\sim}{k}$ in band c is scattering into a state with wavevector $\underset{\sim}{k}'$ in band c'.

Recombination and impact ionization are slow compared to the electron-phonon scattering rates and these processes are not included in Eq. (39). Thus, Eq. (39) is used to determine the electron energy distribution for a fixed number of electrons. This energy distribution is then used to find the impact ionization generation rate. This generation rate is used to find the density of carriers as a function of time for a given optical pulse shape. The recombination rates are very slow (lifetimes on the order of 100 μsec, while the laser pulse we consider is a few tens of nsec or less) and can be ignored. For intensities near the threshold for plasma generation, the intraband scattering rates for the highest energy electron states which are occupied with reasonable probability are fast compared with the impact ionization rates. Thus, our procedure should be reasonable for these intensities. At very high electron energies ($\varepsilon_{e\ell} \gtrsim 1.6$ eV), the impact ionization rates become comparable to the intraband scattering rates we consider and our approach breaks down. However, these very high energy

states are only reached with reasonable probability for intensities considerably larger than the threshold intensity.

For 10μm light the dominant absorption mechanism in n-type germanium is free carrier absorption, where an electron absorbs a photon and is excited to a state in the same band. The cross section for this process is smaller than that for intervalence-band free hole transitions, since in the case of free electron absorption the conservation of energy and crystal momentum cannot both be satisfied without the interaction of a third particle such as a phonon or impurity. In a free-electron approximation, one can derive expressions for the cross section by perturbation methods.[55] The results of these calculations indicate that impurity density plays an important role in determining the cross section.

At low light intensity (linear regime), the free electrons occupy states near the conduction band mimima where the bands can be described by effective mass theory. However, in this problem we are interested in excitation rates for electrons which are highly energetic with energies as high as 2-3 times the bandgap. We assume that the excitation rates depend only on the density of final states to which the electrons can be excited by the absorption of a photon. Thus, the excitation rates depend on the energy of the carrier and increase as the density of final states increases. The constant of proportionality in the excitation rates is determined by requiring that at low light intensities, the calculated value for the cross section agree with the experimental measurements. Thus, the term in Eq. (39), which describes the rate of change of the distribution due to absorption, connects a state with energy ε to the energy surfaces $\varepsilon + \hbar\omega$, where $\hbar\omega$ is the photon energy.

The state with energy ε is depleted by one-photon transitions which excite the electron to energy $\varepsilon + \hbar\omega$, and the state is fed by one-photon transitions from states with energy $\varepsilon - \hbar\omega$. Only one-photon transitions are included in the analysis. Thus, in the calculation, the hot electrons which can undergo impact ionization pair-producing events are generated by successive one-photon transitions.

In order to calculate the occupation probabilities, we must also know the free-electron scattering rates. We consider the region of temperature and impurity density for which the scattering is dominated by lattice scattering. The optical phonon dispersion curve is relatively flat, and we take the optical phonon energy to be discrete with an energy of 37 meV. We consider the scattering of electrons from acoustical phonons to be an elastic process. This approximation is valid for the scattering of electrons from acoustical phonons with small q, but does not account for the energy relaxation of energetic electrons associated with large q electron-acoustical phonon interactions. For electron energies less than the band gap, the rate of energy loss is dominated by optical mode scattering; however, for larger energies, this approximation somewhat underestimates the rate of energy relaxation of the hot electrons by the emission of phonons. Making these assumptions regarding lattice scattering events, the states with energy ε in Eq. (39) directly couple to only the surfaces in $\underset{\sim}{k}$-space with energy ε and $\varepsilon \pm \hbar\omega_0$ by lattice scattering events, where $\hbar\omega_0$ is the optical phonon energy. We describe the scattering due to the combined longitudinal and transverse nonpolar optical phonons by an energy-dependent relaxation time[56]

$$1/\tau_{NPO} = 1/\tau_{AC} \left(\frac{\hbar\omega_0}{K_B T}\right)\left(1/2 \frac{\Xi_{iop}^2}{\Xi_1^2}\right) \left[N_q \left(1 + \frac{\hbar\omega_0}{\varepsilon}\right)^{1/2} + (N_q + 1)\left(1 - \frac{\hbar\omega_0}{\varepsilon}\right)^{1/2}\right] . \tag{40}$$

Here, $1/\tau_{AC}$ is the scattering rate due to the combined longitudinal and traverse acoustical phonons given by[57]

$$1/\tau_{AC} = \frac{2^{1/2}}{\pi} \left(\frac{}{\Xi_1}\right)^2 \frac{(m_t^2 m_\ell)^{1/2} k_B T}{\hbar^4 \rho U_\ell^2} \varepsilon^{1/2} , \tag{41}$$

where $\Xi_1^2 = 0.75\ \Xi_d^2[1.31 + 1.61 \Xi_u/\Xi_d + 1.01\ (\Xi_u/\Xi_d)^2]$. (42)

In Eq. (41) m_t (m_ℓ) is the transverse (longitudinal) effective mass, ρ is the crystal density, U_ℓ is the longitudinal sound velocity, and Ξ_u and Ξ_d are the deformation potential constants as defined by Herring.[58] The quantity τ_{AC} (τ_{NPO}) is the mean free time for a carrier to be scattered out of a state $\epsilon(\underset{\sim}{k})$ by interaction with an acoustical (optical) phonon. Since the matrix elements are independent of the directions of $\underset{\sim}{k}$ and $\underset{\sim}{k}'$ ($= \underset{\sim}{k} + \underset{\sim}{q}$), τ_{AC} and τ_{NPO} are also equal to the relaxation time for this type of scattering given a perturbation which creates a small disturbance from equilibrium. The numerical value for the constants appearing in the scattering rates are shown in Table VI. The value of $(\Xi_{iop}/\Xi_1)^2$ was chosen to be 0.4[59] so the experimentally observed temperature dependence of the mobility could be duplicated without invoking additional scattering

mechanisms. Following Conwell,[59] we determine $\underline{\underline{\Xi}}_1$ using the measured values of the interaction constant D for nonpolar optical modes and the relation

$$D^2 U_\ell^2 / \underline{\underline{\Xi}}_1^2 \ \omega_0^2 = 0.4 \ . \tag{43}$$

The interaction constant D can be determined from high field transport measurements. From the magnitude of the saturation drift velocity[60] one obtains 5×10^8 eV/cm and from the temperature dependence of the saturation drift velocity[61] one obtains 7×10^8 eV/cm. We take an average of these two results $D = 6 \times 10^8$ cm/sec, which gives $\underline{\underline{\Xi}}_1 = 9.1$ eV.

Both the phonon scattering and photon absorption processes tend to randomize the crystal momentum of the final state, although energy conservation still holds in the interactions. As a result, a detailed calculation of $\varepsilon(\underset{\sim}{k})$ is not necessary since one only needs information about the electronic density of states $\rho(\varepsilon)$. The density of states is taken from the nonlocal pseudopotential calculations of Chelikowsky and Cohen.[62]

The rates for the inelastic scattering of electrons by the production of electron-hole pairs are computed by first-order perturbation theory by a method developed by Kane.[63] Because there are three occupied final states, the cross section for impact ionization is a strongly varying function of the hot electron energy near threshold due to density of states considerations. In the impact ionization event, an energetic electron with energy greater than E_g interacts with an electron in the valence band producing a free electron-hole pair. Following Kane,[63] we write the impact ionization rate for an electron with energy ε as

$$w(\varepsilon) = A \int \rho(\varepsilon_2)\rho(\varepsilon_3)\rho(\varepsilon_4)\, \delta(\varepsilon - \varepsilon_2 - \varepsilon_3 - \varepsilon_4)\, d\varepsilon_2 d\varepsilon_3 d\varepsilon_4, \tag{44a}$$

where

$$A = \frac{2\pi}{\hbar} \left[|M_a|^2 + |M_b|^2 - (M_a^* M_b + M_a M_b^*)/2 \right] / (8N_c). \tag{44b}$$

Here, ρ is the density of electron states and N_c is the number of unit cells. M_a and M_b are the direct and exchange screened Coulomb matrix elements defined as

$$M_a = \frac{4\pi e^2}{\epsilon V} \frac{F_{cv}(\underset{\sim}{k}_1, \underset{\sim}{k}_1')\, F_{cc}(\underset{\sim}{k}_2, \underset{\sim}{k}_2')}{|\underset{\sim}{k}_1 - \underset{\sim}{k}_1'|^2 + L_D^{-2}} \tag{45a}$$

and

$$M_b = \frac{4\pi e^2}{V} \frac{F_{cc}(\underset{\sim}{k}_1, \underset{\sim}{k}_2')\, F_{cv}(\underset{\sim}{k}_2, \underset{\sim}{k}_1')}{|\underset{\sim}{k}_2 - \underset{\sim}{k}_1'|^2 + L_D^{-2}} \; . \tag{45b}$$

where

$$F_{nn'}(\underset{\sim}{k}, \underset{\sim}{k}') = \int_{\substack{\text{unit} \\ \text{cell}}} U_n^*(\underset{\sim}{k}, r)\, U_{n'}(\underset{\sim}{k}', r)\, d^3r, \tag{45c}$$

Here, V is the volume, U_n is the periodic part of the Bloch function, and L_D is the Debye Length. In Eqs. (45), $\underset{\sim}{k}_2$ is the wavevector of the initial hot electron in the conduction band, $\underset{\sim}{k}_1$ is the wavevector of the additional electron in the conduction band produced by the impact ionization event, $\underset{\sim}{k}_1'$ is the wavevector of additional hole in the valence band produced by the impact ionization event, and $\underset{\sim}{k}_2'$ is the wavevector of the free electron in the conduction band after the impact ionization. Following Haug and Ekardt,[64] the direct Coulomb term is screened by the dielectric constant, but not the exchange term. Although there are some questions with regard to the validity

of this assumption, this treatment of the exchange terms gives better agreement with the measured Auger recombination rates in Ge and Si.[65-67]

The overlap integrals in Eqs. (45) are estimated to be

$$|F_{nn}|^2 = 1 \ , \tag{46a}$$

and

$$|F_{n'n}|^2 = 0.1 \ . \tag{46b}$$

Here, the value for $|F_{nn}|^2$ follows from $\underset{\sim}{k} \cdot \underset{\sim}{p}$ perturbation theory and the value for $|F_{n'n}|^2$ corresponds to values approximated by Huldt.[68]

Since germanium is indirect with a conduction band minima in the [111] direction at the zone edge, near threshold $|\underset{\sim}{k}_1 - \underset{\sim}{k}_1'| \simeq |\underset{\sim}{k}_2 - \underset{\sim}{k}_1'| \simeq K_{111}/2$, where K_{111} is the minimum non-zero reciprocal lattice vector in the [111] direction. This approximation to the matrix elements is less valid for hot electrons far above the pair-producing threshold. In silicon the variation of the squared matrix element is about 30% for primary electron energies between 5 and 8 eV.[63]

B. Results and Discussion

Using the densities of states of Ref. 62 in Eq. (44a), we calculate the impact ionization rates as shown in Fig. 14. We see that the scattering rates are a strong function of the primary hot electron energy, especially near threshold. The scattering rate for electrons by pair-producing collisions is equal to the scattering rate for electron-phonon interactions for free carriers with an energy of about three times the bandgap.

In the absence of the inelastic pair-producing collisions, the high-intensity light increases the average energy of the free electrons and a steady-state distribution is attained on the time scale of a few picoseconds. Since the laser pulses used in the experiments are much larger than a psec, any transient effects not associated with pair generation would be damped out. We first solve for steady-state solutions of Eq. (39). The occupation probability for a state with energy ε is coupled to the energy surfaces at $\varepsilon \pm \hbar\omega$ and $\varepsilon \pm \hbar\omega_0$. In the numerical calculations, we divide the energy space into a grid with intervals of 1 meV for energies in the range of 0 to 2.50 eV. The equation for $f(\varepsilon)$ is represented by a set of linear algebraic equations as a consequence of the discreteness of the photon and optical phonon energy. For example, for a state with energy greater than the phonon energy $\hbar\omega_0$ and less than the photon energy $\hbar\omega$, the occupation probability is coupled to the energy surface $\varepsilon + \hbar\omega$ by photon absorption and to the energy surfaces $\varepsilon \pm \hbar\omega_0$ by optical phonon interactions. The steady state equation can be written as

$$f(\underset{\sim}{k})\Big|_{\underset{\sim}{E}(\underset{\sim}{k})<\hbar\omega} = f^{e}(\underset{\sim}{k}) - \frac{\beta(I)\, T_{ph}\, [f^{e}(\underset{\sim}{k}) - f_{\varepsilon+\hbar\omega}(I)]}{1 + \beta(I)\, T_{ph}} + \frac{T_{ph}\, F(\varepsilon)}{1+\beta(I) T_{ph}} \,. \quad (47)$$

Here, we have defined the auxiliary functions

$$\frac{1}{T_{ph}(\varepsilon)} = \sum_{c'\underset{\sim}{k}'} R_{c\underset{\sim}{k} \to c'\underset{\sim}{k}'} \,, \quad (48a)$$

$$F(\varepsilon) = \sum_{c'\underset{\sim}{k}'} \left[R_{c'\underset{\sim}{k}' \to c\underset{\sim}{k}} (f_{c'\underset{\sim}{k}'} - f^{e}_{c'\underset{\sim}{k}'}) \right], \quad (48b)$$

$\beta(I)$ is the transition rate by photon absorption out of a state with wavevector $\underset{\sim}{k}$ and $f_{\varepsilon'}(I)$ is the probability that a state on the energy surface

ε' is occupied by an electron. The excitation rate $\beta(I)$ can be written as

$$\beta(I,E) = \frac{\sigma(\varepsilon,\omega)I}{\hbar\omega} \quad , \tag{49}$$

where $\sigma(\varepsilon,\omega)$ determines the free electron absorption cross section for a photon with energy $\hbar\omega$ through the relationship

$$\sigma(\omega) = \sum_{\underset{\sim}{k}} \sigma(\varepsilon(\underset{\sim}{k}),\omega)f(\varepsilon(\underset{\sim}{k})). \tag{50}$$

We assume that $\sigma(\varepsilon,\omega)$ is proportional to the density of electron states at $\varepsilon + \hbar\omega$, where the constant of proportionality is determined using Eq. (50) and requiring that at low light intensities (linear regime), the calculated value for the cross section $\sigma(\omega)$ agree with the experimental results. In solving for the distribution and the constant of proportionality in $\sigma(\varepsilon,\omega)$, we assume that nondegenerate statistics can be used. We use a cross section of 4.8×10^{-17} cm^2 at 10.6μm and room temperature determined from the measurements of Ref. 55. The excitation rates are directly proportional to the product of the free-electron cross section, the light intensity, and the density of final states, so that a different free-electron cross section could be used by scaling the light intensity. All calculations are performed assuming no increase in the lattice temperature, that is, for laser pulses of sufficiently short duration that thermal effects can be ignored. We solve the equations by an iterative method to determine the distribution of free electrons with energies greater than E_g as a function of the laser intensity. We first substitute the thermal equilibrium values for the occupation probabilities on the right hand sides of the set of algebraic equations similar to Eq. (47). Then we continue to iterate the set of equations until convergence. We find that for sufficiently high

intensities, a significant fraction of the total electron density is excited to states with energies greater than the bandgap. For example, the calculated electron density with energy greater than E_g is 0.0017%, 0.070%, and 2.4% of the total electron density for light with a wavelength of 10.6μm, room temperature conditions, and intensities of 20, 50, and 100 MW/cm^2, respectively. We see that for light intensities of about 100 MW/cm^2, a significant fraction of the total electron density are energetically capable of pair-producing inelastic collisions.

In our calculation of the excitation rates, the energy dependence enters through the density of final states, which increases with increasing electron energy up to an energy of about 2 eV.[62] Thus, as the average energy of the electron system is increased by the high intensity light, the average excitation rate by indirect intraband absorption is increased, since there is a larger density of final states to which the electrons can be excited. Using the calculated steady-state values for the intensity dependence of the distribution, we calculate an intensity dependence in the free-electron cross section. The results for $\sigma_e(I)$, normalized to $\sigma_e(I=0)$, are shown in Fig. 15 for room temperature conditions and light having a wavelength of 10.6μm and 9.6μm. We find that the free-electron cross section increases approximately linearly with increasing light intensity. Thus, the absorption coefficient would increase with increasing intensity even in the absence of the pair-production processes.

We now calculate the buildup rate of free electron-hole pairs by the impact ionization events. Using the values for the electron scattering rates by pair production and the calculated values for the steady-state

occupation probabilities for states with energy greater than E_g, we calculate

$$\frac{dN_e}{dt} = \sum_{\substack{i \\ \varepsilon_i > E_g}} n_i w(\varepsilon_i) \quad cN_e, \tag{51}$$

where N_e is the total free electron density and n_i is the free electron density in the i^{th} energy interval. Eq. (51) defines an exponential growth rate c. In the numerical calculations, energy intervals of 1 meV were used in the sum over i in Eq. (51). In Fig. 16, we show the calculated values for the exponential buildup rate for intensities in the range of 0 to 240 MW/cm^2. The calculation was performed for room temperature conditions with the solid line showing the results at 10.6μm, and the dashed line showing the results at 9.6μm. In the calculated values at 9.6μm, a small-signal free electron absorption cross section of 4×10^{-17} cm^2 was used, estimated from the infrared absorption measurements of Ref. 55. We find that the plasma formation thresholds for light at 10.6μm and 9.6μm are approximately the same. For a given light intensity, the exponential buildup factor is slightly larger at 10.6μm primarily due to the larger free-electron cross section, which produces larger excitation rates in Eq. (39).

In Fig. 17, we show the calculated values for the exponential growth rate as a function of the light intensity and temperature for 10.6μm radiation. The curves are for sample temperatures of 200, 300, and 450K for intensities in the range of 0 to 240 MW/cm^2. In the calculation, we use a free electron cross section of 3×10^{-17} cm^2 for T=200K, and 7×10^{-17} cm^2 for T=450K. These values were estimated from the absorption data of Ref. 55. The temperature dependence of the bandgap was taken to be $dE_g/dT = -0.45$ meV/K in the calculation.[69] We find that the exponential growth rate

for a fixed intensity is larger at higher temperatures, and, therefore, the threshold for the formation of the electron-hole plasma becomes lower as the temperature is increased. This is primarily due to the increase in free electron cross section at the larger temperatures. The temperature dependence of the relaxation rates are also important in the analysis. The relaxation rates by electron-phonon interactions increase with increasing temperature so that they in part cancel the effect of the increasing cross sections.

In Fig. 18, we show the fractional change in the free electron density for light with a wavelength of 10.6μm in n-type germanium at room temperature. Since the absorption is time dependent due to the pair production events, the figure shows the fractional change in the free-electron density after passage of an optical pulse with constant power density and pulse durations of 0.5, 2, 10 and 100 nsec. We see that the change in concentration has a large intensity and pulse length dependence. Thus, a direct comparison to experiment requires detailed information about the instantaneous intensities of the input pulse.

We now examine the intensity dependence of the absorption coefficient, including the effect of indirect free electron absorption, indirect free-hole absorption, direct intervalence-band hole absorption, multiphonon absorption, and plasma formation. In Fig. 19, we show values for the absorption coefficient normalized to the small signal absorption for a wavelength of 10.6μm and for intrinsic and optical grade germanium. The values are shown for the absorption coefficient at the end of an optical pulse of constant power density, and a pulse duration of 2 nsec and a pulse with a duration of 40 nsec. The multiphonon absorption coefficient is

taken to be 0.03 cm^{-1},[18] the free hole cross section is taken to be $1x10^{-17}$ cm^2, estimated by Drude-Zener theory, the free-electron cross section is taken to be $4.9x10^{-17}$ cm^2, and the direct intervalence-band cross section is taken to be $6.8x10^{-16}$ cm^2.[7] We use the calculated results in Fig. 15 for the intensity dependence of the free-electron cross section and assume the same intensity dependence for the indirect free-hole cross section. This is not a critical assumption since for intrinsic or n-type materials the indirect free-hole cross section is always much smaller than the other absorption processes. For the intensity dependence of the direct free-hole absorption coefficient $\alpha_D(I)$, we write

$$\alpha_D(I) = \frac{\alpha_D(I=0)}{\sqrt{1 + I/I_s}} \quad , \tag{52}$$

and use $I_s = 4$ MW/cm^2. The increase in free electron-hole pairs is calculated using the values for the exponential growth rate as a function of intensity. In Fig. 19a, we show the calculated values of $\alpha(I)/\alpha(I=0)$ for intrinsic germanium ($N_e = N_h = 2.4x10^{13}$ cm^{-3}) at the end of a 2 nsec pulse and a 40 nsec optical pulse. In each case, the absorption coefficient initially decreases due to the saturation of the intervalence-band absorption as discussed earlier in this paper. The rapidly rising increase in the absorption is the threshold for the electron-hole plasma formation. In Fig. 19b the calculated values for the absorption coefficient are shown for optical grade germanium ($N_e = 1.5x10^{14}$ cm^{-3}). In this case we do not expect to observe absorption saturation since the free hole density is much less than the free electron density in thermal equilibrium, and the saturation of the intervalence-band absorption is approximately cancelled by the

increase in the indirect free electron absorption. Values for the threshold for plasma formation are also shown. From Fig. 19 one sees that the threshold occurs at somewhat higher intensities in intrinsic germanium than in the n-type optical grade germanium. There are two reasons for the higher threshold intensity in the intrinsic case: first, the low intensity absorption coefficient is larger in the intrinsic case owing to the larger density of holes and the large intervalence-band cross section for the holes (thus, a higher density of electron-hole pairs must be generated for the same fractional increase of the absorption coefficient in intrinsic germanium compared with optical grade germanium), and second, there is a smaller density of electrons, which are assumed to be primarily responsible for initiating the impact ionization process, in intrinsic germanium compared with optical grade germanium. However, since the carrier generation rates are very rapidly increasing functions of intensity, the difference in the thresholds for the two cases is rather small.

Experimentally, the transmission as a function of intensity in intrinsic and optical grade germanium has been reported by two groups.[2-3,10] In the work reported in Ref. 10, the laser pulses were approximately Gaussian in time with a FWHM of about 2 nsec. The transmission data was interpreted in terms of electron-hole pair formation. For intrinsic germanium the peak free carrier density as a function of peak laser intensity was reported. The reported free carrier density was weakly dependent on the light intensity for peak intensities less than about 200 MW/cm^2, at which point the free carrier density began to increase rapidly with intensity. These experimental results are in reasonably good agreement with our calculated results. We find a threshold of about 140 MW/cm^2 for a constant intensity

pulse of 2 nsec. (This threshold is taken from Fig. 18 and setting the threshold as the intensity for which $\Delta N_e/N_e = 1.$) For intensities greater than the threshold, we also find a very rapid increase in carrier density with intensity. Considering the various uncertainties in the calculation and the difficulties in direct comparison with the experimental data owing to the pulse shapes, we find this level of agreement satisfactory.

The results in Refs. 2 and 3 are quite different than those of Ref. 10. In this work optical grade Ge was used. The multimode laser pulses used had a spiky structure and the laser intensities quoted were averaged values obtained by assuming a clean pulse with a FWHM of 80 to 90 nsec. Under these conditions, thresholds for electron-hole pair formation of about 12 MW/cm^2 were reported. This is over an order of magnitude smaller than the thresholds reported in Ref. 10. The longer pulse lengths and the use of optical grade rather than intrinsic material do tend to push the thresholds lower. We calculate that for a constant intensity 80 nsec pulse the threshold should be about 80 MW/cm^2. Nonetheless, there is a large discrepancy between the experimental results of these two groups. Our theoretical results, based on the impact ionization model, are consistent with the experimental results of Ref. 10 and they are not consistent with the much lower threshold energies reported in Refs. 2 and 3. If the threshold intensities of Ref. 10 prove correct our calculations support the impact ionization model for the electron-hole pair formation. If the threshold intensities of Refs. 2 and 3 prove correct, our calculation suggest that the electron-hole pair formation cannot be explained by the impact ionization model.

SUMMARY AND CONCLUSIONS

We have presented calculations of the intensity dependence of the absorption by free carriers in p-type and n-type semiconductors. The analysis was divided into two sections, one discussing the absorption of CO_2 laser light by free holes, and the other discussing the absorption by free electrons. In the first section we reviewed a theory of the saturation of heavy- to light-hole band transitions in p-type semiconductors with the diamond or zinc-blend crystal structure. We found that the intensity dependence of the absorption coefficient is closely approximated by an inhomogeneously broadened two-level model, and values of the saturation intensity were presented for most Groups IV and III-V semiconductors for light in the 9-11μm region. For the temperature and concentration range where hole-phonon scattering dominates hole-impurity and hole-hole scattering, I_S is found to be independent of hole density. For larger hole densities where hole impurity and hole-hole scattering are important, the saturation intensity increases monotonically with increasing hole concentration. This behavior is consistent with experimental results. The dependence of the saturation intensity on photon energy has been computed and compared with available experimental results. Good agreement between theory and experiment was found. We have predicted the dependence of the saturation intensity on temperature.

We have also used the theory to describe the intensity dependence of the real part of the dielectric constant in p-Ge due to modifications of the free-hole distribution function by the high intensity laser. We find that the diagonal components of the susceptibility increase monotonically with increasing intensity, and that the increases in the susceptibility are directly proportional to the concentration of free holes in the sample.

We investigated the intensity dependence of the absorption associated with indirect free-electron transitions in germanium. We find that the cross section increases with increasing intensity as the electrons are pumped higher into the conduction band by the absorption of light. As the intensity is further incresed, a significant fraction of the electrons have energy greater than the bandgap. These electrons can relax by inelastic pair-production processes creating an additional electron-hole pair. This leads to a rather abrupt increase in the absorption coefficient with increasing intensity. Once the threshold for plasma formation is attained, the absorption coefficient is a strong function of both the intensity and duration of the laser pulse. Values for the exponential growth are calculated as a function of wavelength, temperature, and the light intensity. Comparison with experiment is required to determine whether impact ionization is indeed responsible for the plasma formation and the resulting increase in absorption. At present, experimental results are in disagreement.

Although calculations for the plasma formation were performed for n-type and intrinsic Ge, a similar process can occur in p-type material. There are two possibilities in p-type material: the impact ionization may be initiated by a hot hole distribution or the small number of electrons initially present may initiate the impact ionization process. For reasons previously discussed, we expect the hole impact ionization process to be somewhat less effective than the electron impact ionization process and, thus, we expect somewhat larger threshold intensities in p-type material than in n-type. However, even if hole impact ionization was completely

ineffective, the threshold intensity of moderately doped p-type Ge would exceed that of *n*-type Ge by less than about a factor of two (at room temperature) owing to the very strong dependence of the excess electron density on intensity shown in Fig. 18. Thus, p-type material is expected to show saturable absorption for intensities less than the threshold intensity for plasma formation, but strongly increasing absorption (with intensity) for intensities greater than this threshold and the threshold intensity in p-type material should somewhat exceed (less than a factor of two) that in n-type material.

ACKNOWLEDGMENTS

The authors thank T. C. McGill and Edgard Schweig for many useful discussions. We are especially grateful to C. R. Phipps, Jr., for communicating *his experimental results prior to publication.* We would also like to thank L. S. Darken, M. E. Mostoller, and J. T. Luck for assistance in the preparation of this manuscript. We acknowledge the support of the U. S. Department of Energy under contract W-7405-eng-26 operated by Union Carbide Corporation and the Air Force of Scientific Research under grant No. AFOSR-77-3216. One of us (R.B.J.) wants to gratefully thank the Director of the Oak Ridge National Laboratory for financial support through the Eugene P. Wigner Fellowship fund, and one of us (D.L.S.) acknowledges support from the Alfred P. Sloan Foundation.

REFERENCES

1. A. F. Gibson, C. A. Rosito, C. A. Raffo, and M. F. Kimmitt, "Absorption saturation in germanium, silicon, and gallium arsenide at 10.6μm," Appl. Phys. Lett., vol. 21, pp. 356-357, 1972.

2. S. Y. Yuen, R. L. Aggarwal, N. Lee, and B. Lax, "Nonlinear absorption of CO_2 laser radiation by nonequilibrium carriers in germanium," Opt. Commun., vol. 28, pp. 237-240, 1979.

3. S. Y. Yuen, R. L. Aggarwal, and B. Lax, "Saturation of transmitted CO_2 laser pulses in germanium," J. Appl. Phys., vol. 51, pp. 1146-1151, 1980.

4. B. J. Feldman and J. F. Figueria, "Generation of subnanosecond CO_2 laser pulses at 10.6μm by pulse compression techniques," Appl. Phys. Lett., vol. 25, pp. 301-303, 1974.

5. A. F. Gibson, M. F. Kimmitt, and B. Norris, "Generation of bandwidth-limited pulses from a TEA CO_2 laser using p-type germanium," Appl. Phys. Lett., vol. 24, pp. 306-307, 1974.

6. A. J. Alcock and A. C. Walker, "Generation and detection of 150-psec mode-locked pulses from a multi-atmosphere CO_2 laser," Appl. Phys. Lett., vol. 25, pp. 299-301, 1974.

7. C. R. Phipps, Jr., and S. J. Thomas, "Saturation behavior of p-type germanium at CO_2 laser wavelengths," Opt. Lett., vol. 1, pp. 93-95, 1977.

8. R. L. Carlson, M. D. Montgomery, J. S. Ladish, and C. M. Lockhart, "Simultaneous multiline saturation of gallium doped germanium and SF_6 on the 10.6μm band," IEEE J. Quantum Electron., vol. 13, p. 35D, 1977.

9. C. R. Phipps, Jr., S. J. Thomas, J. Ladish, S. J. Czuchlewski, and J. F. Figuerira, "Saturation behavior of p-type germanium over the CO_2 laser spectrum," IEEE J. Quantum Electron., vol. 13, p. 36D, 1977.

10. D. E. Watkins, C. R. Phipps, Jr., and S. J. Thomas, "Observation of amplified reflection through degenerate four-wave mixing at CO_2 laser wavelengths in germanium," Opt. Lett., vol. 6, pp. 76-78, 1981. For review of DFWM in semiconductors, see R. K. Jain and M. B. Klein, Optical Phase Conjugation, (R. A. Fisher, ed.), chapter 10, Academic Press, 1982.

11. T. W. Nee, C. D. Cantrell, J. F. Scott, and M. O. Scully, "Nonlinear optical properties of InSb: Hot-electron effects," Phys. Rev. B, vol. 17, pp. 3936-3945, 1978.

12. F. Keilmann, "Infrared saturation spectroscopy in p-type germanium," IEEE J. Quantum Electron., vol. 12, pp. 592-297, 1976.

13. M. Kawai and T. Miyakawa, "Temporal and spectral behavior of absorption saturation in p-Ge around 10.6μm," Jap. J. of Appl. Phys., vol. 20, pp. 369-373, 1981.

14. M. Sargent III, "Relaxation of hot holes in p-Ge," Opt. Commun., vol. 20, pp. 298-302, 1977.

15. E. O. Kane, "Energy band structure in p-type germanium and silicon," J. Phys. Chem. Solids, vol. 1, pp. 82-89, 1956.

16. J. C. Hensel and K. Suzuki, "Quantum resonances in the valence bands of germanium. II. Cyclotron resonances in uniaxially stressed crystals," Phys. Rev. B, vol. 9, pp. 4219-4257, 1974.

17. A. H. Kahn, "Theory of the infrared absorption of carriers in germanium and silicon," Phys. Rev., vol. 97, pp. 1647-1652, 1955.

18. S. J. Fray, F. A. Johnson, J. E. Quarrington, and N. Williams, "Lattice bands in germanium," vol. 85, pp. 153-158, 1965.

19. R. Braunstein and E. O. Kane, "The valence band structure of the III-V compounds," J. Phys. Chem. Solids, vol. 23, pp. 1423-1431, 1962.

20. J. W. Hodby, "Infrared absorption in gallium phosphide-gallium arsenide alloys. II. Absorption in p-type material," Proc. Phys. Soc. (London), vol. 82, pp. 324-326, 1963.

21. G. W. Gobeli and H. Y. Fan, "Infrared absorption and valence band in indium antimonide," Phys. Rev., vol. 119, pp. 613-620, 1960.

22. R. Braunstein, "Intervalence band transitions in gallium arsenide," J. Phys. Chem. Solids, vol. 8, pp. 280-282, 1959.

23. W. M. Becker, A. K. Ramdas, and H. Y. Fan, "Energy band structure of gallium antimonide," J. Appl. Phys., vol. 32, pp. 2094-2102, 1961.

24. F. Matossi and F. Stern, "Temperature dependence of optical absorption in p-type indium arsenide," Phys. Rev., vol. 111, pp. 472-475, 1958.

25. See, for example, A. Abragam, The Principles of Nuclear Magnetism, (Oxford: Clarendon Press, 1961), pp. 272ff.

26. R. B. James and D. L. Smith, "Saturation of intervalence-band transitions in p-type semiconductors," Phys. Rev. B, vol. 21, pp. 3502-3512, 1980.

27. R. B. James and D. L. Smith, "Theory of nonlinear infrared absorption in p-type germanium," Phys. Rev. Lett., vol. 42, pp. 1495-1498, 1979.

28. E. Conwell, "Lattice mobility of hot carriers," J. Phys. Chem. Solids, vol. 8, pp. 234-239, 1959.

29. D. M. Brown and R. Bray, "Analysis of lattice and ionized impurity scattering in p-type germanium," Phys. Rev., vol. 127, pp. 1593-1602, 1962.

30. R. B. James, Edgard Schweig, D. L. Smith, and T. C. McGill, "Experimental investigation of the infrared absorption saturation in p-type germanium and silicon," Appl. Phys. Lett., vol. 40, pp. 231-233, 1982.

31. H. Brooks, Advances in Electronics and Electron Physics (L. Marton, ed.), vol. 7, p. 85, Academic Press, New York, 1955.

32. I. N. Yassievich and I. D. Yaroshetskii, "Energy relaxation and carrier heating and cooling processes in the intraband absorption of light in semiconductors," Fiz. Tekh. Poluprovodn., vol. 9, pp. 857-866, 1975 [Sov. Phys. Semicond., vol. 9, pp. 565-570, 1975].

33. We use the first-order approximation to the distribution as previously discussed. This approximation was shown to produce results for I_s within 15% of the more complete calculation.

34. R. B. James and D. L. Smith, "Dependence of the saturation intensity of p-type germanium on impurity concentration and residual absorption at 10.59μm," Solid State Commun., vol. 33, pp. 395-393, 1980.

35. E. V. Beregulin, P. M. Valov, and I. D. Yaroshetskii, "Experimental investigation of the bleaching of a semiconductor in the case of optical heating and cooling of electrons involving intraband transitions," Fiz. Tekh. Poulprovodn., vol. 12, pp. 239-244, 1978 [Sov. Phys. Semicond., vol. 12, pp. 138-140, 1978].

36. See, for example, E. Bergmann, I. Bigio, B. Feldman, and R. Fisher, "High-efficiency pulsed 10.6μm phase-conjugate reflection via degenerate four-wave mixing," Opt. Lett., vol. 3, pp. 82-84, 1978.

37. R. B. James and D. L. Smith, "Laser induced changes in the dispersive properties of p-Ge due to intervalence-band transitions," Phys. Rev. B, vol. 23, pp. 4044-4048, 1981.

38. J. Wynne, "Optical third-order mixing in GaAs, Ge, Si, and InAs," Phys. Rev., vol. 178, pp. 1295-1303, 1969.

39. D. E. Watkins, C. R. Phipps, Jr., and S. J. Thomas, "Determination of the third-order nonlinear optical coefficients of germanium through ellipse rotation," Opt. Lett., vol. 5, pp. 248-249, 1980.

40. We average the vector potential over all angles.

41. R. B. James and D. L. Smith, "Saturation characteristics of p-type semiconductors over the CO_2 laser spectrum," J. of Appl. Phys., vol. 51, pp. 2836-2839, 1980.

42. R. B. James and D. L. Smith, "Absorption of high intensity CO_2 laser light in p-type semiconductors with small spin-orbit splittings, J. of Appl. Phys., vol. 52, pp. 4238-4240, 1981.

43. P. M. Valov, I. D. Yaroshetskii, and I. N. Yassievich, "Effect of cooling of carriers in semiconductors by light," ZhETF Pis. Red., vol. 20, pp. 448-452, 1974 [JETP Lett., vol. 20, pp. 204-206, 1974].

44. A. F. Gibson and P. N. D. Maggs, "Intraband photoconductivity in p-type germanium at 10.6μm," J. Phys. D: Appl. Phys., vol. 7, pp. 292-297, 1974.

45. V. G. Agafonov, P. M. Valov, B. S. Ryvkin, and I. D. Yaroshetskii, "Experimental investigation of the energy relaxation process in p-type Ge under intraband optical excitation conditions," Fiz. Tekh. Poluprovodn., vol. 9, pp. 867-871, 1975 [Sov. Phys. Semicond., vol. 9, pp. 571-573, 1975].

46. H. Hattori, O. Fujitani, and M. Umeno, "Photoconductivity due to inter-valence band transition in p-type germanium,' J. Phys. Soc. Japan, vol. 36, pp. 485-490, 1974.

47. T. Grave and F. Keilmann, "Relaxation Dynamics and Photoconductivity in p-type germanium," Z. Physik B, vol. 32, pp. 347-354, 1979.

48. P. J. Bishop, A. F. Gibson, and M. F. Kimmitt, "The performance of photon-drag detectors at high laser intensities," IEEE J. of Quantum Electron., vol. QE-9, pp. 1007-1011, 1973. Values of Δ / I quoted were measured by P. Maggs.

49. A. F. Gibson, M. F. Kimmitt, P. N. D. Maggs, and B. Norris, "A wide bandwidth detection and display system for use with TEA CO_2 lasers," J. of Appl. Phys., vol. 46, pp. 1413-1414, 1975.

50. T. Kamibayashi, S. Yonemochi, and T. Miyakawa, "Superlinear dependence of photon drag voltage on incident power density," Appl. Phys. Lett., vol. 22, pp. 119-120, 1973.

51. R. B. James and D. L. Smith, "Theoretical description of the intervalence-band photoconductivity of p-Ge at 10.6μm," Phys. Rev., vol. 23, pp. 4049-4053, 1981.

52. We have assumed that there exists no impact ionization processes in which a hole is sufficiently energetic to relax by an electron-hole pair production. This energy relaxation mechanism is important at very high intensities; however, the experiments of Ref. 6 indicate that this process is small over the range of intensities we consider.

53. Hole-hole scattering is included in the calculation of the distribution f^0, but it is not included in the momentum relaxation rates. For hole-hole scattering, the total momentum is not changed; thus, it has little influence on the mobility.

54. S. A. Jamison and A. V. Nurmikko, "Avalanche formation and high-intensity infrared transmission limit in InAs, InSb, and $Hg_{1-x}Cd_xTe$," Phys. Rev. B, vol. 19, pp. 5185-5193, 1979.

55. H. Y. Fan, W. Spitzer, and R. J. Collins, "Infrared absorption in n-type germanium," Phys. Rev., vol. 101, pp. 566-572, 1956.

56. E. M. Conwell, High Field Transport in Semiconductors. Academic Press, New York, 1967, pp. 149-153.

57. E. M. Conwell, High Field Transport in Semiconductors, Academic Press, New York, 1967, pp. 112-153.

58. C. Herring, "Transport properties of a many-valley semiconductor," Bell System Tech. J., vol. 34, pp. 237-290, 1955.

59. E. M. Conwell, High Field Transport in Semiconductors, Academic Press, New York, 1967, pp. 167-170.

60. H. G. Reik and H. Risken, "Drift velocity and anisotropy of hot electrons in n-germanium," Phys. Rev., vol. 126, pp. 1737-1746, 1962.

61. M. H. Jorgensen, N. I. Meyer, and K. J. Schmidt-Tiedemann, "Hot-electron effects in silicon and germanium," Proc. 7th Intern. Conf. on Phys. of Semicond., pp. 457-466, 1964.

62. J. R. Chelikowsky and M. L. Cohen, "Nonlocal pseudopotential calculations for the electronic structure of eleven diamond and zinc-blende semiconductors," Phys. Rev. B, vol. 14, pp. 556-582, 1976.

63. E. O. Kane, "Electron scattering by pair production in silicon," Phys. Rev., vol. 159, pp. 624-631, 1967.

64. A. Haug and W. Ekardt, "The influence of screening effects on the Auger recombination in semiconductors," Solid State Commun., vol. 17, pp. 267-268, 1975.

65. N. G. Nilsson and K. G. Svanteson, "The spectrum and decay of the recombination radiation from strongly excited silicon," Solid State Commun., vol. 11, pp. 155-159, 1972.

66. R. Conradt and J. Aegenheister, "Minority carrier lifetime in highly doped Ge," Solid State Commun., vol. 10, pp. 321-323, 1972.

67. J. D. Beck and R. Conradt, "Auger-recombination in Si," Solid State Commun., vol. 13, pp. 93-95, 1973.

68. L. Huldt, "Band-to-band Auger recombination in indirect gap semiconductors," Phys. Status Solidi (a), vol. 8, pp. 173-187, 1971.

69. W. C. Dash and R. Newman, "Intrinsic optical absorption in single-crystal germanium and silicon at 77°K and 300°K," Phys. Rev., vol. 99, pp. 1151-1155, 1955.

FIGURE CAPTIONS

Figure 1. Valence band structure of germanium for small k in the [100] direction. Here, an increase in hole energy corresponds to going vertically downward.

Figure 2. Calculated hole distribution functions in p-Ge as a function of k^2 for $\underset{\sim}{k}$ in the [111] and [100] directions. The calculations were performed for λ = 10.6μm, T = 300°K and I = 30 MW/cm^2. The equilibrium distribution functions are shown for comparison. N_c is the effective density of states.

Figure 3. Calculated absorption coefficient normalized to its low intensity value as a function of intensity for p-Ge. The calculations were performed for λ = 10.6μm and T = 295°K. The inhomogeneously broadened two-level model result with I_s = 4.1 MW/cm^2 is also shown.

Figure 4. Calculated saturation intensity as a function of photon energy for p-Ge at 295°K. The experimental results are from Refs. 7, 8, 12, and 30. Error bars are only given in Ref. 7.

Figure 5. Calculated saturation intensity as a function of temperature for p-Ge and light with a wavelength of 10.6μm.

Figure 6. Experimental and calculated values of the saturation intensity I_s vs the hole concentration for p-Ge. The circles (triangles) show the experimental values of I_s for light having a wavelength of 10.6μm (9.6μm). The solid line in the figure shows a calculation of I_s vs N_h taken from Ref. 34 for 10.6μm radiation, and the dashed line shows the calculation of I_s vs N_h for 9.6μm radiation.

Figure 7. Values of the saturation intensity vs hole concentration in p-Ge at 78 K. The solid (dashed) curve shows the calculated values of I_s at 10.6μm (9.5μm).

Figure 8. Calculated values of $\chi'(I)/\chi'(I=0)$ as a function of intensity for unpolarized light in p-Ge. The calculation was done for light with a wavelength of 10.6μm and a temperature of 300K.

Figure 9. The top panel gives the calculated values of the change in the real part of the dielectric constant (divided by the density of free holes) as a function of intensity for p-Ge at λ = 10.6μm, T = 300K, and for unpolarized light. The corresponding values for the change in the index of refraction are given in the lower panel.

Figure 10. Calculated values of the diagonal elements of $\Delta\epsilon$ (divided by the free-hole density) as a function of intensity in p-Ge at 300K for light with a wavelength of 10.6μm. In the top panel the result for [100] polarization is shown. The coordinate system

is chosen to be the crystal axis; ϵ is diagonal in this coordinate system. In the lower panel the result for [110] polarization is shown. For this panel, the X axis is in the [110] direction, the Y axis is in the [1$\bar{1}$0] direction, and the Z axis is in the [001] direction. In this coordinate system ϵ is diagonal.

Figure 11. Values of $(\frac{\Delta\sigma}{\sigma I})$ vs the hole concentration in p-Ge for CO_2 laser excitation at 10.6μm, room temperature and low light intensities. The calculated values of $(-\Delta\sigma/\sigma I)$ are shown by the solid curve. The experimental data are taken from: x, Ref. 44; ▲, Ref. 45; ■, Ref. 46; ●, Ref. 47; and ○, Ref. 48. Error bars are reported only in Refs. 45 and 47.

Figure 12. Calculated values of the normalized change in the conductivity of p-Ge vs temperature for light at 10.6μm, a hole concentration of 2.0×10^{16} cm^{-3} and low intensity excitation. The experimental data are taken from: ▲, Ref. 45 and ●, Ref. 43. Error bars are only reported in Ref. 45.

Figure 13. Values of $(-\Delta\sigma/\sigma I)$ vs the hole concentration in p-Ge for λ = 10.6μm and T = 300K. The solid curves are our calculated values for intensities of 0.05 (linear regime), 1, 5, and 10 MW/cm^2.

Figure 14. Impact ionization rates for germanium at room temperature. w(E) is the scattering rate for pair production for a state with energy E. The zero of the electron energy is taken to be the valence band maximum.

Figure 15. Calculated values for the fractional change in the free electron cross section vs intensity for germanium at room temperature. The solid (dashed) curve is for light with a wavelength of 9.6 (10.6) μm.

Figure 16. Values for the exponential growth rate of the free electron density vs intensity for germanium at T = 300K. The solid (dashed) curve is for light with a wavelength of 10.6 (9.6) μm.

Figure 17. Calculated values for the exponential growth rate of the free electron density vs intensity for germanium and light having a wavelength of 10.6μm. The three curves shown are for lattice temperatures of 200, 300, and 450K.

Figure 18. Normalized change in the free electron density vs intensity for germanium at room temperature and light having a wavelength of 10.6μm. The four curves show the change in the free electron density vs intensity immediately after passage of a light pulse with constant power density in the interaction region and durations of 0.5, 2, 10, and 100 nsec.

Figure 19. Calculated values for the intensity dependence of the absorption coefficient (normalized to its small-signal value) vs intensity for germanium at T = 300K and light with a wavelength of 10.6μm. In the upper and lower figures, the solid (dashed) curve illustrates the normalized change in the absorption coefficient vs intensity at the end of a pulse with constant power density in the interaction region and a pulse duration of 40 (2) nsec. The top figure is for intrinsic germanium ($N_e(I=0) = N_h(I=0) = 2.4\times10^{13}$ cm^{-3}), and the lower figure is for optical grade germanium ($N_e(I=0) = 1.5\times10^{14}$ cm^{-3}).

TABLE 1. Values of the saturation intensity for the laser excitation polarized in the [100], [110] and [111] directions. Also shown is the value of I_s for the case of unpolarized light. All values are for lightly doped p-Ge (doping concentration less than about 3×10^{15} cm^{-3}) and room temperature conditions.

Direction of Light Polarization	I_s(MW/cm^2)
[100]	3.2
[110]	3.4
[111]	3.3
unpolarized	3.5

TABLE II. Saturation intensity and the first derivative of saturation intensity with respect to photon energy and temperature. Values of I_s are given for T_o = 295°K and E_o = 117 meV.

Material	I_s [MW/cm^2]	$\left.\frac{\partial I_s}{\partial E}\right\|_{E_o}$ $\left[\frac{MW}{cm^2}\frac{1}{meV}\right]$	$\left.\frac{\partial I_s}{\partial T}\right\|_{T_o}$ $\left[\frac{MW}{cm^2}\frac{1}{^oK}\right]$
Ge	3.5	0.1	0.03
GaAs	18.	0.5	0.2
GaSb	1.8	0.03	0.02
AlAs	400	9	4
AlSb	24.	0.4	0.2
InAs	5.1	0.1	0.05

TABLE III. Parameters describing the saturation characteristics for heavy-hole to light-hole band transitions, heavy-hole to split-off band transitions, and light-hole to split-off band transitions for $T_0 = 295K$ and $E_0 = 129.8$ meV. Values of the saturation intensity are given due to the cumulative effect of all three direct intervalence-band transitions. Also included are the first derivatives of the saturation intensity with respect to photon energy and temperature. All intensities are given in units of MW/cm^2.

Material	$(I_s)_{h\ell}$	$(I_s)_{hs}$	$(I_s)_{\ell s}$	I_s	$\left.\frac{\partial I_s}{\partial E}\right\|_{E_0}$ $\left[\frac{MW}{cm^2}\ \frac{1}{meV}\right]$	$\left.\frac{\partial I_s}{\partial T}\right\|_{T_0}$ $\left[\frac{MW}{cm^2}\ \frac{1}{^oK}\right]$
Si	301	127	161	175	3.3	1.7
InP[a]	745	---	97	159	8	1.0
GaP	1900	161	332	229	0.9	2.3
AlP	104	190	215	122	3.1	1.0

a) The h↔s transition in InP is not energetically allowed for this photon energy.

TABLE IV. Values of α_{oj}/α_o for transitions between the heavy- and light-hole bands, the heavy- and split-off bands, and the light- and split-off bands. All values are given for a photon energy of 129.8 meV (λ = 9.6μm) and room temperature conditions.

Material	$\frac{(\alpha_o)_{h\to\ell}}{\alpha_o}$	$\frac{(\alpha_o)_{h\to s}}{\alpha_o}$	$\frac{(\alpha_o)_{\ell\to s}}{\alpha_o}$
Si	0.37	0.39	0.24
InP[a]	0.39	----	0.61
GaP	0.14	0.58	0.28
AlP	0.71	0.19	0.10

a) The h→s transition in InP is not energetically allowed for this photon energy.

TABLE V. Measured saturation intensities for uncompensated crystalline p-Si samples. N_h is the concentration of free holes and λ is the wavelength of the light. The silicon samples with doping densities of 7×10^{15} and 3×10^{16} cm^{-3} are doped with boron, and the sample with a doping density of 2×10^{16} cm^{-3} is doped with aluminum.

N_h (cm^{-3})	λ(μm)	I_s(MW/cm^2)
7×10^{15}	10.6	55
3×10^{16}	10.6	71
7×10^{15}	9.6	43
2×10^{16}	9.6	36

TABLE VI. Constants of n-Ge used for calculations. Values of constants taken from Ref. 56.

Quantity	Value
m_t/m_0	0.082
m_ℓ/m_0	1.6
ρ	5.32 gm/cm^3
U_ℓ [a]	5.4×10^5 cm/sec
$\hbar\omega_0$	0.037 eV

[a] This represents an average over different crystallographic directions.

ORNL-DWG 81-18299

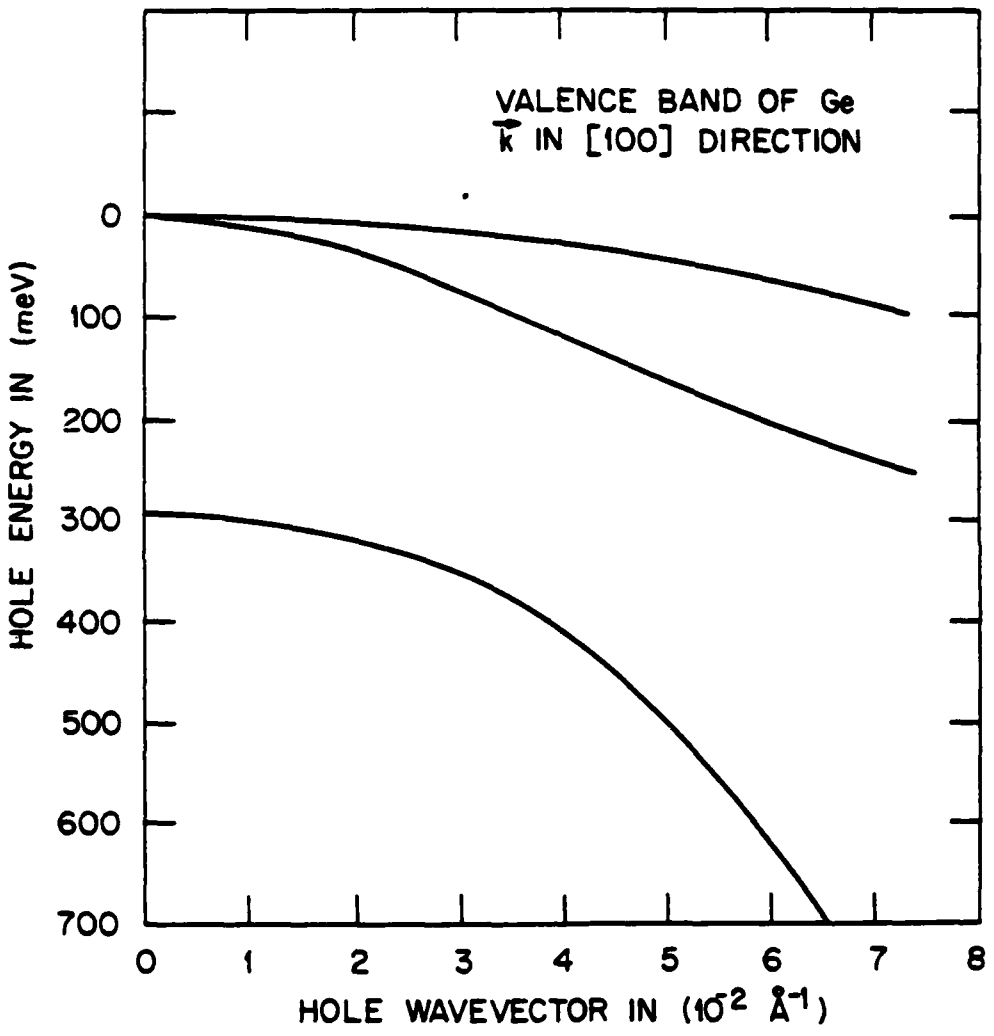

ORNL - DWG 82-8432

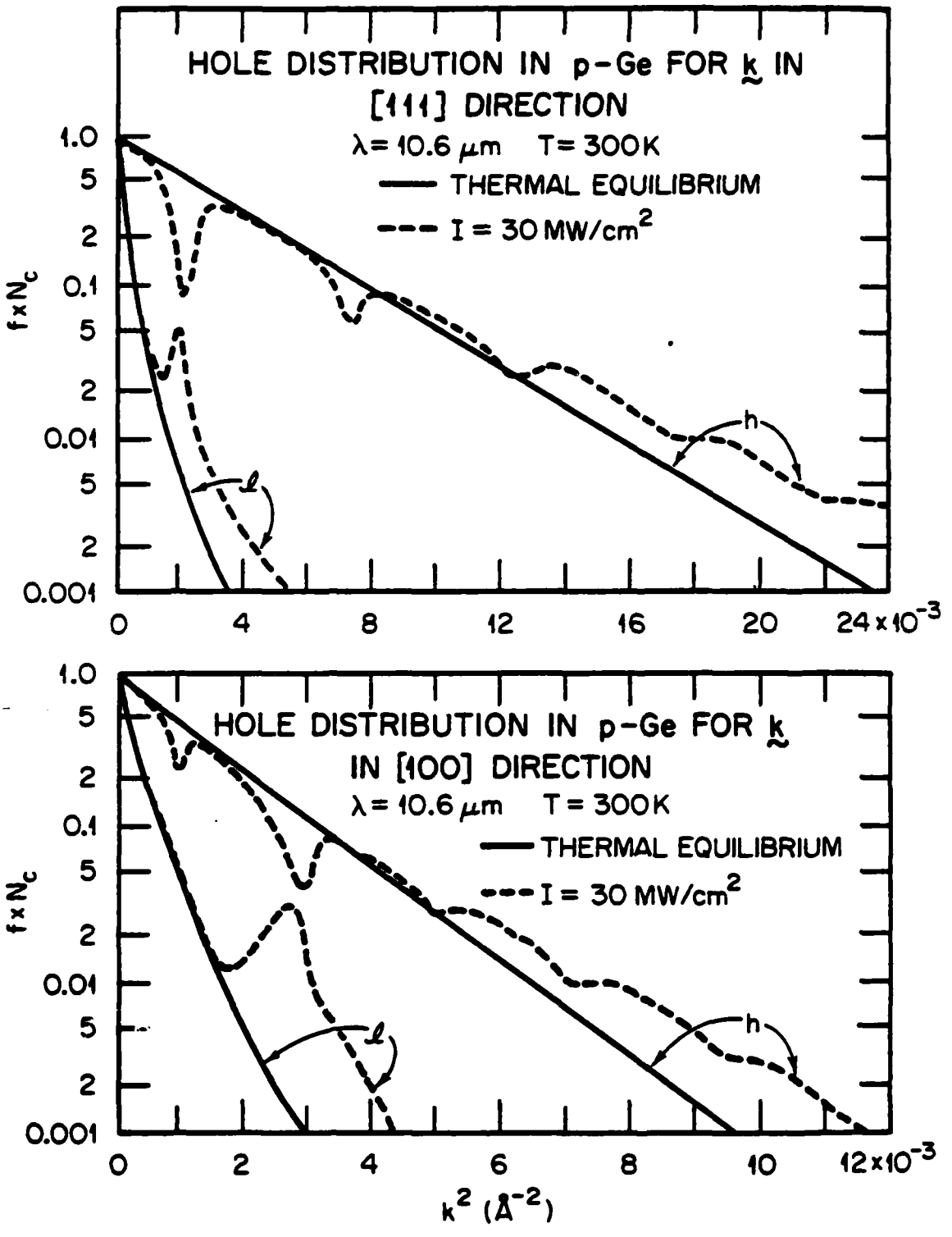

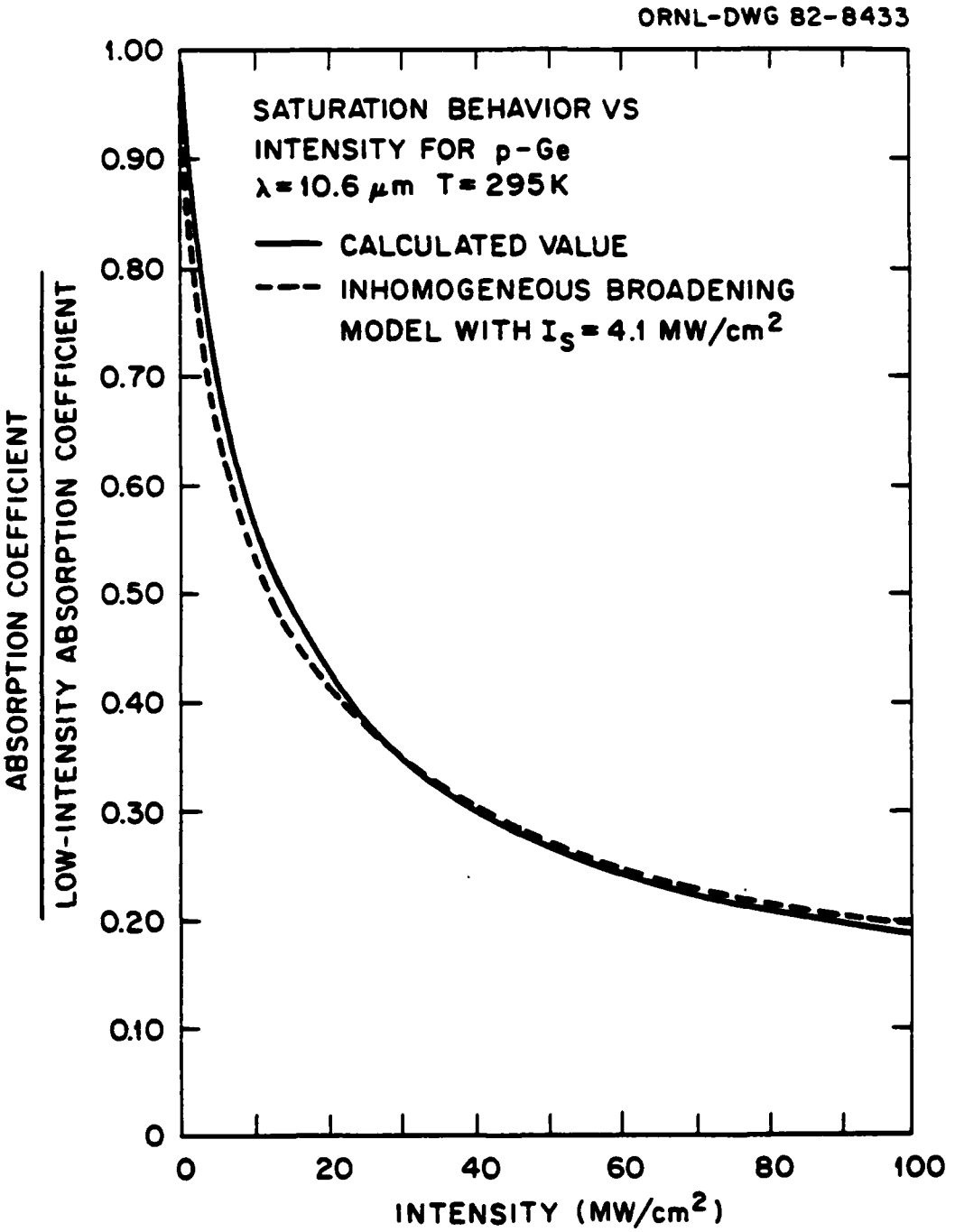
ORNL-DWG 82-8433
SATURATION BEHAVIOR VS
INTENSITY FOR p-Ge
λ=10.6 μm T=295K
CALCULATED VALUE
INHOMOGENEOUS BROADENING
MODEL WITH I_S=4.1 MW/cm^2
ABSORPTION COEFFICIENT / LOW-INTENSITY ABSORPTION COEFFICIENT
1.00
0.90
0.80
0.70
0.60
0.50
0.40
0.30
0.20
0.10
0
0
20
40
60
80
100
INTENSITY (MW/cm^2)

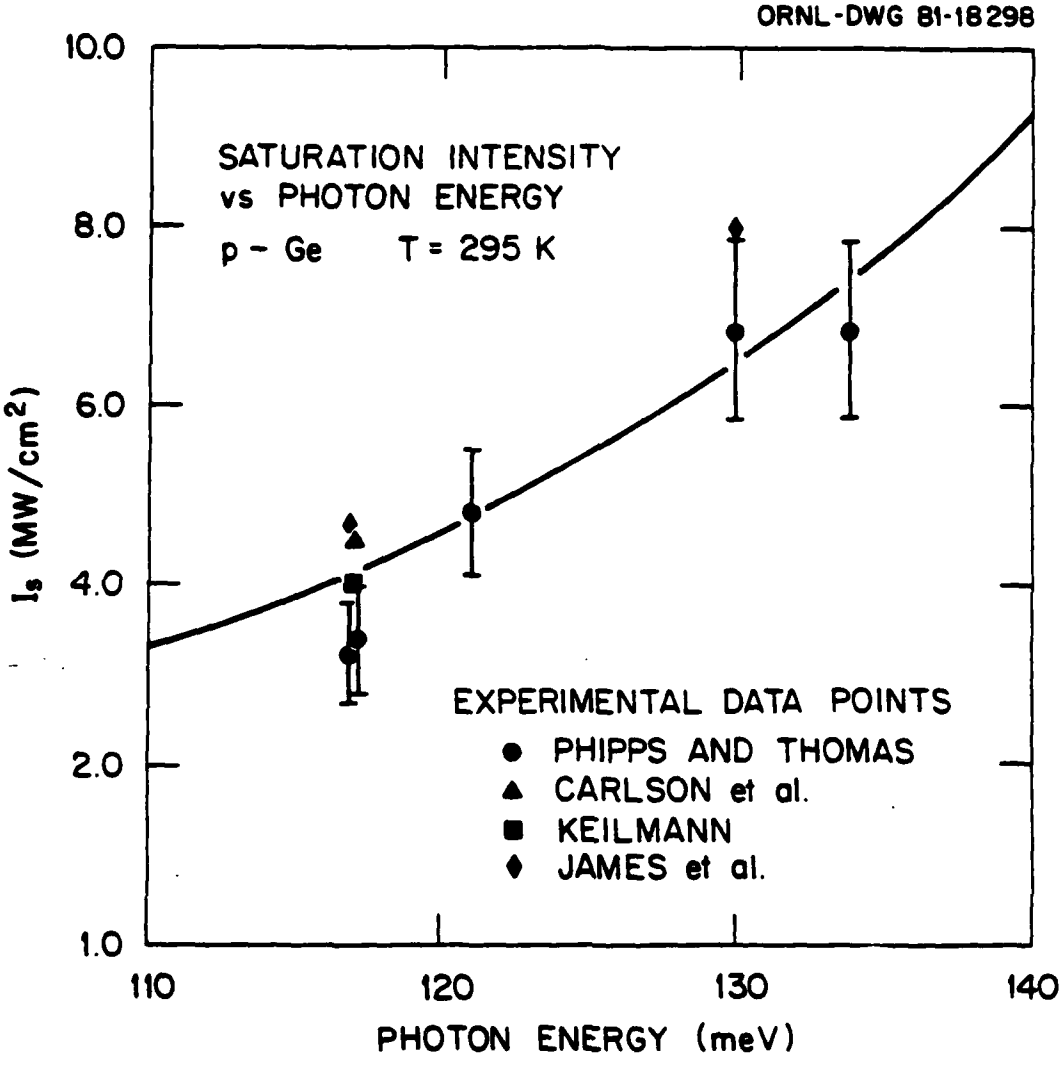
ORNL-DWG 81-18298
SATURATION INTENSITY
vs PHOTON ENERGY
p - Ge T = 295 K
EXPERIMENTAL DATA POINTS
PHIPPS AND THOMAS
CARLSON et al.
KEILMANN
JAMES et al.
I_s (MW/cm^2)
10.0
8.0
6.0
4.0
2.0
1.0
110
120
130
140
PHOTON ENERGY (meV)

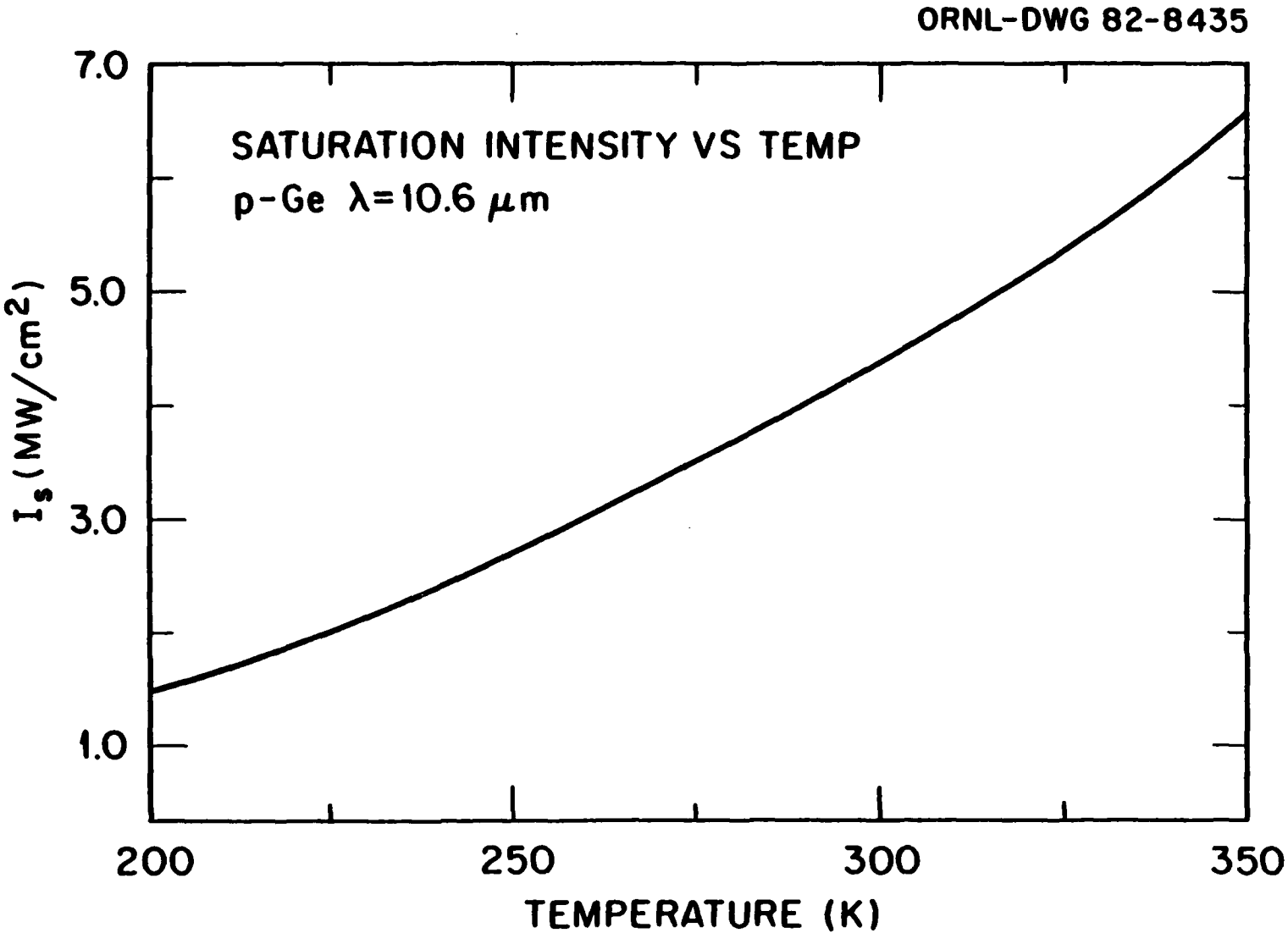
ORNL-DWG 82-8435
SATURATION INTENSITY VS TEMP
p-Ge λ=10.6 μm
7.0
5.0
3.0
1.0
I_s (MW/cm^2)
200
250
300
350
TEMPERATURE (K)

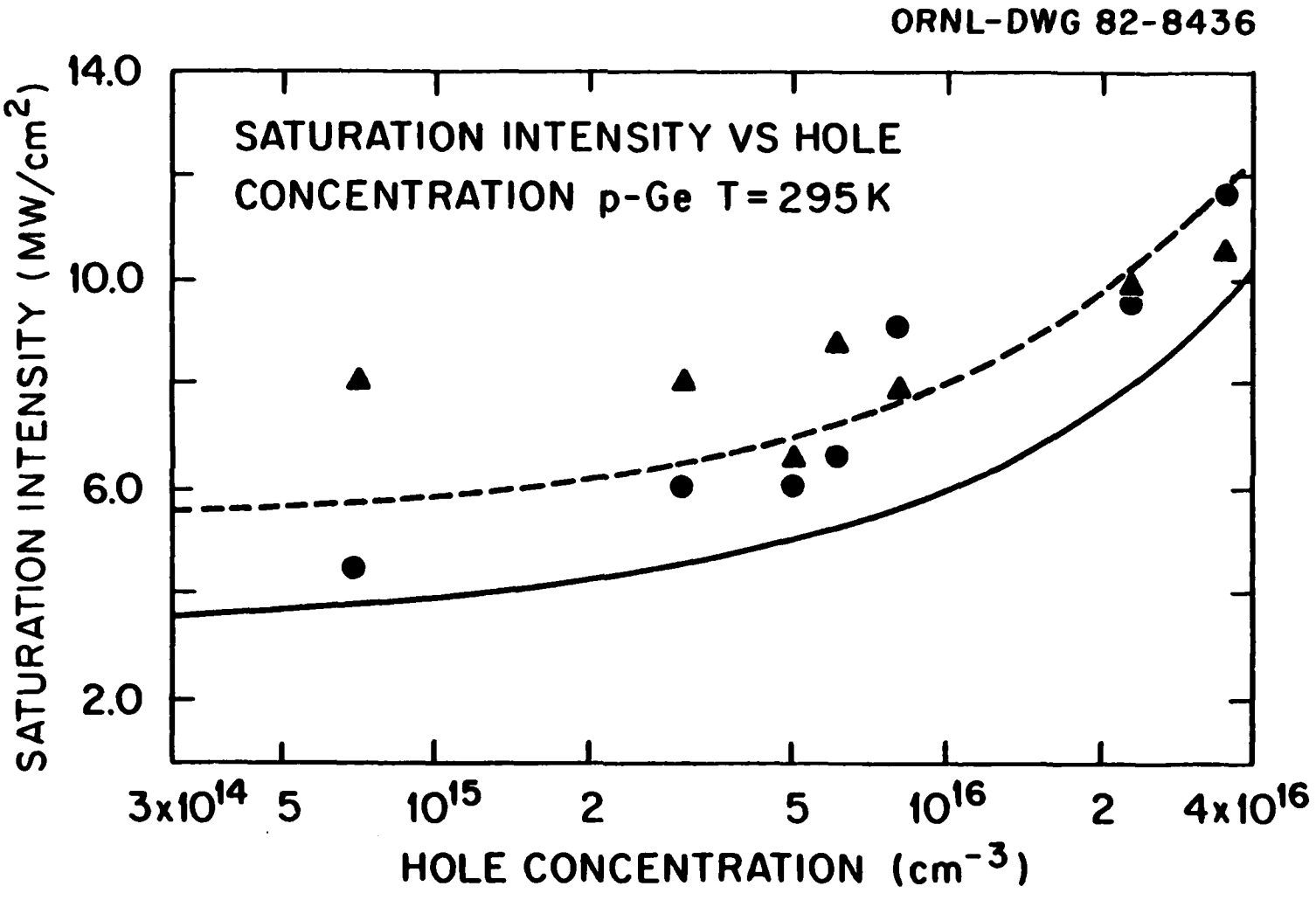
ORNL-DWG 82-8436
SATURATION INTENSITY VS HOLE CONCENTRATION p-Ge T=295K
SATURATION INTENSITY (MW/cm²)
14.0
10.0
6.0
2.0
3x10¹⁴
5
10¹⁵
2
5
10¹⁶
2
4x10¹⁶
HOLE CONCENTRATION (cm⁻³)

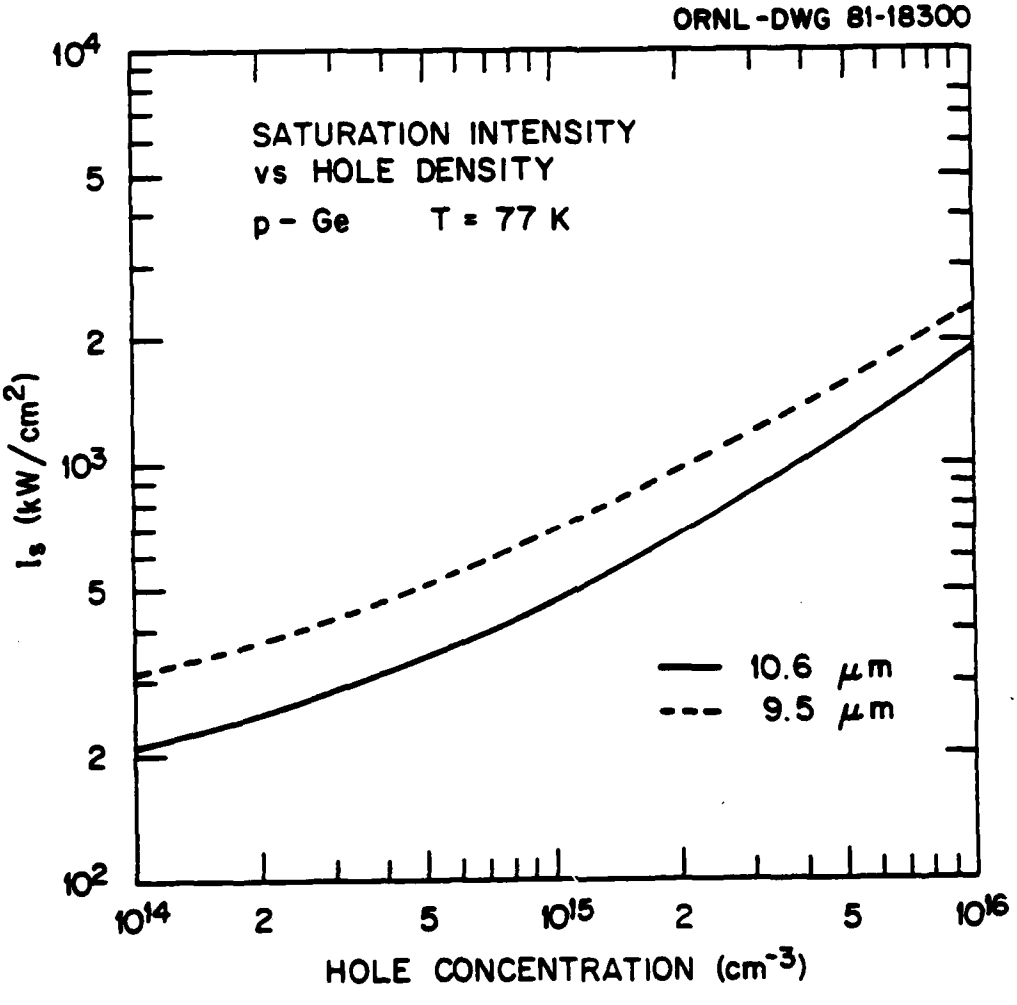
ORNL-DWG 81-18300
SATURATION INTENSITY
vs HOLE DENSITY
p - Ge T = 77 K
10.6 μm
9.5 μm
I_s (kW/cm^2)
HOLE CONCENTRATION (cm^{-3})
10^4
5
2
10^3
5
2
10^2
10^{14}
2
5
10^{15}
2
5
10^{16}

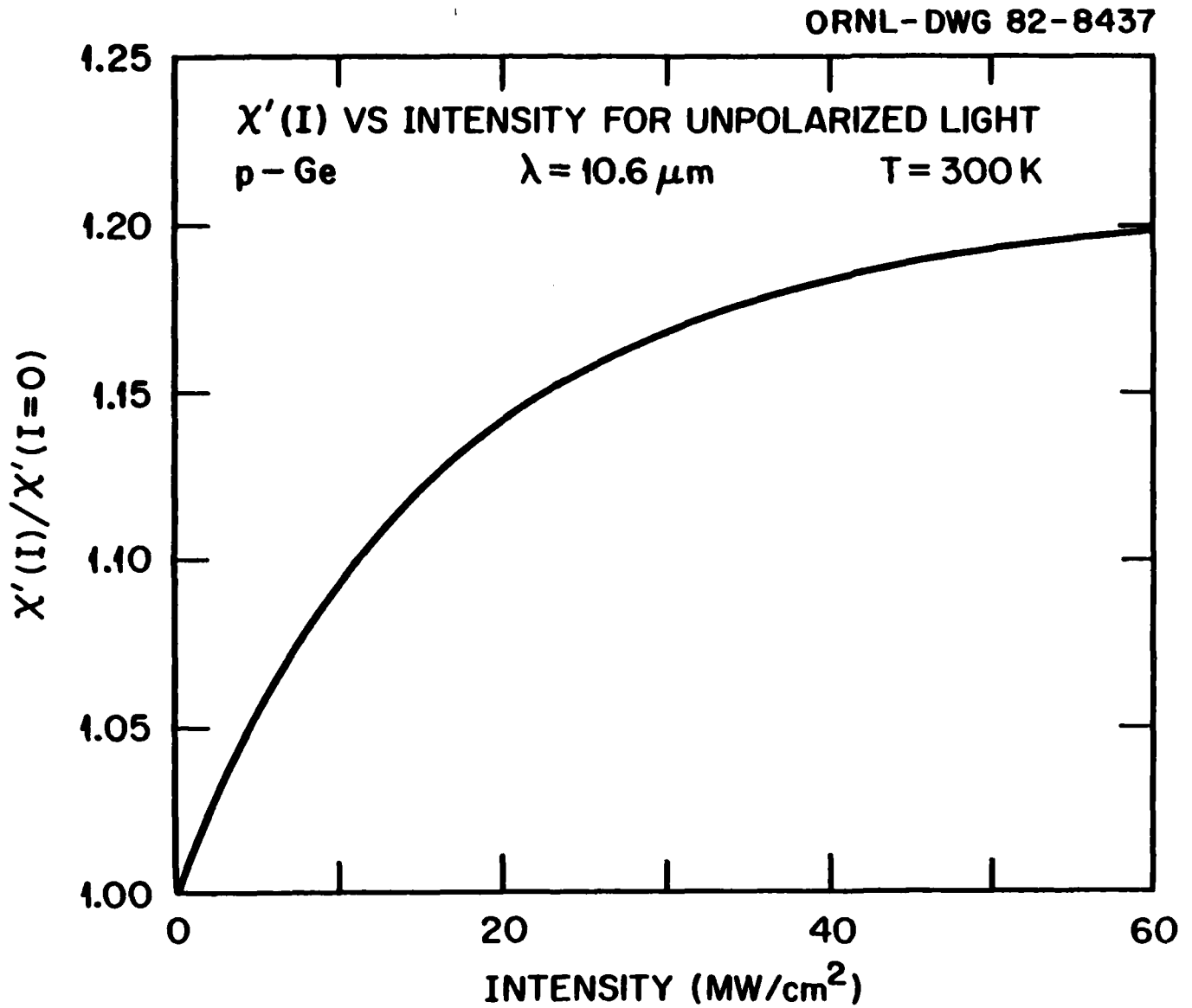
ORNL-DWG 82-8437
χ'(I) VS INTENSITY FOR UNPOLARIZED LIGHT
p – Ge
λ = 10.6 μm
T = 300 K
χ'(I)/χ'(I=0)
1.25
1.20
1.15
1.10
1.05
1.00
0
20
40
60
INTENSITY (MW/cm²)

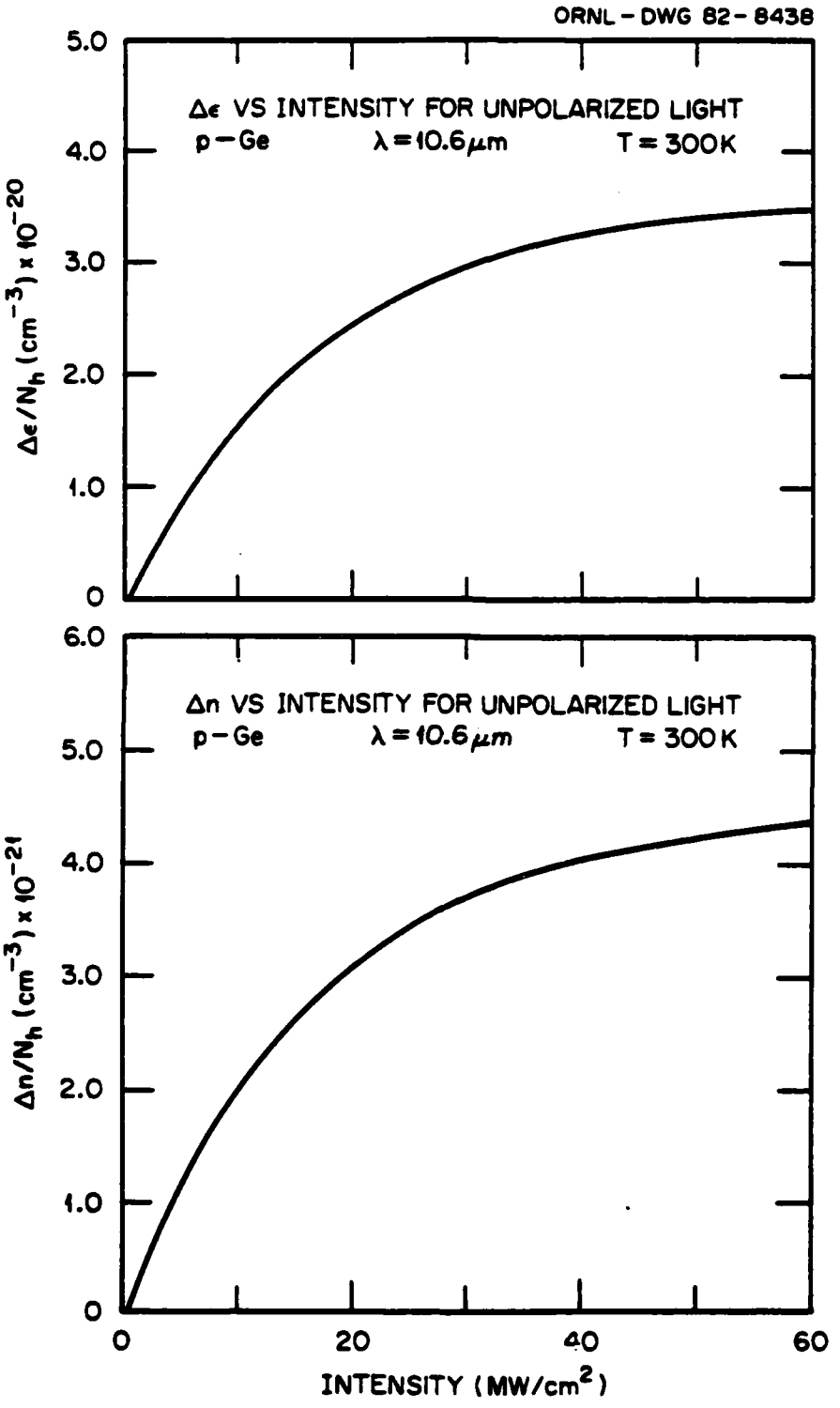
ORNL - DWG 82 - 8438
Δε VS INTENSITY FOR UNPOLARIZED LIGHT
p - Ge λ = 10.6 μm T = 300K
Δε/N_h (cm^-3) x 10^-20
5.0
4.0
3.0
2.0
1.0
0
Δn VS INTENSITY FOR UNPOLARIZED LIGHT
p - Ge λ = 10.6 μm T = 300K
Δn/N_h (cm^-3) x 10^-21
6.0
5.0
4.0
3.0
2.0
1.0
0
0
20
40
60
INTENSITY (MW/cm^2)

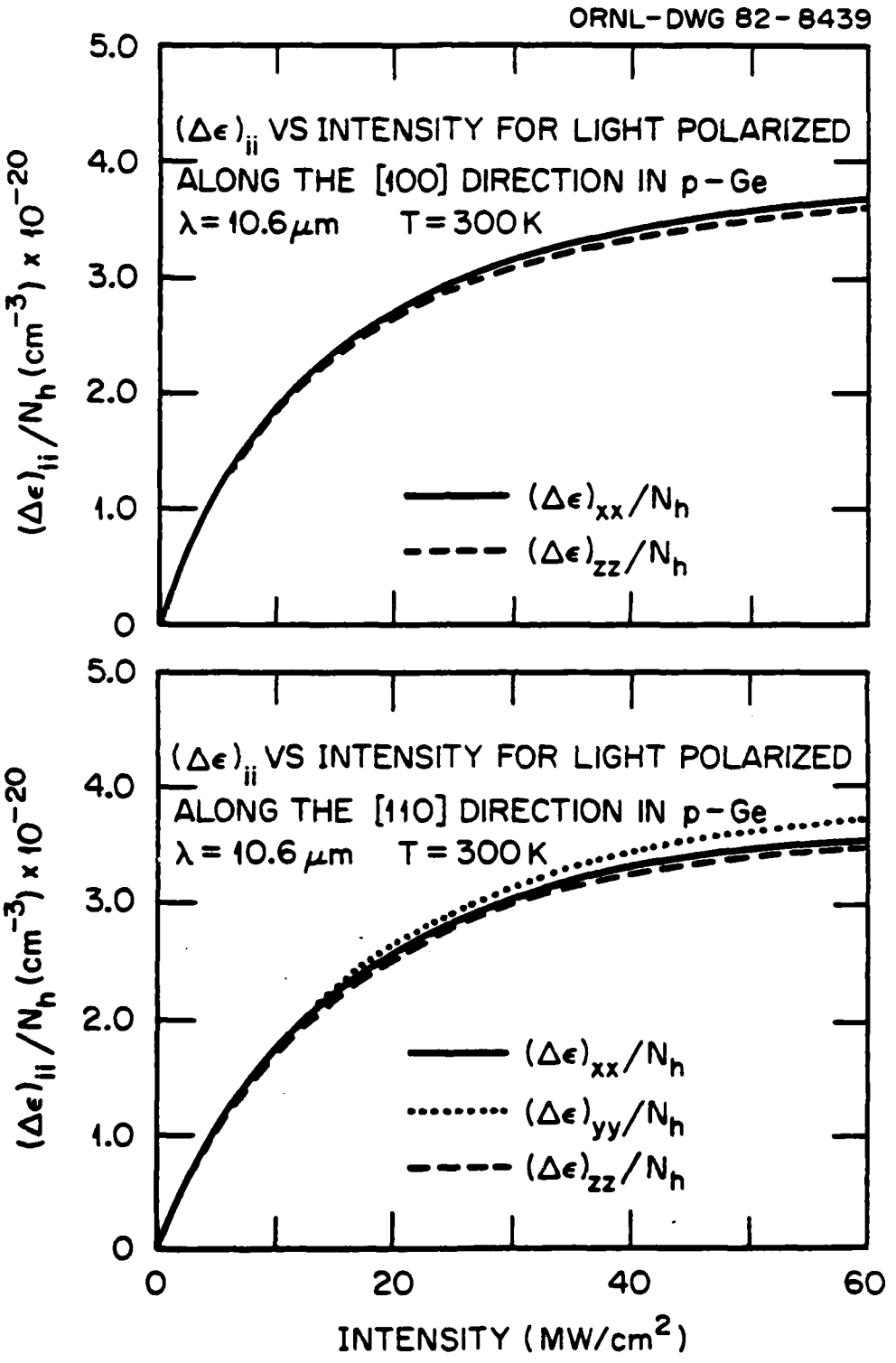
ORNL-DWG 82-8439
$(\Delta\epsilon)_{ii}$ VS INTENSITY FOR LIGHT POLARIZED
ALONG THE [100] DIRECTION IN p-Ge
$\lambda = 10.6\,\mu m$ T = 300 K
$(\Delta\epsilon)_{xx}/N_h$
$(\Delta\epsilon)_{zz}/N_h$
$(\Delta\epsilon)_{ii}/N_h\,(cm^{-3}) \times 10^{-20}$
$(\Delta\epsilon)_{ii}$ VS INTENSITY FOR LIGHT POLARIZED
ALONG THE [110] DIRECTION IN p-Ge
$\lambda = 10.6\,\mu m$ T = 300 K
$(\Delta\epsilon)_{xx}/N_h$
$(\Delta\epsilon)_{yy}/N_h$
$(\Delta\epsilon)_{zz}/N_h$
$(\Delta\epsilon)_{ii}/N_h\,(cm^{-3}) \times 10^{-20}$
0
1.0
2.0
3.0
4.0
5.0
0
20
40
60
INTENSITY (MW/cm^2)

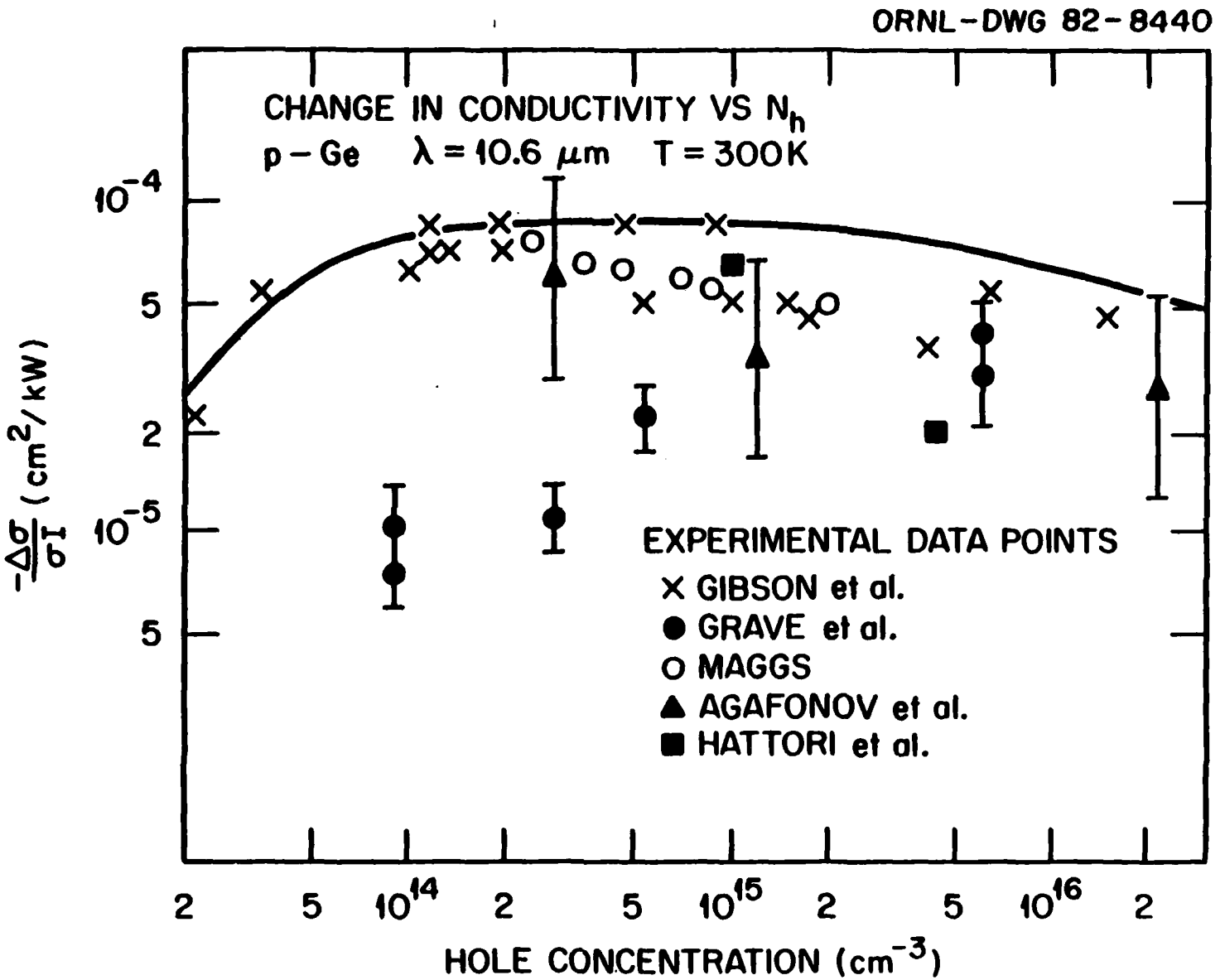
ORNL-DWG 82-8440
CHANGE IN CONDUCTIVITY VS N_h
p – Ge λ = 10.6 μm T = 300K
$-\frac{\Delta\sigma}{\sigma I}$ (cm²/kW)
10^{-4}
5
2
10^{-5}
5
EXPERIMENTAL DATA POINTS
× GIBSON et al.
● GRAVE et al.
O MAGGS
▲ AGAFONOV et al.
■ HATTORI et al.
2 5 10^{14} 2 5 10^{15} 2 5 10^{16} 2
HOLE CONCENTRATION (cm^{-3})

ORNL-DWG 82-8434

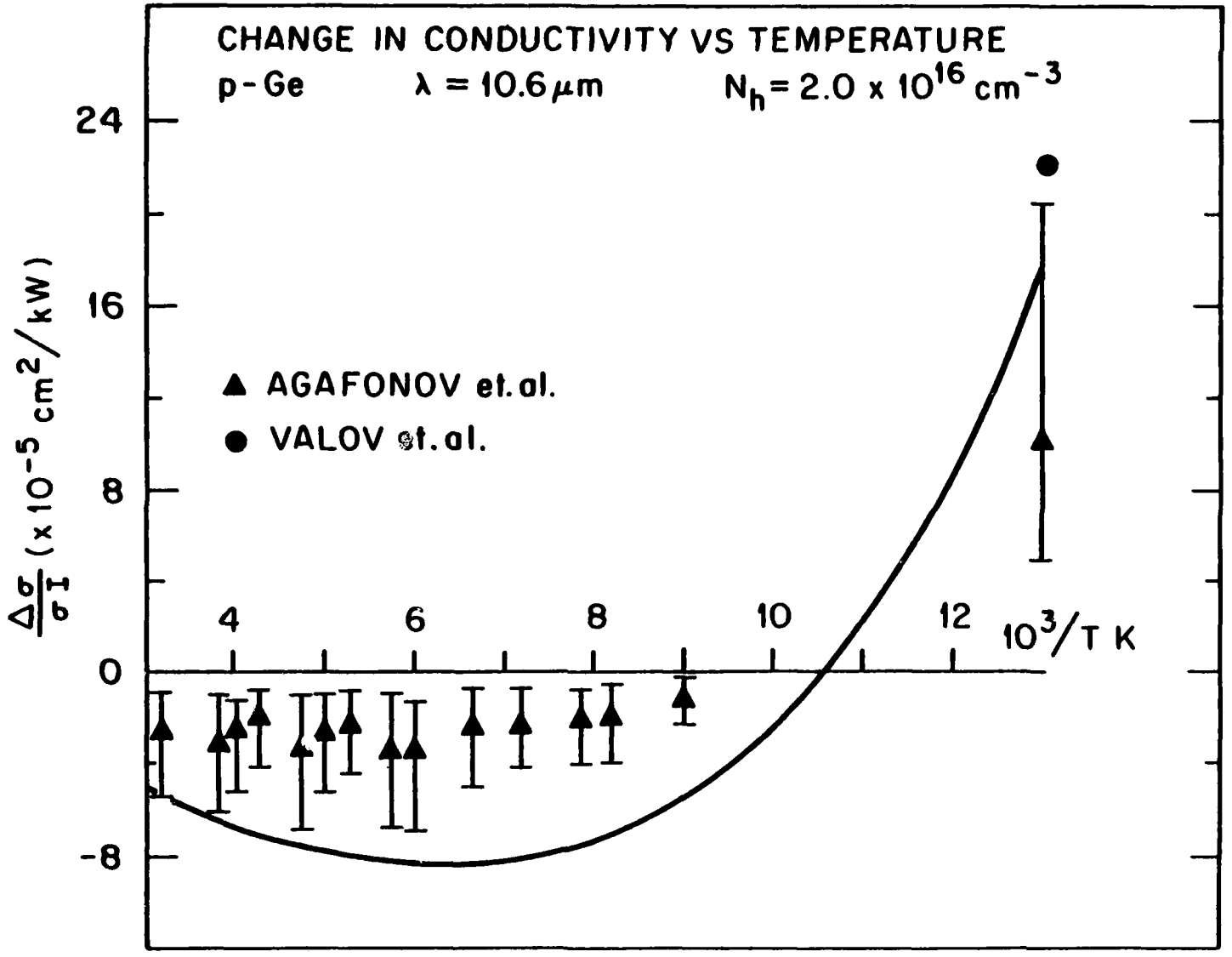

AD-A119 264 CALIFORNIA INST OF TECH PASADENA F/G 20/5
OPTICAL PROPERTIES OF SMALL BAND GAP SEMICONDUCTORS SUBJECT TO --ETC(U)
1982 T C MCGILL, D L SMITH AFOSR-77-3216
UNCLASSIFIED AFOSR-TR-82-0678 NL

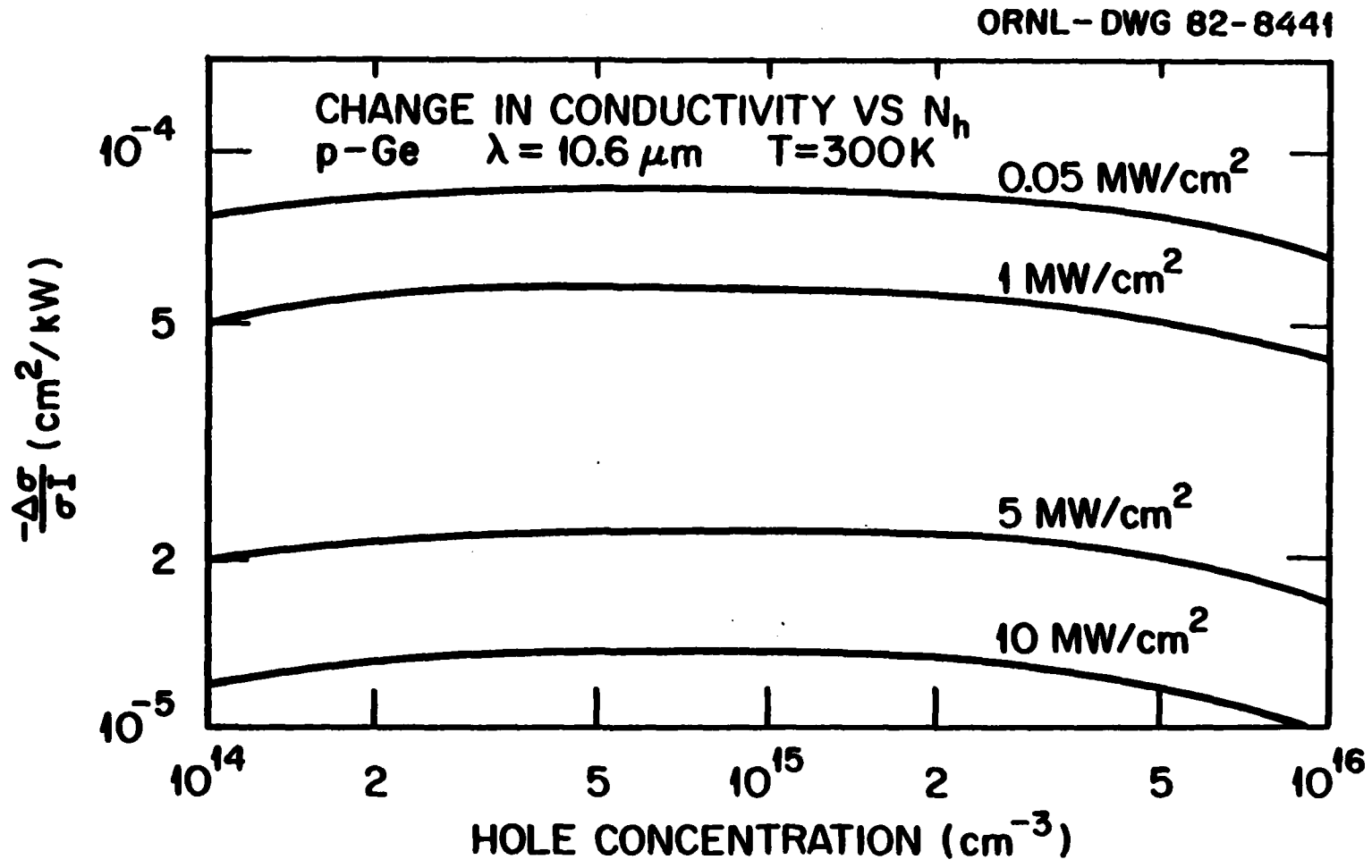
ORNL-DWG 82-8441
CHANGE IN CONDUCTIVITY VS N_h
p-Ge $\lambda = 10.6\ \mu m$ T=300K
0.05 MW/cm^2
1 MW/cm^2
5 MW/cm^2
10 MW/cm^2
$-\frac{\Delta\sigma}{\sigma I}$ (cm^2/kW)
10^{-4}
5
2
10^{-5}
10^{14}
2
5
10^{15}
2
5
10^{16}
HOLE CONCENTRATION (cm^{-3})

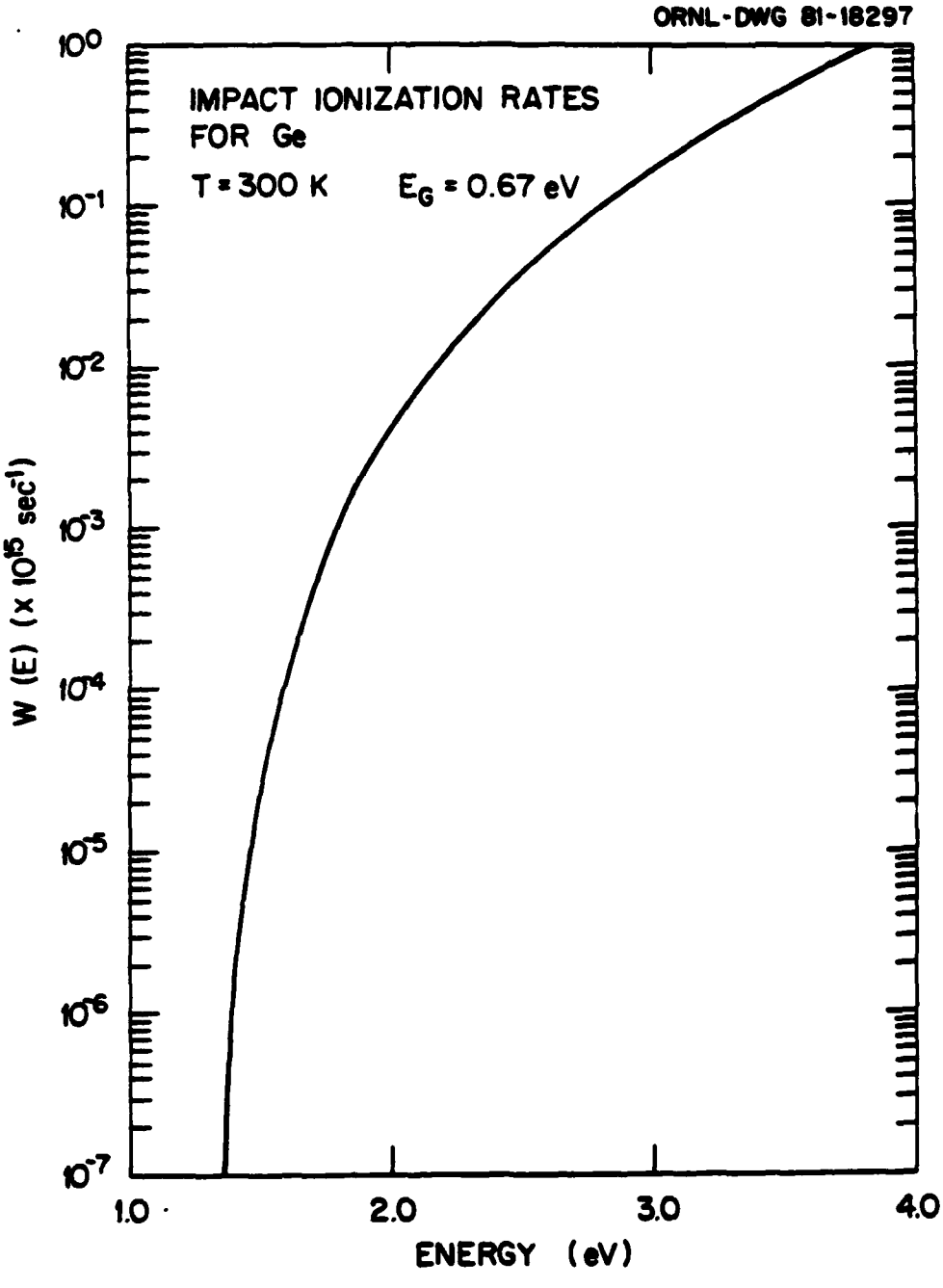
ORNL-DWG 81-18297
IMPACT IONIZATION RATES
FOR Ge
T = 300 K
E_G = 0.67 eV
W (E) (x 10^{15} sec^{-1})
10^{0}
10^{-1}
10^{-2}
10^{-3}
10^{-4}
10^{-5}
10^{-6}
10^{-7}
1.0
2.0
3.0
4.0
ENERGY (eV)

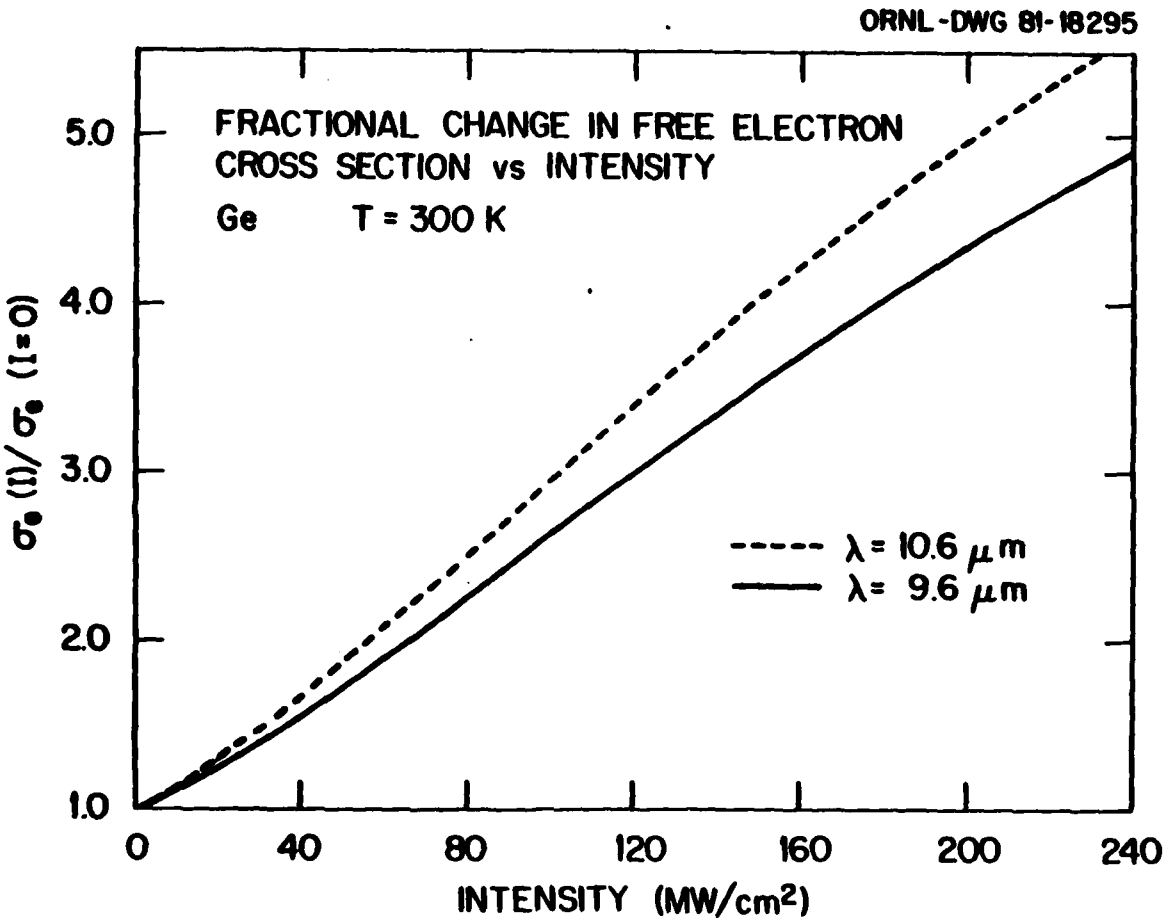
ORNL-DWG 81-18295
FRACTIONAL CHANGE IN FREE ELECTRON CROSS SECTION vs INTENSITY
Ge T = 300 K
$\sigma_e(I)/\sigma_e(I=0)$
5.0
4.0
3.0
2.0
1.0
0
40
80
120
160
200
240
INTENSITY (MW/cm²)
λ = 10.6 μm
λ = 9.6 μm

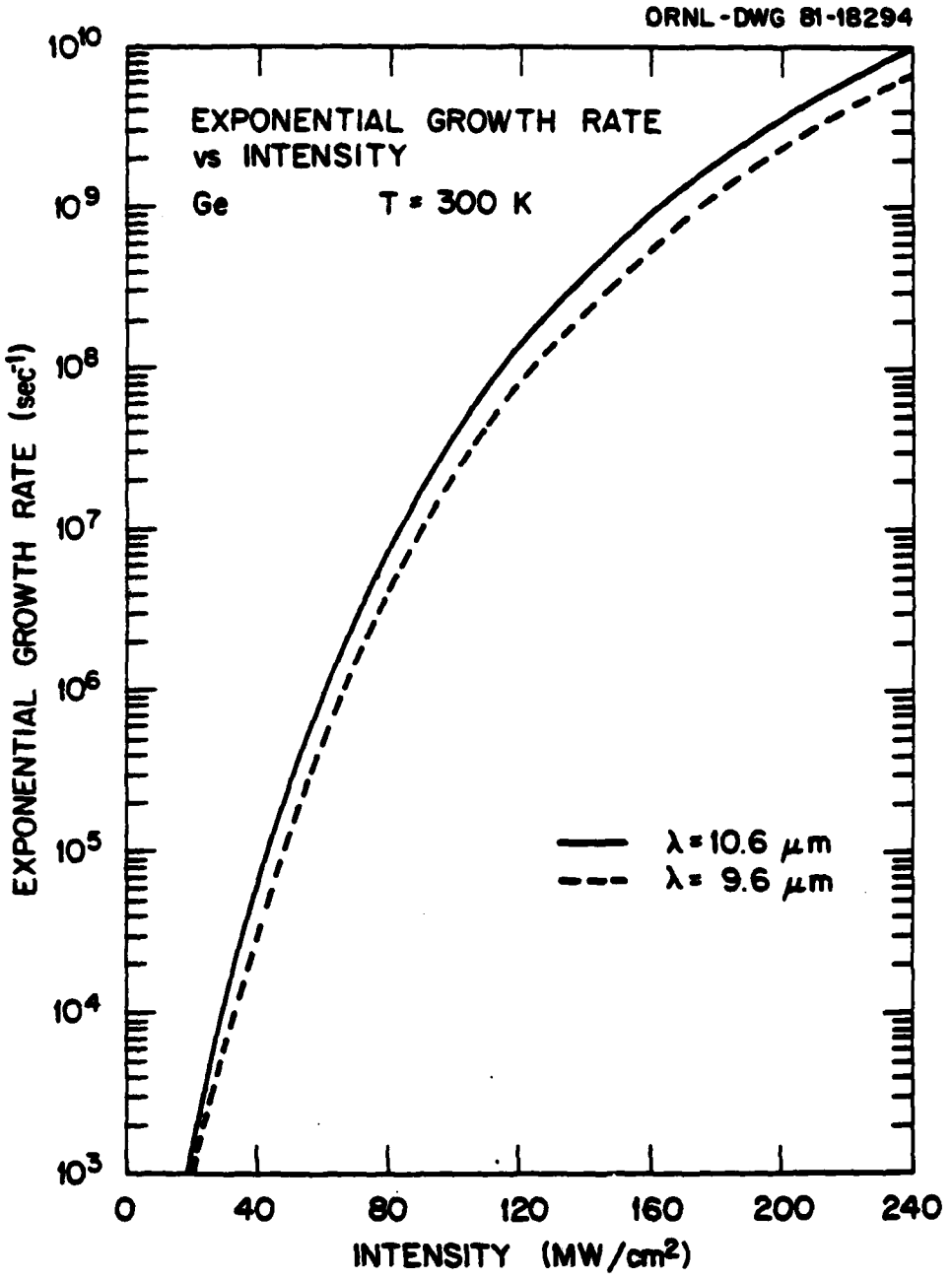
ORNL-DWG 81-18294
EXPONENTIAL GROWTH RATE
vs INTENSITY
Ge
T = 300 K
EXPONENTIAL GROWTH RATE (sec⁻¹)
10¹⁰
10⁹
10⁸
10⁷
10⁶
10⁵
10⁴
10³
λ = 10.6 μm
λ = 9.6 μm
0
40
80
120
160
200
240
INTENSITY (MW/cm²)

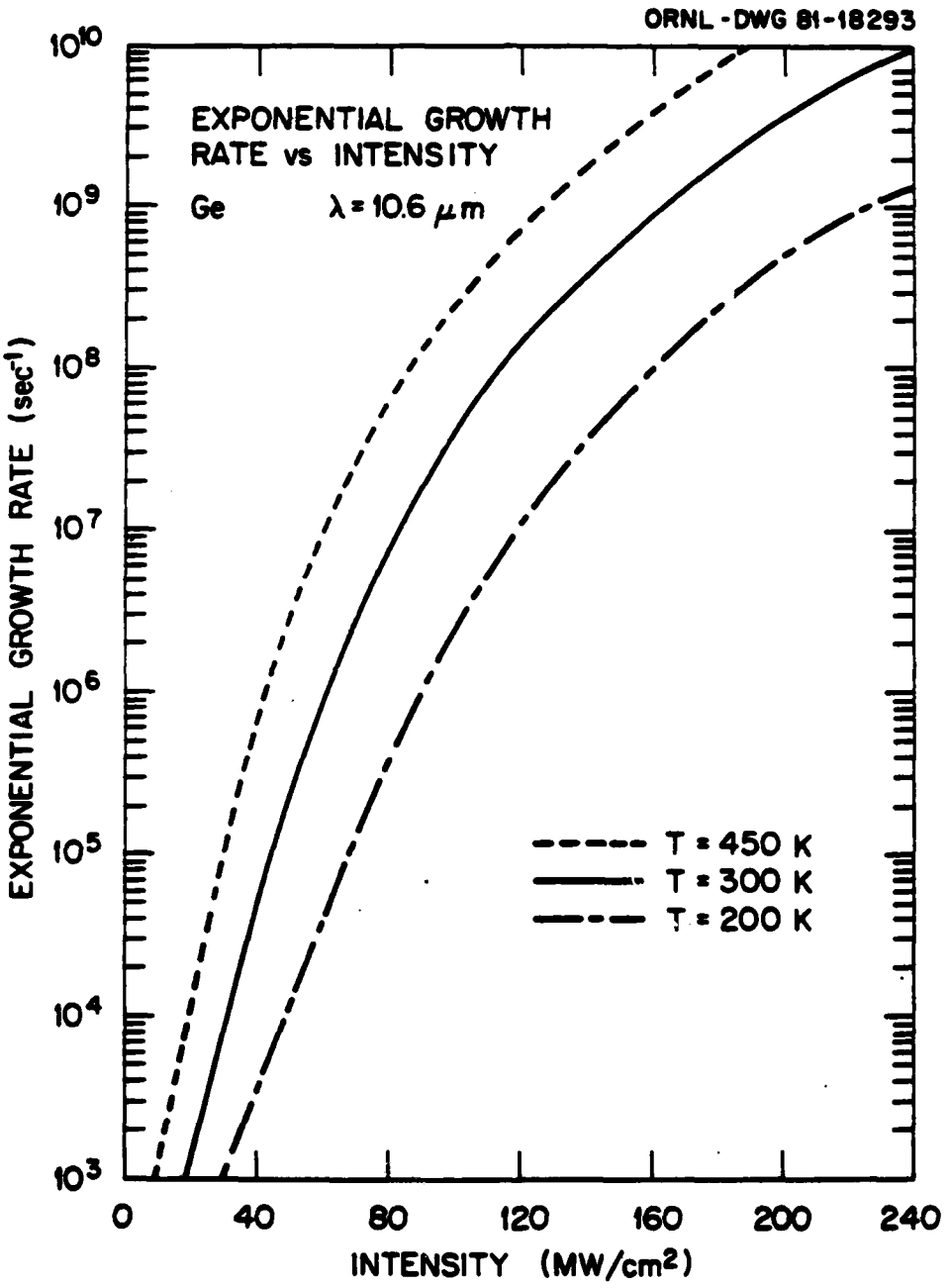
ORNL - DWG 81-18293
EXPONENTIAL GROWTH
RATE vs INTENSITY
Ge
λ = 10.6 μm
EXPONENTIAL GROWTH RATE (sec⁻¹)
10¹⁰
10⁹
10⁸
10⁷
10⁶
10⁵
10⁴
10³
T = 450 K
T = 300 K
T = 200 K
0
40
80
120
160
200
240
INTENSITY (MW/cm²)

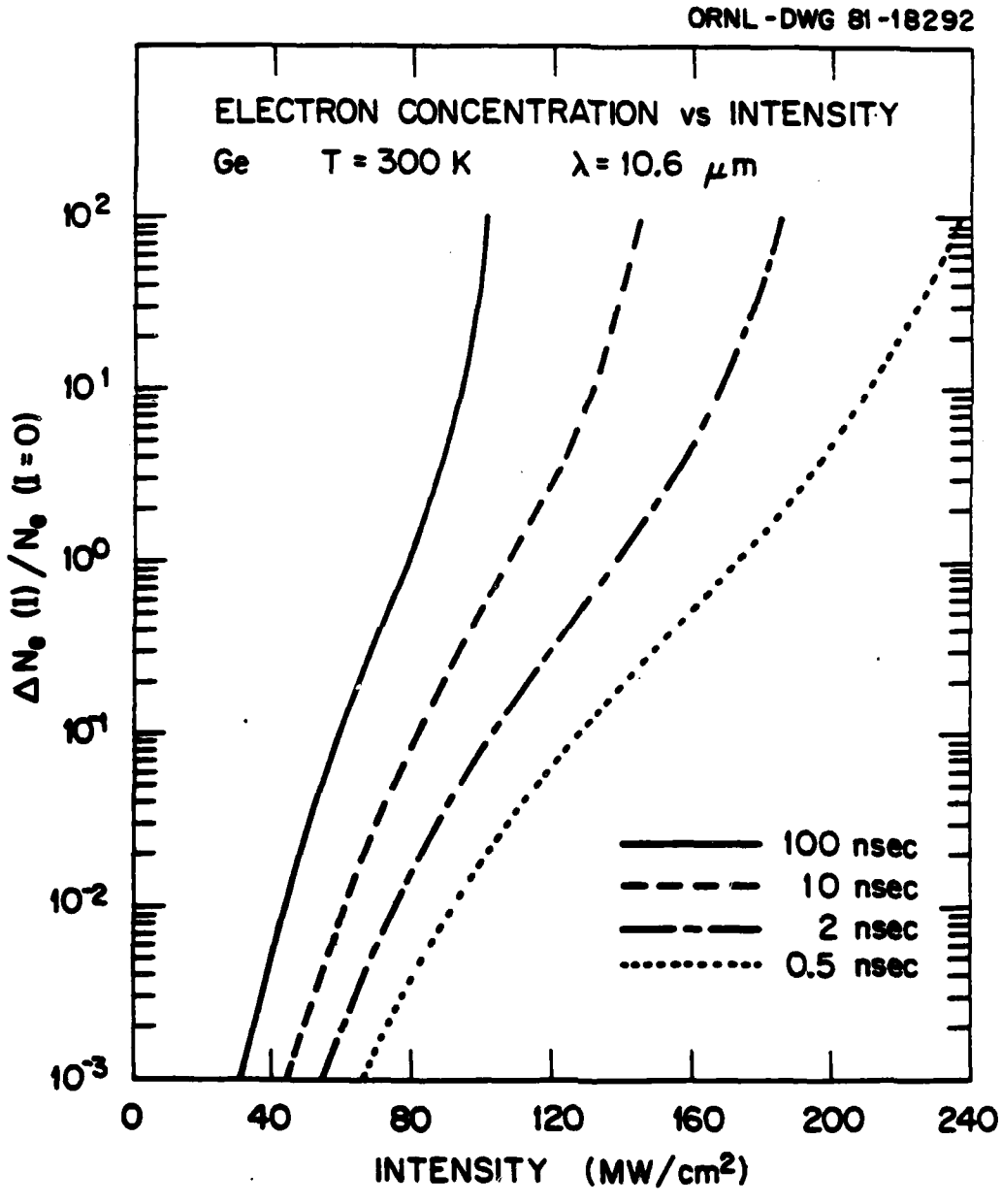
ORNL-DWG 81-18292
ELECTRON CONCENTRATION vs INTENSITY
Ge T = 300 K λ = 10.6 μm
$\Delta N_e(I)/N_e(I=0)$
10^2
10^1
10^0
10^{-1}
10^{-2}
10^{-3}
0
40
80
120
160
200
240
INTENSITY (MW/cm²)
100 nsec
10 nsec
2 nsec
0.5 nsec

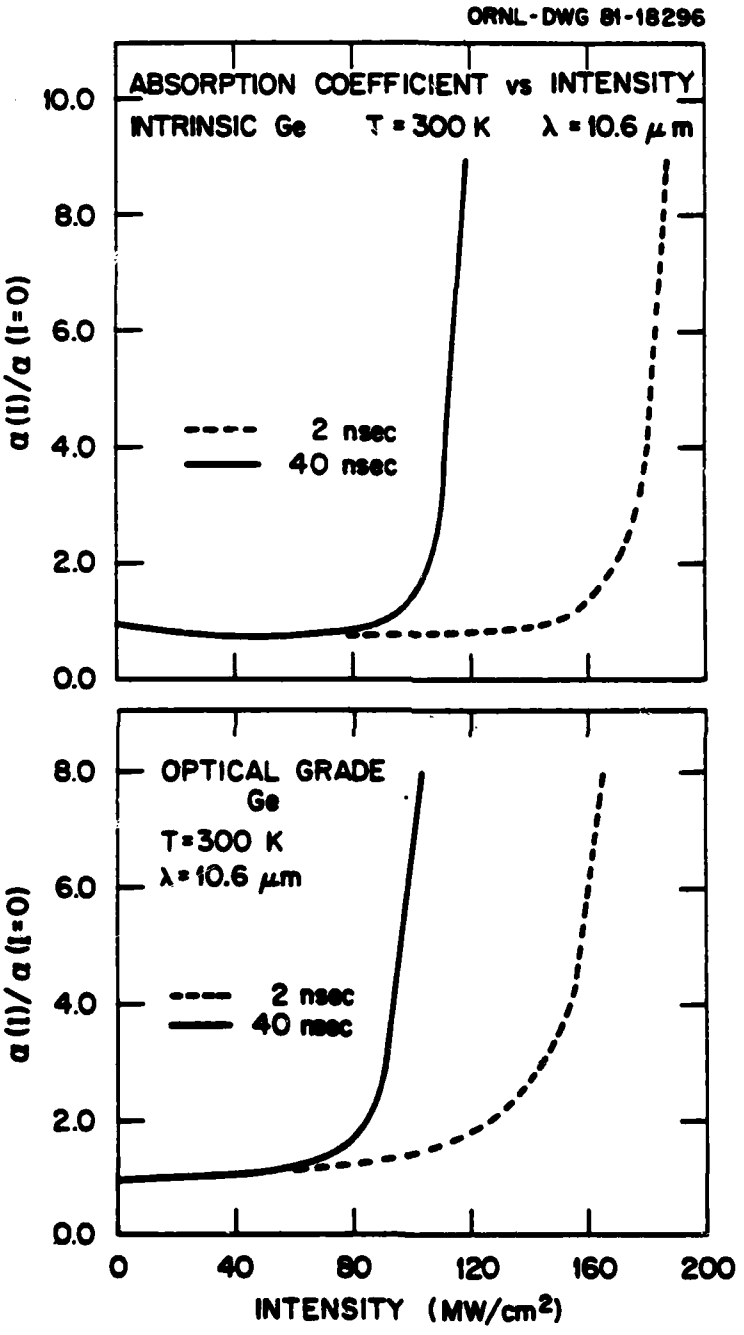
ORNL-DWG 81-18296
ABSORPTION COEFFICIENT vs INTENSITY
INTRINSIC Ge T = 300 K λ = 10.6 μm
α (I)/α (I=0)
10.0
8.0
6.0
4.0
2.0
0.0
2 nsec
40 nsec
OPTICAL GRADE
Ge
T=300 K
λ=10.6 μm
0
40
80
120
160
200
INTENSITY (MW/cm²)